

Spring 5-15-2015

Ketone Body Metabolism Preserves Hepatic Function during Adaptation to Birth and in Overnutrition

David Graham Cotter
Washington University in St. Louis

Follow this and additional works at: https://openscholarship.wustl.edu/art_sci_etds

 Part of the [Biology Commons](#)

Recommended Citation

Cotter, David Graham, "Ketone Body Metabolism Preserves Hepatic Function during Adaptation to Birth and in Overnutrition" (2015). *Arts & Sciences Electronic Theses and Dissertations*. 444.
https://openscholarship.wustl.edu/art_sci_etds/444

This Dissertation is brought to you for free and open access by the Arts & Sciences at Washington University Open Scholarship. It has been accepted for inclusion in Arts & Sciences Electronic Theses and Dissertations by an authorized administrator of Washington University Open Scholarship. For more information, please contact digital@wumail.wustl.edu.

WASHINGTON UNIVERSITY IN ST. LOUIS

Division of Biology & Biomedical Sciences
Molecular Cell Biology

Dissertation Examination Committee:

Peter Crawford, Chair

Thomas Baranski

Brian Finck

Shin-ichiro Imai

Joel Schilling

Clay Semenkovich

Ketone Body Metabolism Preserves Hepatic Function during Adaptation to Birth and in Overnutrition

by

David Graham Cotter

A dissertation presented to the
Graduate School of Arts and Sciences
of Washington University in
partial fulfillment of the
requirements for the degree
of Doctor of Philosophy

May 2015

St. Louis, Missouri

© 2015, David Graham Cotter

Table of Contents

1. List of Figures.....	iii
2. List of Tables.....	vi
3. Acknowledgements.....	vii
4. Abstract.....	ix
5. Body of Dissertation	
a. Chapter 1: Introduction: Ketone Body Metabolism and Cardiovascular Disease.....	2
b. Chapter 2: Obligate role for ketone body oxidation in neonatal metabolic homeostasis.....	30
c. Chapter 3: Successful adaptation to ketosis by mice with tissue-specific deficiency of ketone body oxidation	54
d. Chapter 4: Impact of peripheral ketolytic deficiency on hepatic ketogenesis and gluconeogenesis during the transition to birth.	81
e. Chapter 5: PPAR α -dependent ketogenesis prevents hepatic steatosis in neonatal mice.....	121
f. Chapter 6: Ketogenesis prevents diet-induced fatty liver injury and hyperglycemia through coenzyme A recycling.....	138
g. Chapter 7: ^{13}C -edited proton NMR spectroscopy method for measurement of gluconeogenesis from pyruvate in the perfused mouse liver.....	176
h. Chapter 8: Impaired fasting glucose and hepatic steatosis in ketogenesis insufficient mice.....	181
i. Concluding Remarks.....	184
6. Literature Cited.....	191
7. Curriculum Vitae.....	212

List of Figures

Figure 1.1: Ketone body metabolism pathways.....	24
Figure 1.2: Hepatic integration of ketogenesis.....	25
Figure 1.3: Ketogenic flux through CoA transferase.....	26
Figure 1.4: Regulatory mechanisms for HMGCS2 and CoA transferase (SCOT).....	27
Figure 1.5: Diverse roles of CoA transferase in mitochondrial function.....	28
Figure 2.1: Ketolysis-deficient <i>Oxct1</i> ^{-/-} mice.....	45
Figure 2.2: Metabolic resuscitation of <i>Oxct1</i> ^{-/-} mice.....	46
Figure 2.3: Normal glucose disposal but refractory hyperketonemia in glucose-resuscitated suckling <i>Oxct1</i> ^{-/-} mice.....	47
Figure 2.4: Increased phosphorylation of AMPK α within brain of <i>Oxct1</i> ^{-/-} mice.....	48
Figure 2.5: Enhanced autophagy in brain of <i>Oxct1</i> ^{-/-} mice.....	49
Figure 2.6: Tissue-specific adaptations to ketolytic insufficiency.....	50
Figure S.2.1: Absence of terminal ketone body oxidation in muscle and brain of <i>Oxct1</i> ^{-/-} mice.....	52
Figure 3.1: Strategy for the generation of transgenic overexpresser and tissue-specific SCOT-KO mice.....	71
Figure 3.2: Restoration of ketone body oxidative capacity selectively within cardiomyocytes of germline SCOT-KO mice.....	72
Figure 3.3: Absence of CoA transferase protein and enzymatic activity in tissue-specific SCOT-KO mouse strains.....	73
Figure 3.4: Circulating metabolites in neonatal tissue-specific SCOT-KO strains.....	74
Figure 3.5: Increased glucose consumption by brains of neonatal SCOT-Neuron-KO mice.....	75
Figure 3.6: Adult tissue-specific SCOT-KO mice tolerate starvation.....	76
Figure 3.7: Diminished total body ketone body oxidative capacity impairs adaptation to ketotic nutrient states.....	77
Figure 4.1: Absence of extrahepatic ketone body oxidation engages an hepatic gluconeogenic program in neonatal mice.....	102
Figure 4.2: Alterations of terminal fatty acid oxidation and pyruvate handling in livers of SCOT-KO mice.....	103
Figure 4.3: Mother's milk-induced impairment of de novo β OHB production in neonatal SCOT-KO liver.....	104

Figure 4.4: Normal in vitro hepatic ketogenesis of livers from SCOT-KO mice.....	105
Figure 4.5: D-βOHB inhibits neonatal hepatic ketogenesis in vivo.....	106
Figure 4.6: Oxidized hepatic redox potential in P1 SCOT-KO mice.....	107
Figure S4.1: PDH-E1α Ser293 phosphorylation in P1 Liver.....	108
Figure S4.2: Normal oxidative and ketogenic machinery in livers of P1 SCOT-KO mice.....	109
Figure S4.3: Normal hepatic fractional enrichment of ¹³ C-glutamate from [¹³ C]octanoate in P0 SCOT-KO mice.....	110
Figure S4.4: Normal oxidative and ketogenic machinery in livers of milk-fed P0 SCOT-KO mice.....	111
Figure S4.5: Relative abundances of mRNAs encoding mediators of NAD ⁺ metabolism and signaling in livers of P0 and P1 mice.....	112
Figure S4.6: CoA transferase protein abundance in neonatal tissues.....	113
Figure 5.1: PPARα-KO mice exhibit neonatal hypoglycemia.....	132
Figure 5.2: PPARα promoted gluconeogenesis from glycerol in neonatal mice.....	133
Figure 5.3: Normal hepatic fatty acid oxidation in PPARα-KO neonates.....	134
Figure 5.4: PPARα-KO neonates exhibit hypoketonemia due to decreased expression of ketogenic enzymes.....	135
Figure 5.5: Ketogenic suppression is associated with neonatal hepatic steatosis.....	136
Figure 6.1: Ketogenic insufficiency in mice treated with <i>Hmgcs2</i> ASO.....	161
Figure 6.2: Hepatic injury in ketogenesis insufficient HFD-fed mice.....	162
Figure 6.3: Hepatic metabolic reprogramming in ketogenesis insufficient mice.....	163
Figure 6.4: Replenishing CoA precursors restores gluconeogenesis and TCA cycle intermediate abnormalities in livers of ketogenesis insufficient mice.....	164
Figure S6.1: Metabolic parameters of ketogenesis insufficient neonatal mice, specificity of HMGCS2 ASO treatment in adult mice, and quantification of ketogenesis in perfused livers.....	165
Figure S6.2: Metabolic parameters of ketogenesis insufficient adult mice fed a standard chow diet.....	166
Figure S6.3: Serum metabolites of ASO-treated mice fed a 60% HFD.....	167
Figure S6.4: Body weight, energy intake, and body composition of ketogenesis insufficient mice fed either a 60% HFD or a 40% fat diet.....	168
Figure S6.5: Metabolite concentrations and gene expression in livers of ketogenesis insufficient mice.....	169
Figure S6.6: Hepatic injury in ketogenesis insufficient mice fed a 40% HFD.....	170

Figure S6.7: Elevation of short- and medium-chain blood acylcarnitines in ketogenesis insufficient mice fed a 40% fat diet.....	171
Figure S6.8: Hepatic glucose pools in livers perfused with supplemental CoASH precursors.....	172
Figure 7.1: Fasting alters pyruvate fate in perfused livers.....	180
Figure 8.1: Fasting-induced hyperglycemia is associated with hepatic steatosis in ketogenesis insufficient mice.....	182
Figure 8.2: Altered hepatic pyruvate fate in ketogenesis insufficient mice.....	183

List of Tables

Table 1.1: Implications of ketone body metabolism.....	29
Table 2.1: Plasma metabolite concentrations in P0-P1 mice.....	51
Table S2.1: Oligonucleotide primer sequences used for PCR in this study.....	53
Table 3.1: Genotyping primer sequences.....	78
Table 3.2: RT-qPCR primer sequences.....	79
Table 3.3: Serum AcAc-to-D-βOHB ratios in adult mice.....	80
Table S4.1: RT-qPCR Primers.....	114
Table S4.2: P0 Hepatic Taurine Concentrations.....	115
Table S4.3: P1 Hepatic Taurine Concentrations.....	116
Table S4.4: P0 Blood Amino Acid Profile.....	117
Table S4.5: P1 Blood Amino Acid Profile.....	118
Table S4.6: P1 Blood Acylcarnitine Profile.....	119
Table S4.7: P0 Blood Acylcarnitine Profile.....	120
Table 5.1: RT-qPCR Primers.....	137
Table S6.1: Blood acylcarnitine profiles of ASO-treated mice fed a chow diet.....	173
Table S6.2: Blood acylcarnitine profile of ASO-treated mice fed a 40% fat diet.....	174
Table S6.3: RT-qPCR Primers.....	175

Acknowledgements

This work was supported in part by NIH grants HL007873, DK091538, plus grants from the Diabetic Cardiovascular Disease Center at Washington University, and the March of Dimes.

Many people have contributed to my scientific development. During my undergraduate training, I was extremely fortunate to find outstanding mentors, including Frank van Breukelen, Peter Starkweather, Abayomi Animashaun, Matt Lawrenz, Jon Lenz, and Virginia Miller. As a graduate student, past and present members of the Crawford lab, including Rebecca Schugar, Baris Ercal, Jamison Leid, Ashley Moll, Annie Wentz, Mary Weber, Charles Shyng, and Debra Whorms, have provided numerous helpful conversations and technical assistance. In particular, Rebecca Schugar and her fiancé have become treasured friends. Baris Ercal and Jamison Leid, the ASO squad, have always made work fun. The studies presented herein have greatly benefitted from helpful discussions with and experimental assistance from many collaborators, including Dennis Dietzen, Brian Finck, Shin Imai, Trey Coleman and Clay Semenkovich, Tom Baranski, and D. Andre d'Avignon. No one has spent more time in the trenches with me than Andre, who has even come into work at 11:30 PM, beer in hand, to help me trouble shoot instrument problems. Most importantly, this work would not exist without the unwavering support, guidance, and friendship of my thesis advisor Peter Crawford. Peter, thank you for helping me to obtain and to maintain “momentum.”

Science offers unique psychological challenges. Without extracurricular outlets, one could easily unravel. Fortunately, my best friends, James Byers and Anthony Marlon, helped me maintain sanity through martial arts, hiking, and all around “fun-having.” My mother- and father-in-law have offered unrivaled love and support. Brian and Valerie, thank you for letting me into your home and into your lives. Most of all, my beautiful, strong, and loving wife Brianna has made tremendous personal sacrifices to stand beside me in pursuit of this degree. Bri, I would be lost without you.

Dedication

Quinn, even as I write, your mother and I eagerly await your arrival. All that I have done and will ever do
is for you.

ABSTRACT OF THE DISSERTATION

Ketone Body Metabolism Preserves Hepatic Function during Adaptation to Birth and in Overnutrition

by

David Graham Cotter

Doctor of Philosophy in Biology & Biomedical Sciences
Molecular Cell Biology

Washington University in St. Louis, 2015

Professor Peter Crawford, Chair

Mammalian ketone body metabolism partially oxidizes hepatic acyl-chains to ketone body intermediates, which can serve as alternative fuels in extrahapetic tissues during carbohydrate restricted states. Ketone body production (ketogenesis) occurs primarily in liver, due to hepatocyte-specific expression of the fate committing ketogenic enzyme, mitochondrial 3-hydroxymethylglutaryl-CoA synthase (HMGCS2). In contrast, the fate committing enzyme of ketone body oxidation, mitochondrial Succinyl-CoA:3-oxoacid CoA Transferase (SCOT), is expressed ubiquitously, except in liver. Here I demonstrate novel roles for ketone body metabolism during a classically ketogenic period, the transition to birth, and in a classically ‘non-ketogenic’ state, overnutrition, using novel genetic mouse models, high-resolution measures of dynamic metabolism using ^{13}C -labeled substrates, and systems physiology approaches. I show that germline SCOT-knockout (KO) mice cannot oxidize ketone bodies in any tissue. These mice developed lethal hyperketonemia and hypoglycemia within the first 48 hr of life and died in a manner that phenocopied human sudden infant death syndrome. Nonetheless, my studies of tissue-specific SCOT-KO mice revealed that ketone body oxidation is dispensable during the transition to birth and during starvation in the adult when individually eliminated in neurons, cardiomyocytes, or skeletal myocytes, which comprise the three largest consumers of ketone bodies. Surprisingly, the inability to dispose of ketone bodies in germline SCOT-KO mice drove derangements of carbohydrate and fatty acid metabolism, oxidized redox potential, and inhibited ketogenesis in liver. Moreover, I show that adult-onset loss of HMGCS2 ablated the liver’s capacity to effectively convert fat into ketone bodies, and thus

induced ketogenesis insufficiency. Ketogenesis insufficient mice exhibited increased hepatic gluconeogenesis from pyruvate and mild hyperglycemia in the fed state. High-fat diet feeding of ketogenesis insufficient mice caused extensive hepatocyte injury and inflammation that was associated with decreased glycemia due to fatty acid-induced sequestration of free coenzyme A that caused secondary derangements of hepatic tricarboxylic acid (TCA) cycle intermediate concentrations and impaired gluconeogenesis. Together, my studies have revealed a critical and novel role for ketone body metabolism in preservation of the dynamic intermediary metabolic network in liver during the adaptation to birth and in overnutrition.

Epigraph

"Though it be in deep sadness and pain,
in cold or heat...
gasping after breath... I will go on!
Now! Open the Gate!"

... Along the Road of the Sun L he journeyed—
one league he traveled...,
dense was the darkness, light there was none,
neither what lies ahead nor behind does it allow him to see.

Two leagues he traveled...,
dense was the darkness, light there was none,
neither what lies ahead nor behind does it allow him to see.

[22 lines are missing here.]

Four leagues he traveled...,
dense was the darkness, light there was none,
neither what lies ahead nor behind does it allow him to see.

Five leagues he traveled...,
dense was the darkness, light there was none,
neither what lies ahead nor behind does it allow him to see.

Six leagues he traveled...,
dense was the darkness, light there was none,
neither what lies ahead nor behind does it allow him to see.

Seven leagues he traveled...
dense was the darkness, light there was none,
neither what lies ahead nor behind does it allow him to see.

Eight leagues he traveled and cried out!
dense was the darkness, light there was none,
neither what lies ahead nor behind does it allow him to see.

Nine leagues he traveled... the North Wind.
It licked at his face,
dense was the darkness, light there was none,
neither what lies ahead nor behind does it allow him to see.

Ten leagues he traveled...
... is near,
... four leagues
...Eleven leagues he traveled and came out before the sun(rise).

Twelve leagues he traveled and it grew brilliant.
...it bears lapis lazuli as foliage,
bearing fruit, a delight to look.

From *The Epic of Gilgamesh*
Translated by Maureen Gallery Kovacs
Electronic Edition by Wolf Carnahan, 1998

Chapter 1: Introduction

Ketone Body Metabolism and Cardiovascular Disease

The work presented in this chapter has been adapted from:

Cotter, D. G., Schugar, R. C., and Crawford, P. A. (2013). *Am J Physiol Heart Circ Physiol* **304**(8), H1060-1076

Abstract

Ketone bodies are metabolized through evolutionarily conserved pathways that support bioenergetic homeostasis, particularly in brain, heart, and skeletal muscle when carbohydrates are in short supply. The metabolism of ketone bodies interfaces with the tricarboxylic acid cycle, β -oxidation of fatty acids, de novo lipogenesis, sterol biosynthesis, glucose metabolism, the mitochondrial electron transport chain, hormonal signaling, intracellular signal transduction pathways, and the microbiome. Here we review the mechanisms through which ketone bodies are metabolized, and how their signals are transmitted. We focus on the roles this metabolic pathway may play in cardiovascular disease states, the bioenergetic benefits of myocardial ketone body oxidation, and prospective interactions among ketone body metabolism, obesity, metabolic syndrome, and atherosclerosis. Ketone body metabolism is non-invasively quantifiable in humans and is responsive to nutritional interventions. Therefore, further investigation of this pathway in disease models and in humans may ultimately yield tailored diagnostic strategies and therapies for specific pathological states.

I. Introduction

Metabolism of ketone bodies is conserved among Eukarya, Bacteria, and Archaea (1-3). Ketone bodies are synthesized in liver from acetyl-CoA derived primarily from fatty acid oxidation and are transported to extrahepatic tissues for terminal oxidation during physiological states characterized by limited carbohydrate and surplus fatty acid availability [reviewed in (4,5); **(Figs. 1.1A-B)**]. Ketone body oxidation becomes a significant contributor to overall energy metabolism within extrahepatic tissues in numerous physiological states, including the neonatal period, starvation, post-exercise, and adherence to low carbohydrate diets, when circulating ketone body concentrations increase from $\sim 50 \mu\text{M}$ in the

normal fed state to up to 7 mM. Circulating ketone body concentrations rise to ~1 mM after 16-20h of fasting in healthy adult humans, but can accumulate to as high as 20 mM in pathological states like diabetic ketoacidosis (2,4,6). Ketone body metabolism is not solely rooted in energy metabolism, as ketone bodies also serve as lipogenic and sterol biosynthetic substrates in many tissues, including the developing brain, lactating mammary gland, and liver (7-10) (**Fig. 1.1C**). Furthermore, hepatic ketogenesis interfaces with fatty acid β -oxidation, the tricarboxylic acid (TCA) cycle, and gluconeogenesis (**Fig. 1.2**). Derangements of ketone body metabolism occur in numerous disease states, including types 1 and 2 diabetes and heart failure, and ketone body metabolism changes over the course of normal aging (11-19). In this review we examine (i) the biochemistry of ketone body metabolism and its regulation (**Section II**), (ii) the roles of ketone body metabolism in normal and pathological states of the myocardium (**Sections III-IV**), (iii) the concept, and prospective cardiovascular disease relevance of extrahepatic ketone body production, which may channel ketone bodies into lipogenesis (**Section 1.V; Fig. 1.3**), and (iv) intersections among ketone body metabolism, cellular signaling pathways, and the gut microbiota (**Sections VI-VII**). Analysis of the known and prospective cardiovascular disease targets of ketone body metabolism is also provided (**Section VIII**). The effects of ketone body metabolism are summarized in **Table 1.1**.

II. Ketone body metabolism

The fundamental biochemical and physiological roles of ketone body metabolism have been extensively studied and reviewed (4,5,20). In this Section, we provide a brief overview of ketone body metabolism, and then focus on recent studies revealing novel aspects of the pathway's regulatory mechanisms.

A. Hepatic ketogenesis. In liver, 3-hydroxymethylglutaryl-CoA synthase 2 (encoded by the nuclear gene *Hmgcs2*) catalyzes a fate committing ketogenic reaction: condensation of β -oxidation-derived acetoacetyl-CoA (AcAc-CoA) and acetyl-CoA to generate HMG-CoA, which is cleaved by HMG-CoA lyase (HMGCL) to generate acetoacetate (AcAc). AcAc is reduced to D- β -hydroxybutyrate (D- β OHB), in an NAD^+ /NADH-coupled near equilibrium reaction catalyzed by phosphatidylcholine-dependent

mitochondrial D- β OHB dehydrogenase (BDH1), in which the K_{eq} favors D- β OHB formation (21,22) (**Fig. 1.1A**). Because the BDH1 catalyzed reduction/oxidation of AcAc and D- β OHB is common to the final reaction of ketogenesis and the first reaction of ketone body oxidation (**Figs. 1.1A-B**) (22,23), BDH1 modulates mitochondrial redox potential in liver and extrahepatic tissues, wherein the AcAc/ β OHB ratio is directly proportional to the mitochondrial $NAD^+/NADH$ ratio (24). A cytoplasmic D- β OHB-dehydrogenase (BDH2) with only 20% sequence identity to BDH1 has been identified (25). More work is needed to elucidate the mechanisms by which the BDH enzymes are regulated and function *in vivo*. AcAc is also non-enzymatically decarboxylated to acetone. Ketone bodies are released by the liver via solute carrier 16A (SLC16A) family members 1, 6, and 7 and circulate to extrahepatic tissues where they primarily undergo terminal oxidation (26,27).

A.1. Ketogenic substrates. Ketogenesis occurs predominantly in liver mitochondria at rates proportional to β -oxidation when dietary carbohydrates are limiting, and is highly integrated with the TCA cycle and gluconeogenesis (**Fig. 1.2**). Biochemical studies by pioneering investigators including Krebs, McGarry, and Foster demonstrated that hepatic metabolic fluxes of acetyl-CoA govern rates of ketogenesis [reviewed in (5,20)]. Fatty acid β -oxidation-derived AcAc-CoA and acetyl-CoA are the primary ketogenic substrates. Glucose metabolism accounts for less than 1% of circulating ketone bodies in states of low carbohydrate intake because pyruvate enters the hepatic TCA cycle predominantly via carboxylation to oxaloacetate or malate, rather than decarboxylation (to acetyl-CoA) (28-30). In addition, amino acid catabolism accounts for a small percentage of circulating ketone bodies, with leucine catabolism generating up to 4% of circulating ketone bodies in the post-absorptive state (31).

A.2. Regulation of ketogenic mediators. Key regulatory steps in ketogenesis include lipolysis of fatty acids from triacylglycerols, transport to and across the hepatocyte plasma membrane, transport into mitochondria via allosterically-regulated carnitine palmitoyltransferase 1 (CPT1), the β -oxidation spiral, and the hormonal regulators of these processes, predominantly glucagon and insulin. These classical mechanisms have been reviewed (5,32-34). Hepatic ketogenesis is a spillover pathway for β -oxidation-derived acetyl-CoA generated in excess of the liver's energetic needs (**Fig. 1.2**). Acetyl-CoA subsumes

several roles integral to hepatic intermediary metabolism beyond ATP generation via terminal oxidation. Acetyl-CoA allosterically activates (i) pyruvate carboxylase, thereby activating a metabolic control mechanism that augments anaplerotic entry of metabolites into the TCA cycle (35,36) and (ii) pyruvate dehydrogenase kinase, which phosphorylates and inhibits pyruvate dehydrogenase (37), thereby further enhancing flow of pyruvate into the TCA cycle via anaplerosis. Furthermore, cytoplasmic acetyl-CoA, whose pool is augmented by transport mechanisms that convert mitochondrial acetyl-CoA to transportable metabolites (see **Section V.B.**), inhibits fatty acid oxidation: acetyl-CoA carboxylase catalyzes the conversion of acetyl-CoA to malonyl-CoA, the lipogenic substrate and an allosteric inhibitor of mitochondrial CPT1, decreasing delivery of acyl chains to the mitochondrial matrix for terminal oxidation [reviewed in (5,38)]. Thus, the mitochondrial acetyl-CoA pool regulates and is regulated by the spillover pathway of ketogenesis, which orchestrates key aspects of hepatic intermediary metabolism. The studies described below focus on recently discovered mechanisms of ketogenic regulation.

Following procession through β -oxidation, ketogenic fate is determined by HMGCS2, whose regulatory mechanisms are schematized in **Fig. 1.4A**. Because of its ability to support high rates of hepatic ketogenesis, divergence of this mitochondrial HMGCS ~500 Mya from the gene encoding cytoplasmic HMGCS1 may have supported the emergence of increasing brain-weight/body-weight ratios during vertebrate evolution (39-41). The *Hmgcs2* gene and encoded protein are regulatory targets during the transition to extrauterine life, starvation, diabetes, during adherence to low carbohydrate/high fat (ketogenic) diets, and in aging (2,11,20,42-44). The *Hmgcs2* gene is dynamically regulated at the transcriptional level. Methylation of 5' regulatory sequences within the *Hmgcs2* gene silences its transcription in fetal liver, and in non-ketogenic adult tissues (45). At birth, hepatic *Hmgcs2* becomes hypomethylated and thereby becomes responsive to circulating hormones (34,46). Insulin suppresses *Hmgcs2* transcription, prospectively via phosphorylation-induced sequestration of FOXA2 from the nucleus, while glucagon induces it via activation of the cAMP regulatory element binding protein (44-49). In addition, free fatty acids induce *Hmgcs2* in a peroxisome proliferator activated receptor (PPAR)- α dependent manner (50,51). In fact, *Hmgcs2* is induced *in vivo* in the post-absorptive state and by

adherence to ketogenic diet through the activities of the fibroblast growth factor (FGF)-21/PPAR α axis (50,52,53). HMGCS2 may also reciprocally induce *Fgf21* gene expression (54). In addition, following cysteine palmitoylation, HMGCS2 translocates to the nucleus, physically interacts with PPAR α , and potentiates its own gene transcription (55,56). Inhibition of mTORC1 signaling has been identified as a primary mechanism responsible for de-repression of PPAR α -mediated transcriptional changes responsible for the induction of ketogenesis in the post-absorptive state (11,57). Hepatic *Bdh1* also exhibits a developmental expression pattern, increasing in brain and liver from birth to weaning, and is also induced by ketogenic diet in an FGF21 dependent-manner (53,58).

In addition to cysteine palmitoylation, HMGCS2 enzymatic activity is responsive to forms of post-translational modification. Mitochondrial activity of HMGCS2 is inhibited through allosteric regulation by succinyl-CoA (44,59,60) and through succinylation of lysine residues (44,46,47,61). While the regulatory mechanisms remain to be determined, desuccinylation is stimulated by glucagon (47), and recent discoveries that identify sirtuin (silent mating type information regulation 2 homolog) 5 (SIRT5) as a mitochondrial NAD⁺ dependent lysine desuccinylase prompt the hypothesis that SIRT5 function dynamically regulates mitochondrial HMGCS2 activity (62,63). HMGCS2 activity is also induced in the post-absorptive state by SIRT3, a mitochondrial NAD⁺ dependent deacetylase (64). Because SIRT3 regulates multiple enzymatic mediators of β -oxidation, sirtuins may be multi-tiered regulators of ketogenesis. Genetically obese mice were recently shown to exhibit increased hepatic HMGCS2 serine phosphorylation, a post-translational modification that enhances HMGCS2 activity *in vitro* and was correlated with elevated serum D- β OH levels *in vivo* (65).

Despite all of the described transcriptional and post-translational mechanisms that regulate HMGCS2, it is unknown if regulation of *Hmgcs2* gene expression correlates with changes in protein abundance, and if these changes in gene expression directly regulate ketogenesis. Importantly, it remains undetermined if HMGCS2 post-translational modification itself is a primary determinant of ketogenic flux. Nonetheless, HMGCS2 activity is required for the normal ketogenic response to states of diminished

carbohydrate intake, as its absence in humans yields hypoketotic hypoglycemia and fatty liver in states of diminished carbohydrate intake (66-68).

B. Ketone body utilization. Ketone body catabolism generates acetyl-CoA that can be terminally oxidized within the TCA cycle or utilized for sterol biosynthesis and de novo lipogenesis (DNL). Ketone bodies are an alternative and glucose-sparing fuel source, avidly oxidized in heart and muscle. Moreover, neurons do not effectively generate high-energy phosphates from fatty acids, and consequently oxidize ketone bodies during starvation and in the neonatal period [presented and reviewed in (2,4,69-71)]. Below we review the biochemical activities of the enzymes of ketone body utilization, focusing on recent studies that reveal the precise physiological roles of ketone body utilization *in vivo*.

B.1. Ketone body oxidation. Ketone bodies are extracted from the circulation by peripheral tissues via SLC16A1 and -7 (26). Within mitochondria of peripheral organs, BDH1 catalyzes the oxidation of D- β OHB to AcAc. AcAc is activated to AcAc-CoA by succinyl-CoA:3-oxoacid-CoA transferase (SCOT, CoA transferase), the only mammalian CoA transferase, which catalyzes a near equilibrium reaction that exchanges coenzyme A between succinate and AcAc (**Fig. 1.1B**). The free energy released by hydrolysis of AcAc-CoA is greater than that of succinyl-CoA (72,73). Therefore, the equilibrium of this reaction thermodynamically favors the formation of AcAc, [(74), also see **Section V**]. Thus, ketone body oxidative flux occurs by mass action: an abundant supply of AcAc and rapid utilization of acetyl-CoA through citrate synthase favors AcAc-CoA formation and contribution of ketone bodies to the TCA cycle. A reversible AcAc-CoA thiolase reaction yields two molecules of acetyl-CoA, which enter the TCA cycle (**Fig. 1.1B**) (4,74-76). CoA transferase is necessary, but not sufficient, for ketone body oxidation in mice and humans [see below and (77-81)].

Ketone body oxidation becomes a primary contributor to bioenergetic homeostasis during ketotic states, during which ketone bodies are oxidized in proportion to their delivery in heart, brain, and muscle until saturation of either uptake or oxidation occurs (2,43,71,82-84). Relative to ketogenesis, little is known about the regulation of mediators of ketone body oxidation. Perhaps paradoxically, expression of the gene encoding CoA transferase (*Oxct1*), CoA transferase protein abundance, and CoA transferase

enzymatic activity are all diminished in rodent heart and muscle during states of sustained ketosis (51,85-89). In pathological contexts such as diabetic ketoacidosis, diminution of CoA transferase abundance and activity limit ketone body disposal, while insulin deficiency (or severe impairment of its signaling) stimulates peripheral fatty acid mobilization and unabated hepatic ketogenesis. This mismatch of ketogenesis and peripheral disposal predisposes to the extreme hyperketonemia that can emerge in diabetic ketoacidosis.

In ketotic states, expression of *Oxct1* may be negatively regulated through mechanisms involving PPARs that are abrogated by insulin [(51); **Fig. 1.4B**]. Myocardial *Oxct1* expression may also be down-regulated under select non-ketotic metabolic states, as transgenic mice overexpressing the non-insulin-dependent glucose transporter (GLUT1/SLC2A1) in cardiomyocytes exhibit decreased *Oxct1* expression and diminished ketone body oxidation (90). Future experiments are needed to determine whether regulation of *Oxct1* expression occurs through transcriptional or post-transcriptional mechanisms (or both), which may help support insight into whether these events are adaptive or maladaptive. Post-translational modification of CoA transferase occurs through non-enzymatic tyrosine nitration, which has been observed in hearts of endotoxin-treated rats, hearts of streptozotocin-treated rats, and hearts of *db/db* mice (86,91,92). Tyrosine nitration correlates with impairments of enzymatic activity (**Fig. 1.4B**). Conversely, nitration of CoA transferase on tryptophan residues in aged rat hearts and kidneys appears to augment enzymatic activity (93,94). Molecular mechanisms of residue-specific nitration or de-nitration designed to modulate CoA transferase activity may exist and require elucidation, as do additional prospective post-translational modifications of CoA transferase.

Although touted as energy efficient substrates (95,96), an energetic requirement for ketone body oxidation at the cellular level has never been demonstrated, even in states of diminished carbohydrate supply. Nonetheless, human inborn errors of ketone body oxidation do result in clinically significant disease, as approximately 30 CoA transferase-deficient patients have been identified. These patients present early in life with severe ketoacidosis that results in lethargy, vomiting, and coma, requiring aggressive intravenous hydration, bicarbonate, and glucose and insulin therapy (79-81,97-101). Some

CoA transferase deficient patients also present with hypoglycemia, and CoA transferase deficiency may contribute to a subset of idiopathic ketotic hypoglycemia cases (79,102-106). If maintained on carbohydrate-rich diets that are mildly reduced in protein content, CoA transferase-deficient patients seem to thrive, albeit with persistent hyperketonemia. To mechanistically dissect the homeostatic roles of ketolysis, germline CoA transferase-knockout (SCOT-KO) mice were developed (78). These mice cannot oxidize ketone bodies, and invariably die within 48h of extrauterine life due to hyperketonemic hypoglycemia that is marked by hypolactatemia and an increase in the serum AcAc/D- β OHB ratio. The mechanisms and consequences of this unusually high ratio remain to be determined. Despite the critical nature of CoA transferase and ketone body disposal at an organismal level, recently published studies demonstrated that mice with selective loss of CoA transferase in either cardiomyocytes, neurons, or skeletal myocytes – the three greatest consumers of ketone bodies (4,107) – survive the neonatal period and starvation as adults, with only subtle metabolic abnormalities in these two states (108). Future studies using these and related models will be important to determine the metabolic and bioenergetic adaptations to CoA transferase deficiency and the inability to derive energy from ketone bodies.

B.2. Non-oxidative metabolism of ketone bodies. Ketone bodies also contribute to lipogenesis and sterol biosynthesis in developing brain, lactating mammary gland, and liver following enzymatic and endergonic activation of AcAc to AcAc-CoA by cytoplasmic acetoacetyl-CoA synthetase (AACS) [(7-10) and **Fig. 1.1C**]. While AcAc-CoA serves as a direct substrate for cytoplasmic HMGCS1, which catalyzes the fate-committing step of sterol biosynthesis, channeling of AcAc-CoA into DNL requires a thiolytic cleavage reaction (*i.e.*, cytoplasmic ketolysis) to yield acetyl-CoA, which becomes the lipogenic substrate malonyl-CoA upon carboxylation (8,109-112). Recent studies support the physiological importance of ketone bodies as anabolic substrates. Genetic knockdown of AACS in mouse liver lowered total blood cholesterol *in vivo*, and *in vitro* AACS knockdown impaired differentiation of primary mouse embryonic neurons, and inhibited adipocyte differentiation of 3T3-L1 cells [(113-115), also see **Section V**]. While lipogenic fates of ketone bodies may support essential biological functions, these pathways do not serve as a primary pathway for disposal of ketone bodies when hepatic ketogenesis is stimulated, because CoA

transferase deficiency in mice and humans, which abrogates terminal ketone body oxidation, causes severe hyperketonemia (77-81). Nonetheless, future studies in models of AACCS disruption are merited to firmly establish the physiological roles for non-oxidative fates of ketone bodies.

III. Bioenergetics of Myocardial Ketone Body Oxidation

In the normal adult heart, mitochondrial oxidative phosphorylation provides more than 95% of the ATP generated for its mechanical, electrical, and homeostatic activities. Fatty acid oxidation provides up to 70% of the ATP produced by the heart, with metabolism of glucose, lactate, amino acids, and ketone bodies supplying the balance [reviewed in (116)]. Cardiomyocytes demonstrate considerable metabolic flexibility during dynamic alterations of nutrient state and hemodynamic stress – conferring an important adaptive property to the myocardium (117-120). Myocardium is the highest ketone body consumer per unit mass (2,43,76). Cardiomyocytes oxidize ketone bodies in proportion to their delivery, at the expense of terminal fatty acid oxidation and glucose oxidation (90,117,121-126). Competition between oxidation of ketone bodies and fatty acids is independent of changes in myocardial malonyl-CoA concentrations (127).

Ketone body oxidation is more energetically efficient than terminal fatty acid oxidation. While terminal fatty acid oxidation yields the highest theoretical payoff of ATP per C₂ unit of all the myocardial substrates, the initial ATP investment required to activate long chain fatty acids for oxidation (i.e. to generate a fatty acyl-CoA thioester) and fatty acid-induced expression of uncoupling proteins may actually confer greater energetic density to ketone bodies (96). Furthermore, unlike terminal fatty acid oxidation all of the reducing equivalents generated by ketone body oxidation are delivered via NADH to complex I within the electron transport chain. Oxidation of β OHB also increases the redox span between complexes I and III, by keeping mitochondrial ubiquinone oxidized. This may increase the potential energy harvested from oxidation of ketone bodies (relative to fatty acids), thereby yielding more energy available for ATP synthesis per molecule of oxygen invested (P/O ratio), improving the energetic

efficiency of oxidizing ketone bodies over fatty acids (95,96,128). Because unrestrained mitochondrial fatty acid oxidation may augment the generation of reactive oxygen species (ROS) to levels that exceed scavenging mechanisms, competitive contribution of ketone bodies to the TCA cycle in cardiomyocytes may be adaptive under conditions in which the ability to switch between fatty acids and glucose becomes impaired (95,96,128). Moreover, ketone bodies diminish oxidative stress by scavenging free radicals and by maintaining ubiquinone in the oxidized state (**Fig. 1.5**) (96,129,130).

CoA transferase dependent activation of AcAc to AcAc-CoA sequesters free CoA-SH (131,132). Rodent hearts perfused *ex vivo* with AcAc alone exhibit depleted free CoA-SH pools and require addition of either CoA precursors or anaplerotic substrates to maintain anaplerotic and TCA cycle flux, and to prevent functional decline in cardiac performance (132-134). Although ketone bodies do not serve as the sole myocardial fuel under any *in vivo* circumstance, these studies underscore the important role of cardiac anaplerosis in maintaining myocardial bioenergetic homeostasis and cardiac function, a topic that was recently reviewed by Des Rosiers and colleagues (135).

Until recently, it was not known how the myocardium adapts to chronic ketosis – an important question relevant to the role that ketone body metabolism may serve in myopathic hearts. Mouse models of physiologic ketotic nutritional states (24h of fasting or four weeks of a ketogenic diet) demonstrate that the myocardium engages a transcriptional program including, as described above, transcriptional suppression of *Oxct1* and diminution of CoA transferase protein (51). Consistent with diminution of CoA transferase, nuclear magnetic resonance (NMR) profiling demonstrated that maintenance on a ketogenic diet decreased myocardial ¹³C-enrichment of glutamate from ¹³C-labeled ketone bodies that were delivered *in vivo* or *ex vivo* by 25%, indicating diminished terminal oxidation of ketone bodies in the TCA cycle (51,136). Furthermore, attenuation of ketone body oxidation correlated with failure of ketone bodies to inhibit contribution of fatty acids to the TCA cycle. Together, these results indicate that ketotic nutrient environments induce mechanisms that modulate myocardial utilization of ketone bodies. Because hemodynamic parameters were preserved in hearts of mice fed a ketogenic diet, these results suggest that modulation of ketone body metabolism may be adaptive in the setting of sustained ketosis.

IV. Ketone Bodies and Myocardial Disease

Numerous experimental approaches have established that cardiomyopathy is associated with changes in cardiac substrate and energy metabolism, and that altered energy metabolism can cause cardiomyopathy [reviewed in (116,135,137-144)]. Both metabolic and bioenergetic lines of evidence indicate that ketone body metabolism could play a significant role in the myopathic heart. Hepatic ketogenesis is stimulated and ketone bodies circulate at increased concentrations in the setting of heart failure – in a relationship directly proportional to filling pressure (13-17). As previously noted, the myocardium oxidizes ketone bodies at the expense of fatty acid oxidation (117,124,127,145), and thus reductions of myocardial fatty acid oxidation that occur during the development of advanced cardiomyopathy may not be coupled to reductions of ketone body oxidation (116,141,144). A study in humans with advanced heart failure indicated that myocardial extraction of delivered ketone bodies is maintained in the failing heart, but not skeletal muscle (146). Similarly, the contribution of ketone bodies to cardiac energy metabolism may be elevated in patients with dilated and hypertrophic cardiomyopathies (147). Therefore, while the data on ketone body metabolism in heart failure are currently very limited, diminished myocardial ketone body oxidation could promote pathological outcomes. Of the identified CoA transferase-deficient patients, two were reported to present with dilated cardiomyopathy (98,148,149). Future studies in humans that specifically measure CoA transferase function and ketone body oxidation in cardiomyopathic states, complemented by mechanistic studies using tissue-selective genetic rodent models, will be required to definitively determine how myocardial ketone body metabolism changes in pathophysiological states, and the contexts in which myocardial ketone body utilization may be adaptive or maladaptive.

Studies in rodents demonstrate a possible role for ketone body metabolism in myocardial adaptation to ischemia/reperfusion injury. In two studies using *ex vivo* perfusion approaches in rat hearts, maintenance on low carbohydrate diets prior to ischemia/reperfusion protocols gave conflicting results with regard to infarct size and hemodynamic performance (150,151). Prospective cardioprotective effects of a low carbohydrate diet may be attributable to an increase in the number of myocardial mitochondria or transcriptional upregulation of key mediators of oxidative phosphorylation (150,152). Cardioprotective

effects have been observed using *in vivo* ischemia/reperfusion approaches in rats subjected to starvation-induced ketosis, initiated through prolonged fasting, and also via intravenous injection of DL- β OHB immediately prior to ischemic injury, which conferred a significant decrease in both infarct size and myocardial cell death (153,154). These studies should stimulate further investigation using genetic and pharmacological approaches to determine the validity and mechanisms of these preliminary studies, and whether the observations actually relate to myocardial metabolism of ketone bodies.

Relationships among ketone body metabolism, membrane excitability, and arrhythmogenesis have also been reported. Metabolomic and proteomic analysis of atrial tissue harvested during cardiac surgeries demonstrated an increase in both myocardial β OHB content and CoA transferase abundance in patients with atrial fibrillation, compared to control patients (155). Although myocardial ketone body utilization in the setting of atrial fibrillation has not been investigated, mechanisms that directly link ketone bodies to membrane excitability and arrhythmogenesis have been preliminarily assessed. β OHB blocks the transient outward K^+ current (I_{to}) in murine ventricular myocytes, causing action potential prolongation (156). However, only L- β OHB inhibits the I_{to} current. L- β OHB is measurable in myocardial extracts, but does not circulate and likely results from hydrolysis of the β -oxidation intermediate L- β OHB-CoA (157-160). Hepatic ketogenesis only produces D- β OHB, which is the only form that is a BDH substrate, and thus, a substrate for oxidation. SLC16A transporters in rat myocytes demonstrate no stereoselectivity for β OHB (161). Prospective pathophysiological significance of the L- β OHB stereoisomer requires investigation.

V. Reversibility of the CoA Transferase Reaction Extends Cardiovascular Disease Targets of Ketone Body Metabolism

Each enzyme involved in ketone body oxidation catalyzes a reversible reaction. Thus, each tissue that oxidizes ketone bodies has the enzymatic potential to synthesize them.

A. Pseudoketogenesis. Brunengraber and colleagues quantified exchange between isotopically labeled fatty acids and unlabeled ketone bodies in rat hearts perfused *ex vivo* (162). Des Rosiers *et al.*

subsequently quantified dilution of labeled ketone bodies in hepatectomized dogs *in vivo* (163). This isotopic dilution by extrahepatic tissues was termed pseudoketogenesis, which occurs because CoA transferase and AcAc-CoA thiolase catalyze reversible reactions. While a physiological role for pseudoketogenesis has yet to be established, the process leads to overestimation of ketone body turnover in whole-body tracer dilution studies, because its rate is up to one-third of the rate of ketone body uptake (162).

B. CoA transferase-dependent ketogenesis in extrahepatic tissues. CoA transferase is expressed in all mammalian cells that harbor mitochondria, except hepatocytes, but not all cell types oxidize ketone bodies, suggesting that CoA transferase may mediate non-oxidative metabolic functions in certain tissues or physiological states (74,107,164,165). Because AcAc exits mitochondria via monocarboxylate transporters, ketogenic flux through thiolase and CoA transferase may permit carbon efflux from mitochondria independent of citrate synthase, thus generating a monocarboxylate transport system that complements both citrate-dependent tricarboxylate transport (**Fig. 1.3**) and acetylcarnitine transport (166). Such a role for CoA transferase reflects its dual evolutionary history as an enzyme of ketone body production and utilization (167,168). Ketogenic flux through mitochondrial thiolase and CoA transferase may be poised to regulate discrete cellular functions directly relevant to metabolic syndrome, diabetes, and atherosclerosis, because ketone bodies are substrates for cytoplasmic DNL and sterol biosynthesis [**Fig. 1.3** and (8,109-111)]. A series of studies have implicated ketogenic flux through CoA transferase as a putative mechanism through which ketone bodies act as insulin secretagogues in pancreatic β cells (169-172). The authors of these reports demonstrated that ketone bodies and ketone body precursors potentiate insulin release, possibly by contributing to formation of cytoplasmic short-chain acyl-CoAs (169,171,172), and that diminished CoA transferase expression correlated with impaired glucose stimulated insulin secretion in a rat insulinoma cell line (170). Future experiments will be required to determine the biological roles of ketogenic flux in cell types not classically associated with lipogenesis, including β cells of the pancreas and cardiomyocytes.

An additional non-oxidative role for CoA transferase may emerge in macrophages, which exhibit robust CoA transferase enzymatic activity, but do not terminally oxidize ketone bodies (173,174). Recent discoveries have highlighted the importance of macrophage metabolism in cardiovascular disease [reviewed in (175)]. As macrophage-specific deficiency of the enzyme required for DNL, fatty acid synthase (FAS), ameliorates diet-induced atherosclerosis in mice (176), it is intriguing to consider that anabolic procession of metabolites through mitochondrial thiolase and CoA transferase acts upstream of FAS to contribute to macrophage DNL flux. CoA transferase is also abundantly expressed in adipose tissue, in which the enzyme that catalyzes the reaction downstream from CoA transferase, AACS (**Fig. 1.3**), is dynamically regulated by PPAR γ , a key mediator of adipogenesis and adipocyte function (113,177,178). Adipocyte-specific FAS deficiency increases baseline energy expenditure and improves diet-induced obesity in mice (179). Because ketone bodies have been proposed as quantitatively significant DNL substrates in multiple cell types (8,180), these recent findings suggest that use of genetic models is warranted to draw mechanistic and cardiovascular disease-relevant links among CoA transferase, lipogenesis from ketone bodies, and metabolic and vascular diseases.

VI. Signaling Roles for Ketone Bodies

Because serum ketone body concentrations vary over a large dynamic range, they may act as physiologically relevant signals for cell-surface and intracellular receptors. In fact, D- β OHB is an endogenous ligand for a niacin receptor, G protein-coupled receptor 109A (GPR109A), with an EC₅₀ of 770 nM (181). Like niacin, D- β OHB can inhibit adipose tissue lipolysis, which has been proposed to create a negative feedback loop in which ketosis curtails ketogenesis by limiting delivery of non-esterified fatty acids to the liver (182,183). GPR109A signaling also promotes reverse cholesterol transport in macrophages (184). It is unknown if D- β OHB plays a role in this cascade.

β OHB signaling may also influence cardiovascular biology through additional G protein-Coupled Receptors (GPCRs). A recent study in mice revealed that β OHB decreases sympathetic outflow and reduces heart rate and total energy expenditure by antagonizing (through an unknown mechanism)

GPR41, a $G_{i/o}$ -coupled receptor for short chain fatty acids (SCFAs, *e.g.*, acetate, propionate, and butyrate) that is abundantly expressed in sympathetic ganglia (185). Thus, evidence implicating ketone bodies as signaling molecules further supports roles for ketone bodies that transcend energy metabolism, indicating that additional experimentation is required to elucidate the receptors and mechanisms through which ketone bodies serve as extracellular signals.

Recently published findings also demonstrated that D- β OHB inhibits Class I histone deacetylases (HDACs), resulting in increased histone acetylation, and thus, increased expression of genes encoding mediators of resistance to oxidative stress (186). The molecular effects of D- β OHB were observed at high IC_{50} concentrations (2.4 – 5.3 mM, depending on the HDAC isoform), and were recapitulated by caloric restriction, fasting, or AcAc. To determine if these effects were dependent on D- β OHB metabolism, small interfering RNAs (siRNAs) against BDH1/2 were transfected into cells, which were then treated with D- β OHB. The authors observed that, up to 3 mM D- β OHB, the effects on histone acetylation were preserved, leading to the conclusion that most of the influence of D- β OHB on HDAC function was independent of D- β OHB metabolism. However, residual BDH persisted in the siRNA-transfected cells, and the control experiment confirming diminished D- β OHB oxidation in BDH ‘knockdown’ cells was not performed. Thus, it remains plausible that oxidation of D- β OHB to AcAc by BDH1 could alter mitochondrial redox potential, and that CoA transferase-dependent contribution of AcAc to the TCA cycle for terminal oxidation could alter cellular energy metabolism (see **Section II.B.1** and **Fig. 1.5**), each of which may contribute to the observed effects on histone acetylation. Nonetheless, these observations reveal exciting roles for ketone body metabolism in a multitude of disease states, which will benefit from the development and application of both pharmacological and genetic tools.

VII. Ketone Body Metabolism, the Microbiota, and Cardiovascular Biology and Disease

A therapeutically tractable interface between ketone body metabolism and cardiovascular disease is offered through the dynamic community of microorganisms living on our cutaneous and mucosal surfaces – the microbiota. This ecosystem of ~100 trillion cells – 10 times the total number of our own cells –

comprises a ~1 kg ‘organ’ that harbors a massive aggregate of genomes (the microbiome) encoding millions of genes – 100 times that of the human genome – that influence the human metabolome and coordinate immune function [recently reviewed in (187-195)]. The data supporting causal links between the microbiota and host cardiovascular disease, in both rodent models and humans, are compelling. Gut microbial ecology undergoes marked transformation in obese and type 2 diabetic humans and rodents, and the dynamic energy-harvesting capacity of the gut microbial community plays a significant contributing role to energy homeostasis in the host (196-209). Acting in synergy, the host’s genome and microbiome coordinate ‘supraorganismal’ metabolic processes, creating a suite of co-metabolites that influence a panoply of pathophysiological processes including nonalcoholic fatty liver disease (NAFLD), hypertension, insulin resistance, and atherosclerosis (210-213). Furthermore, the ability of indigenous microbial communities to coordinate the functions of the host’s immune system is likely a key influence over the development of cardiovascular disease [reviewed in (189)], including the development of type 1 diabetes (214). Together, comparative genomics, metabolomics, and gnotobiotic studies (Greek roots: *gnosis*, knowledge; *bios*, life; a technology that allows cultivation of experimental animal models in the presence of defined microbial communities) may usher an era that ultimately allows caregivers to administer individualized forms of therapy that configure the microbiota using probiotics and prebiotics to ameliorate cardiovascular disease.

Studies of gnotobiotic animals have revealed intriguing relationships among the microbiota, ketone bodies, and cardiovascular biology. Normalized to tibial length or body weight, hearts of germ free mice, which are born and raised in sterile gnotobiotic isolators, are ~15% smaller than those of normally-colonized mice, but myocardial mass increases within two weeks of microbial colonization (126). *In vivo* and *ex vivo* functional parameters of hearts of germ free mice are normal, but myocardial glucose oxidation rates are higher. A systematic assessment of substrate delivery and metabolism in germ free mice revealed that while circulating ketone body concentrations were not significantly different under fed conditions, ketosis was blunted during nutrient deprivation in germ free mice, due to diminished hepatic ketogenesis (126). While reduced adiposity of germ free mice (205) is a likely contributor to blunted

ketogenesis during fasting, hepatic ketogenic machinery, including expression of *Hmgcs2*, was curtailed in fasting germ free mice. The reduction in cardiac size and alterations of systemic and myocardial metabolism were abrogated when germ free mice were maintained on a ketogenic diet (126). It is also intriguing to consider the aforementioned cross-talk between SCFAs and ketone bodies [(185); see **Section VI**]. SCFAs are produced through the fermentative actions of glycan-digesting enzymes uniquely-encoded by the microbiome, contributing to the host's energy harvest and to signaling through GPR41 (185,215). Thus, the microbiome may supervise an expansive and integrated network in which ketone bodies influence cardiac metabolism, size, and physiology. Future studies using genetically-modified gnotobiotic animals will permit further construction of the relationship between ketone metabolism and the microbiome in diseases of the heart and vasculature.

VIII. Diagnostic and Therapeutic Targets of Ketone Body Metabolism

The diversity of metabolic and signaling processes in which ketone body metabolism participates provides a range of diagnostic and therapeutic applications, only a subset of which is under active investigation.

A. Abnormalities of Ketone Body Oxidation. CoA transferase deficient humans typically present early in life with severe ketoacidosis that can result in vomiting, coma, and death if intravenous glucose and insulin therapy is not rapidly instituted (79,97,98). Neonatal mice with complete loss of terminal ketone body oxidation (SCOT-KO mice) invariably die within the first 48 hr of life in a manner that mimics human sudden infant death syndrome (SIDS) (78). Furthermore, a recent observational study that performed metabolic autopsies on 255 SIDS patients found that three exhibited underlying disorders of ketone body metabolism (216). Therefore, a small subset of cases that ultimately receive a diagnosis of SIDS may actually be attributable to latent abnormalities of CoA transferase function. However, statewide neonatal screening protocols in the United States do not currently detect newborns with isolated disorders of ketone body oxidation, who exhibit hyperketonemia, but generally normal organic acid and acylcarnitine profiles (99). Improved screening methods, measuring both AcAc and D- β OHB, may detect

patients with latent deficiency of ketone body oxidation, further reduce SIDS incidence, and predict metabolic complications which may manifest later in life.

B. Dietary Therapies: Ketogenic Diets, Ketone Esters, and Odd-Chain Fatty Acids. Ketogenic diets are actively used for weight loss and anticonvulsant therapy, and are intensively studied as potential adjunctive therapy for brain cancers and neurodegenerative diseases including Parkinson's and Alzheimer's diseases (217-221). Additionally, limited studies raise the possibility that humans with NAFLD could benefit from low carbohydrate diet therapy (222,223). An experimental ketogenic diet has been used to mitigate a mitochondrial cardiomyopathy in mice (152). The full scope of cardiovascular diseases responsive to nutritional and/or pharmacological manipulation of ketone body metabolism, and the associated metabolic mechanisms remain underexplored.

Ketogenic diets are often unpalatable, which leads to poor patient compliance. Additionally, such diets raise blood cholesterol and free fatty acids, and increase the risk of nephrolithiasis and cause constipation (224-226). Therefore, Veech and Clarke developed and tested ingestible ketone ester compounds, which can rapidly generate ketoses exceeding 5 mM in rats and humans (227-229), while sparing the adverse consequences of high fat diets. A small preliminary study indicates that oral ketone esters are safe in humans (227). Rodents fed these compounds acutely decrease food intake. Although these animals do not exhibit changes in body weight over an extended time period, they do become more insulin sensitive, possibly due to increased expression of uncoupling proteins in brain and brown adipose tissue (228,229). Further studies will evaluate the efficacy of these compounds in the mitigation and prevention of metabolic, myocardial, and neurological diseases in rodent and human subjects.

In the last decade, studies analyzing the beneficial roles of the anaplerotic five-carbon (C5)-ketone bodies and their precursor odd-chain fatty acids for the treatment of long chain fatty acid oxidation (LCFAO) disorders have emerged (230,231). Conventional management of LCFAO disorders consists of dietary therapy with the medium-chain fatty acid octanoate. Substitution of octanoate for the odd-chain fatty acid heptanoate (given as the triglyceride triheptanoin) further improves clinical outcomes, specifically by reducing the incidence of rhabdomyolysis and cardiomyopathy (230,231). While only

trace levels of C5 ketone bodies are normally found in human body fluids (232,233), ingestion of odd chain fatty acids promotes hepatic C5-ketogenesis: β -oxidation of odd chain fatty acids yields propionyl-CoA, an anaplerotic substrate, which, in the liver, can also be packaged into C5 ketone bodies (234). Oxidation of C5-ketone bodies in peripheral tissues occurs through CoA transferase (235), regenerating propionyl-CoA. However, as oxidation of heptanoate within myocytes locally generates anaplerotic propionyl-CoA, direct evidence linking C5-ketone body metabolism to improved clinical outcome in LCFAO disorders currently remains lacking. Thus, it may be useful to cross experimental models of tissue-specific CoA transferase deficiency to existing models of LCFAO defects (108,236) to establish the metabolic roles of C5-ketone body metabolism in myocyte oxidation. Future studies of the role of these three approaches: low carbohydrate ketogenic diets, ketone ester-containing diets, or anaplerotic odd-chain fatty acid-containing diets in cardiomyopathy remain to be systematically performed, but are warranted (135,237).

C. Modifying Ketone Body Enzymatic Pathways: Targeting HMGCS2 and CoA transferase. As both nutrients and hormonal factors affect ketogenic regulation, it is not surprising that ketone body metabolism is dynamically regulated in mouse models of diet-induced obesity and in humans with metabolic syndrome. Hepatic ketogenesis becomes suppressed at later stages of the evolution of hyperinsulinemic obesity (12,42,238-240). Because transgene mediated *Hmgcs2* overexpression within hepatocytes enhances ketogenesis and simultaneously diminishes circulating free fatty acid concentrations *in vivo* (241), regulation of HMGCS2 activity (**Section II.A.2**) becomes a prospective therapeutic target. Diversion of hepatic fatty acyl chains into ketone bodies could diminish carbon that would otherwise require terminal oxidation, storage, or packaging into lipoproteins for secretion, prospectively mitigating hepatic steatosis and insulin resistance.

Whole-body ketone body turnover is non-invasively quantifiable in humans, as is tissue-level oxidative flux of ketone bodies via positron emission tomography using ^{11}C -labeled ketone body tracers, which have been used for studies in brain, but not yet in other organs (242,243). Additionally, ketone body metabolism and the mitochondrial enzyme CoA transferase are amenable to a number of nutritional,

and perhaps ultimately, pharmacological therapies. Importantly, as described above, myocardial CoA transferase activity plays an important role in the regulation of substrate selection, mitochondrial ROS generation, and cardiac work and bioenergetic efficiency (**Fig. 1.5**). Therefore, analysis of animal models with sophisticated genetic manipulations of ketone body metabolism, coupled with pharmacological targeting strategies may provide rationale for a suite of translational and clinical studies that validate ketone body metabolism as a myocardial therapeutic target. Additionally, CoA transferase and AACS activities may ultimately serve as therapeutic targets in contexts in which the ketone body-lipogenic pathways play significant roles, particularly within adipocytes, hepatocytes, and macrophages.

IX. Conclusions

Ketone body metabolism maintains bioenergetic homeostasis when dietary carbohydrates are limiting. Defects in either the synthetic or oxidative arms of ketone body metabolism result in disease pathogenesis in humans, and ketone body oxidation is required for maintenance of glycemia and survival in neonatal mice. Ketone bodies regulate mitochondrial metabolism, energetics, and ROS production via their oxidation, and may therefore have significant signaling roles within cardiomyocytes. Ketogenic flux through CoA transferase channels ketone bodies to lipogenesis, which could regulate signaling processes in many cell types, including macrophages, adipocytes and pancreatic β cells, which express CoA transferase abundantly, but may have relatively diminished need to harvest energy from ketone bodies. Therefore, the metabolism of ketone bodies may influence numerous human disease states relevant to cardiovascular disease, including obesity, diabetes, atherosclerosis, and heart failure. Because both CoA transferase and HMGCS2 experience multi-tiered regulation, these enzymes may be tractable to pharmacological manipulation. Before these ends are achieved, the scope of viable therapeutic targets of ketone body metabolism must first be developed. Integrative experiments in both animal models and humans that exploit the convergence of sophisticated genetic approaches, quantitative substrate fate-mapping ('fluxomics'), metabolomic profiling, physiological studies, and quantification of mitochondrial

function are needed to elucidate the mechanisms through which ketone body metabolism influences cardiovascular pathophysiological processes.

Figure Legends

Fig. 1.1. Ketone body metabolism pathways. (A) Ketogenesis within hepatic mitochondria is the primary source of circulating ketone bodies. (B) The primary metabolic fate of ketone bodies is terminal oxidation within mitochondria of extrahepatic tissues via CoA transferase (SCOT). Substrate competition with pyruvate-derived and fatty acyl-CoA-derived (the corkscrew arrows represent the activities of the β -oxidation spiral) acetyl-CoA are shown. (C) Cytoplasmic DNL and cholesterol synthesis are non-oxidative metabolic fates of ketone bodies. For simplicity of panel C, only acetoacetate (AcAc) is depicted, although β -hydroxybutyrate (β OHB) is also a substrate for lipogenesis after it has been oxidized to AcAc via mitochondrial β OHB dehydrogenase (BDH1). Additional abbreviations: AACS, acetoacetyl-CoA synthetase; ACC, acetyl-CoA carboxylase; AcAc-CoA, acetoacetyl-CoA; ATP, adenosine triphosphate; CoA-SH, free coenzyme A; FAS, fatty acid synthase; HMG-CoA, 3-hydroxymethylglutaryl-CoA; HMGCL, HMG-CoA lyase; HMGCS1, cytoplasmic HMG-CoA synthase; HMGCS2, mitochondrial HMG-CoA synthase; HMGCR, HMG-CoA reductase; NAD⁺(H), nicotinamide adenine dinucleotide oxidized (reduced); PDH, pyruvate dehydrogenase; SCOT, succinyl-CoA:3-oxoacid-CoA transferase; TCA, tricarboxylic acid; mThiolase, mitochondrial thiolase; cThiolase, cytoplasmic thiolase. Thiolase activity is encoded by at least six genes: *ACAA1*, *ACAA2* (encoding an enzyme known as T1 or CT), *ACAT1* (encoding T2), *ACAT2*, *HADHA*, and *HADHB*.

Fig. 1.2. Hepatic integration of ketogenesis. Integration of hepatic ketogenesis with hepatic TCA cycle, DNL, and pyruvate cycling/glucose metabolism. FAO, β -oxidation of fatty acids; GDH, glutamate dehydrogenase; OAA, oxaloacetate; ME, malic enzyme; PEPCK, phosphoenolpyruvate carboxykinase; PC, pyruvate carboxylase; PDH, pyruvate dehydrogenase; PK, pyruvate kinase; PEP, phosphoenol pyruvate; CS, citrate synthase; DNL, de novo lipogenesis.

Fig. 1.3. Ketogenic flux through CoA transferase. Because CoA transferase catalyzes an equilibrium reaction, select spatiotemporal metabolic conditions may favor channeling of mitochondrial acetyl-CoA to AcAc, generating a monocarboxylate shuttle that complements the citrate-dependent tricarboxylate shuttle and permits mitochondrial efflux of β -oxidation-derived acetyl-CoA independent of the TCA cycle. ACLY, ATP-citrate lyase.

Fig. 1.4. Regulatory mechanisms for HMGCS2 and CoA transferase (SCOT). (A) HMGCS2 and (B) SCOT both undergo transcriptional (red) and post-translational modes of regulation (blue). Some regulatory factors exhibit both classes of effects (violet). mTORC1, mammalian target of rapamycin complex 1; PPAR α , peroxisome proliferator activated receptor- α ; PTM; post-translational modification; SIRT3, sirtuin (silent mating type information regulation 2 homolog) 3.

Fig. 1.5. Diverse roles of CoA transferase in mitochondrial function. β OHB and AcAc cross the plasma membrane via SLC16A family members, and may employ these or other transporters to enter the mitochondrial matrix. Within the mitochondria, D- β OHB is oxidized to AcAc by the inner-membrane bound and phosphatidylcholine-dependent BDH1. CoA transferase (SCOT) catalyzes a near equilibrium reaction through which coenzyme A is exchanged between succinate and AcAc. Oxidation of ketone bodies occurs by mass action, and may diminish reactive oxygen species (ROS) formation, compared to oxidation of fatty acids. See text for details. ADP, adenosine diphosphate; ANT, adenine nucleotide transporter; CPT, carnitine palmitoyltransferase; Cyt C, cytochrome C; e^- , electron; H^+ , hydrogen ion; I, II, III, IV, complexes I-IV of the electron transport chain; IMM, inner mitochondrial membrane; OMM, outer mitochondrial membrane; Q, ubiquinone; ψ_m , electrochemical potential across the inner mitochondrial membrane; SLC, solute ligand carrier protein; Tr, translocase; UCPs, uncoupling proteins.

Figure 1.1

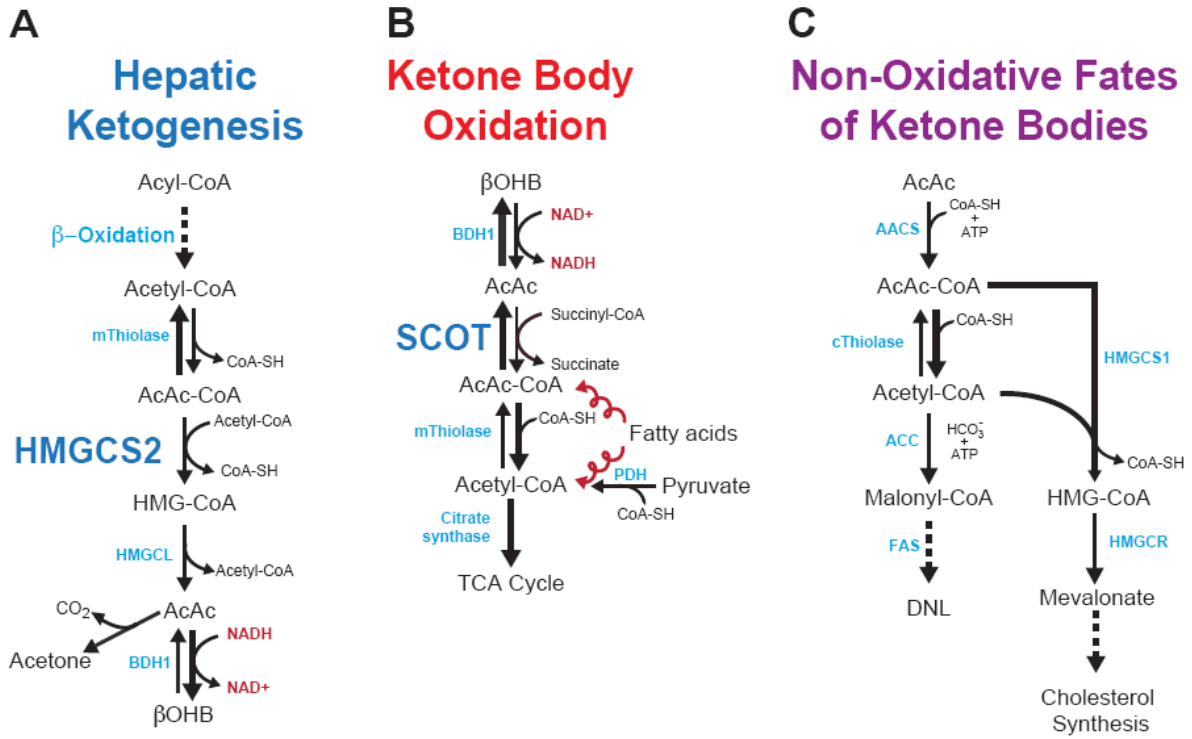


Figure 1.2

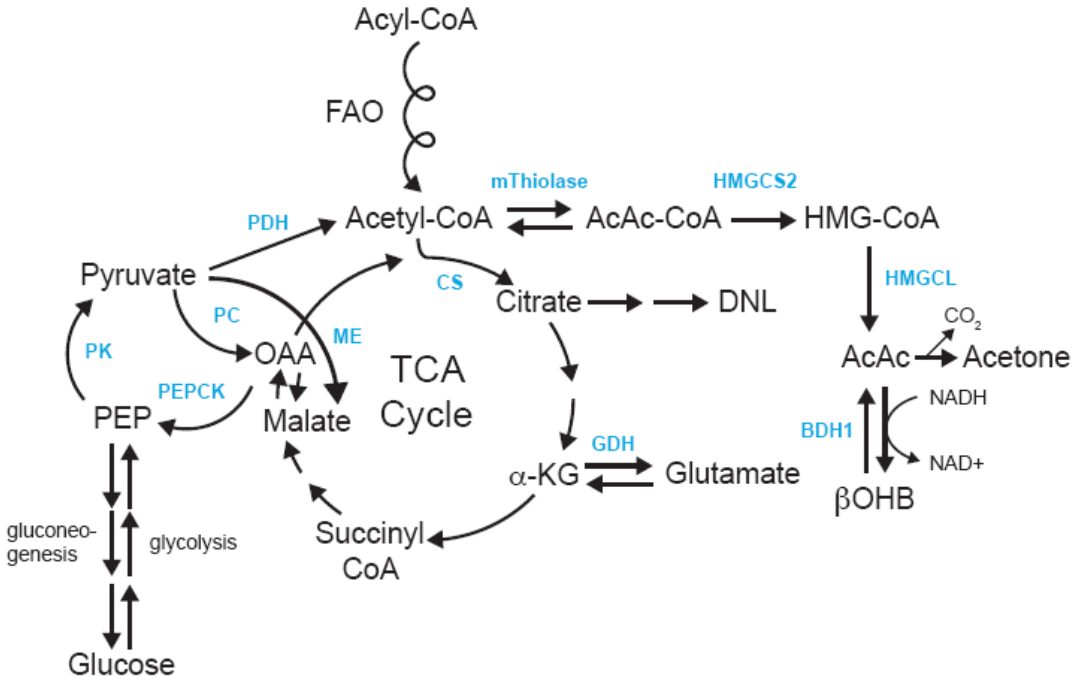


Figure 1.3

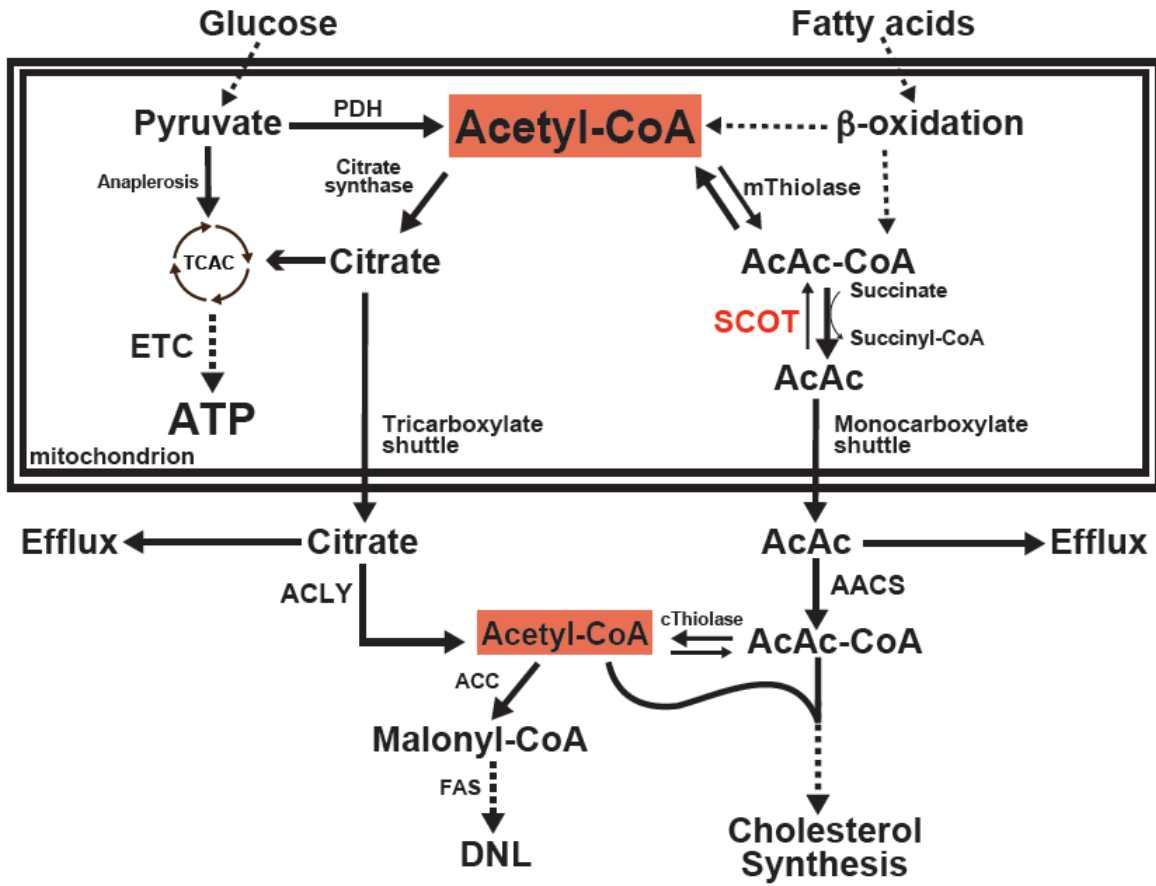


Figure 1.4

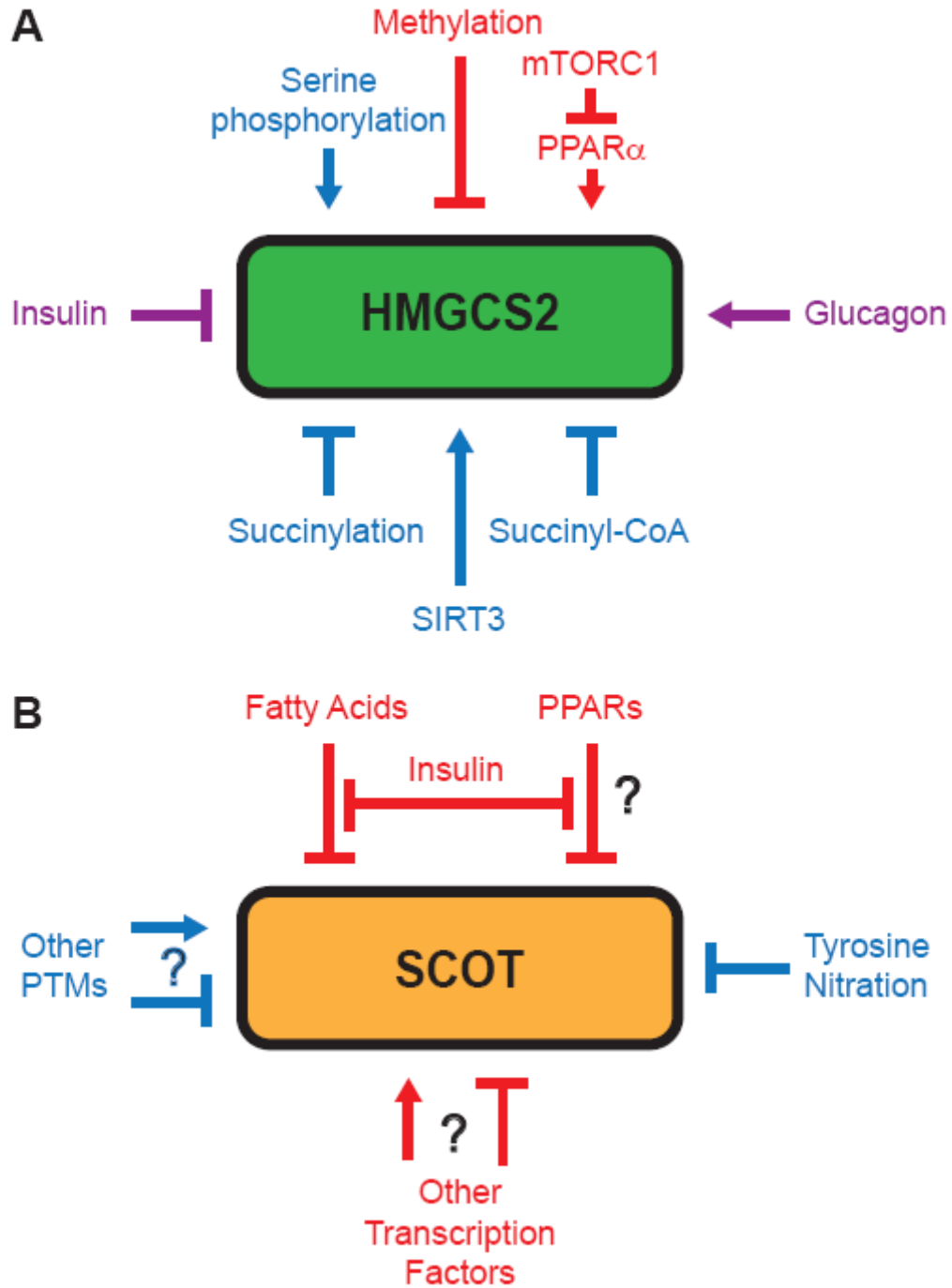


Figure 1.5

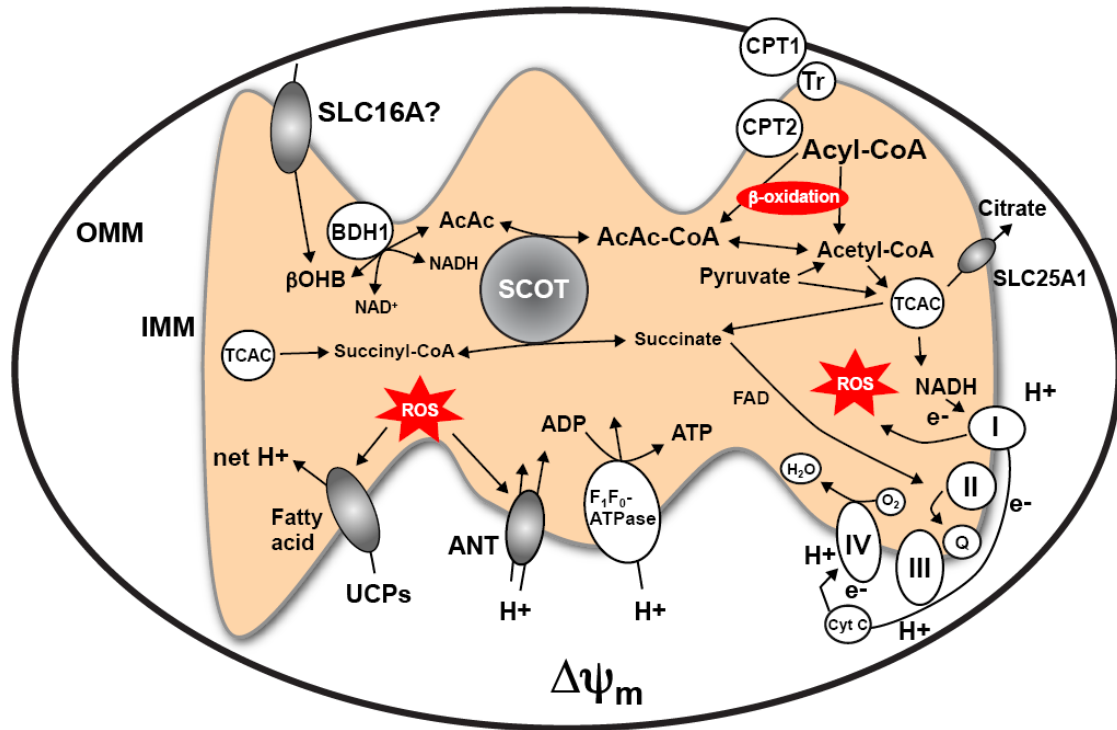


Table 1.1

Table 1. *Implications of ketone body metabolism*

-
-
- I. Metabolic and bioenergetic fates of ketone bodies
 - A. Hepatic ketogenesis: spillover pathway for β -oxidation-derived acetyl-CoA (Figs. 1 and 2)
 - B. Oxidation (Figs. 1 and 5)
 - 1. Improves P-to-O ratio (energetic efficiency)
 - 2. Diminishes ROS production and influences redox potential
 - 3. Substrate competition: favored over fatty acids
 - C. DNL and sterol synthesis (Figs. 1 and 3)
 - D. Ketogenic flux through CoA transferase (Fig. 3), generating a citrate synthase-independent DNL substrate
 - II. Signaling roles of ketone bodies
 - A. GPCR
 - 1. GPR109A
 - 2. GPR41 (?)
 - B. Membrane excitability
 - C. HDAC-dependent regulation of mediators of the response to oxidative stress: ligand versus metabolism-dependent effects
-

P-to-O ratio, ATP yielded per oxygen invested; ROS, reactive oxygen species; DNL, de novo lipogenesis; GPCR, G protein-coupled receptor; GPR109A, GPCR 109A; HDAC, histone deacetylase.

Chapter 2

Obligate role for ketone body oxidation in neonatal metabolic homeostasis

The work presented in this chapter has been adapted from:

Cotter, D. G., d'Avignon, D. A., Wentz, A. E., Weber, M. L., and Crawford, P. A. (2011) *J Biol Chem* 286(9), 6902-6910

Abstract

To compensate for the energetic deficit elicited by reduced carbohydrate intake, mammals convert energy stored in ketone bodies to high-energy phosphates. Ketone bodies provide fuel particularly to brain, heart, and skeletal muscle in states that include starvation, adherence to low carbohydrate diets, and the neonatal period. Here, we use novel *Oxct1*^{-/-} mice, which lack the ketolytic enzyme succinyl-CoA:3-oxo-acid CoA-transferase (SCOT), to demonstrate that ketone body oxidation is required for postnatal survival in mice. Although *Oxct1*^{-/-} mice exhibit normal prenatal development, all develop ketoacidosis, hypoglycemia, and reduced plasma lactate concentrations within the first 48 h of birth. *In vivo* oxidation of ¹³C-labeled β-hydroxybutyrate in neonatal *Oxct1*^{-/-} mice, measured using NMR, reveals intact oxidation to acetoacetate but no contribution of ketone bodies to the tricarboxylic acid cycle. Accumulation of acetoacetate yields a markedly reduced β-hydroxybutyrate:acetoacetate ratio of 1:3, compared with 3:1 in *Oxct1*⁺ littermates. Frequent exogenous glucose administration to actively suckling *Oxct1*^{-/-} mice delayed, but could not prevent, lethality. Brains of newborn SCOT-deficient mice demonstrate evidence of adaptive energy acquisition, with increased phosphorylation of AMP-activated protein kinase α, increased autophagy, and 2.4-fold increased *in vivo* oxidative metabolism of [¹³C]glucose. Furthermore, [¹³C]lactate oxidation is increased 1.7-fold in skeletal muscle of *Oxct1*^{-/-} mice but not in brain. These results indicate the critical metabolic roles of ketone bodies in neonatal metabolism and suggest that distinct tissues exhibit specific metabolic responses to loss of ketone body oxidation.

Introduction

Transition from the intrauterine to the extrauterine environment incurs a marked shift in nutrient delivery and energy metabolism. A continuous pipeline replete with glucose and lactate, but calorically reduced in lipid, is replaced by a reduced carbohydrate, high fat milk diet that is cyclically interrupted by periods of nutrient deprivation (20,71,244). High energy-requiring organs like heart and skeletal muscle are poised to meet the energetic demands of this new nutrient environment because they are endowed with enzymatic machinery that avidly generates high energy phosphates from oxidative metabolism of fatty acids and lactate (245). Unlike cardiomyocytes and skeletal myocytes, most neurons oxidize fatty acids poorly and therefore remain dependent on hepatic gluconeogenesis to support energetic needs (69,70,246,247). However, because newborn brain comprises 10% of body weight and requires up to 60% of total body energy expenditure, maintenance of energetic homeostasis in the nervous system requires allocation of multiple fuels for metabolic homeostasis in the neonatal period. The rate of ketone body extraction by human neonatal brain is up to 40-fold higher than adult brain. Furthermore, ketones contribute uniquely to maturation within the nervous system (2,4,9,20,71,76,82,244,248-250).

Most ketogenesis occurs in the liver and is driven primarily by rates of fatty acid oxidation. Mitochondrial fatty acid oxidation-derived acetoacetyl-CoA (AcAc-CoA) and acetyl-CoA together serve as the primary ketogenic substrates. Ketogenic reactions are sequentially catalyzed by HMG-CoA synthase 2 and HMG-CoA lyase, generating acetoacetate (AcAc), which is converted to D- β -hydroxybutyrate (β OHB) in an NAD^+ / NADH -coupled redox reaction catalyzed by β OHB dehydrogenase. AcAc and β OHB diffuse into the bloodstream and are delivered to ketolytic organs, in which they are exceptionally energy-efficient substrates (5,39,76,95,96,251,252). Within mitochondria of ketolytic organs, β OHB is oxidized back to AcAc in a reaction catalyzed by β OHB dehydrogenase. AcAc receives a CoA moiety from succinyl-CoA, generating AcAc-CoA in a reaction catalyzed by succinyl-CoA:3-oxo-acid CoA-transferase (SCOT, EC 2.8.3.5), encoded by nuclear *Oxct1*. This enzyme is not expressed in liver (76,164). Mitochondrial AcAc-CoA thiolase catalyzes conversion of AcAc-CoA to acetyl-CoA, which is terminally oxidized within the tricarboxylic acid cycle.

Reports of ~20 individuals who harbor homozygous or compoundheterozygous *OXCT1* loss-of-function mutations (Online Mendelian Inheritance in Man 245050) indicate that afunctional allele is required for ketone body oxidation, and as such patients typically present in infancy with spontaneous ketoacidosis (79-81,98,100,148,149,253). Numerous single-nucleotide polymorphisms have been identified within the human *OXCT1* locus, but functional significance has been ascribed to relatively few of them.

Adverse consequences of ketoacidosis are well appreciated, and physiological states that increase ketone body turnover have been extensively analyzed. Nonetheless, experimental models to date have not definitively revealed whether loss of ketone oxidation can be energetically tolerated, particularly at the tissue level, and the metabolic adaptations to ketolytic insufficiency are unknown. In this study, we use novel *Oxct1*^{-/-} mice to examine the metabolic roles of ketone body oxidation in the neonatal period and the adaptations to its absence.

Experimental Procedures

Animals— *Oxct1*^{-/-} C57BL/6 mouse embryonic stem (ES) cells (clone EPD0082-1-CO2) were acquired through the National Institutes of Health knock-out mouse project (KOMP) consortium. The targeting sequence inserts two transcriptional terminators (pA) within intron 5 of the *Oxct1* locus, which is upstream from sequence that encodes critical catalytic SCOT residues (**Fig. 2.1A**) (254,255). Genotyping was performed using primer sets schematized in Fig. 1A and listed in **supplemental Table S2.1**. ES cells were microinjected into embryonic day 3.5 (E3.5) C57BL/6 blastocysts, and four chimeric mice (determined by tail biopsy PCR) were obtained. Transmission of the targeted allele was achieved by breeding chimeric males to C57BL/6 wild-type females. Heterozygote (*Oxct1*^{+/-}) progeny were then crossed to generate *Oxct1*^{-/-} mice. All mice were maintained on standard polysaccharide-rich chow diet (Lab Diet 5053) and autoclaved water *ad libitum*. Lights were off between 1800 and 0600. All P0 litters were obtained at 0900, and tissues/blood were harvested mid-morning. All experiments were performed using protocols approved by the Animal Studies Committee at Washington University.

Plasma Metabolite and Insulin Measurement— Measurements of plasma glucose, AcAc, β OHB, free fatty acids, and triglycerides were performed using biochemical assays coupled to colorimetric substrates (Wako), as described previously (51). Plasma lactate was measured using a colorimetric assay (BioVision). Blood glucose was measured in duplicate using a glucometer (Aviva). Measurement of plasma insulin was performed by ELISA (Millipore) as described previously (51).

Gene Expression Analysis— Quantification of gene expression was performed using real-time RT-quantitative PCR using the $\Delta\Delta$ Ct approach as described, normalizing to *Rpl32*, using primer sequences listed within **supplemental Table S2.1** (51).

Immunoblotting— Immunoblots, using protein lysates from neonatal brain, heart, and quadriceps/hamstring muscles to detect Oxct1/SCOT (rabbit anti-SCOT; Proteintech Group) were performed as described (51). Detection of phospho-AMPK α (*p*-AMPK α Thr-172) and total AMPK α was performed as described previously (126). Microtubule-associated protein 1 light chain 3 (LC3) was detected using rabbit polyclonal anti-LC3 (NB100-2220; Novus Biologicals) and donkey anti-rabbit IgG conjugated to horseradish peroxidase (NA9340; GE Healthcare). Band intensities were quantified densitometrically using QuantityOne software (Bio-Rad).

Measurement of in Vivo Substrate Utilization— P0 mice were injected intraperitoneally with 10 μ mol of sodium [2,4- 13 C₂] β OHB, [1- 13 C]glucose, or sodium [3- 13 C]lactate (Cambridge Isotope Laboratories) per g of body weight. Because P1 *Oxct1*^{-/-} mice are hypoglycemic and hypolactatemic, 13 C-isotope injections were supplemented in these animals with either 20 μ mol/g naturally occurring glucose, for [1- 13 C]glucose studies, or 10 μ mol/g naturally occurring lactate, for [3- 13 C]lactate studies, to ensure tissue delivery of total and 13 C-labeled substrate would remain equal among genotypes. After the indicated incubation durations in minutes, neonatal mice were killed by decapitation, and tissues were rapidly freeze-clamped in liquid N₂. Neutralized perchloric acid extracts were profiled using gradient heteronuclear single-quantum correlation 13 C-edited proton NMR measured at 11.75 T. Quantification of integrals of carbon 2 of [1- 13 C]taurine (a normalizing metabolite whose tissue concentrations were constant across conditions and which is not enriched by administration of these substrates) and [1- 13 C]glutamate (carbon 4) was performed

as described previously (51). Signals were collected from extracts dissolved in 300 μ l of D2O + 1 mM trimethylsilyl propionate, loaded into high precision, thin walled 5-mm tubes (Shigemi).

Statistical Analyses—Analyses were performed using GraphPad software (Prism), using tests described under “Results.”

Results

Ketolytic Deficiency in $Oxct1^{-/-}$ Mice—To determine the energetic role of ketone bodies in the neonatal period, $Oxct1^{-/-}$ mice were generated on the C57BL/6 genetic background (**Fig. 2.1, A and B**). Genotyping analysis of $Oxct1^{+/-}$ X $Oxct1^{+/-}$ live progeny from 12 litters examined on postnatal days 0–1 (P0–P1) indicated that progeny are born in a Mendelian ratio: 19 $+/+$, 40 $+/-$, and 25 $-/-$ mice ($\chi^2 = 0.5$, $p = 0.78$). Body weights among $+/+$, $+/-$, and $-/-$ mice did not vary on P0 or P1; gastric milk spots were observed with equal frequency within each genotype; and no gross anatomic or behavioral abnormalities were observed in P0–P1 $Oxct1^{-/-}$ mice (Table 1). As expected, $Oxct1$ mRNA and SCOT protein were reduced \sim 50% in P0 $Oxct1^{+/-}$ mice and were absent in $Oxct1^{-/-}$ mice (**Fig. 2.1, C and D**). Independent measurements of plasma biochemical metabolites on P0 and P1 revealed marked and progressive hyperketonemia in $Oxct1^{-/-}$ mice, with total ketone body concentrations increasing to \sim 16mM in $Oxct1^{-/-}$ mice on P1, consistent with accumulation of unmetabolized substrate (**Table 2.1**). An abnormally increased ratio of AcAc to β OHB is also consistent with a ketolytic lesion at the reaction catalyzed by SCOT: ligation of a CoA moiety to AcAc. Measurement of *in vivo* metabolism of [13 C] β OHB in skeletal muscle of P0 $Oxct1^{-/-}$ mice, using 13 C-edited proton NMR of extracts acquired 30 min after labeled substrate administration, confirmed the absence of 13 C-enriched glutamate, a quantitative surrogate for procession of carbon through the tricarboxylic acid cycle, and accumulation of [13 C]acetone and [13 C]AcAc, products of [13 C] β OHB that remain unmetabolized due to the absence of SCOT (**Fig. 2.1E**) (51,136). These findings were corroborated in P1 skeletal muscle and in P0 and P1 brain (**supplemental**

Fig. S2.1). Taken together, these results indicate that (i) *Oxct1*^{-/-} mice are ketolysis-deficient and (ii) ketone body oxidation in mice does not notably proceed through SCOT-independent pathways.

Ketoacidosis, Hypoglycemia, and Neonatal Lethality of Oxct1^{-/-} Mice— Unlike P0–P1 progeny of *Oxct*^{+/-} X *Oxct1*^{+/-} pairings, genotyping analysis of live progeny from 14 litters between P2 and P10 yielded 34 +/+, 50 +/-, and zero -/-mice ($\chi^2 = 24.7$, $p = 0.0001$). No lethality phenotype was evident in heterozygotes ($\chi^2 = 0.92$, $p = 0.34$). In addition to hyperketonemia, hypoglycemia and reduced plasma lactate concentrations were also observed in P1, but not P0 *Oxct1*^{-/-} animals. Significant differences in plasma insulin, free fatty acid, and triglyceride concentrations were not observed (**Table 2.1**). In particular, the rise in plasma free fatty acid concentrations that occurs after birth in association with suckling of high fat milk was preserved in P1 *Oxct1*^{-/-} mice(256,257).

Although P1 *Oxct1*^{-/-} mice exhibit marked hyperketonemia, relatively reduced plasma glucose and plasma lactate concentrations indicate that ketolytic insufficiency also results in diminution of other circulating metabolic fuels. To determine whether suckling *Oxct1*^{-/-} mice could be rescued from these metabolic abnormalities and prospective energetic deficiency, we performed metabolic resuscitation experiments using newborn progeny of *Oxct*^{+/-} X *Oxct1*^{+/-} mice. Serial subcutaneous injections of 155 mM NaHCO₃ ± 10% glucose were delivered to suckling neonates (50 µl every 3–6 h; seven injections were administered/24 hr period). Although NaHCO₃ partially buffers the acidifying effects of ketone bodies, glucose provides an additional energetic substrate that stimulates insulin release, thereby inhibiting ketogenesis and prospectively curtailing ketoacidosis in suckling *Oxct1*^{-/-} mice (12,258). As expected, survival analysis revealed that control suckling *Oxct1*^{-/-} mice injected with 155mM NaHCO₃ alone exhibited similar survival and weight course as uninjected suckling *Oxct1*^{-/-} animals, indicating that partial buffering of the acidifying effects of ketone bodies had no impact on survival (**Fig. 2.2**, $n = 20$ pups/group). On the other hand, serial administration of NaHCO₃ + glucose markedly improved the survival and weight trajectory of suckling *Oxct1*^{-/-} mice in the first 48 h of life. However, by P3, *Oxct1*^{-/-} animals maintained on the NaHCO₃ + glucose regimen had fallen off a normal growth curve, and all

gradually died over an additional 2–3 days. No significant effects of the NaHCO_3 + glucose, or NaHCO_3 alone regimens were observed in *Oxct1*^{+/+} or *Oxct1*^{+/-} animals.

To determine whether the failure-to-thrive phenotype observed within NaHCO_3 + glucose-resuscitated *Oxct1*^{-/-} animals was attributable to an insufficiency of glucose uptake, plasma glucose concentrations were measured in resuscitated animals 30 and 180 min after NaHCO_3 + glucose administrations in P2 *Oxct1*^{+/+}, *Oxct1*^{+/-}, and *Oxct1*^{-/-} mice. In addition, because SCOT-dependent ketone body metabolism within pancreatic β cells may influence glucose-stimulated insulin secretion, we also measured plasma insulin 30 min after NaHCO_3 + glucose administration in these mice (169,170). Our results indicate that postinjection glucose disposal and plasma insulin concentrations were not reduced in *Oxct1*^{-/-} mice (**Fig. 2.3, A and B**). However, despite treatment with the resuscitation regimen, suckling *Oxct1*^{-/-} mice still developed marked hyperketonemia (**Fig. 2.3C**). These results indicate that although systemic glucose uptake is intact in *Oxct1*^{-/-} mice, the lethal metabolic consequences of ketolytic insufficiency in suckling mice are refractory to frequent glucose administration.

Metabolic Adaptations of Oxct1^{-/-} Mice— To determine whether the development of hypoglycemia and reduced plasma lactate concentrations result from metabolic adaptations to the loss of ketolytic capacity, we performed a series of experiments in neonatal *Oxct1*^{-/-} mice and their littermates. First, we measured the abundance of the phosphorylated (active) form of the energy sensor/effector AMPK α in skeletal muscle, heart, and brain of untreated P0 *Oxct1*^{-/-} mice and their P0 *Oxct1*^{+/+} littermates. To ensure that measured responses of *Oxct1*^{-/-} mice were not downstream consequences of ketoacidosis and hypoglycemia, P0 mice were harvested within 3 h of birth. Protein lysates from skeletal muscle and heart of *Oxct1*^{-/-} mice did not reveal evidence of AMPK α activation, but the phosphorylated form of AMPK α was augmented 6.9 ± 1.4 -fold in brain of *Oxct1*^{-/-} mice, suggesting tissue-specific adaptation to the absence of ketolysis ($n = 7/\text{group}$, $p = 0.01$; **Fig. 2.4**).

Second, we determined whether autophagy was altered in *Oxct1*^{-/-} mice. Autophagy is an AMPK-activated self-degradative intracellular process in which organelles are recycled, prospectively in part for the purpose of energy conservation during periods of nutrient deprivation (259-261). Adaptation to

extrauterine life requires normal autophagic progression (262). To determine whether ketolytic deficiency in brain of P0 *Oxct1*^{-/-} mice is accompanied by induction of autophagy, we measured a key biomarker of autophagic progression, the differential processing/migration of protein LC3 on SDS-PAGE (263). The relative abundance of the faster migrating form of LC3 (LC3-II:LC3-I ratio) was increased 2.0 ± 0.2 -fold ($n = 7/\text{group}$, $p = 0.001$) in brain lysates of *Oxct1*^{-/-} mice (**Fig. 2.5**). This result, which was not observed in skeletal muscle (data not shown), is consistent with a proautophagic response to energy deficiency in brain of *Oxct1*^{-/-} mice.

Third, to determine whether ketolytic insufficiency and the associated ultimate development of reduced plasma glucose and lactate concentrations were linked to increases in glucose and lactate utilization by tissues that normally oxidize ketones in *Oxct1*^{-/-} mice, we used NMR to measure *in vivo* oxidative metabolism of independently administered [¹³C]glucose or [¹³C]lactate in brains and skeletal muscle of P0 and P1 *Oxct1*^{-/-} mice and their littermates. Brain extracts obtained from P0 neonates 30 min after intraperitoneal administration of 10 $\mu\text{mol/g}$ body weight [¹³C]glucose revealed 2.4 ± 0.2 -fold increased accumulation of ¹³C-enriched glutamate in brains of *Oxct1*^{-/-} mice compared with *Oxct1*⁺ mice (from $3.6 \pm 0.8\%$ to $8.5 \pm 1.7\%$; $n = 7/\text{group}$, $p = 0.002$; **Fig. 2.6A**; no differences were observed between *Oxct1*^{+/+} and *Oxct1*^{+/-} mice, which are combined and represented as *Oxct1*⁺). As expected, at the time of tissue harvest, tissue ¹³C enrichment of glucose (35.3% and 41.3% in *Oxct1*⁺ and *Oxct1*^{-/-} mice, respectively, $p = 0.51$) and total blood glucose concentrations were also equivalent between groups that received [¹³C]glucose, indicating that increased ¹³C-enrichment of glutamate could not be explained by increased delivery of ¹³C-substrate. These findings were corroborated in brain extracts of P0 animals collected 45 min after substrate injection: ¹³C-enrichment of glutamate was increased 2.8 ± 0.3 -fold in brains of *Oxct1*^{-/-} mice ($n = 5/\text{group}$, $p = 0.02$). Evidence for increased glucose utilization persisted in brains of *Oxct1*^{-/-} mice on P1, which exhibited 1.8 ± 0.2 -fold greater ¹³C-enrichment of glutamate in *Oxct1*^{-/-} brains than by brains of *Oxct1*⁺ littermates 30 min after substrate administration ($n = 7/\text{group}$, $p = 0.02$; **Fig. 2.6A**). Because P1 *Oxct1*^{-/-} mice are hypoglycemic, this experiment was performed by administering a mixture of ¹³C-labeled and naturally occurring glucose (see “Experimental Procedures”),

which prevented disproportionately high delivery of labeled glucose to brains of *Oxct1^{-/-}* mice. Taken together, these results are consistent with a higher rate of glucose oxidation in brains of *Oxct1^{-/-}* mice on both P0 and P1, which possibly contributes to the ultimate development of hypoglycemia.

Unlike brain of *Oxct1^{-/-}* mice, evidence for increased glucose oxidation was not observed in skeletal muscle, which, after 30 min of [¹³C]glucose administration, revealed only scant ¹³C-enrichment of glutamate in *Oxct1⁺* ($1.4 \pm 0.2\%$) or *Oxct1^{-/-}* mice ($1.9 \pm 0.3\%$). After 45 min, ¹³C-enrichment of glutamate increased equally to $\sim 3\%$ in *Oxct1⁺* and *Oxct1^{-/-}* mice. Similar results were observed in muscle of P1 mice.

To obtain surrogates of *in vivo* lactate oxidation in neonatal mice, we measured [¹³C]glutamate in brains and skeletal muscles of P0 animals 30 min after administration of $10 \mu\text{mol/g}$ [¹³C]lactate. In *Oxct1⁺* and *Oxct1^{-/-}* mice, ¹³C labeling of glutamate in brain was greater through [¹³C]lactate than that delivered through [¹³C]glucose. Nonetheless, there was no difference between brains of *Oxct1⁺* and *Oxct1^{-/-}* mice ($11.1 \pm 3.0\%$ and $12.0 \pm 3.7\%$, respectively, $n = 5/\text{group}$, $p = 0.84$). Conversely, ¹³C enrichment of glutamate from lactate was enhanced in skeletal muscle of P0 *Oxct1^{-/-}* mice by 1.7 ± 0.2 -fold compared with skeletal muscle of *Oxct1^{-/-}* mice ($7.9 \pm 0.8\%$ and $4.5 \pm 0.7\%$, respectively, $n = 5/\text{group}$, $p = 0.02$; **Fig. 2.6B**). As expected, ¹³C enrichment of substrate was not greater in skeletal muscle of P0 *Oxct1^{-/-}* mice. Increased lactate oxidation rates did not persist to P1 in skeletal muscle, which were $5.5 \pm 0.4\%$ and $5.0 \pm 0.8\%$ in P1 *Oxct1⁺* and *Oxct1^{-/-}* mice, respectively ($n = 5/\text{group}$, $p = 0.6$; **Fig. 2.6B**). Taken together, these results indicate (i) increased oxidation of lactate in skeletal muscle of P0 but not P1 and *Oxct1^{-/-}* mice and (ii) adaptation of both neonatal brain and skeletal muscle to ketolytic insufficiency.

Discussion

Introduction to the extrauterine environment creates new metabolic and energetic demands. Studies of metabolic flux and ketone turnover have indicated that ketone bodies serve an important role in neonatal rodents and humans (20,71,244,248,256,257). This is the first study to use a genetic model to demonstrate that oxidation of ketones is required for postnatal survival in mice. *Oxct1^{-/-}* mice exhibit no evidence of

terminal ketone body oxidation and develop ketoacidosis, indicating that the SCOT pathway is required for ketolysis in mice. Furthermore, plasma glucose and lactate levels become depleted in *Oxct1*^{-/-} mice after the first 24 h of extrauterine life. Increased oxidation of glucose and lactate is observed, starting prior to the depletion of these metabolites in plasma, suggesting that increased consumption, at least in part, contributes to their depletion.

Although reduced nutrient ingestion could also contribute to ketoacidosis, hypoglycemia, and hypolactatemia, our results, together with those of prior investigators, strongly suggest that these abnormalities occur in actively suckling neonatal *Oxct1*^{-/-} mice. First, because mice and rats (unlike humans) possess very little white adipose stores at birth, neonatal ketogenesis, robust in *Oxct1*^{-/-} mice, is dependent on suckling (256,257,264). Second, plasma free fatty acid concentration, a reporter of milk intake and a key determinant of ketogenesis, exhibited increases in P1 *versus* P0 *Oxct1*^{-/-} mice, comparable with the increase observed in *Oxct1*⁺ littermates. Plasma triglyceride concentrations were also not reduced in *Oxct1*^{-/-} mice. Although ingested milk volumes were not formally quantified, *Oxct1*^{-/-} mice exhibited gastric milk spots with equal frequency to their littermates on P0 and P1. Thus, these studies indicate that loss of ketone oxidation in postnatal mice provokes a metabolic state that ultimately proves lethal, despite access to metabolic fuels through milk.

Reduced plasma glucose and lactate concentrations in P1 *Oxct1*^{-/-} mice are prospectively explained by increased oxidation of glucose and lactate, but hypoglycemia and hypolactatemia also may occur due to insufficient biosynthesis. During the rodent suckling period, biosynthesis of glucose and lactate are driven by hepatic gluconeogenesis and extrahepatic glycolysis, respectively (20). Altered mitochondrial redox potential of *Oxct1*^{-/-} mice could contribute to prospective synthetic deficiencies. In neonatal *Oxct1*⁺ mice, plasma β OHB:AcAc ratio is 3:1, consistent with reported ratios in ketotic states (2,258). In hyperketonemic *Oxct1*^{-/-} mice, this ratio is markedly reduced to 1:2 on P0, due to oxidation of β OHB to, and no further than, AcAc, which significantly alters mitochondrial [NAD⁺]:[NADH] ratio, particularly in extrahepatic tissues. Altered mitochondrial redox potential could in turn impair flux through the malate-aspartate shuttle, whose function is important for glycolysis, the source of lactate. In

turn, curtailed lactate production deprives the liver of a key gluconeogenic substrate, via the Cori cycle. Furthermore, in P1 *Oxct1*^{-/-} mice, plasma concentrations of β OHB and AcAc accumulate to very high concentrations, while remaining in a ratio of 1:3, which may evoke extrahepatic and hepatic impairments of the tricarboxylic acid cycle and fatty acid oxidation. Oxidative impairment within liver disrupts gluconeogenesis (20,265-267). Emergence of attenuated extrahepatic oxidative capacity was evident in *Oxct1*^{-/-} mice on P1, when glucose oxidation in brain and lactate oxidation in skeletal muscle were both reduced in *Oxct1*^{-/-} mice, relative to P0 *Oxct1*^{-/-} mice.

An additional abnormality of ketone metabolism may also occur in *Oxct1*^{-/-} mice. In humans, up to 37% of AcAc is spontaneously decarboxylated to acetone (268). Therefore, with accumulation of high concentrations of AcAc, it is likely that acetone also accumulates in normally ketolytic tissues of *Oxct1*^{-/-} mice, a notion supported by our NMR findings. Acetone is disposed through breath and urine, but a significant proportion of acetone can also be used as a substrate for anabolic and catabolic processes through SCOT-independent pathways (268). High circulating concentrations of acetone may also cause central nervous system depression.

It is important to note that the precise roles of neonatal ketone metabolism differ between mice and humans. Humans are born at a more mature point in development, and as indicated above, at the time of birth, body fat percentage is higher in humans than in rats and mice (256,264,269-271). In these neonatal rodents, ketogenesis is driven by suckling, rather than fasting (256,257). Moreover, due to increased fat/carbohydrate ratio, rodent milk is more ketogenic than most human milk and infant formulas (9,20). It is likely for these reasons that two features of *Oxct1*^{-/-} mice are distinct from those of SCOT deficient humans: (i) autosomal recessive *OXCT1* mutations in humans are compatible with life (albeit with aggressive nutritional support), whereas analysis of ~100 litters of *Oxct1*^{+/-} X *Oxct1*^{+/-} pairings has yet to reveal any male or female *Oxct1*^{-/-} neonate that spontaneously survives past 48 h of extrauterine life; and (ii) *Oxct1*^{-/-} mice develop hypoglycemia, unlike most SCOT-deficient humans. Despite these differences, deficiencies of ketone metabolism in neonatal mice bear significant relevance to human infant metabolism. First, physiological ketosis (1-2mM) occurs in the early neonatal period in both

humans and mice (2,71,244,272,273). Second, human infants are particularly prone to develop hyperketonemia and thus, increased energetic utilization of ketones, in response to relatively short periods of nutrient deprivation, due to adipose lipolysis (2,4,20,248,274). Consequences of common viral illnesses can rapidly trigger ketosis. Third, human milk exhibits significant variations of macronutrient content distribution, even within the same mother over different collections (275,276). Therefore, it is plausible that energetic crisis and/or ketoacidosis could emerge in infants with unsuspected ketolytic insufficiency. Current newborn screening regimens do not detect individuals with isolated ketolytic disorders, who exhibit ketosis but normal acylcarnitine and organic acid profiles (99). Therefore, a small subset of cases which ultimately receive a diagnosis of sudden infant death syndrome (SIDS) may actually be attributable to SCOT deficiency.

Although our studies did not directly measure prospective changes in glycolytic flux or metabolic shifts within myocardium (the particularly low mass of neonatal mouse heart, ~10 mg, prevented tractable NMR approaches), these results indicate both toxic effects of and metabolic adaptation to ketolytic insufficiency in the neonatal period. Future experiments will determine definitively the relative contributions of ketoacidosis, hypoglycemia, and energy deficiency to lethality of *Oxct1*^{-/-} mice. Further measurement of the energetic roles of ketone bodies in mouse models will be best supported through studies in which (i) a lower fat nonketogenic nutrient formula replaces mother's milk in the neonatal period and/or (ii) additional genetic approaches selectively induce a ketolytic defect within individual tissues. Such studies will ultimately permit determination of energetic and disease-modifying roles of ketolysis in neonates and adults in conditions that include nutrient deprivation, maintenance on low carbohydrate diets, and diabetes. Finally, with increasing utilization of low and very low carbohydrate diets in clinical trials for conditions including adult obesity, pediatric and adult epilepsy, and malignancies of the central nervous system, it is important to consider the metabolic and clinical consequences of latent ketolytic defects that are revealed later in life, possibly caused by single nucleotide polymorphisms within the *OXCT1* locus; case reports describe marked variations of tolerance to ketogenic milieus (277-279). These studies indicate the critical metabolic role that ketone body oxidation

serves and adaptations to its absence in the reduced carbohydrate nutrient environment of the neonatal period.

Figure legends

Figure 2.1. Ketolysis-deficient *Oxct1*^{-/-} mice. **A**, targeting strategy for the *Oxct1* locus in ES cells. **WT**, wild-type locus; **Null**, loss-of-function allele. **Arrows** indicate locations of genotyping PCR primers. See supplemental Table S1 for a list of primer sequences. **B**, PCR genotyping of *Oxct1*^{-/-} P0 mice. **NTC**, no template control. **C**, expression of *Oxct1* mRNA in heart of P0 *Oxct1*^{+/+}, *Oxct1*^{+/-}, and *Oxct1*^{-/-} mice, determined by RT-quantitative PCR; **n** = 5/group. **D**, immunoblot of SCOT and actin using protein lysates from brain, heart, and quadriceps/hamstrings skeletal muscle of P0 *Oxct1*^{+/+}, *Oxct1*^{+/-}, and *Oxct1*^{-/-} mice. **E**, ¹³C-edited proton NMR spectrum (2.1–2.5 ppm, relative to chemical shift of trimethylsilyl propionate internal standard) from quadriceps/hamstrings of P0 *Oxct1*^{+/+} and *Oxct1*^{-/-} mice that had been injected with [2,4-¹³C₂]βOHB 30 min prior to collection of tissues and generation of extracts. [¹³C]Glutamate is a reporter of tricarboxylic acid flux of a ¹³C-labeled substrate that is selectively absent in extracts from *Oxct1*^{-/-} mice. *C2* and *C4* correspond to carbon position.

Figure 2.2. Metabolic resuscitation of *Oxct1*^{-/-} mice. **A**, Kaplan-Meier curves for neonatal mice in the untreated, treated with 155 mM NaHCO₃ alone, or treated with 155 mM NaHCO₃ + 10% glucose (**glc**) states. Subcutaneous injections were performed every 3–6 h, starting within 3h of birth, with seven injections over a 24-h period. *Oxct1*^{+/+} and *Oxct1*^{+/-} mice showed no differences and were pooled (noted as *Oxct1*⁺). Within the first 90 h of life, no statistically significant differences were observed among treated *Oxct1*⁺ mice, untreated *Oxct1*⁺ mice, and *Oxct1*^{-/-} mice treated with NaHCO₃ + glucose. Likewise, no statistically significant difference was observed between *Oxct1*^{-/-} mice treated with NaHCO₃ alone and untreated *Oxct1*^{-/-} mice. However, addition of glucose to the NaHCO₃ regimen significantly improved survival of *Oxct1*^{-/-} mice in the first 90 h of life (**p** < 0.001 by log-rank test, **n** = 20/group). **B**, relative weights of animals within the genotype and treatment groups described in **A**. *******, **p** < 0.001 by two-way

ANOVA with post hoc Bonferroni testing, independently compared with each of the other treatment groups.

Figure 2.3. Normal glucose disposal but refractory hyperketonemia in glucose-resuscitated suckling *Oxct1*^{-/-} mice. **A**, blood glucose concentrations measured on P2 within neonatal mice treated with the NaHCO₃ + glucose resuscitation regimen every 3–6 h. Measurements were taken independently 30 and 180 min after administration of NaHCO₃ + glucose. **B**, plasma insulin concentrations within resuscitated mice, 30 min after NaHCO₃ + glucose administration. NS, not significant. **C**, total plasma ketone concentration (β OHB + AcAc) within resuscitated mice, 30 min after NaHCO₃ + glucose administration. For all comparisons, *Oxct1*^{+/+} and *Oxct1*^{-/-} mice showed no differences and were pooled (noted as *Oxct1*⁺). n = 7/group; ***, p < 0.001 by Student's *t* test.

Figure 2.4. Increased phosphorylation of AMPK α within brain of *Oxct1*^{-/-} mice. **A–C**, immunoblots of lysates from untreated animals: skeletal muscle (**A**), heart (**B**), and brain (**C**) protein lysates from P0 *Oxct1*^{+/+} and *Oxct1*^{-/-} mice for phospho-AMPK α (p-AMPK α), total AMPK α , SCOT, and actin. **D**, densitometric quantification of p-AMPK α :AMPK α ratio in brain lysates. **, p < 0.01 by Student's *t* test.

Figure 2.5. Enhanced autophagy in brain of *Oxct1*^{-/-} mice. **A**, immunoblots of P0 brain protein lysates for LC3 and actin. **B**, densitometric quantification of LC3-II:LC3-I ratios in brain lysates. ***, p < 0.001 by Student's *t* test.

Figure 2.6. Tissue-specific adaptations to ketolytic insufficiency. **A**, accumulation of [¹³C]glutamate carbon 4 (*C4*) in brains of P0 (*left*) and P1 (*right*) mice injected with [1-¹³C]glucose, measured by ¹³C-edited proton NMR. n = 7/group. **B**, accumulation of [¹³C]glutamate in skeletal muscle of P0 (*left*) and P1 (*right*) mice injected with [3-¹³C]lactate, measured by ¹³C-edited proton NMR. n = 5/group; **, p < 0.01

by Student's *t* test.

Figure S2.1. Absence of terminal ketone body oxidation in muscle and brain of *Oxct1*^{-/-} mice. ¹³C-edited proton NMR spectra (2.1-2.5 ppm, relative to chemical shift of TSP internal standard) from extracts derived from muscle (A) and brain (B) of P0 (left panels) or P1 (right panels) *Oxct1*^{+/+} and *Oxct1*^{-/-} mice. Animals were injected with 10 μmol/g body weight [2,4-¹³C₂]βOHB 30 min prior to collection of tissues and generation of extracts. ¹³C-glutamate (glu; resonances of protons on carbon #4 are shown) is a reporter of tricarboxylic acid flux of a ¹³C-labeled substrate that is selectively absent, above naturally-occurring enrichment (1.1% abundance), in extracts from *Oxct1*^{-/-} mice.

Figure 2.1

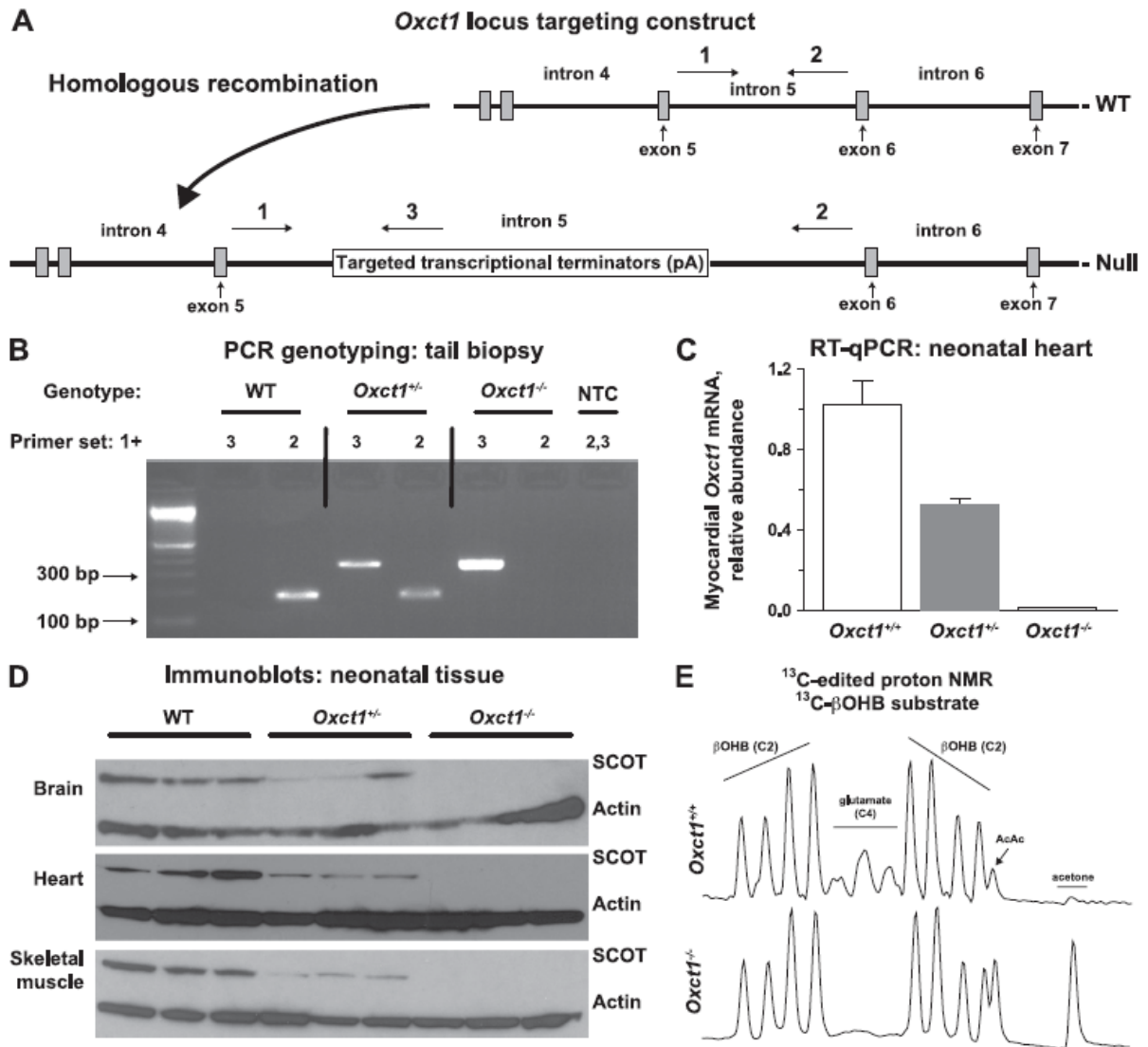


Figure 2.2

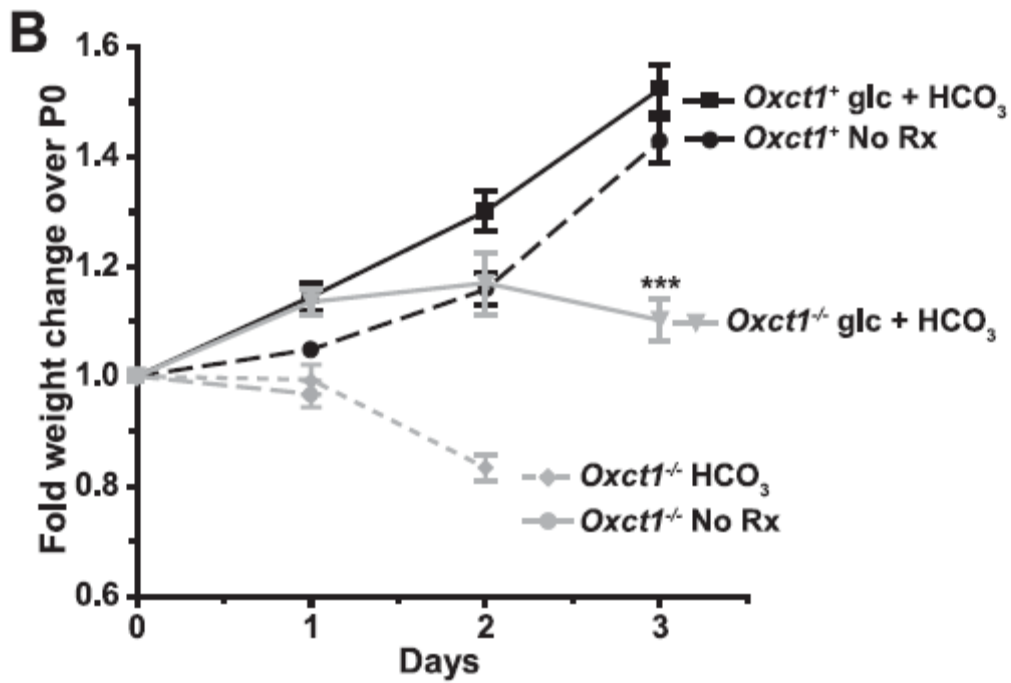
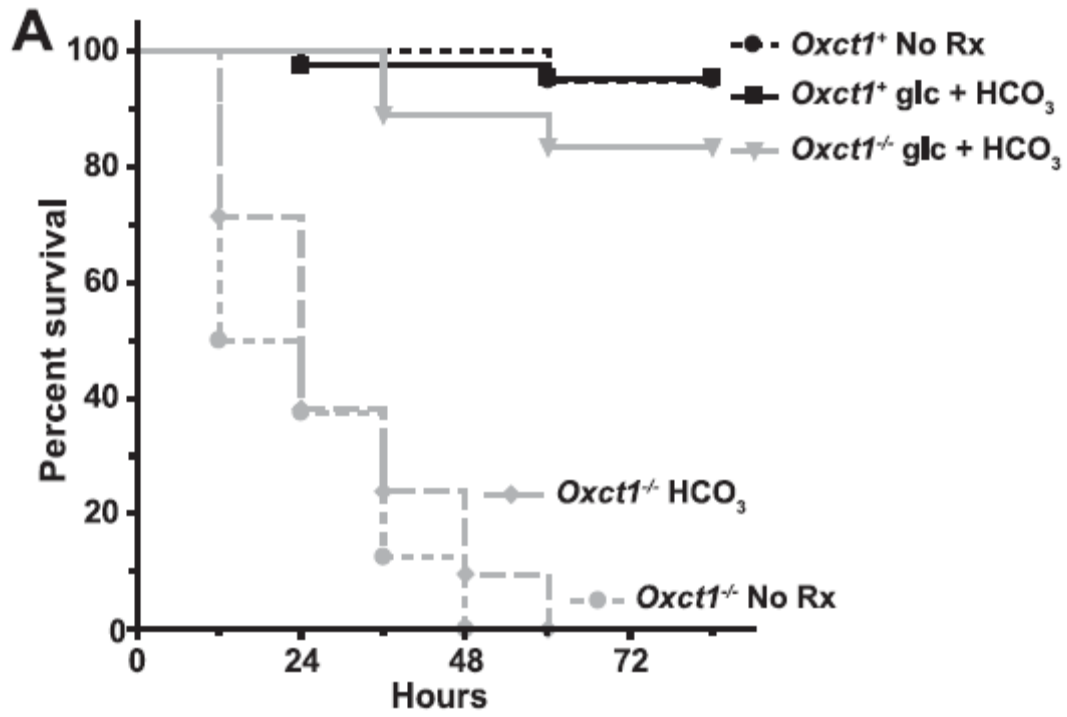


Figure 2.3

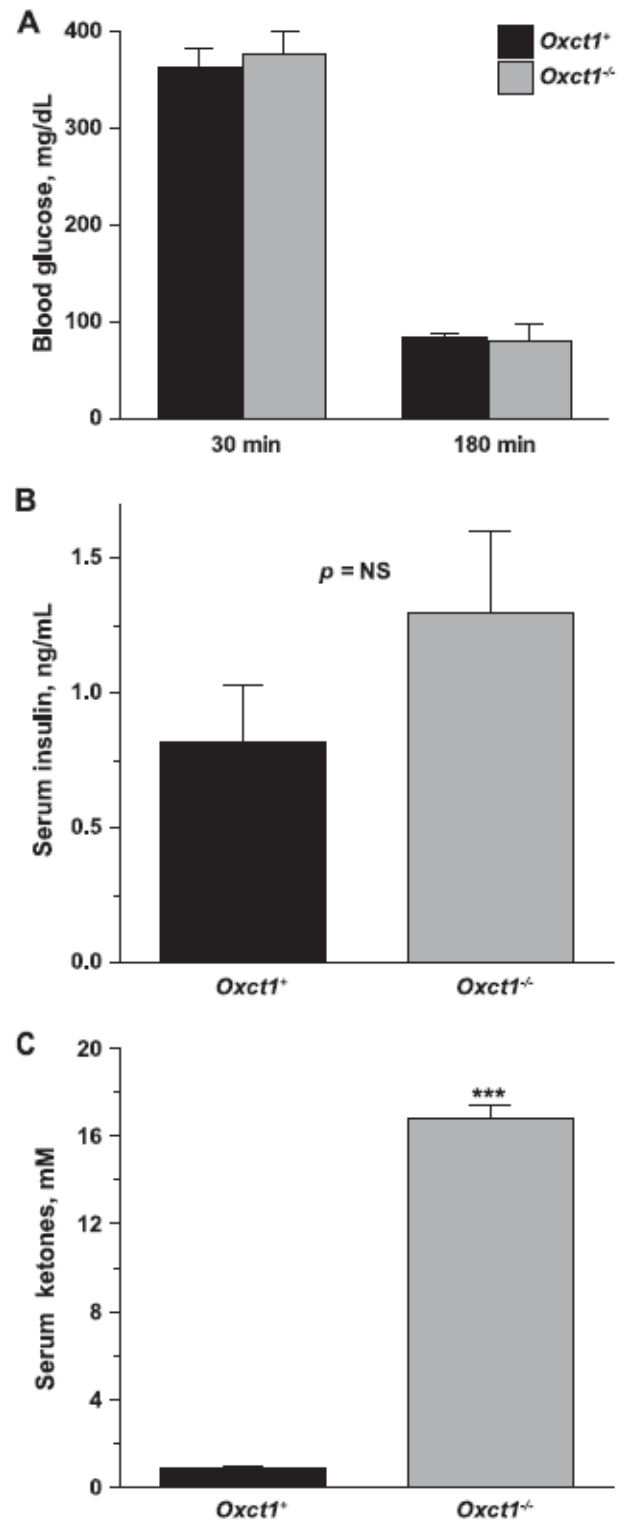


Figure 2.4

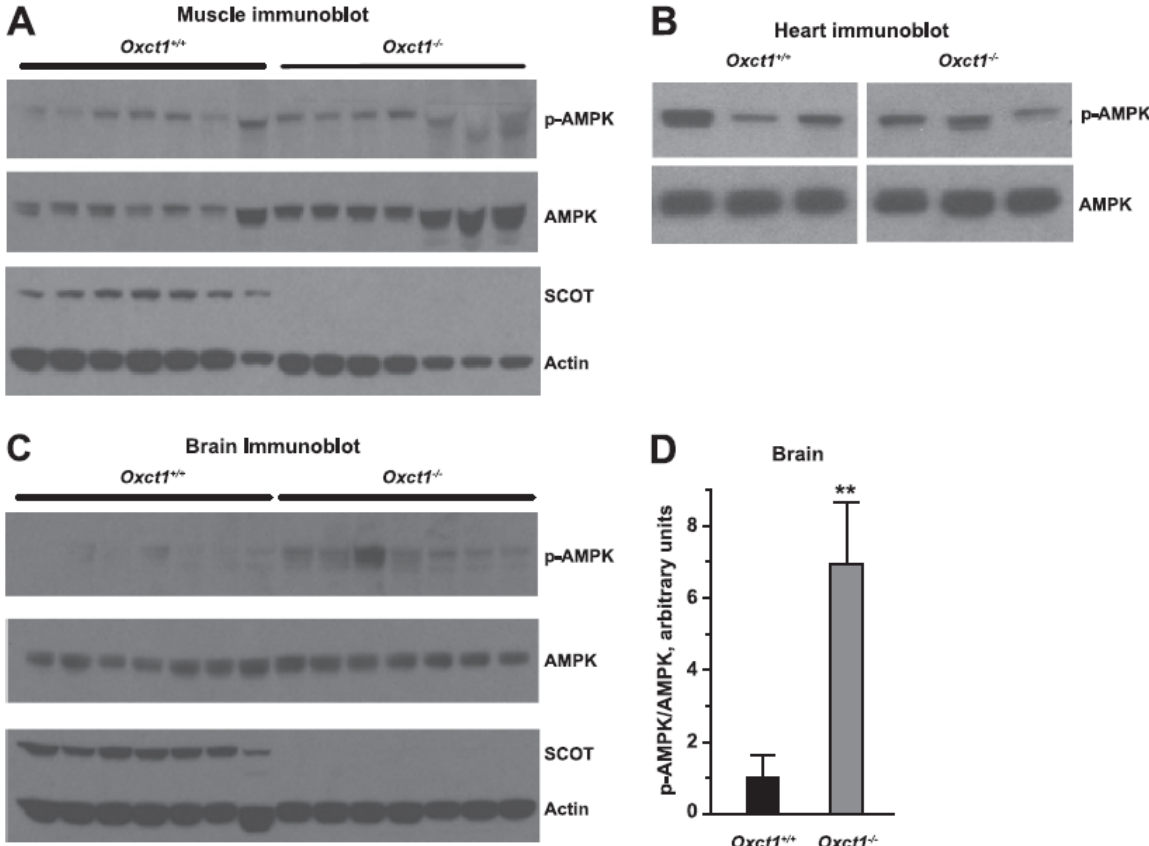


Figure 2.5

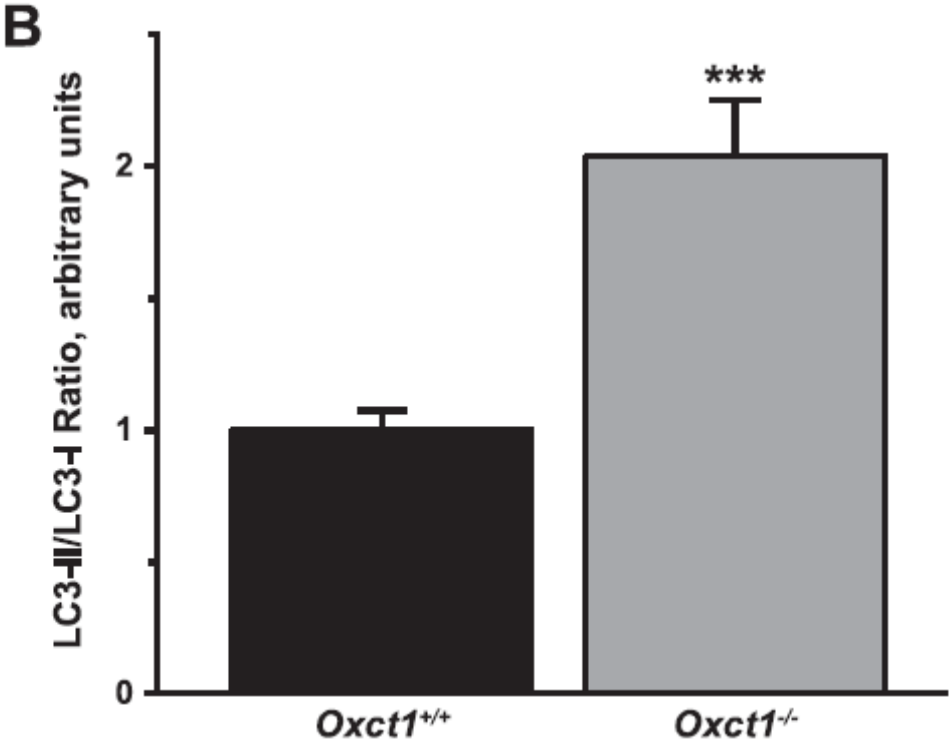
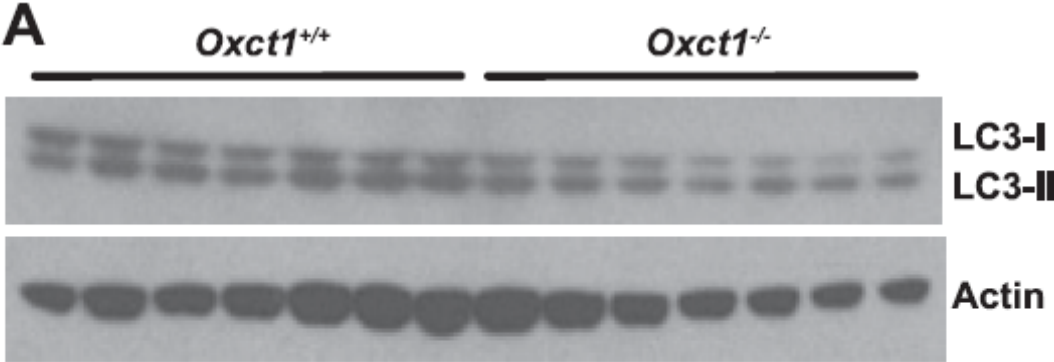


Figure 2.6

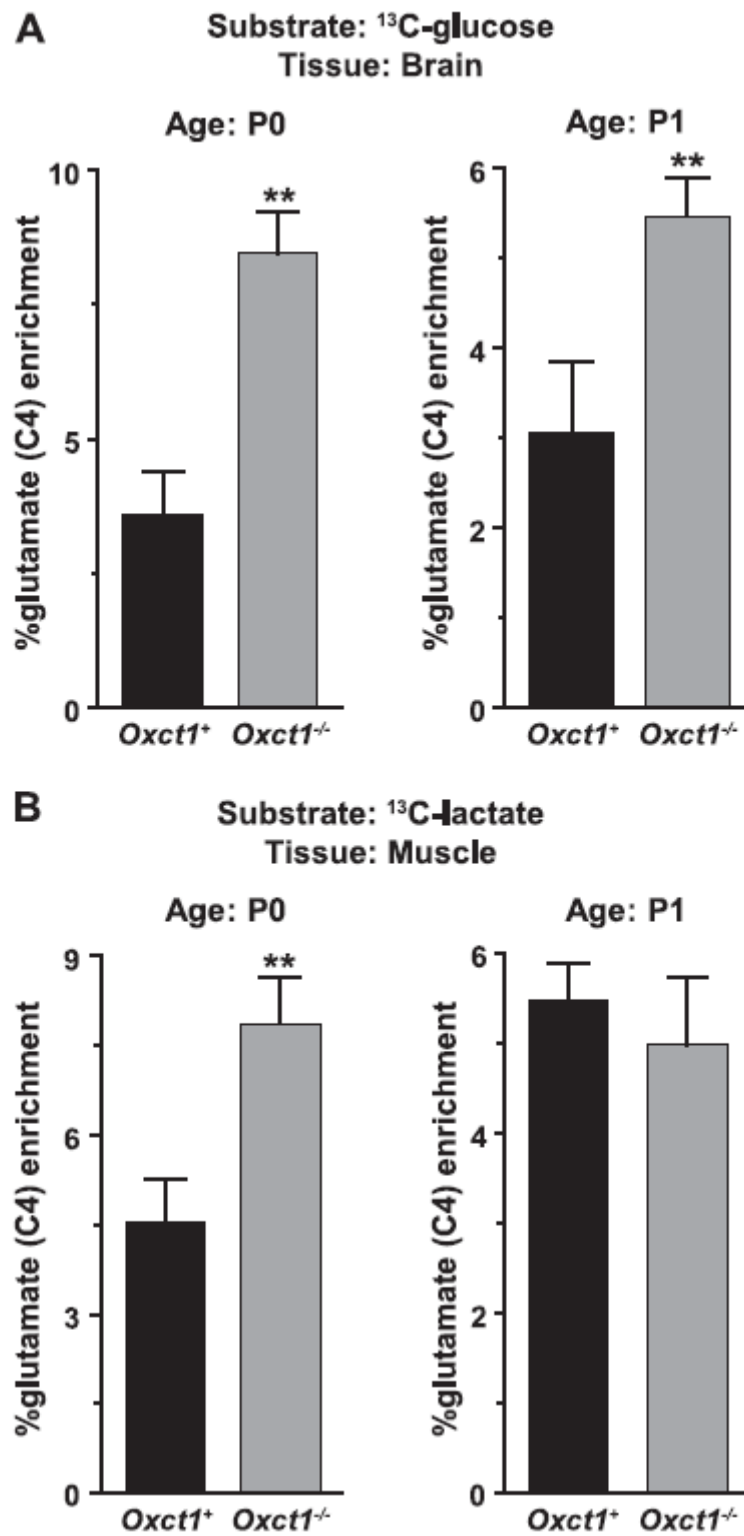


Table 2.1

TABLE 1

Plasma metabolite concentrations in P0–P1 mice

TG, triglycerides; FFA, free (nonesterified) fatty acids; $n = 6-10/\text{group}$; **, $p < 0.01$ compared with +/–; †, $p < 0.01$ compared with +/+; aa, $p < 0.01$ and a, $p < 0.05$ compared with the same genotype at P0. Data are presented as mean \pm S.E.; comparisons are two-way ANOVA with Bonferroni post hoc testing.

<i>Oxct1</i> genotype and age	Weight	β OHB	AcAc	Glucose	Insulin	FFA	Lactate	TG
	mg	mm	mm	mg/dl	ng/ml	mm	mm	mg/dL
+/+, P0	1,339 \pm 37	0.29 \pm 0.07	0.08 \pm 0.02	46 \pm 19	0.47 \pm 0.09	0.28 \pm 0.09	1.09 \pm 0.11	72.5 \pm 20.6
+/-, P0	1,285 \pm 28	0.50 \pm 0.12	0.17 \pm 0.06	49 \pm 10	0.53 \pm 0.16	0.24 \pm 0.04	1.11 \pm 0.06	72.4 \pm 11.0
-/-, P0	1,301 \pm 29	1.40 \pm 0.36 ^{**,†}	3.10 \pm 1.07 ^{**,†}	38 \pm 11	0.30 \pm 0.01	0.28 \pm 0.05	1.10 \pm 0.07	82.0 \pm 19.0
+/+, P1	1,384 \pm 60	0.66 \pm 0.04	0.06 \pm 0.1	65 \pm 7	0.38 \pm 0.04	0.96 \pm 0.40 ^{aa}	1.36 \pm 0.20	80.7 \pm 16.0
+/-, P1	1,435 \pm 36	0.67 \pm 0.09	0.20 \pm 0.06	56 \pm 4	0.62 \pm 0.16	0.77 \pm 0.14 ^a	1.50 \pm 0.11	74.8 \pm 23.4
-/-, P1	1,322 \pm 36	4.39 \pm 0.53 ^{**,†,a}	11.8 \pm 0.8 ^{**,†,aa}	19 \pm 1 ^{**,†,a}	0.42 \pm 0.06	1.14 \pm 0.30 ^{aa}	0.67 \pm 0.04 ^{**,†,aa}	127.8 \pm 21.6

Figure S2.1

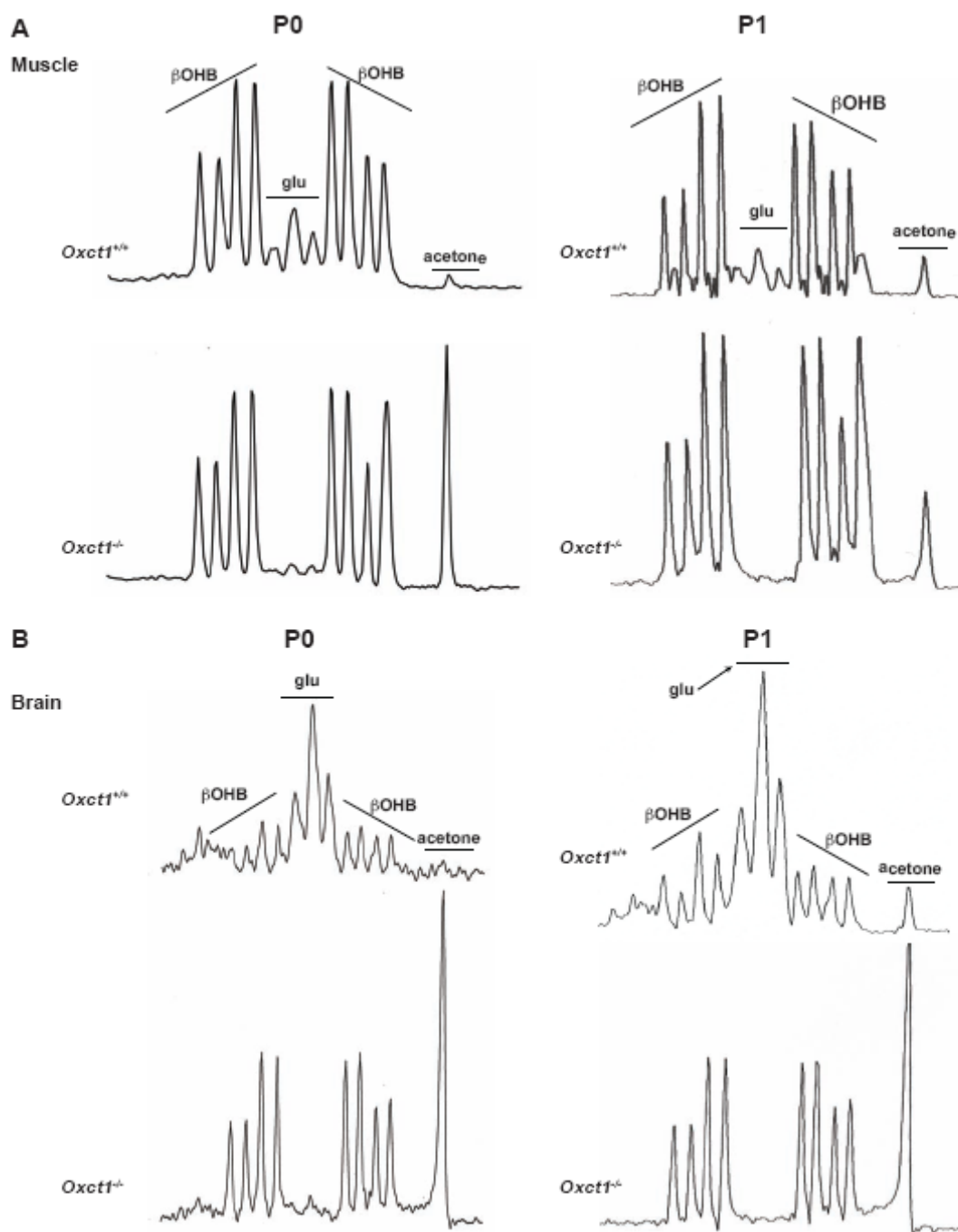


Table S2.1

Supplemental Table S1. Oligonucleotide primer sequences used for PCR in this study.		
Gene	NCBI #	Sequence
<i>Oxct1</i> Genomic Forward (1)	NC_000081.5	CCAAGGAAGTAAATGAAGATGCTCCTA
<i>Oxct1</i> Genomic Reverse (2)		ACGTGTATGTTACAAGAAATGGCTTACC
<i>Oxct1</i> Genomic- targeted Reverse (3)	<i>Oxct1</i> ^{tm1a(KOMP)Wtsi}	CCAACTGACCTTGGGCAAGAACAT
<i>Oxct1</i> mRNA Forward	NM_024188.6	TGGCCAACCTGGATGATACCTGG
<i>Oxct1</i> mRNA Reverse		TCCATGGTGACCACCACTTTGG
<i>Rpl32</i> Forward	NM_172086	CCTCTGGTGAAGCCCAAGATC
<i>Rpl32</i> Reverse		TCTGGGTTTCCGCCAGATTT

Chapter 3

Successful adaptation to ketosis by mice with tissue-specific deficiency of ketone body oxidation

The work presented in this chapter has been adapted from:

Cotter, D. G., Schugar, R. C., Wentz, A. E., d'Avignon, D. A., and Crawford, P. A. (2013) *Am J Physiol Endocrinol Metab* 304(4), E363-374

Abstract

During states of low carbohydrate intake, mammalian ketone body metabolism transfers energy substrates originally derived from fatty acyl chains within the liver to extrahepatic organs. We previously demonstrated that the mitochondrial enzyme CoA transferase (succinyl-CoA:3-oxoacid CoA transferase, SCOT, encoded by nuclear *Oxct1*) is required for oxidation of ketone bodies, and that germline SCOT-knockout (KO) mice die within 48h of birth due to hyperketonemic hypoglycemia. Here, we use novel transgenic and tissue-specific SCOT-KO mice to demonstrate that ketone bodies do not serve an obligate energetic role within highly ketolytic tissues during the ketogenic neonatal period or during starvation in the adult. While transgene-mediated restoration of myocardial CoA transferase in germline SCOT-KO mice is insufficient to prevent lethal hyperketonemic hypoglycemia in the neonatal period, mice lacking CoA transferase selectively within neurons, cardiomyocytes, or skeletal myocytes, are all viable as neonates. Like germline SCOT-KO neonatal mice, neonatal mice with neuronal CoA transferase deficiency exhibit increased cerebral glycolysis and glucose oxidation, and while these neonatal mice exhibit modest hyperketonemia, they do not develop hypoglycemia. As adults, tissue-specific SCOT-KO mice tolerate starvation, exhibiting only modestly increased hyperketonemia. Finally, metabolic analysis of adult germline *Oxct1*^{+/-} mice demonstrates that global diminution of ketone body oxidation yields hyperketonemia, but hypoglycemia emerges only during a protracted state of low carbohydrate intake. Together, these data suggest that, at the tissue level, ketone bodies are not a required energy substrate in the newborn period or during starvation, but rather that integrated ketone body metabolism mediates adaptation to ketogenic nutrient states.

Introduction

Adaptation to limited carbohydrate availability and increased fatty acid supply, as encountered during the initial transition to extrauterine life, starvation, and adherence to low-carbohydrate diets, requires shifts in metabolic substrate utilization (2,4,5,20). While many organs are poised to meet the bioenergetic demands imposed by fat-dominated energy economies, neurons do not effectively derive high-energy phosphates from fatty acids (69,70). Thus, provision of alternate fuel sources may be required to preserve bioenergetic homeostasis within some tissues when carbohydrates are limiting. Ketone body metabolism supports this function by oxidizing hepatic fatty acyl-coenzyme A species (acyl-CoAs) to water-soluble four carbon ketone body intermediates (via ketogenesis) that are shared with extrahepatic tissues for terminal oxidation. Most ketogenesis occurs within hepatic mitochondria, at rates proportional to β -oxidation of fatty acids (5). Sequential ketogenic reactions catalyzed by mitochondrial thiolase, hydroxymethylglutaryl-CoA synthase (HMGCS2) and hydroxymethylglutaryl-CoA lyase convert acetyl-CoA to the ketone body acetoacetate (AcAc), which is reduced by mitochondrial D- β -hydroxybutyrate (β OHB)-dehydrogenase (BDH1) to D- β OHB in an NAD^+ /NADH-coupled redox reaction (44). D- β OHB and AcAc are secreted from the liver via monocarboxylate SLC16A transporters, transported into extrahepatic cells via SLC16A transporters, and oxidized in the mitochondrial matrix (4,26,27). Mitochondrial BDH1 re-oxidizes D- β OHB to AcAc, and covalent activation of AcAc by CoA is catalyzed by the mitochondrial matrix enzyme succinyl-CoA:3-oxoacid CoA transferase [SCOT (encoded by the nuclear gene *Oxct1*), the only mammalian CoA transferase] to generate AcAc-CoA, which upon thiolytic cleavage, liberates acetyl-CoA that enters the tricarboxylic acid (TCA) cycle for terminal oxidation (74). CoA transferase catalyzes a near equilibrium reaction in which CoA is exchanged between succinate and AcAc (72,280). As such, unlike glucose and fatty acids, ketone bodies do not directly require commitment of ATP for activation of the substrate prior to oxidation.

Ketone bodies are efficient energetic substrates that are oxidized in proportion to their delivery (4,20). The neonatal brain extracts ketones at rates up to 40 times those of the adult brain, and ketone body oxidation can support as much as 25% of the neonate's basal energy requirements (71,248).

Neurons oxidize fatty acids poorly, and glucose utilization accounts for only 70% of the postnatal brain's energetic needs (69,71). Thus, ketogenesis, which converts up to two-thirds of hepatic β -oxidation-derived acetyl-CoA into ketones (281), has been proposed as a facilitator of evolution of the vertebrate brain and of human brain size (40,41). Nonetheless, an energetic requirement for ketone body oxidation has never been demonstrated, even though it is thought to become a primary contributor to bioenergetic homeostasis (2,84). Ketogenesis is also required for normal fitness in humans, as loss-of-function mutations in the gene encoding the fate-committing hepatic ketogenic enzyme HMGCS2 result in pediatric hypoketonemic hypoglycemia (66,68), and CoA transferase deficiency in humans manifests as spontaneous pediatric ketoacidosis (80,81,98), which is associated with hypoglycemia in severe cases, and may account for a subset of cases of idiopathic ketotic hypoglycemia (79,102). Germline SCOT-KO mice, which cannot terminally oxidize ketone bodies in any tissue, universally die within 48 hr of birth due to hyperketonemic hypoglycemia (78). Here we use novel genetic mouse models of gain- and loss-of-CoA transferase function to determine whether ketone body oxidation is required within specific cell types for metabolic adaptation and survival during the neonatal period and in adult starvation.

Materials and Methods

Animals. *Oxct1*^{-/-} (germline SCOT-KO) mice were previously generated by using targeted C57BL/6 mouse embryonic stem cells obtained from the NIH-Knockout Mouse Project (clone EPD0082-1-CO2), which were obtained and injected into C57BL/6 blastocysts in house (78). Transgenic mice that overexpress CoA transferase in cardiomyocytes (SCOT-Heart-OVEX mice) were generated on the C57BL/6 background. Murine *Oxct1* cDNA was sub-cloned downstream of the α -MHC (myosin heavy chain, *Myh6*) promoter (282), and after liberation of vector sequences, the expression cassette (**Fig. 3.1A**) was purified and injected into the male pronucleus of fertilized oocytes prior to implantation. One founder strain expressing the transgene was obtained, and these SCOT-Heart-OVEX mice are viable, fertile, and indistinguishable from wild-type littermates. SCOT-Heart-OVEX mice were successively crossed to *Oxct1*^{+/-} mice to generate α -MHC-*Oxct1*;*Oxct1*^{-/-} mice (SCOT-Heart-OVEX; SCOT-KO mice).

The targeting construct for the gene that encodes CoA transferase, *Oxct1*, permitted a ‘germline knockout first’ (283) approach that allows subsequent generation of a conditional ‘floxed’ allele. To generate tissue-specific SCOT-KO mice, *Oxct1*^{+/-} mice were first crossed to C57BL/6 mice that ubiquitously express Flp recombinase (β-actin-Flp, Jackson Laboratory) to generate *Oxct1*^{+/*lox*} mice, through germline recombination. An additional round of breeding yielded *Oxct1*^{*lox/lox*} mice (**Fig. 3.1B**). *Oxct1* exon 6 contains 107 nucleotides, which in the *Oxct1*^{*lox*} allele (which encodes functional CoA transferase) is flanked by *loxP* recognition sequences for Cre recombinase. Therefore, when excised by cell type-specific Cre recombinase, the recombination event results in a nonsense coding mutation. See **Table 3.1** for a list of primers used for genotyping.

Cardiomyocyte-, skeletal muscle-, or neuron-specific SCOT-KO mice were generated by successive rounds of breeding of *Oxct1*^{*lox/lox*} mice independently to three strains expressing Cre recombinase, each on the C57BL/6 background: *α-MHC-Cre*, *HSA-Cre* (human skeletal muscle actin promoter), or *Synapsin I-Cre*, respectively (284-286). Each of these strains effects cell type-specific recombination through *loxP* recognition sites by embryonic day (E)12.5 (284-287). In addition, *Synapsin I-Cre* mediates recombination of floxed alleles in the male germline (288). This facilitated generation of SCOT-Neuron-KO mouse lines with either one (*lox/rec*) or two (*lox/lox*) functional *Oxct1* alleles in the germline (**Fig. 3.1B**). Mice with the germline *lox/rec* genotype are functionally whole-body heterozygotes, and germline *lox/lox* mice are functionally wild-type mice.

Unless otherwise noted, all mice were maintained on standard polysaccharide-rich chow diet (Lab Diet 5053) and autoclaved water *ad libitum*. For the ketogenic diet studies, mice were maintained for two weeks on a low protein, very low carbohydrate, and high fat ketogenic diet (Bio-Serv F3666) in which 94.1% of calories are from fat, 4.6% from protein, and 1.3% from carbohydrates. Lights were off between 1800 and 0600. All postnatal day (P)0 (*i.e.*, the first day of extrauterine life) litters were obtained at 0900 and tissues and blood were harvested mid-morning. Mice were housed in groups of 3-5 for fasting experiments on sawdust bedding. Fasting and ketogenic diet were initiated in six week-old male mice. All

experiments were conducted using protocols approved by the Animal Studies Committee at Washington University.

CoA transferase activity assay. CoA transferase enzymatic activity was measured in neonatal tissue lysates using an adapted protocol (92). Neonatal tissues were collected and snap frozen in liquid nitrogen and stored at -80° C until processing. Tissues were homogenized in phosphate-buffered saline (PBS, pH 7.2) with protease inhibitors (complete mini EDTA-free protease inhibitor cocktail, Roche) in a glass dounce homogenizer on ice. Lysates were centrifuged at 20,000 x g at 4° C for 20 min and supernatants were used as a source of CoA transferase. Assays contained 100 µg protein (determined by Micro BCA Protein Assay Kit, Thermo Scientific) in a final volume of 100 µL, consisting of 50 mM Tris-HCl pH 8.5, 10 mM MgCl₂, and 4 mM iodoacetamide. Absorbance at 313 nm, at which AcAc-CoA absorbs maximally, was followed in unstimulated and stimulated (1 mM succinyl-CoA + 10 mM AcAc) replicates for 2 min and normalized to an AcAc-CoA standard curve to determine rates of AcAc-CoA production. Base hydrolysis of ethyl-AcAc (Sigma W241512) was performed by addition of 50% NaOH to pH 12 and incubation at 60° C for 30 min. Base hydrolyzed AcAc was adjusted to pH 8.5, and [AcAc] was confirmed using standard biochemical assays coupled to colorimetric substrates (Wako), as described previously (51).

Serum metabolite measurements. Measurements of serum AcAc, D-βOHB, free fatty acids, and glucose were performed using standard biochemical assays coupled to colorimetric substrates (Wako), as described previously (51). AcAc concentrations were determined by measuring total ketone body (TKB) concentrations and subtracting the corresponding measured D-βOHB concentration. Neonatal blood glucose was measured in duplicate using glucometers (Aviva).

Gene expression analysis. Quantification of gene expression was performed using real-time RT-quantitative PCR using the ΔΔCt approach as described, normalizing to *Rpl32*, using primer sequences listed within **Table 3.2** (51).

Immunoblotting. Lysates from neonatal brain, heart, and quadriceps/hamstring muscles were generated in a protein lysis buffer: 20 mM Tris-HCl, 150 mM NaCl, 1 mM EDTA, 1% Triton X-100, 1% phosphatase inhibitor cocktail (Sigma), and protease inhibitor cocktail (complete mini EDTA-free, Roche), pH 7.5. Immunoblots to detect CoA transferase (rabbit anti-SCOT, Proteintech Group) and actin (rabbit anti-actin, Sigma) were performed as described (78). Band intensities were quantified densitometrically using QuantityOne software (Bio-Rad). For hippocampal immunoblots, brains were rapidly isolated and hippocampal dissections were performed in PBS on ice using a dissecting microscope.

In vivo substrate utilization. Neonatal mice were injected intraperitoneally with 10 μ mol [1- 13 C]glucose (Cambridge Isotope Laboratories) per g of body weight. After 30 min incubation durations, neonatal mice were killed by decapitation, and tissues were rapidly freeze-clamped in liquid N₂. Neutralized and lyophilized perchloric acid extracts were profiled using gradient heteronuclear single-quantum correlation [13 C]edited proton nuclear magnetic resonance (NMR) measured at 11.75 T. Signals were collected from extracts dissolved in 275 μ L D₂O + 1 mM trimethylsilyl propionate, loaded into high precision, thin walled 5-mm tubes (Shigemi). Quantification of integrals of carbon 2 of [13 C]taurine (a normalizing metabolite whose tissue concentrations were constant across conditions and which is not enriched by administration of these substrates), [13 C]lactate (carbon 2), and [13 C]glutamate (carbon 4) was performed as described previously (78).

Measurements of body composition. Percent body fat and lean body mass were determined in awake adult animals using an EchoMRI instrument (Echo Medical Systems, Houston, TX).

Results

Restoration of myocardial ketone body oxidation in germline SCOT-KO mice does not prevent lethal hyperketonemic hypoglycemia. Tissues that lack CoA transferase protein and activity cannot terminally oxidize ketone bodies, and germline SCOT-KO mice invariably die within 48 hr of birth due to lethal hyperketonemic hypoglycemia (78). Myocardium is the highest ketone body consumer per unit mass (2,43,76). To determine if selective restoration of myocardial CoA transferase activity was sufficient to

prevent lethal hyperketonemic hypoglycemia in SCOT-KO mice, transgenic mice harboring *Oxct1* cDNA under control of the α -MHC promoter (*α -MHC-Oxct1*) were successively bred to *Oxct1*^{+/-} heterozygous mice to ultimately yield SCOT-Heart-OVEX; SCOT-KO mice (**Fig. 3.1**). Selective restoration of CoA transferase expression and activity on the first postnatal day, P0, was confirmed by immunoblot (**Fig. 3.2A**) and CoA transferase enzyme activity assays (**Fig. 3.2B**) using neonatal tissue extracts. Despite restoration of myocardial CoA transferase activity to a magnitude that modestly exceeded wild type levels, SCOT-Heart-OVEX; SCOT-KO mice still develop hyperketonemic hypoglycemia with abnormally elevated AcAc/D- β OHB serum ratios (**Fig. 3.2C-D**). Genotypic analysis of > 25 litters derived from *α -MHC-Oxct1*; *Oxct1*^{+/-} crosses did not yield any SCOT-Heart-OVEX; SCOT-KO mice after P1 (data not shown), indicating that neonatal lethality ensues despite restoration of myocardial ketolysis in germline SCOT-KO mice.

Tissue-specific CoA transferase knockout mice are viable. To mechanistically dissect the energetic roles of ketone body oxidation in individual tissues, we individually eliminated CoA transferase from the three cell types most adapted to ketone body oxidation (2,76) – cardiomyocytes, skeletal myocytes, and neurons – to generate SCOT-Heart-KO, SCOT-Muscle-KO, and SCOT-Neuron-KO mice, respectively (see **Fig. 3.1B**). Tissue-specific loss of CoA transferase protein was confirmed in each tissue-specific mouse strain on P0 by immunoblot and CoA transferase activity assay (**Fig. 3.3A-C**). CoA transferase is present and active in astrocytes (70,289), and likely explains residual enzymatic activity in brains of SCOT-Neuron-KO neonates (**Fig. 3.3C**). Absence of CoA transferase in neurons of SCOT-Neuron-KO mice was further confirmed by immunoblot of protein lysates derived from adult hippocampi (hippocampus exhibits an increase in neuronal density relative to other brain regions) (**Fig. 3.3D**). Each tissue-specific SCOT-KO mouse strain is viable, exhibits normal body size (see below), and is fertile. Unlike germline SCOT-KO mice, which develop neonatal hyperketonemic hypoglycemia with abnormally elevated plasma AcAc/ β OHB ratios by the second postnatal day (P1) [**Fig. 3.2C** and ref (78)], tissue-specific SCOT-KO neonatal mice do not exhibit hypoglycemia, marked hyperketonemia, or abnormal ratios of serum AcAc/ β OHB (**Fig. 3.4A-B**). The *Synapsin-1-Cre* transgene, used to generate

SCOT-Neuron-KO mice, also mediates recombination of floxed alleles within the male germline, resulting in a null (*rec*) allele (**Fig. 3.1B**), which is transmitted to most progeny (288). This enabled generation of SCOT-Neuron-KO and control mice with either one (*flox/rec*) or two (*flox/flox*) functional *Oxct1* alleles in the germline. Hypoglycemia and hyperketonemia do not develop in neonatal *flox/rec* mice (**Fig. 3.4**), consistent with previous observations of neonatal *Oxct1*^{+/-} mice (78). Of the three tissue-specific models of CoA transferase deficiency, only SCOT-Neuron-KO mice develop mild hyperketonemia on P1 (mean serum total ketone body concentrations 0.85 ± 0.05 mM vs. 1.60 ± 0.25 mM, in *flox/flox* control and SCOT-Neuron-KO mice on the *flox/flox* germline background, respectively, n = 5-8 per group, *p* < 0.001) (**Fig. 3.4B**). On P1, ketonemia did not differ between SCOT-Neuron-KO mice on the *flox/flox* and *flox/rec* germline backgrounds (**Fig. 3.4B**). Furthermore, unlike the large increase in AcAc/βOHB ratios of germline SCOT-KO mice compared to littermate controls (**Fig. 3.2C**), these ratios did not significantly differ in any of the tissue-specific models (**Fig. 3.4B**).

Neuronal CoA transferase deficiency results in increased glucose utilization in the neonatal brain. Because brains of neonatal germline SCOT-KO mice exhibit increased glucose oxidation (78), we quantified the fates of [¹³C]glucose in brains of P2 SCOT-Neuron-KO mice (*flox/rec* background) and genotype control mice, and observed increased glycolytic and oxidative metabolism of glucose in brains SCOT-Neuron-KO mice: [¹³C]lactate abundance, a reporter of glycolytic metabolism, was 2.31 ± 0.45 fold greater (*p* < 0.05, n = 4/group **Fig. 3.5A**), and [¹³C]glutamate abundance, which quantitatively reports the rate of entry of [¹³C]acetyl-CoA into the TCA cycle for terminal oxidation (136), was 2.11 ± 0.29 fold greater in SCOT-Neuron-KO mice, compared to *flox/rec* control neonatal mice (*p* < 0.05, n = 4/group; **Fig. 3.5B**). Nevertheless, SCOT-Neuron-KO mice remain euglycemic (**Fig. 3.4A**) and do not exhibit molecular signatures of enhanced hepatic gluconeogenesis [expression of the mRNA encoding phosphoenolpyruvate carboxykinase (*Pck1*) is normal in livers of SCOT-Neuron-KO mice], or altered ketogenesis (hepatic *Hmgcs2* and *Bdh1* expression were also normal, **Fig. 3.5C**).

Oxidation of ketone bodies within neurons, cardiomyocytes, and skeletal myocytes is dispensable during moderate starvation in the adult. Ketone body metabolism supports bioenergetic homeostasis when

carbohydrate supply is limited, such as in starvation, by providing an alternative fuel source to energy sensitive tissues (2,4). To directly test the hypothesis that individual tissues require ketone bodies for energy transfer to support survival and glycemia in the post-absorptive state, SCOT-Neuron-KO (on the *flox/flox* and *flox/rec* germline backgrounds), SCOT-Heart-KO, and SCOT-Muscle-KO mice were fasted for 48h. Surprisingly, none of these tissue-specific SCOT-KO mouse strains exhibited fasting-induced hypoglycemia, compared to fasted genotype- and age-matched control mice (**Fig. 3.6A**). While SCOT-Muscle-KO and SCOT-Neuron-KO mice exhibit hyperketonemia compared to SCOT-Heart-KO and *flox/flox* control mice (**Fig. 3.6B**), mice from each of these strains exhibited normal serum AcAc/D- β OHB ratios after a 48h fast (**Table 3.3**) and normal fasting-induced weight loss (**Fig. 3.6C**). In addition, adult SCOT-Neuron-KO mice on the *flox/flox* and *flox/rec* backgrounds are metabolically indistinguishable during moderate starvation: these SCOT-Neuron-KO mouse strains do not differ in serum ketone body concentrations, blood glucose, body weight, or serum AcAc/D- β OHB ratios during fasting (**Fig. 3.6 and Table 3.3**). Conversely, germline *flox/rec* mice with intact neuronal CoA transferase do develop hyperketonemia relative to *flox/flox* control mice at 48h starvation (**Fig. 3.6B**). Taken together, these results indicate that ketone body oxidation is not required for energy transfer at the cellular or tissue level in the post-absorptive state for survival or preservation of glycemia.

Relative deficiency of ketone body oxidation influences the response to a chronic ketogenic nutrient milieu. While tissue-specific SCOT-KO models have utility in determining the metabolic roles of ketolysis within individual tissues, naturally-occurring variations in ketone body oxidative capacity in humans likely affect all ketolytic cell types (79-81,97,101,148,149,290). Germline CoA transferase heterozygous (*Oxct1*^{+/-}) mice are metabolically indistinguishable from *Oxct1*^{+/+} (wild-type) littermates in the ketogenic neonatal period, despite ~50% diminution of CoA transferase protein abundance in *Oxct1*^{+/-} mice (78). To determine if metabolic abnormalities emerge in adult mice with ubiquitous, but partial, reduction of catalytically active CoA transferase, wild type and *Oxct1*^{+/-} littermate mice were exposed to ketogenic milieus at six weeks of age. First, to measure the consequences of acute ketosis, male *Oxct1*^{+/-} and wild type littermate control mice were subjected to a 48h period of starvation. Body composition and

total body weight was not different between genotypes at the onset of fasting: body fat percentage was $16.7 \pm 0.2\%$ in wild type mice vs. $16.3 \pm 0.3\%$ in *Oxct1*^{+/-} mice; n = 6/group, and mice from each genotype exhibited equivalent weight loss during the fast (**Fig. 3.7A**). As expected, fasting induces ketosis in both genotypes, but *Oxct1*^{+/-} mice developed greater ketonemia than control mice after 24 and 48h of fasting, consistent with a global reduction in ketone body oxidative capacity (**Fig. 3.7B**). Serum AcAc/D-βOHB ratios were not different between *Oxct1*^{+/-} and control mice after 48 hr of fasting (**Table 3.3**). Furthermore, fasting serum glucose and free fatty acid concentrations did not significantly differ between genotypes (**Fig. 3.7C-D**). Next, to determine if reduced ketone body oxidative capacity impairs adaptation to a chronic ketogenic nutrient milieu, we placed *Oxct1*^{+/-} and littermate control mice on a low protein, very low carbohydrate, and high fat ketogenic diet that has been extensively used by our lab and others to study ketotic states in mice (51,53,126,291-295). Adherence to this diet for 2 weeks induces ketosis in both genotypes, but ketonemia was nearly three-fold greater in *Oxct1*^{+/-} mice (**Fig. 3.7E**). Furthermore, compared to wild type controls, ketogenic diet-fed *Oxct1*^{+/-} mice exhibited relative hypoglycemia (**Fig. 3.7F**). Taken together, these results indicate that partial ketolytic defects become metabolically evident after brief periods of nutrient deprivation and upon adherence to low carbohydrate diet regimens.

Discussion

We have used novel mouse models of CoA transferase deficiency to demonstrate that the inability to oxidize ketone bodies individually within neurons, cardiomyocytes, or skeletal myocytes does not impair the ability of mice to survive the ketogenic neonatal period, or moderate-length durations of starvation in the adult. However, transgene-mediated restoration of myocardial ketone body oxidation in an animal lacking the ability to oxidize ketone bodies elsewhere does not prevent lethal hyperketonemic hypoglycemia in the neonatal period. Taken together, these results support the notion that organism-wide CoA transferase activity provides a ketolytic reservoir that is required to maintain bioenergetic homeostasis in states of diminished carbohydrate intake, and that no single organ or cell type exhibits an

obligate energetic requirement for ketone body oxidation to support survival or preserve glycemia under the conditions tested. The inability of SCOT-Heart-OVEX; SCOT-KO mice to survive the ketogenic neonatal period, and the mild hyperketonemic hypoglycemia exhibited by adult *Oxct1*^{+/-} mice maintained on a ketogenic diet indicate that incremental defects of the global ketolytic reservoir has significant impact on metabolic homeostasis in ketogenic milieus.

Of the tissue-specific SCOT-KO mouse strains examined in the neonatal period, only SCOT-Neuron-KO mice develop mild hyperketonemia, which supports previous observations indicating that neurons are a significant consumer of ketone bodies in the neonatal period (71,105). Moreover, loss of ketone body oxidation within neurons increases glycolysis and oxidative metabolism of glucose, strongly suggesting that ketolytic impairment in neurons requires additional glucose to meet the energetic demands of the neonatal brain. Given the relative inability of neurons to oxidize fatty acids for energy (69,70), increased cerebral consumption of glucose in SCOT-Neuron-KO neonates is not unexpected. The liver is the most important source of glucose for the neonatal brain, which normally accounts for 60-70% of total energy expenditure in this period, even though the neonatal brain only comprises 10% of total body weight (2,71). Loss of terminal ketone body oxidation in neurons may therefore increase the liver's glucogenic burden. Increased hepatic glucose production may initially be met through increased glycogenolysis, although hepatic glycogen stores are normally depleted rapidly after birth (20). Furthermore, gluconeogenic gene expression markers were not increased in livers of SCOT-Neuron-KO mice, suggesting that counterregulatory programs are not engaged in these mice. Thus, an alternative explanation for preservation of euglycemia in newborn SCOT-Neuron-KO mice is that ketone body oxidation within tissues that remain competent to terminally oxidize ketone bodies spares glucose for the neonatal brain.

As in the neonatal period, ketone body oxidation subsumes an important role in energy transfer in the post-absorptive state (2,4). Interestingly, in mice subjected to 48h starvation, survival is maintained and glycemia is preserved when ketone body oxidation is individually eliminated from neurons, cardiomyocytes, or skeletal myocytes. However, in this state, SCOT-Muscle-KO and SCOT-Neuron-KO

mice exhibit hyperketonemia compared to fasted SCOT-Heart-KO and control strains. Hyperketonemia in these two models suggests that skeletal muscle and neurons each provide a major component of the ketolytic reservoir in the adult, consistent with previous observations indicating that ketone body oxidation can account for as much as two-thirds of cerebral metabolism during starvation (2,296). Due to bioethical considerations, these studies were not designed to determine if tissue-specific energetic requirements for ketone body oxidation emerge in extremes of starvation. Nevertheless, it is striking that animals challenged to a ketotic 48h fast, during which ~25% of total body weight is lost, do not require ketone body oxidation in neurons, cardiomyocytes, or skeletal myocytes for survival or maintenance of glycemia. In particular, SCOT-Neuron-KO mice on the *flox/rec* germline background have lost a substantial proportion of total ketone body oxidative capacity. Nonetheless, these mice do not exhibit greater starvation-induced ketonemia than SCOT-Neuron-KO mice on the *flox/flox* germline background, despite the fact that germline *flox/rec* (functionally whole-body heterozygote) mice, which have preserved neuronal ketolytic capacity, manifest greater starvation-induced ketonemia than *flox/flox* (functionally wild-type) mice with normal neuronal ketolytic capacity (**Figs. 3.6B, 3.7B**). Therefore, as dynamic variation of glucose metabolism occurs in these models, as described above, dynamic variations of both ketogenic and ketolytic capacity are likely to occur in mice on these genetic backgrounds to meet the collective energetic demands of all tissues.

In contrast to genetic animal models of tissue-specific ketolytic deficiency, sporadic CoA transferase deficiency in humans likely affects all cells that oxidize ketones. Studies of CoA transferase deficient infants and their parents reveal that heterozygous carriers for loss-of-function *OXCT1* mutations exhibit reduced CoA transferase enzymatic activity (290). Thus, we subjected germline adult *Oxct1*^{+/-} mice to a series of ketogenic provocations. Compared to wild type littermate controls, *Oxct1*^{+/-} mice developed hyperketonemia upon fasting, but glycemia was preserved. Prospectively, hypoglycemia may ensue in *Oxct1*^{+/-} mice at the extremes of starvation, when readily-available gluconeogenic substrate pools are depleted to meet the increased gluconeogenic demand imposed by ketolytic insufficiency. This notion is supported by the hyperketonemic hypoglycemic response of *Oxct1*^{+/-} mice maintained on a low protein,

very low carbohydrate, and high fat ketogenic diet for 2 weeks. These findings suggest that latent ketolytic defects may emerge in humans upon introduction to ketogenic nutrient milieus. Indeed, case reports indicate sporadic but rapid development of severe hyperketonemia with modest durations of nutrient deprivation or upon adherence to Atkins-style ketogenic diets for weight loss (278,279). Because ketogenic diets are increasingly employed for treatment of obesity, nonalcoholic fatty liver disease, and neurological diseases including epilepsy, attentiveness to latent ketolytic insufficiency, and the possibility of functional consequences of single nucleotide polymorphisms in loci that encode and regulate the enzymatic mediators of ketone body oxidation, is warranted.

While these studies indicate that cell-type specific preservation of ketone body oxidation is not required for survival of the murine neonatal period or a moderate degree of starvation in the adult mouse, these tissue-specific models will also permit highly-penetrating analyses of the diverse bioenergetic roles that ketone body oxidation plays through physiological and pathophysiological states relevant to each tissue. For example, within the heart, cardiomyocytes oxidize ketone bodies in proportion to their delivery, at the expense of fatty acid oxidation and glucose oxidation (90,117,121-127). Compared to fatty acids, oxidation of ketone bodies is more energetically efficient. Unlike fatty acid oxidation, all of the reducing equivalents generated by ketone body oxidation are delivered through NADH to complex I within the electron transport chain (ETC). In addition, oxidation of ketone bodies increases the redox span between complexes I and III by keeping mitochondrial ubiquinone oxidized. This increases the potential energy of the mitochondrial proton gradient, thereby yielding more energy available for ATP synthesis per molecule of oxygen invested, improving the energetic efficiency of ketone bodies, and attenuating production of reactive oxygen species by the ETC (95,96,128,297). Furthermore, numerous studies indicate prospective therapeutic applications of harnessing the benefits of ketone body metabolism in neurons and astrocytes within the central nervous system (9,221,289,298). Therefore, these new models provide opportunities for metabolic and bioenergetic dissection of both ketone body metabolism and CoA transferase function in disease pathogenesis relevant to each organ.

The ability to derive conclusions from tissue-specific loss-of-function models is a function of the spatiotemporal fidelity of the gene inactivation system employed. The Cre-expressing strains used in this study effect robust and cell-type-specific recombination during mouse embryogenesis (284-287,299). *HSA-Cre* expresses Cre recombinase in a pan-fiber type distribution of skeletal myocytes; *α -MHC-Cre* drives the expression of the recombinase abundantly and specifically within cardiac myocytes, and the *Synapsin1-Cre* model was selected because it specifically expresses Cre recombinase in a pan-neuronal manner. Nevertheless, the complexity of the central and peripheral nervous systems is reflected by the >40 Cre-expressing mouse strains that are employed to target select neuronal and glial populations (300). Thus, it is likely that novel phenotypes will emerge from study of CoA transferase deficiency through use of other strains expressing Cre recombinase in other experimental settings. Finally, loss of CoA transferase during embryogenesis may promote adaptation to the absence of terminal ketone body oxidation, prospectively limiting the emergence of robust phenotypes in adult tissue-specific SCOT-KO mice. Use of conditionally-induced Cre expressing strains will support further insight into the metabolic consequences of ketolytic insufficiency in the adult animal.

In conclusion, we demonstrate that, to sustain survival and glycemia during moderate-duration starvation, ketone body oxidation is not required for energy transfer in the three cell types that exhibit the greatest capacity to oxidize ketone bodies: neurons, skeletal myocytes, and cardiomyocytes. However, diminished ketone body oxidative capacity predisposes to metabolic abnormalities, including the development of hyperketonemia during fasting, and hyperketonemic hypoglycemia upon adherence to a low carbohydrate, high fat diet. A minimum threshold of organism-wide ketone body oxidation must be maintained to preserve bioenergetic homeostasis and support compatibility with life.

Acknowledgments

The authors thank Jeffrey Milbrandt for helpful discussions, Laura Kyro for assistance with graphics, and Ashley Moll, Baris Ercal, and Charles Shyng for technical assistance. This work was supported in part by grants from the NIH DK091538 (to PAC), DK020579 (Diabetes Research Center), HL007873 (DGC),

HL007275 (RCS), and grants from the Diabetic Cardiovascular Disease Center at Washington University, and the March of Dimes (both to PAC).

Figure Legends

Fig. 3.1. Strategy for the generation of transgenic overexpresser and tissue-specific SCOT-KO mice.

(A) SCOT-Heart-OVEX mice. Mouse *Oxct1* cDNA was sub-cloned downstream of the α -MHC promoter to generate mice overexpressing CoA transferase specifically within cardiomyocytes. ATG, initiator methionine codon; TGA, stop codon; kb, kilobase; UTR, untranslated region. **(B)** Schematics depict the endogenous *Oxct1* mouse gene (**Wild-type**); targeted **Null** allele (the germline knockout allele); **Flox** allele, which encodes normal CoA transferase protein; and the recombined **Rec** (also a null) allele. Polyadenylation (pA) signals in the **Null** locus terminate transcription after exon 5, and a splice acceptor (SA)/internal ribosomal entry sequence (IRES) results in a truncated and catalytically inactive product from residual message. Flp recombinase recognition target (FRT) sites flank the β -gal and neomycin resistance cassettes and the pA signals. Thus, Flp recombinase mediates removal of the pA transcriptional stop signals and *lacZ*/neomycin cassette, restoring an active *Oxct1* **Flox** allele in the germline. Exon 6 is flanked by *loxP* recognition sequences in the **Flox** allele for cell type-specific Cre recombinase-mediated recombination and inactivation. Genotyping primers for each allele are indicated as horizontal arrows (see **Table 3.1** for sequences). β gal, β -galactosidase-encoding *lacZ* gene; β -act:neo, neomycin resistance gene driven by the β -actin promoter.

Fig. 3.2. Restoration of ketone body oxidative capacity selectively within cardiomyocytes of germline SCOT-KO mice.

(A) Immunoblot for CoA transferase (SCOT) and actin in myocardial protein lysates derived from P0 hearts of wild type mice, SCOT-KO mice with transgene mediated restoration of cardiomyocyte CoA transferase (SCOT-Heart-OVEX; SCOT-KO mice), and SCOT-KO mice. **(B)** CoA transferase activity was measured spectrophotometrically in tissue lysates derived from hearts of P0 wild-type and SCOT-KO mice, and hearts and brains of P0 SCOT-Heart-OVEX; SCOT-KO mice. n = 3/group. ***, p < 0.001 by linear regression *t* test vs. SCOT-Heart-OVEX; SCOT-KO heart. †††, p < 0.001 by

linear regression *t* test vs. wild type heart. **(C)** Serum ketone bodies (mM) in P1 wild type, SCOT-KO, SCOT-Heart-OVEX, and SCOT-Heart-OVEX; SCOT-KO mice. *n* = 5-6/ group; ***, *p* < 0.001; *, *p* < 0.05 for β OHB; †††, *p* < 0.001 for AcAc; †††, *p* < 0.001 for AcAc/D- β OHB ratio by 2-way ANOVA, compared to genotype control on the *Oxct1*^{+/+} (wild-type) background. **(D)** Blood glucose (mg/dL) in P1 mice. *n* = 4-6/group, ***, *p* < 0.001; *, *p* < 0.05 by 2-way ANOVA.

Fig. 3.3. Absence of CoA transferase protein and enzymatic activity in tissue-specific SCOT-KO mouse strains. CoA transferase activity was measured spectrophotometrically (left) in tissue lysates derived from **(A)** heart, **(B)** skeletal muscle (quadriceps/hamstrings), and **(C)** brains of P0 mice. *n* = 3-6/group. ***, *p* < 0.001 by linear regression *t* test. Brains of SCOT-Neuron-KO mice on both *flox/flox* and *flox/rec* genetic backgrounds were analyzed (depicted as *flox/x*). Immunoblots for CoA transferase (SCOT) and actin (right). **(D)** Immunoblot (left) and densitometric quantification (right) of CoA transferase protein abundance, normalized to actin in isolated hippocampi from adult SCOT-Neuron-KO mice. Brains of SCOT-Neuron-KO mice on both *flox/flox* and *flox/rec* genetic backgrounds were analyzed and did not reveal significant differences in CoA transferase protein abundances. ***, *p* < 0.001, **, *p* < 0.01, *, *p* < 0.05 by 1-way ANOVA. ns, not significant.

Fig. 3.4. Circulating metabolites in neonatal tissue-specific SCOT-KO strains. **(A)** Blood glucose (mg/dL) in P1 mice. **(B)** Serum AcAc and D- β OHB in P1 mice. *n* = 5-8/group. ***, *p* < 0.001; **, *p* < 0.01 for serum [ketone] vs. *flox/flox* by 1-way ANOVA. ††, *p* < 0.01 for serum [ketone] vs. *flox/rec* by 1-way ANOVA.

Fig. 3.5. Increased glucose consumption by brains of neonatal SCOT-Neuron-KO mice. **(A)** [¹³C]glucose labeling of lactate, a surrogate for glycolysis in brains of SCOT-Neuron-KO (on the *flox/rec* germline background) and control mice, 30 min after intraperitoneal injection of [¹³C]glucose into P2 animals. **(B)** ¹³C labeling of glutamate (surrogate for terminal oxidation in the TCA cycle) in these same cerebral extracts. *n* = 4/group. *, *p* < 0.05 by Student's *t* test. **(C)** Relative mRNA abundance of

gluconeogenic (*Pck1*) and ketogenic (*Hmgcs2*, *Bdh1*) genes in livers of P2 SCOT-Neuron-KO and control mice. n = 5/group.

Fig. 3.6. Adult tissue-specific SCOT-KO mice tolerate starvation. (A) Serum glucose, (B) serum total ketone bodies (TKB), and (C) body weight were measured in fasting SCOT-Heart-KO, Muscle-KO, Neuron-KO, and control adult mice after the indicated durations of nutrient withdrawal. ***, $p < 0.001$; **, $p < 0.01$; and *, $p < 0.05$, by 2-way ANOVA, compared to same genotype at 4 hr. †††, $p < 0.001$; ††, $p < 0.01$ by 2-way ANOVA, compared to *flox/flox* at same time point. †††, $p < 0.001$ by 2-way ANOVA, compared to *flox/rec* control; $n \geq 6$ /group for each measurement at all time points and for each genotype.

Fig. 3.7. Diminished total body ketone body oxidative capacity impairs adaptation to ketotic nutrient states. Metabolic parameters were measured in six week-old *Oxct1*^{+/-} and *Oxct1*^{+/+} (wild-type littermate control) male mice subjected to ketotic nutrient states. (A) Total body weight, (B) total serum ketone bodies (TKB), (C) serum glucose, and (D) serum free fatty acids (FFA) were measured in fasting mice. (E) Total serum ketone bodies and (F) serum glucose were also measured in eight week-old male *Oxct1*^{+/-} and littermate *Oxct1*^{+/+} (wild-type) mice maintained either on a standard polysaccharide rich (Chow) diet or low protein, low carbohydrate, high fat ketogenic diet (KD) for two weeks. n = 7/group; ***, $p < 0.001$; **, $p < 0.01$; *, $p < 0.05$, by 2-way ANOVA.

Figure 3.1

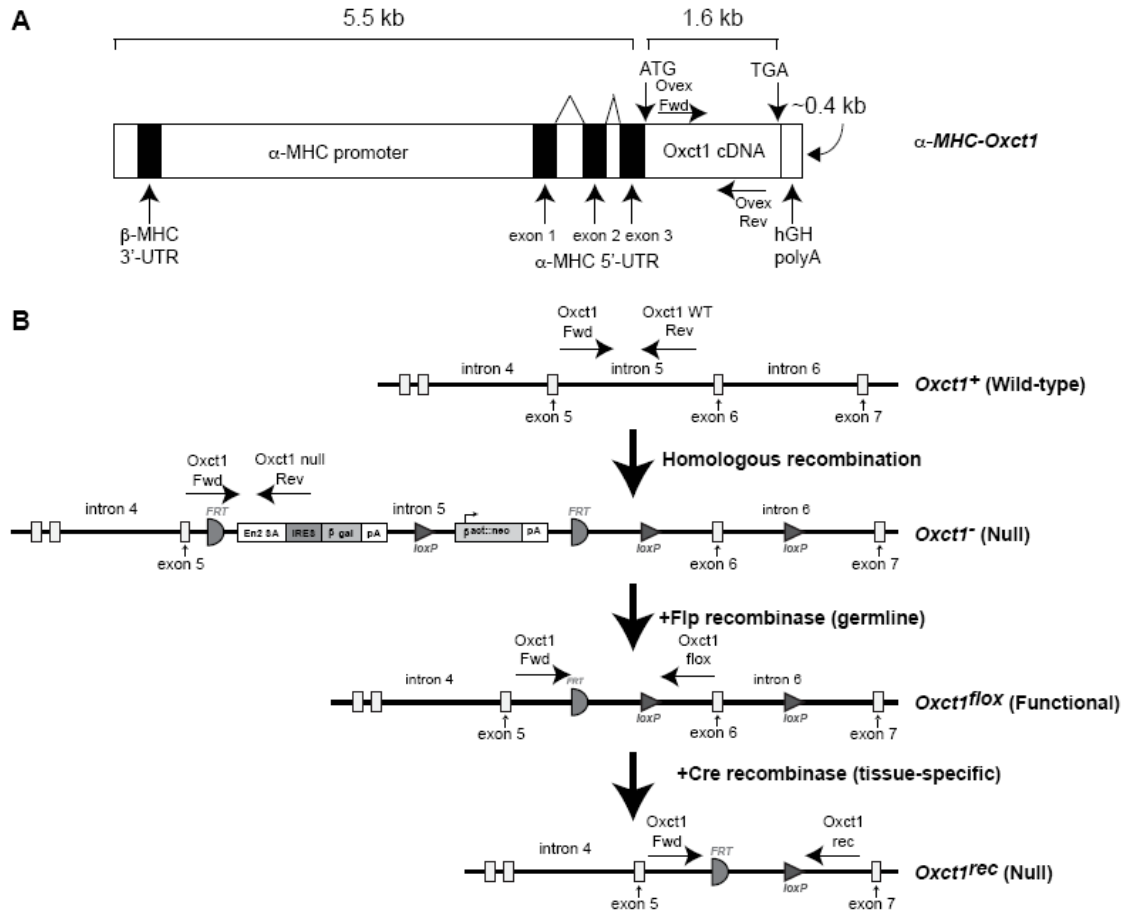


Figure 3.2

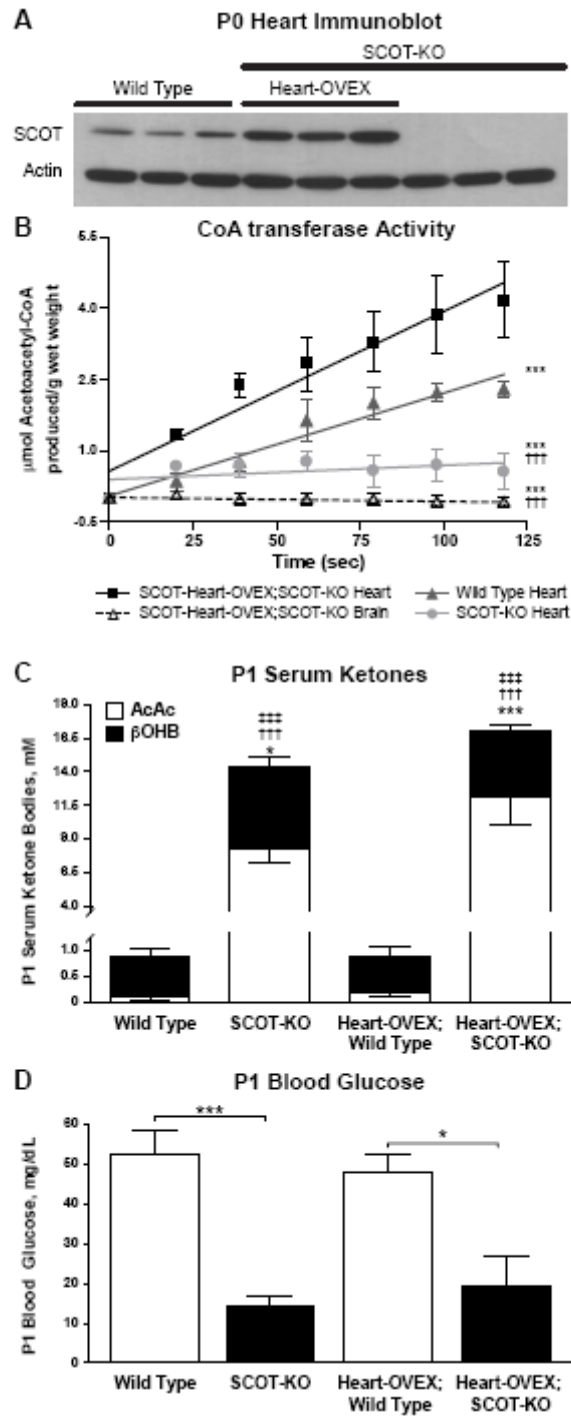
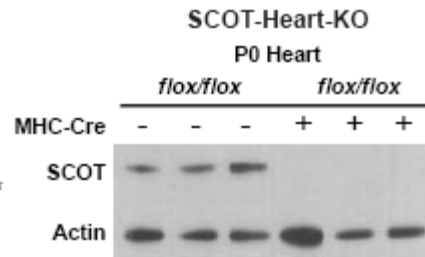
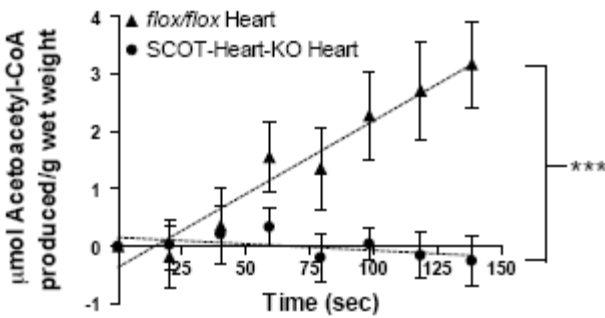
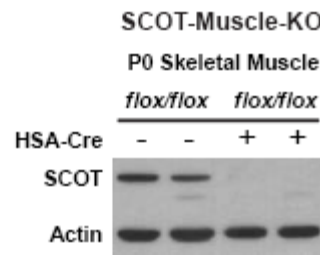
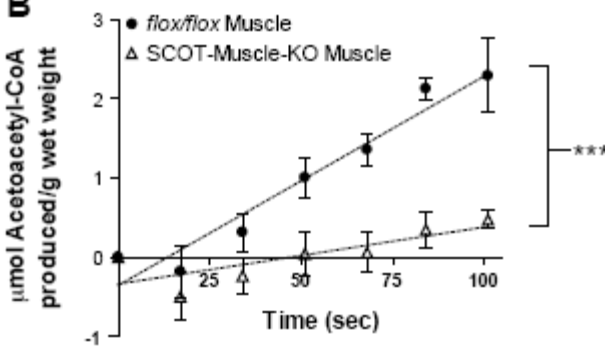


Figure 3.3

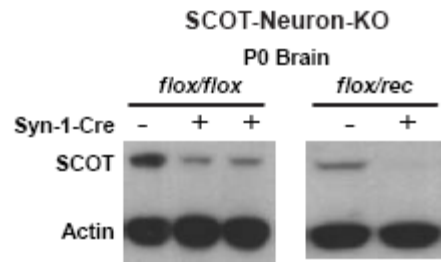
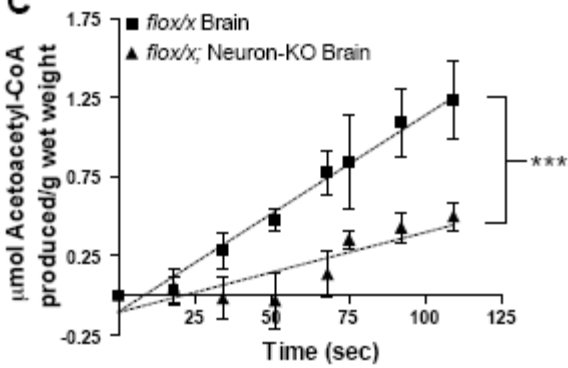
A



B



C



D

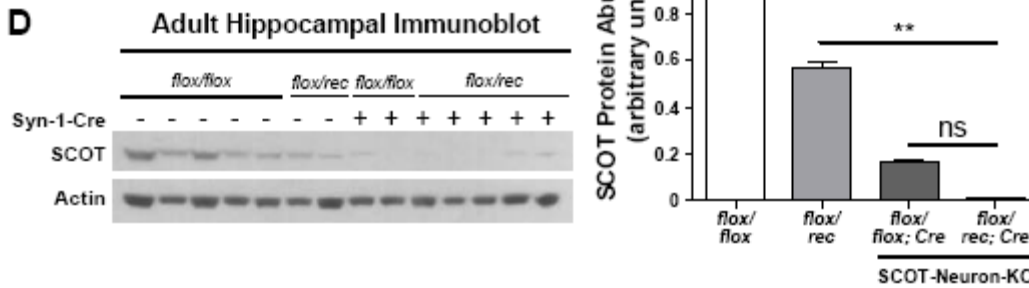


Figure 3.4

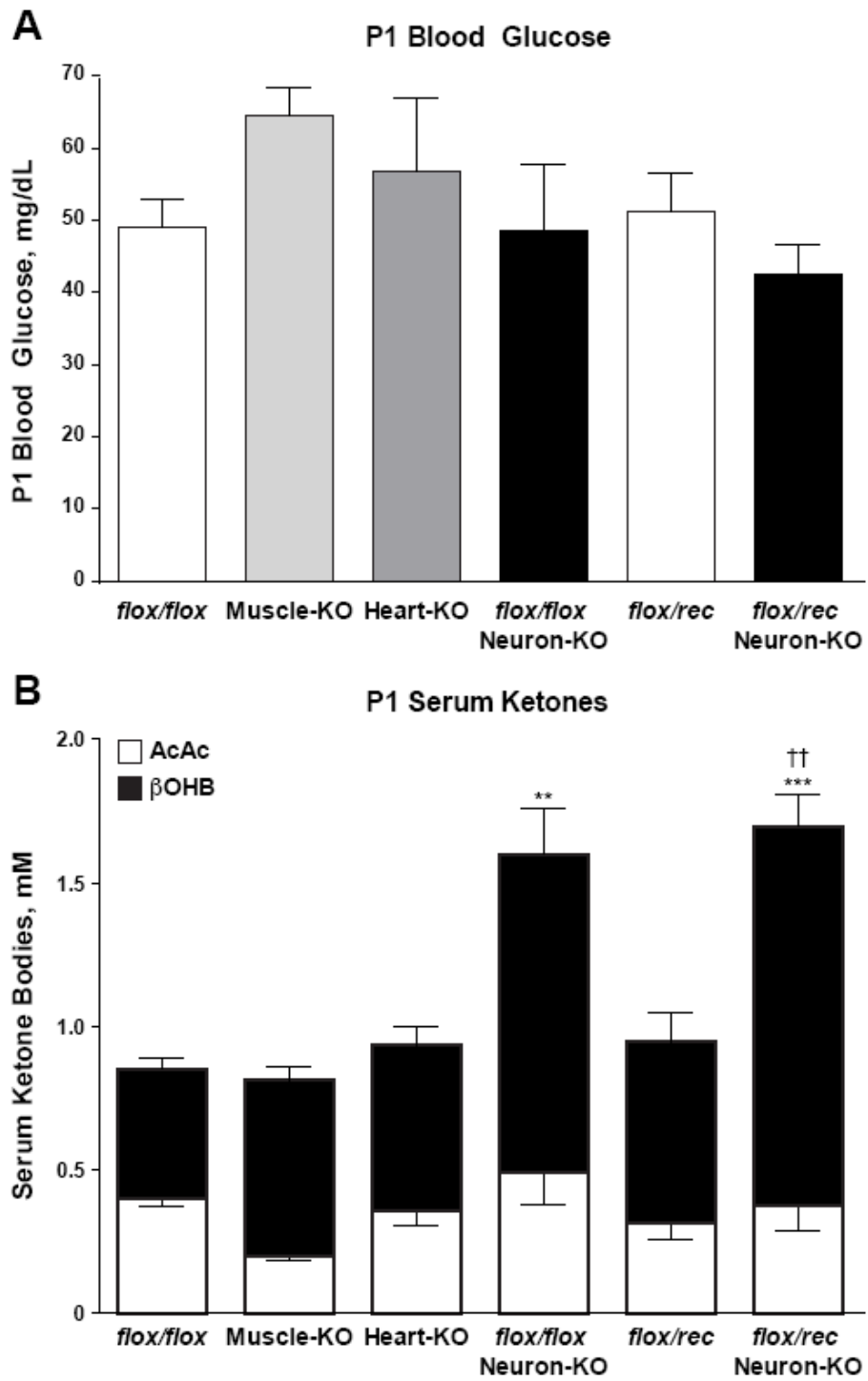


Figure 3.5

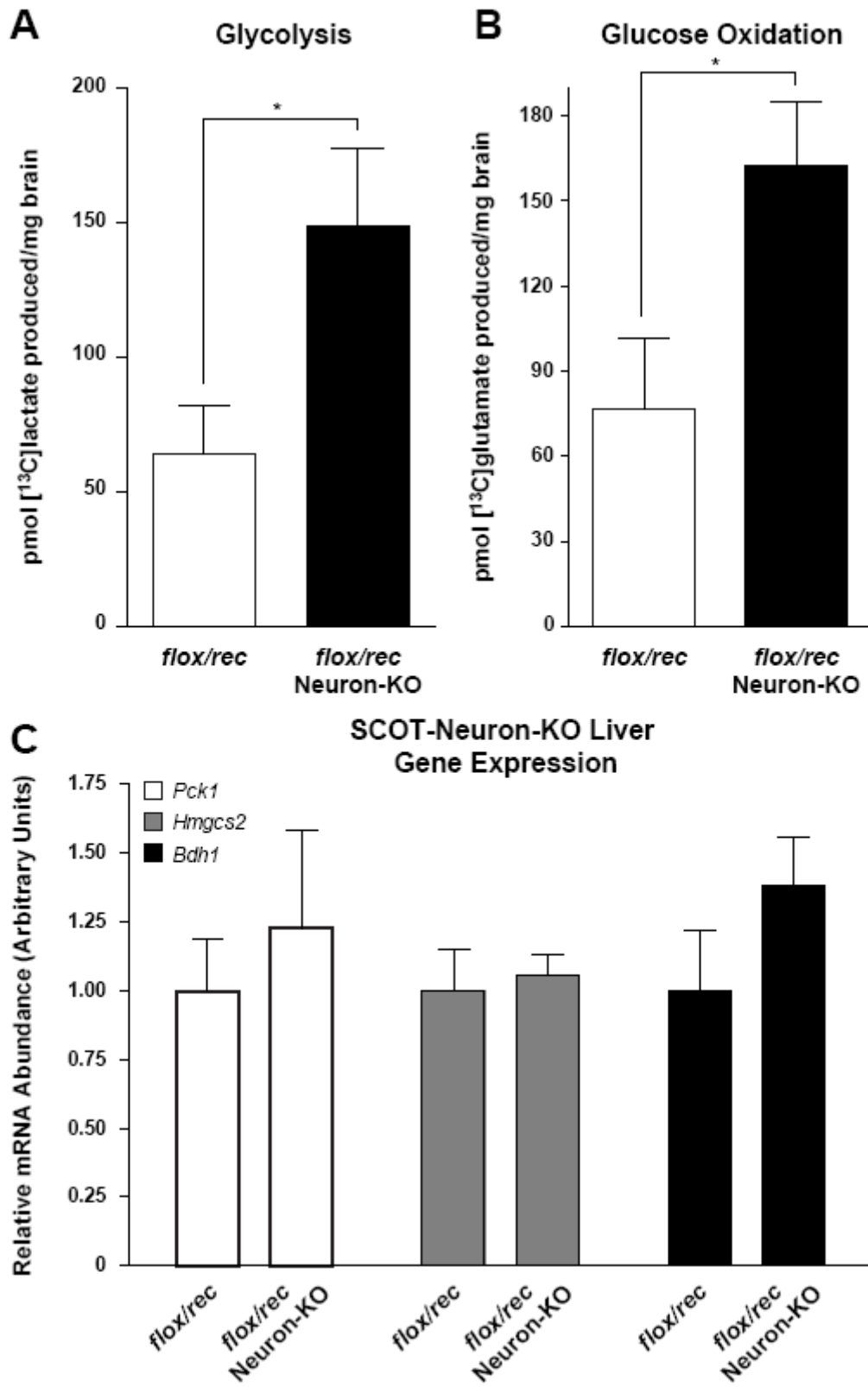


Figure 3.6

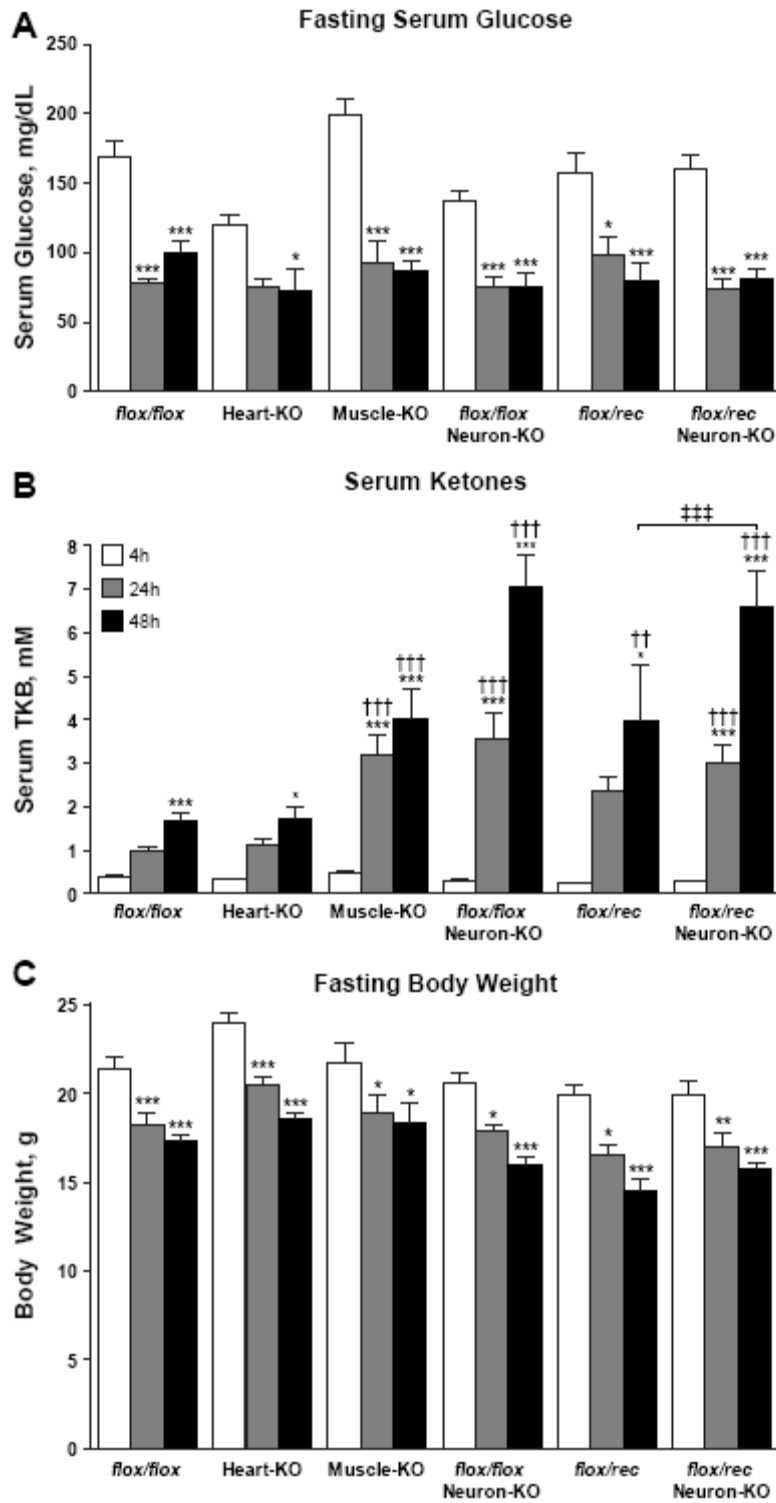


Figure 3.7

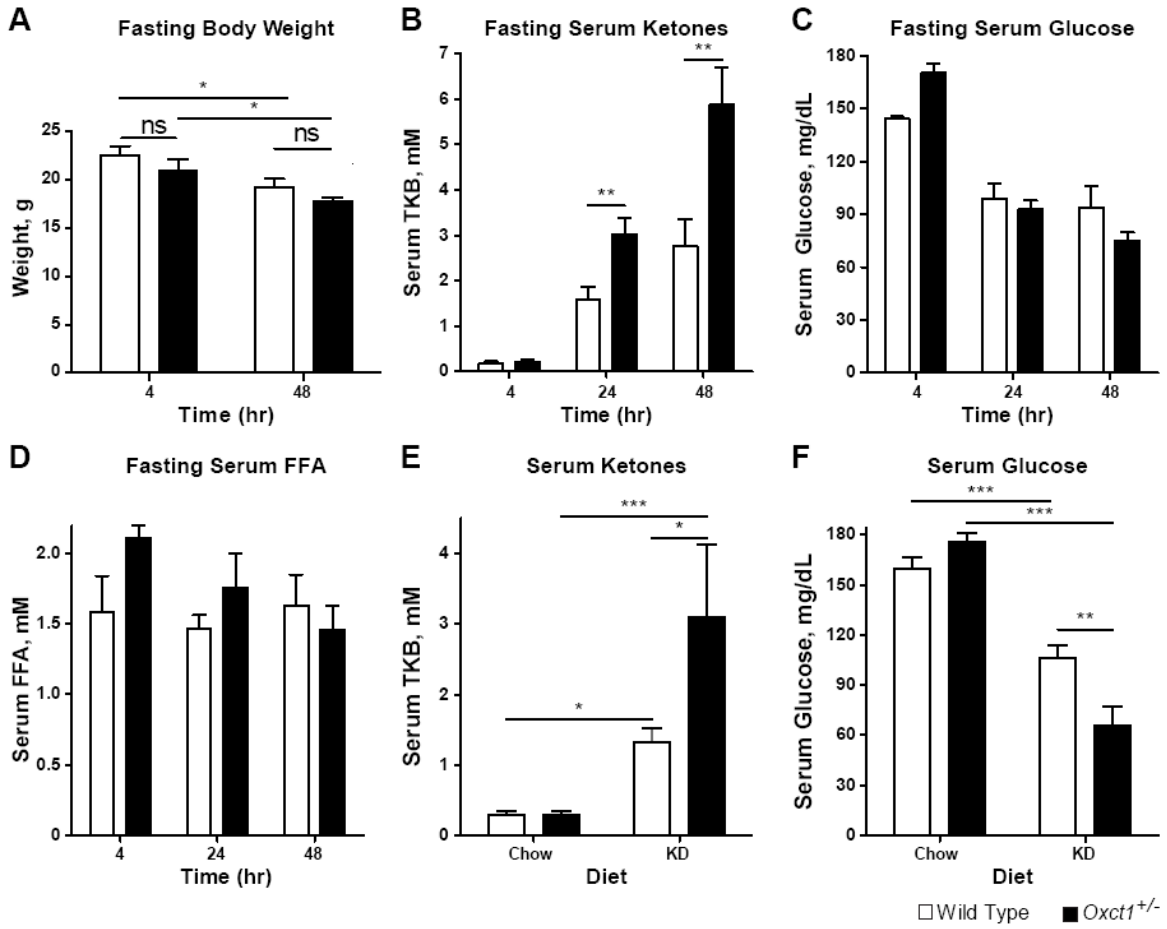


Table 3.1Table 1. *Genotyping primer sequences*

Genotyping Primers	Sequence (5'-3')		Product Size	Dissociation Temperature, °C
	Forward	Reverse		
<i>Oxct1</i> wild-type allele	CCAAGGAAGTAAATGAAGATGCTCCTA	ACGTGTATGTTACAAGAAATGGCTTACC	179	80.5
<i>Oxct1</i> null allele	CCAAGGAAGTAAATGAAGATGCTCCTA	CCAACTGACCTTGGGCAAGACAT	355	84.5
<i>Oxct1 flox</i> allele	CCAAGGAAGTAAATGAAGATGCTCCTA	ACGTGTATGTTACAAGAAATGGCTTACC	383	83.5
<i>Oxct1 rec</i> allele	CCAAGGAAGTAAATGAAGATGCTCCTA	ATGGCGAGCTCAGACCATAACTTCG	270	83
Cre	GCGGTCTGGCAGTAAAACTATC	GTGAAACAGCATTGCTGTCACTT	100	84
<i>MHC-Oxct1</i>	TGGCCAACCTGGATGATACCTGG	TCCATGTTGACCACCACTTTGG	97	80.8

MHC, myosin heavy chain.

Table 3.2Table 2. *RT-qPCR primer sequences*

RT-qPCR Primers	Sequence (5'-3')		Product Size	Dissociation Temperature, °C
	Forward	Reverse		
<i>Pck1</i>	GGAAGGACAAAGATGGCAAGTTC	AGGCGTTTTCTTAGGGATGTAG	138	87.3
<i>Hmgcs2</i>	TGGTTCAAGACAGGGACACAGAAC	AGAGGAATACCAGGGCCCAACAAT	98	84.1
<i>Bdh1</i>	TGCAACAGTGAAGAGGTGGAGAAG	CAAACGTTGAGATGCCTGCGTTGT	109	85
<i>Rpl32</i>	CCTCTGGTGAAGCCCAAGATC	TCTGGGTTTCGCCAGTTT	102	81.8

Pck1, phosphoenolpyruvate carboxykinase 1; *Hmgcs2*, hydroxymethylglutaryl-CoA synthase 2; *Bdh1*, D-β-hydroxybutyrate dehydrogenase.

Table 3.3**Table 3. Serum AcAc-to-D- β OHB ratios in adult mice**

<i>Oxct1</i> Genotype, condition	<i>n</i>	AcAc-to-D- β OHB Ratio
<i>flox/flox</i> , 48-h fast	12	0.30 \pm 0.11
Heart-KO, 48-h fast	7	0.37 \pm 0.12
Muscle-KO, 48-h fast	4	0.54 \pm 0.14
<i>flox/flox</i> ; Neuron-KO, 48-h fast	10	0.60 \pm 0.13
<i>flox/rec</i> , 48-h fast	3	0.88 \pm 0.33
<i>flox/rec</i> ; Neuron-KO, 48-h fast	10	0.39 \pm 0.07
<i>+/+</i> , 48-h fast	8	0.61 \pm 0.17
<i>+/-</i> , 48-h fast	6	0.69 \pm 0.18
<i>+/+</i> , 2-wk KD	9	0.17 \pm 0.04
<i>+/-</i> , 2-wk KD	6	0.20 \pm 0.03

n, No. of mice. AcAc, acetoacetate; D- β OHB, D- β -hydroxybutyrate; KO, knockout; KD, low-protein, very-low-carbohydrate, and high-fat ketogenic diet.

Chapter 4

Impact of peripheral ketolytic deficiency on hepatic ketogenesis and gluconeogenesis during the transition to birth

The work presented in this chapter has been adapted from:

Cotter, D. G., Ercal, B., d'Avignon, D. A., Dietzen, D. J., and Crawford, P. A. (2013) *J Biol Chem*

288(27), 19739-19749

Summary

Preservation of bioenergetic homeostasis during the transition from the carbohydrate-laden fetal diet to the high fat, low carbohydrate neonatal diet requires inductions of hepatic fatty acid oxidation, gluconeogenesis, and ketogenesis. Mice with loss-of-function mutation in the extrahepatic mitochondrial enzyme CoA transferase (succinyl-CoA:3-oxoacid CoA transferase, SCOT, encoded by nuclear *Oxct1*) cannot terminally oxidize ketone bodies and develop lethal hyperketonemic hypoglycemia within 48 hr of birth. Here we use this model to demonstrate that loss of ketone body oxidation, an exclusively extrahepatic process, disrupts hepatic intermediary metabolic homeostasis after high fat mother's milk is ingested. Livers of SCOT-knockout (SCOT-KO) neonates induce the expression of the genes encoding PGC-1 α , PEPCK, pyruvate carboxylase, and glucose-6-phosphatase, and the neonate's pools of gluconeogenic alanine and lactate are each diminished by 50%. NMR-based quantitative fate mapping of ¹³C-labeled substrates revealed that livers of SCOT-KO newborn mice synthesize glucose from exogenously administered pyruvate. However, the contribution of exogenous pyruvate to the TCA cycle as acetyl-CoA is increased in SCOT-KO livers, and is associated with diminished terminal oxidation of fatty acids. After mother's milk provokes hyperketonemia, livers of SCOT-KO mice diminish *de novo* hepatic β -hydroxybutyrate synthesis by 90%. Disruption of β -hydroxybutyrate production increases hepatic NAD⁺/NADH ratios three-fold, oxidizing redox potential in liver but not skeletal muscle. Together, these results indicate that peripheral ketone body oxidation prevents hypoglycemia and supports hepatic metabolic homeostasis, which is critical for the maintenance of glycemia during the adaptation to birth.

Introduction

At birth, a transplacental nutrient stream replete with carbohydrates is terminated and replaced with a high fat, low carbohydrate milk diet that is cyclically interrupted by periods of nutrient deprivation. Hepatic glucose production plays a critical role in providing fuel, particularly to the developing brain (20). Nonetheless, glucose utilization is thought to support only ~70% of the neonatal brain's energetic needs, and additional substrates, including ketone bodies, are required to supply the balance (71). To meet this demand, a coordinated hepatic metabolic program integrates β -oxidation and terminal oxidation of fatty acids, gluconeogenesis, and ketogenesis (20). Ketone body metabolism mediates energy transfer by partially oxidizing hepatic fatty acids to water-soluble four-carbon ketone body intermediates that are transported to extrahepatic organs for terminal oxidation during physiological states characterized by limited carbohydrate supply (4,5,301). As such, contributions of ketone body metabolism to neonatal bioenergetic homeostasis are two-fold: (i) because the neonatal diet has high lipid content, ketogenesis provides a spill-over pathway for excess fatty acid oxidation-derived acetyl-CoA that would otherwise require terminal oxidation, storage, or secretion (5,42,302), and (ii) extrahepatic ketone body oxidation diminishes hepatic gluconeogenic demand because ketone body oxidation spares glucose utilization in peripheral tissues (4).

Most ketogenesis occurs within hepatic mitochondria, at rates proportional to β -oxidation of fatty acids (5). Sequential ketogenic reactions catalyzed by mitochondrial thiolase, mitochondrial hydroxymethylglutaryl-CoA synthase (HMGCS2), and hydroxymethylglutaryl-CoA lyase (HMGCL) convert β -oxidation-derived acetyl-CoA to the ketone body acetoacetate (AcAc), which is reduced by mitochondrial D- β -hydroxybutyrate (D- β OHB)-dehydrogenase (BDH1) to D- β OHB in an NAD⁺/NADH-coupled redox reaction (21,22,44). Within extrahepatic organs, mitochondrial BDH1 re-oxidizes D- β OHB to AcAc. Covalent activation of AcAc by CoA is catalyzed by the mitochondrial matrix enzyme succinyl-CoA:3-oxoacid CoA transferase [SCOT (encoded by the nuclear gene *Oxct1*), the only mammalian CoA transferase] to generate AcAc-CoA, which upon thiolytic cleavage, liberates acetyl-CoA that enters the tricarboxylic acid (TCA) cycle for terminal oxidation (74). CoA transferase catalyzes a near equilibrium

reaction in which coenzyme A is exchanged between succinate and AcAc (72). Ketone bodies are efficient energetic substrates that are oxidized in proportion to their delivery (4,5,20). The neonatal brain extracts ketones at rates up to 40-fold greater than the adult brain and ketone body oxidation can support as much as 25% of the neonate's total basal energy requirements (71,248). Because neurons oxidize fatty acids poorly (69,71), ketogenesis has been proposed as a key determinant in vertebrate evolution and the evolution of human brain size (41).

Prior analysis of germline CoA transferase knockout (SCOT-KO) mice revealed that CoA transferase is required for terminal ketone body oxidation. SCOT-KO mice are born normal, but exhibit increased cerebral glucose oxidation. These mice ultimately develop hyperketonemic hypoglycemia and die within 48h of birth unless their lifespan is prolonged by frequent glucose administration (78). Unlike mice with a global CoA transferase defect, recent studies using cell type-specific SCOT-KO mice reveal that the selective absence of ketone body oxidation individually within neurons, cardiomyocytes, or skeletal myocytes – the three greatest consumers of ketone bodies (4,107) – does not cause hyperketonemia or hypoglycemia, and does not impair survival during the neonatal period or starvation in adulthood. As observed in brains of germline SCOT-KO neonates, selective absence of neuronal CoA transferase activity was associated with increased glycolysis and glucose oxidation in the neonatal brain (108). Taken together, the phenotypes of germline and tissue-specific SCOT-KO mice reveal that ketolytic cells do not require the energy stored in ketone bodies, but ketone body oxidation is necessary for maintenance of glycemia, and therefore survival in the neonatal period.

During states in which dietary carbohydrates are in short supply, the balance of hepatic glucose output with extrahepatic glucose consumption coordinates glucose homeostasis. Increased extrahepatic glucose consumption in neonatal germline SCOT-KO mice may therefore contribute to the development of hypoglycemia. To determine whether the absence of extrahepatic ketone body oxidation influences hepatic glucose production and intermediary metabolic homeostasis, we used biochemical approaches to quantify dynamic metabolism in livers of germline neonatal SCOT-KO mice.

Methods

Animals. *Oxct1^{-/-}* (germline SCOT-KO) mice were generated on the C57BL/6 genetic background (78). To obtain unfed neonatal mice, pups were collected within one hour of birth. Pups without gastric milk spots were confirmed by open examination of the stomach and intestine at the time of sacrifice. Fed postnatal day zero (P0, the first day of postnatal life) mice were collected within 4 hr of birth. All P1 mice were maintained with the dam through the first 30h after birth, and were milk fed. All mice were maintained at 22°C on standard polysaccharide-rich chow diet (Lab Diet 5053) and autoclaved water *ad libitum*. Lights were off between 1800 and 0600. All experiments consisted of mouse pups that were harvested from at least three litters from three different breeder pairings. All experiments were conducted using protocols approved by the Animal Studies Committee at Washington University.

Plasma metabolite measurements. Measurements of plasma AcAc and D-βOHB were performed using standard biochemical assays coupled to colorimetric substrates (Wako), as described previously (51). AcAc concentrations were determined by measuring total ketone body (TKB) concentrations and subtracting the corresponding measured D-βOHB concentration. Plasma lactate and pyruvate were measured using colorimetric and fluorescent biochemical assays, respectively (Biovision). Blood glucose was measured in duplicate using glucometers (Aviva).

Gene expression analysis. Quantification of gene expression was performed using real-time RT-quantitative PCR using the $\Delta\Delta C_t$ approach as described, normalizing to *Rpl32*, using primer sequences listed within supplemental **Table S4.1** (51).

Immunoblotting. Immunoblots, using protein lysates from neonatal brain, heart, liver, and quadriceps/hamstring muscles to detect SCOT (rabbit anti-SCOT; Proteintech Group), actin (rabbit anti-actin; Sigma), HMGCS2 (rabbit anti-mHMGCS; Santa Cruz Biotechnology), PDH-E1 α (rabbit anti-Pyruvate Dehydrogenase E1-alpha subunit antibody; abcam ab155096), phospho-serine 293 PDH-E1 α [PhosphoDetect™ Anti-PDH-E1 α (pSer293) Rabbit Antibody; Millipore AP1062], and BDH1 (rabbit anti-BDH1; Proteintech Group) were performed as previously described (34). Band intensities were quantified densitometrically using QuantityOne software (Bio-Rad).

In vitro ketogenesis of hepatic explants. Neonatal mice were sacrificed by decapitation. Livers were collected, weighed, and each liver was placed in a single well of a 6-well tissue culture plate containing 2 mL of phosphate-buffered saline (PBS) on ice. Livers were minced and transferred to a 2 mL eppendorf tube. Tissues were allowed to settle on ice and were centrifuged at 500 x g for 1 min. Minced-liver pellets were resuspended in 1 mL of assay media [Dulbecco's Modified Eagle's Medium supplemented with 2.78 mM glucose (which reflects glycemia in neonatal mice), 0.63 mM sodium pyruvate, and 150 μ M oleic acid (conjugated to bovine serum albumin in a 2:1 molar ratio)]. Each liver preparation was plated in a single well of a 12-well plate containing 1 mL of media, and incubated at 37°C. At time points indicated in the figure legends, 50 μ L of media was removed to quantify ketone body concentrations.

Tissue triglyceride, glycogen, and nicotinamide metabolite quantifications. Hepatic triacylglycerol (TAG) concentrations were determined using a Folch extract of liver and biochemical quantification using a biochemical assay (Wako), as previously described (126). Hepatic glycogen and NAD⁺(H) concentrations were measured in liver lysates using fluorescent biochemical assays (Biovision).

In vivo substrate utilization. P0 or P1 mice were injected intraperitoneally with 10 μ mol of sodium [1,2,3,4-¹³C₄]octanoate, 10 μ mol sodium [3-¹³C]pyruvate, or co-injected with 10 μ mol of sodium [1,2,3,4-¹³C₄]octanoate, plus 20 μ mol naturally-occurring sodium pyruvate, sodium D- β OHB, sodium L- β OHB, or AcAc per g of body weight (vendor for stable isotopes: Cambridge Isotope Laboratories). Base hydrolysis of ethyl-AcAc (Sigma W241512) was performed by addition of 50% NaOH to pH 12 and incubation at 60° C for 30 min. The pH of base hydrolyzed AcAc was adjusted to pH 8.5, and [AcAc] was confirmed using standard biochemical assays coupled to colorimetric substrates (Wako), as described previously (51). After intraperitoneal injections, neonatal mice were maintained on a heating pad for the indicated durations (see text and figure legends), killed by decapitation, and tissues were rapidly freeze-clamped in liquid N₂. Neutralized perchloric acid tissue extracts were profiled using ¹³C-edited proton nuclear magnetic resonance (NMR) measured at 11.75 T (Varian/Agilent Direct Drive-1) via first increment gradient heteronuclear single-quantum correlation (gHSQC). The majority of studies were carried out using a traditional probe, but extracts generated from mice injected with sodium [3-¹³C]pyruvate were

analyzed using a high-sensitivity cold probe at 11.75 T (Varian/Agilent Direct Drive-1). Signals were collected from extracts dissolved in 275 μL of D_2O + 1 mM trimethylsilyl propionate (TSP), loaded into high precision, thin walled 5-mm tubes (Shigemi). Quantification of signals by integration from the $^1\text{H}\{^{13}\text{C}\}$ and ^{13}C -edited (gHSQC) collections of carbon 2 for taurine, carbon 4 for βOHB , carbon 1 for glucose, carbon 4 for glutamate, and $^1\text{H}\{^{13}\text{C}\}$ of carbons 3 for lactate and alanine were all performed as described previously (78). Tissue concentrations (pool size) of glucose, taurine, glutamate, and βOHB were calculated by normalizing the integrals for each metabolite obtained from the $^1\text{H}\{^{13}\text{C}\}$ collections to TSP and tissue weight. Because tissue taurine concentrations were constant across conditions (**Tables S4.2-S4.3**) and taurine is not enriched by administration of these experimental substrates (51,136), taurine was used as a normalizing metabolite between the $^1\text{H}\{^{13}\text{C}\}$ and gHSQC collections to calculate the moles of ^{13}C -labeled metabolites present in each sample. The moles of ^{13}C -labeled metabolites produced from the labeled substrate in each sample were calculated by subtracting the moles of ^{13}C -labeled metabolites attributable to the metabolite pool size (*i.e.*, in the absence of any enrichment from exogenous ^{13}C -labeled substrates, 1.1% of the metabolites within the entire pool are expected to be ^{13}C -labeled, based upon the natural abundance of ^{13}C) from the total amount of ^{13}C -labeled metabolites detected in the gHSQC collections. Fractional enrichments of ^{13}C -labeled glutamate and βOHB were then calculated as described (51), by dividing taurine-normalized integral values for each queried metabolite derived from the gHSQC collections by the corresponding integral value obtained from the $^1\text{H}\{^{13}\text{C}\}$ collections.

Tandem mass spectrometry (MS/MS) analysis of blood amino acids and acylcarnitines. Neonatal blood was spotted onto 1.3 cm spots on Whatman 903 filter paper. Amino acids were quantified as butyl ester derivatives using multiple precursor/product combinations in a reversed-phase liquid chromatography protocol coupled to MS/MS (303). Carnitine esters were measured by scanning for the precursors of the common m/z 85 carnitine fragment. Quantification was achieved in all cases using stable isotope (^2H) labeled internal standards using an electrospray ionization source coupled to an API 3200-Qtrap tandem mass spectrometer (Applied Biosystems, Foster City CA, USA).

Results

Neonatal SCOT-KO mice engage an hepatic gluconeogenic gene program. The liver is the most important source of glucose for the neonatal brain (2,71), which increases its reliance on this vital fuel when CoA transferase inactivation prevents ketone body oxidation in the entire brain (78) or selectively within neurons (108). Therefore, we hypothesized that neonatal germline SCOT-KO mice, which cannot terminally oxidize ketone bodies, engage compensatory mechanisms in the liver to meet increased peripheral glucose demand. Increased abundances of the mRNAs encoding peroxisome proliferator activated receptor gamma-1a (PGC-1 α , encoded by *Ppargc1a*), pyruvate carboxylase (PC, encoded by *Pcx*), phosphoenolpyruvate carboxykinase (PEPCK, encoded by *Pck1*), and glucose-6-phosphatase (encoded by *G6pc*) were observed in livers of postnatal day 1 (P1, the day immediately following delivery) SCOT-KO mice (**Fig. 4.1A**), and as expected, hepatic glycogen content was depleted in livers of P1 SCOT-KO mice (**Fig. 4.1B**). Consistent with increased gluconeogenic demand, tandem mass spectrometry (MS/MS) analysis of circulating amino acids demonstrated that alanine, which becomes the gluconeogenic substrate pyruvate following transamination (36), was diminished 51% in blood of P1 SCOT-KO mice (**Fig. 4.1C**). Serine, which is deaminated to pyruvate by serine dehydratase, also trended lower in these mice. In addition, blood concentrations of the anaplerotic amino acid glutamate, which can replenish TCA cycle intermediates following conversion to α -ketoglutarate, were diminished 40% in SCOT-KO neonates. This contrasted with many glucogenic/ketogenic, glucogenic, ketogenic, and urea cycle amino acids, whose circulating concentrations were increased in P1 SCOT-KO mice (**Fig. 4.1D**; see **Tables S4.4-S4.5** for complete P0 and P1 blood amino acid profiles, respectively, of wild type and SCOT-KO mice), suggesting enhanced skeletal muscle proteolysis in P1 SCOT-KO mice. In addition, the total circulating pyruvate pool (the sum of pyruvate plus lactate, which form a redox couple with NAD⁺/NADH), a critical source of gluconeogenic precursors via the Cori cycle, was diminished 53% in P1 SCOT-KO mice (**Fig. 4.1E**). In SCOT-KO neonates, increased extrahepatic glucose and lactate consumption (78,108) are likely contributors to hypoglycemia. Unlike wild-type littermates, endogenous hepatic content of free glucose was below the limit of detection by proton NMR in P1 SCOT-KO mice

(**Fig. 4.1F, left**), suggesting that hepatic glucose generated from residual endogenous substrates is rapidly cleared to meet increased peripheral demands, and that this production is insufficient to support the glycemic requirements for survival in these mice. However, intraperitoneal supplementation of P1 SCOT-KO mice with exogenous [^{13}C]pyruvate 30 min prior to harvest of the liver demonstrated robust generation of ^{13}C -glucose (**Fig. 4.1F, right**). Taken together, these data suggest that neonatal hepatic glucose production is increased to meet enhanced peripheral requirements, but is limited in these mice by precursor availability and not intrinsic synthetic capacity.

Reprogrammed intermediary metabolism in livers of neonatal SCOT-KO mice. Given marked hypoglycemia, hyperketonemia, alterations of gluconeogenic precursor pools, and increased concentrations of circulating amino acids, we hypothesized that livers of P1 SCOT-KO mice would exhibit alterations of terminal fatty acid oxidation and pyruvate metabolism. Therefore, to determine if livers of P1 germline SCOT-KO mice exhibit diminished terminal oxidation of acyl-CoA-derived acetyl-CoA, we quantified the contribution of the fatty acid [1,2,3,4- $^{13}\text{C}_4$]octanoate (10 $\mu\text{mol/g}$ body weight, via the intraperitoneal route) to the acetyl-CoA entering the TCA cycle, by using ^{13}C -glutamate fractional enrichment as a quantitative surrogate, because glutamate is in equilibrium with the TCA cycle intermediate α -ketoglutarate (51,78,108,136,304,305). Hepatic enrichment of ^{13}C -glutamate did not differ between P1 wild type and SCOT-KO mice that received [^{13}C]octanoate alone (**Fig. 4.2A, left**), indicating equal contributions of labeled octanoate to the acetyl-CoA entering the TCA cycle. However, SCOT-KO mice exhibited a significantly decreased glutamate pool size (**Fig. 4.2A, right**; 1.03 ± 0.17 nmol glutamate/mg liver in P0 wild type mice, versus 0.56 ± 0.09 nmol glutamate/mg liver in P1 SCOT-KO mice, $p = 0.046$, $n = 6-8/\text{group}$). Therefore, to determine if hepatic terminal fatty acid oxidation remains equal when glutamate pool sizes in livers of P1 wild-type and SCOT-KO mice are equal, we co-administered [^{13}C]octanoate with unlabeled pyruvate, which augments TCA cycle intermediates by stimulating anaplerosis. Co-administration of unlabeled pyruvate with [^{13}C]octanoate increased hepatic glutamate pool sizes in livers of both wild type and SCOT-KO neonatal mice, and abrogated the diminution of this pool size in livers of SCOT-KO mice (**Fig. 4.2B, right**). However, compared to livers

of wild-type P1 mice, hepatic glutamate enrichment from [¹³C]octanoate was diminished nearly 50% in livers of P1 SCOT-KO mice delivered this combination of substrates (22.9±3.05% in wild type mice versus 11.8±3.0% in SCOT-KO mice, $p = 0.026$, $n = 6-7$ /group; **Fig. 4.2B**, *left*), indicating diminished contribution of labeled octanoate to the acetyl-CoA entering the TCA cycle in livers of P1 SCOT-KO mice. The only competing sources of acetyl-CoA in the livers of neonatal mice in this experimental context are (i) endogenous fatty acids or (ii) pyruvate that is decarboxylated via the pyruvate dehydrogenase (PDH) complex. Thus, we directly quantified the contribution of pyruvate to the acetyl-CoA entering the TCA cycle by administering [3-¹³C]pyruvate (10 μmol/g body weight), which labels > 95% of the circulating pyruvate pool in both wild type and SCOT-KO mice, and measured hepatic glutamate enrichment. Hepatic ¹³C-enrichment of glutamate was 2.7-fold greater in SCOT-KO neonates administered [¹³C]pyruvate (5.95±1.92% versus 16.32±2.87% in livers of wild-type and SCOT-KO P1 mice, respectively, $p=0.04$, $n=4$ /group; **Fig. 4.2C**). As observed in mice receiving unlabeled pyruvate (**Fig. 4.2B**), hepatic glutamate pools were not different between wild type and SCOT-KO neonates injected with [¹³C]pyruvate (data not shown). Increased ¹³C-glutamate enrichment from [¹³C]pyruvate occurred in SCOT-KO neonates in the absence of altered phosphorylation of PDH on the E1 α subunit, a post-translational modification that increases the K_m of PDH (138,306,307) (**Fig. S4.1**).

Because the contribution of labeled fatty acids to the acetyl-CoA entering the TCA cycle was diminished in livers of P1 SCOT-KO mice when glutamate pools were rendered equal by administration of unlabeled pyruvate, we hypothesized that signatures of diminished fatty acid oxidation would be evident in livers of these mice. To determine if there was a defect in the β -oxidation spiral, we quantified blood acylcarnitines of untreated P1 germline SCOT-KO mice by MS/MS. While medium and long chain acylcarnitine species were normal (**Table S4.6**), short chain acylcarnitine concentrations were elevated in P1 SCOT-KO mice (**Fig. 4.2D**). This result is consistent with an intact β -spiral, but diminished entry of its products into the TCA cycle. Abundances of transcripts encoding key mediators of fatty acid transport and oxidation, including *Fabp1*, *Fgf21*, *Cpt1a*, and *Acadm* mRNAs, were all normal in SCOT-KO mice (**Fig. S4.2A**). However, hepatic triacylglycerol content trended higher in P1 SCOT-KO mice (**Fig. 4.2E**;

12.7±5.0 µg/mg liver versus 3.5±1.7, respectively, $p = 0.09$, $n=5-6/\text{group}$), also suggesting impaired terminal fatty acid oxidation in livers of SCOT-KO mice.

To determine whether signatures of diminished terminal fatty acid oxidation in livers of SCOT-KO neonatal mice are innate, or the result of a perturbed metabolic environment, we delivered [¹³C]octanoate to newborn P0 SCOT-KO mice that had been collected prior to their first milk feed, and observed that hepatic ¹³C-glutamate fractional enrichment and glutamate pool size were both normal, as they were in livers of fed P0 SCOT-KO mice (**Fig. S4.3**). Moreover, unlike the observation of increased short chain acylcarnitines in the circulation of P1 SCOT-KO mice, blood acylcarnitine species did not differ between fed, but untreated P0 wild-type and SCOT-KO mice (**Table S4.7**). Taken together, these findings indicate that the observed abnormalities of fatty acid and pyruvate metabolism are likely secondary to increased gluconeogenic demand and the hyperketonemic state that develops in P1 SCOT-KO mice.

Accumulated D-βOHB suppresses normal ketogenesis in neonatal liver. Due to (i) the alterations of hepatic fatty acid oxidation and pyruvate metabolism in SCOT-KO mice, and (ii) our previous observation that the AcAc/βOHB ratio was significantly elevated in the circulation of markedly hyperketonemic P1 SCOT-KO mice (78), we hypothesized that regulation of hepatic ketogenesis would also be altered in these mice. To determine the effects of peripheral ketolytic deficiency on hepatic ketogenesis, we measured the hepatic ¹³C fractional enrichment and pool sizes of βOHB in neonatal mice injected with [¹³C]octanoate. ¹³C-βOHB enrichment from [¹³C]octanoate was decreased 15-fold in livers of P1 SCOT-KO mice (15.26±1.34% versus 1.21±0.08%, $p < 0.0001$, $n = 6-8/\text{group}$ **Fig. 4.3A, left**). Commensurate with the marked increase in the concentration of circulating ketone bodies in P1 SCOT-KO mice, the total hepatic βOHB pool size was expanded in P1 SCOT-KO mice (0.51±0.07 nmol βOHB/mg liver and 3.27±0.73 nmol βOHB/mg liver in wild-type and SCOT-KO mice, respectively, $p = 0.0009$, $n = 6-8/\text{group}$; **Fig. 4.3A, middle**). Therefore, to confirm that the decreased ¹³C-βOHB fractional enrichment from [¹³C]octanoate in livers of SCOT-KO mice reflects diminished *de novo* production of βOHB (rather than merely an increase in the total pool), we quantified the ¹³C-βOHB abundance in livers

of these mice, and observed a 90% decrease in livers of P1 SCOT-KO mice (72.4 ± 12.5 pmol ^{13}C - βOHB /mg liver and 6.3 ± 2.1 pmol ^{13}C - βOHB produced/mg liver in wild-type and SCOT-KO mice, respectively, $p = 0.0007$, $n=6-8/\text{group}$; **Fig. 4.3A**, *right*). Messenger mRNAs encoding the ketogenic mediators FGF21 and HMGCS2 were both normal, while *Bdh1* mRNA abundance was decreased 50% in livers of P1 SCOT-KO mice (**Fig. S4.2A**). At the protein level, SCOT-KO livers exhibited $\sim 25\%$ increased HMGCS2, and normal BDH1 protein abundance (**Fig. S4.2B-C**).

To determine if the marked impairment of βOHB production in livers of P1 SCOT-KO mice was innate or acquired, we quantified ^{13}C - βOHB production from [^{13}C]octanoate in livers of unfed P0 SCOT-KO mice. Hepatic ^{13}C - βOHB enrichment, βOHB pool size, and ^{13}C - βOHB production were all normal in unfed P0 SCOT-KO mice (**Fig. 4.3B**). Prior to milk feeding, endogenous plasma ketones were nearly undetectable and did not differ between wild type and SCOT-KO mice (**Fig. 4.3C**). However, after only a single feed, plasma ketone bodies exceeded 3 mM in SCOT-KO mice (versus ~ 0.3 mM in wild-type littermate controls), with both D- βOHB and AcAc exhibiting significant increases in SCOT-KO neonates (**Fig. 4.3D**). In contrast to the robust ^{13}C -labeling of hepatic βOHB in unfed SCOT-KO neonates administered [^{13}C]octanoate, suckling-induced hyperketonemia correlated with the emergence of a 90% decrease in ^{13}C - βOHB enrichment in milk-fed P0 SCOT-KO mice, compared to littermate controls (**Fig. 4.3E**, *left*). Similar to the observations in the pools of βOHB in P1 SCOT-KO mice, suckling in P0 mice correlated with a marked expansion of the hepatic βOHB pool in SCOT-KO neonates, and was associated with an 80% decrease in the abundance of ^{13}C - βOHB (**Fig. 4.3E**, *middle and right*). Diminished ^{13}C - βOHB enrichment from [^{13}C]octanoate occurred in livers of fed P0 SCOT-KO mice despite normal abundances of *Fabp1*, *Cpt1a*, *Acadm*, *Hmgcs2*, and *Bdh1* mRNAs, and a 38% increase in HMGCS2 protein (**Fig. S4.4**). Together, these results indicate that suckling-induced hyperketonemia in SCOT-KO neonates diminishes the generation of ^{13}C - βOHB from [^{13}C]octanoate, without impairment of the upstream β -spiral or diminution of expression of the enzymatic mediators of fatty acid oxidation and ketogenesis.

To determine whether the acquired deficiency of *de novo* hepatic β OHB production in livers of SCOT-KO mice was mediated by hyperketonemia, we measured ketogenesis in livers explanted into culture from unfed and fed P0 SCOT-KO and littermate control mice, in order to isolate them from a hyperketonemic milieu. As expected, explants from unfed wild type and SCOT-KO neonatal mice did not differ in ketogenic rate (**Fig. 4.4A**). However, in contrast to the defect in *de novo* synthesis of β OHB exhibited by fed P0 SCOT-KO mice *in vivo*, livers explanted from fed SCOT-KO mice exhibited normal ketogenic rates, despite the increased baseline ketone body abundance in these explants (**Fig. 4.4B**). Therefore, to test the hypothesis that the acquired ketogenic impairment in livers of SCOT-KO mice requires an environment in which ketone bodies accumulate, we determined the effects of hyperketonemia on hepatic β OHB production *in vivo* by performing intraperitoneal co-injections in fed wild-type P0 mice. Unlabeled AcAc, D- β OHB, or L- β OHB [L- β OHB is a by-product of fatty acid oxidation that is neither produced during hepatic ketogenesis, nor is a substrate for BDH1 (158,160)] were co-injected intraperitoneally with [13 C]octanoate into milk-fed P0 wild-type neonatal mice, and the hepatic β OHB pool sizes, fractional enrichments of hepatic 13 C- β OHB, and molar contents of 13 C- β OHB/mg tissue were quantified. Co-administered AcAc, L- β OHB and D- β OHB each expanded the total β OHB pool significantly, although hepatic β OHB concentrations were greater in neonates co-injected with L- or D- β OHB compared to neonates co-injected with AcAc (**Fig. 4.5A**). While fractional 13 C-enrichments of β OHB from [13 C]octanoate were decreased in livers of mice co-injected with each of the three unlabeled ketone bodies, neonatal mice co-injected with L- or D- β OHB exhibited greater suppression of 13 C- β OHB enrichment than neonates co-injected with AcAc (**Fig. 4.5B**). However, only co-administered D- β OHB decreased the molar content/mg tissue of 13 C- β OHB in livers of wild-type mice (by 75%), while neither AcAc nor L- β OHB produced this effect (**Fig. 4.5C**). Because oxidation of D- β OHB to AcAc by BDH1 concomitantly reduces NAD^+ to NADH (22,24,308), these results suggest that the exogenously delivered D- β OHB diminished *de novo* β OHB production by shifting the equilibrium of the BDH1-catalyzed reaction towards AcAc formation.

Diminished β OHB production by livers of neonatal SCOT-KO mice results in oxidation of hepatic redox potential. Despite the impairment of *de novo* synthesis of β OHB, livers of SCOT-KO neonates continue to channel fatty acid oxidation-derived acetyl-CoA to AcAc, which exhibits a four-fold increase in plasma concentration between P0 and P1 in SCOT-KO mice (78). Because AcAc and D- β OHB exist in an NAD⁺ and NADH-coupled equilibrium, we hypothesized that preservation of AcAc formation, but impairment of its reduction to D- β OHB would oxidize hepatic redox potential. While plasma AcAc/ β OHB molar ratios were elevated 3.5-fold ($p = 0.03$, $n=8-9$ /group) in fed P0 SCOT-KO mice over wild-type littermate controls, these ratios spanned a large dynamic range among SCOT-KO animals (**Fig. 4.6A**), and abundances of total NAD⁺ and NADH were normal in both livers and skeletal muscle of fed P0 SCOT-KO mice (**Fig. 4.6B-C**). Plasma AcAc/ β OHB ratios were increased 10-fold ($p = 1.98 \times 10^{-8}$, $n=11-14$ /group) in P1 SCOT-KO mice compared to littermate controls, but in contrast to fed P0 SCOT-KO mice, they exhibited less variability (**Fig. 4.6D**). Correspondingly, livers of P1 SCOT-KO mice exhibited a three-fold increased ratio of NAD⁺/NADH concentrations (**Fig. 4.6E**). This effect was neither attributable to, nor contributed to altered hepatic abundances of mRNAs encoding NAMPT, CD38, SIRT1, or Rictor (**Fig. S4.5**). Redox potential was unaltered in skeletal muscles of P1 SCOT-KO mice (**Fig. 4.6F**), consistent with the notion that persistent AcAc production by the liver is the primary driver of the redox abnormality of P1 SCOT-KO mice. Because SCOT is normally considered absent in hepatocytes (74,107,164), and only a scant amount of SCOT was detected in neonatal hepatic lysates (**Fig. S4.6**), these results indicate that peripheral disposal of ketone bodies is required to prevent oxidation of hepatic redox potential.

Discussion

Ketone bodies provide an alternative fuel in states of diminished carbohydrate supply (4,5,20). Ketone body oxidation is required for adaptation to birth in mice, and for adaptation to low carbohydrate states in humans (78,97). Here we show that extrahepatic ketone body oxidation is essential for preservation of hepatic metabolic homeostasis during the ketogenic neonatal period because the absence of ketone body

oxidation causes impaired hepatic terminal fatty acid oxidation, altered pyruvate metabolism, and diminished *de novo* β OHB production, which results in oxidation of hepatic redox potential.

Germline SCOT-KO neonates succumb to neonatal hypoglycemia. Increased peripheral oxidation of lactate and glucose contribute to hypolactatemia and hypoglycemia (78), and increase the gluconeogenic burden of SCOT-KO livers. These mice also develop increased blood amino acid concentrations, indicating that hypoglycemia and the inability to derive high-energy phosphates from ketone bodies likely stimulate skeletal muscle proteolysis. While increased blood amino acid concentrations indicate that amino acid supply exceeds hepatic utilization, a subset of these amino acids yields gluconeogenic carbon backbones within liver and replenishes TCA cycle intermediates via anaplerosis (36). Notably, blood alanine concentrations are decreased in SCOT-KO neonates, although absolute plasma pyruvate concentrations are preserved, suggesting that pyruvate generation via both the glucose-alanine and Cori cycles increase to support increased gluconeogenic demand. Because livers of SCOT-KO neonates successfully produce glucose from exogenously delivered pyruvate, impairments of the hepatic gluconeogenic machinery do not account for hypoglycemia. In fact, gluconeogenic enzymes, which normally exhibit significant postnatal inductions (20), are further induced in livers of SCOT-KO neonates. Together, these data suggest that the availability of gluconeogenic substrates (*i.e.*, alanine and the lactate + pyruvate pool), and not expression of enzymatic mediators of gluconeogenesis, exacerbates the mismatch between neonatal hepatic glucose production and extrahepatic glucose requirements in mice that lack CoA transferase activity. In states of limited dietary carbohydrate supply, >60% of hepatic gluconeogenesis is derived from pyruvate (267). Upon carboxylation by PC, pyruvate supplies the TCA cycle with the intermediate oxaloacetate, which can either remain in the cycle to facilitate terminal oxidation of acetyl-CoA, or efflux into the gluconeogenic pathway through PEPCK-dependent conversion to phosphoenolpyruvate (36,309). Such 'pyruvate cycling' governs rates of anaplerosis and TCA cycle intermediate efflux (309), which normally exceed the rate of TCA cycle flux in the liver (30). Although limited pyruvate pool availability precludes preservation of euglycemia, transcriptional induction of these

enzymatic mediators of pyruvate cycling may initially help support gluconeogenesis in livers of SCOT-KO mice.

Hyperketonemic states, both physiological and pathophysiological, are almost always characterized by plasma AcAc/ β OHB molar ratios that are < 1 . SCOT-KO mice present a unique hyperketonemic state in which the AcAc/ β OHB molar ratio is > 1 . Following their first high fat, low carbohydrate milk meal, SCOT-KO mice develop hyperketonemia, which becomes associated with diminished *de novo* production of D- β OHB. NMR studies in wild type mice co-injected with the fatty acid [^{13}C]octanoate and unlabeled ketone bodies indicate that increased circulating D- β OHB in germline SCOT-KO mice diminishes hepatic production of β OHB. In the final ketogenic reaction, AcAc is reduced to D- β OHB in an NAD^+/NADH coupled equilibrium reaction catalyzed by BDH1 that normally favors β OHB production (21,22,44). However, the equilibrium of the BDH1 reaction is sensitive to concentrations of both AcAc and D- β OHB, such that increases in the molar concentrations of one partner of the couple diminish the reduction/oxidation of the other (308). Because livers of SCOT-KO mice initially produce D- β OHB in a normal fashion (**Figs. 4.3B and 4.4**), a model emerges in which loss of peripheral ketone body oxidation results in pooling of D- β OHB, which causes the equilibrium of BDH1 to shift towards AcAc, such that AcAc becomes the primary ketone body synthesized by *de novo* hepatic ketogenesis. Rising AcAc concentrations initially counteract the propensity of D- β OHB to reduce hepatic redox potential, explaining why hepatic NAD^+/NADH ratios are normal in fed P0 SCOT-KO mice. Continued channeling of β -oxidation-derived acetyl-CoA to AcAc ultimately results in the high plasma AcAc/ β OHB ratios, and thus elevated hepatic NAD^+/NADH ratios observed in P1 germline SCOT-KO mice.

The development of oxidized hepatic redox potential may partially explain the alteration of pyruvate and fatty acid handling in livers of P1 SCOT-KO mice. In states of high fat/low carbohydrate nutrient supply, the vast majority of pyruvate delivered to the liver enters the TCA cycle via carboxylation, rather than decarboxylation to acetyl-CoA via the PDH complex (29). While the pyruvate carboxylation pathway is active, and possibly augmented in livers of P1 SCOT-KO mice, the ^{13}C -

fractional enrichments of glutamate observed in both (i) the [^{13}C]octanoate + unlabeled pyruvate and (ii) the [^{13}C]pyruvate experiments both suggest that flux of pyruvate through PDH is relatively increased in livers of SCOT-KO mice. Phosphorylation of the E1 a subunit of PDH was not diminished in livers of P1 SCOT-KO mice, which suggests equal PDH activity. However, pyruvate concentrations in these experiments were high enough that PDH flux could be governed by the concentrations of its cofactor, NAD^+ , and one of its allosteric inhibitors, NADH, whose concentrations are increased and decreased, respectively, in livers of P1 SCOT-KO neonates (138,307,310). These findings are consistent with the notion that increased gluconeogenic demand, and an oxidized hepatic redox potential together support a state of increased pyruvate consumption that culminates in the diminished pyruvate pools that lead to hypoglycemia in SCOT-KO mice. An additional consequence of augmented contribution of pyruvate to the TCA cycle through acetyl-CoA is diminished contribution of fatty acid oxidation-derived acetyl-CoA. While the NMR studies of P1 SCOT-KO mice injected with [^{13}C]octanoate alone indicated equal fractional enrichment of ^{13}C -glutamate, this observation was obtained in the context of a diminished total glutamate pool, raising the possibility that absolute flux of fatty acids through terminal oxidation is reduced in livers of P1 SCOT-KO neonates. Increased circulating concentrations of short-chain acylcarnitines in P1 SCOT-KO mice support this hypothesis. These integrated mechanisms merit further evaluation in the pathogenesis of human neonatal hypoglycemia, a high-morbidity condition with an incidence of 10% (311).

At birth, mammals experience a shift towards a lipid-dominated energy economy, inducing hepatic fatty acid oxidation, ketogenesis, and gluconeogenesis (20). Although rodents are born at an earlier developmental stage and exhibit lower neonatal body fat percentages, they suckle milk with higher fat contents than humans, and physiological ketosis develops rapidly after birth in both (2,20,71). Case reports indicate that HMGCS2- and SCOT-deficient humans adapt poorly to nutrient states that are marked by diminished carbohydrate intake. Human HMGCS2 deficiency results in pediatric hypoketonemic hypoglycemia (68), and human CoA transferase deficiency manifests as spontaneous pediatric ketoacidosis (81,98), which in severe cases is associated with hypoglycemia, and may account

for a subset of idiopathic ketotic hypoglycemia cases (79,102). SCOT-KO mice die in a manner that mimics human sudden infant death syndrome (SIDS)/sudden unexpected death in infancy (SUDI), the leading cause of death of U.S. infants after the age of one month (312). Inborn errors of ketone body oxidation are not currently assessed on any statewide screening protocols in the U.S. (99). Therefore, these metabolic abnormalities merit further evaluation, as supported by a recent observational study in which metabolic autopsies performed on 255 SIDS patients detected three individuals with underlying disorders of ketone body metabolism (216). Thus, a small subset of sudden infant death cases could be attributable to undetected defects in ketone body oxidation.

Due to their small size and delicate nature, steady state analyses of metabolic flux in neonatal mice are not currently possible. Therefore, we performed NMR substrate fate mapping after bolus injections of octanoate to quantify hepatic fatty acid fate in neonatal mice. This medium chain fatty acid avidly enters the mitochondrial matrix independently of allosterically regulated mitochondrial carnitine palmitoyltransferase 1a (5), and thus reports the activities of β -oxidation, fractional contribution to the TCA cycle, and ketogenesis.

We have demonstrated that global disruption of ketone body oxidation reprograms hepatic intermediary metabolism, initiating a cascade that alters ketogenesis and oxidizes hepatic redox potential, and ultimately consumes pyruvate at the expense of terminal hepatic fatty acid oxidation, resulting in accumulation of circulating short chain acylcarnitines and hepatic triacylglycerols. Thus, extrahepatic ketone body oxidation helps integrate hepatic ketogenesis, redox potential, fatty acid oxidation, and glucose production in the neonatal period. Future studies will be needed to determine whether these relationships extend to other physiological and pathophysiological states characterized by excess fatty acid availability and limited carbohydrate supply (or inefficient carbohydrate utilization), including starvation, adherence to low carbohydrate diets, and Types 1 and 2 diabetes.

Acknowledgements

The authors thank Shin-ichiro Imai and Rebecca Schugar for helpful discussions, Laura Kyro for assistance with graphics, and Ashley Moll and Debra Whorms for technical assistance. This work was supported by grants from the NIH [DK091538 (to PAC) and HL007873 (a training grant that supports DGC)], the March of Dimes, and the Children's Discovery Institute through St. Louis Children's Hospital (to PAC).

Figure legends

Figure 4.1. Absence of extrahepatic ketone body oxidation engages an hepatic gluconeogenic program in neonatal mice. (A) Relative mRNA abundance of encoded mediators of pyruvate metabolism and gluconeogenesis in livers of P1 mice. n = 5/group. (B) Liver glycogen content (μg glycogen/mg tissue) in P1 neonates. n = 8/group. p = 0.06 by Student's *t* test. (C) Blood alanine, serine, and glutamate concentrations (μM) in P1 mice. n = 5-7/group. (D) Circulating amino acid concentrations (μM) in blood of P1 mice. n = 5-10/group. (E) Plasma pyruvate pool (pyruvate + lactate) in P1 mice. n = 8-11/group. (F) Endogenous hepatic glucose concentration (left) and accumulated [^{13}C]glucose in livers (right) of P1 mice that had been injected with [$3\text{-}^{13}\text{C}$]pyruvate (10 μmol per g body weight) 30 min prior to collection of tissues and generation of extracts for NMR. n = 4/group. *, p < 0.05; **, p < 0.01; ***, p < 0.001 by Student's *t* test. *Ppargc1a*, PPAR γ coactivator 1 α ; *Pcx*, pyruvate carboxylase; *Pck1*; phosphoenolpyruvate carboxykinase; *G6pc*, cytoplasmic glucose-6-phosphatase.

Figure 4.2. Alterations of terminal fatty acid oxidation and pyruvate handling in livers of SCOT-KO mice. (A) Hepatic fractional ^{13}C -enrichments of glutamate (left) and total hepatic glutamate pools (right) 20 min after ip injection of sodium [$1,2,3,4\text{-}^{13}\text{C}_4$]octanoate (10 μmol per g body weight) in P1 mice. n=6-8/group. (B) Fractional ^{13}C -enrichments of glutamate (left) and total hepatic glutamate pools

(right) 20 min after ip injection of sodium [1,2,3,4-¹³C₄]octanoate (10 μmol per g body weight) + unlabeled pyruvate (20 μmol/g) in livers P1 mice. n=6-7/group. (C) Fractional ¹³C-enrichments of glutamate 30 min after ip injection of sodium [3-¹³C]pyruvate (10 μmol per g body weight) in livers P1 mice. n=4/group. (D) Short-chain acylcarnitine concentrations in blood of untreated P1 mice. n = 5-10/group. (E) Hepatic triacylglycerol (TAG) content in livers of untreated P1 mice. n = 5-6/group. *, p < 0.05; **, p < 0.01; ***, p < 0.001 by Student's *t* test.

Figure 4.3. Mother's milk-induced impairment of *de novo* βOHB production in neonatal SCOT-KO liver. (A) Hepatic fractional ¹³C-enrichments of β-hydroxybutyrate (βOHB) (left), total βOHB pools (middle), and ¹³C-βOHB concentration (right) 20 min after ip injection of sodium [1,2,3,4-¹³C₄]octanoate (10 μmol per g body weight) in P1 mice. n=6-8/group. (B) Fractional ¹³C-enrichments of βOHB (left), total βOHB pools (middle), and ¹³C-βOHB concentration (right) 20 min after ip injection of sodium [1,2,3,4-¹³C₄]octanoate (10 μmol per g body weight) in livers of unfed P0 mice. n=6/group. (C) Plasma total ketone body (TKB) concentration, mM, measured in P0 wild type and SCOT-KO mice prior to the onset of suckling. n = 4/group. (D) Plasma TKB, mM, measured in P0 wild type and SCOT-KO mice within 2 hours after the onset of suckling. The distributions of D-βOHB and AcAc are shown. n = 8-10/group. †, p < 0.05 for AcAc; *, p < 0.05 for βOHB. n = 6-7/group. (E) Fractional ¹³C-enrichments of βOHB (left), total βOHB pools (middle), and ¹³C-βOHB concentration (right) 20 min after ip injection of sodium [1,2,3,4-¹³C₄]octanoate (10 μmol per g body weight) in milk-fed P0 mice. n = 6-7/group. ***, p < 0.001 by Student's *t* test. AcAc, acetoacetate.

Figure 4.4. Normal *in vitro* hepatic ketogenesis of livers from SCOT-KO mice. Determination of ketone body production (pmol ketone/mg liver), 0.25, 1, and 8 hr after stimulation with BSA-conjugated oleic acid (150 μM), was used to derive ketogenic rate (pmol/mg/liver/hr) in liver explants derived from

(A) unfed and (B) fed P0 mice. n = 4/group for unfed pups and n = 8-10/group for fed pups. **, p < 0.01; ***, p < 0.001 by 1-way ANOVA.

Figure 4.5. D-βOHB inhibits neonatal hepatic ketogenesis *in vivo*. (A) Total βOHB pools, (B) fractional ¹³C-enrichments of βOHB, and (C) ¹³C-βOHB concentrations, 20 min after ip injection of sodium [1,2,3,4-¹³C₄]octanoate (10 μmol per g body weight) alone, or co-injected with [¹³C]octanoate plus 20 μmol per g body weight unlabeled AcAc, L-βOHB, or D-βOHB, in livers of milk-fed P0 mice. The [¹³C]octanoate alone datasets (the white bars in these panels) are reproduced from **Fig. 3E** for comparison. n = 5-7/group for each panel. *, p < 0.05; **, p < 0.01; ***, p < 0.001 vs. wild type neonates injected with [¹³C]octanoate alone, or as indicated by 1-way ANOVA. ††, p < 0.01, †††, p < 0.001 vs. AcAc co-injected neonates.

Figure 4.6. Oxidized hepatic redox potential in P1 SCOT-KO mice. (A) Plasma AcAc/D-βOHB molar ratios in milk-fed P0 mice. n = 8-9/group. (B) NAD⁺/NADH ratios, NAD⁺, NADH, and total NAD [NAD⁺ + NADH; NADt (nmol/g tissue)] in livers (n = 5/group) and (C) skeletal muscles of fed P0 neonates (n = 6/group). (D) Plasma AcAc/D-βOHB molar ratios in P1 mice. n = 11-14/group. (E) NAD⁺/NADH ratios, [NAD⁺], [NADH], and [NADt] (nmol/g tissue) in livers and (F) skeletal muscles of P1 wild type and SCOT-KO mice. n = 13-14/group. **, p < 0.01; ***, p < 0.001 by Student's *t* test.

Figure S4.1. PDH-E1α Ser293 phosphorylation in P1 Liver. (A) Immunoblot for phosphorylated Ser293 of Pyruvate Dehydrogenase (PDH) E1α subunit (PDH-p293) and total PDH-E1α (PDHt) in protein lysates derived from livers of P0 mice. (B) Densitometric quantification of phosphorylated Ser293 of PDH-E1α (pSer293-PDHE1α) normalized to total PDHE1α. n = 7/group.

Figure S4.2. Normal oxidative and ketogenic machinery in livers of P1 SCOT-KO mice. (A) Relative mRNA abundances of *Fabp1*, *Fgf21*, *Cpt1a*, *Acadm*, *Hmgcs2*, and *Bdh1* in livers of P1 mice. n = 5/group. (B) Immunoblots for HMGCS2 and actin in protein lysates derived from livers of P1 mice. Densitometric quantification normalized to actin below. n = 4/group. (C) Immunoblots for BDH1 and actin in protein lysates derived from livers of P1 mice. Densitometric quantification normalized to actin below. n = 7/group. *, p < 0.05 by Student's t test.

Figure S4.3. Normal hepatic fractional enrichment of ¹³C-glutamate from [¹³C]octanoate in P0 SCOT-KO mice. (A) Fractional ¹³C-enrichments of glutamate (left) and total hepatic glutamate pools (right) 20 min after intraperitoneal injection of sodium [1,2,3,4-¹³C₄]Octanoate (10 μmol per g body weight) in livers of unfed (n=6-7/group) and (B) milk-fed P0 mice (n = 6/group).

Figure S4.4. Normal oxidative and ketogenic machinery in livers of milk-fed P0 SCOT-KO mice. (A) Relative mRNA abundance of *Fabp1*, *Cpt1a*, *Acadm*, *Hmgcs2*, and *Bdh1* in livers of fed P0 mice. n = 5/group. (B) Immunoblots for HMGCS2 and actin in protein lysates derived from livers of P0 mice. Densitometric quantification normalized to actin on right. n = 4/group. *, p < 0.05 by Student's t test.

Figure S4.5. Relative abundances of mRNAs encoding mediators of NAD⁺ metabolism and signaling in livers of P0 and P1 mice. n = 5/group. *Nampt*, nicotinamide adenine dinucleotide phosphoribosyl transferase. *Sirt1*, silent mating type information regulation 2 homolog 1.

Figure S4.6. CoA transferase protein abundance in neonatal tissues. CoA transferase (SCOT) and actin immunoblots of protein lysates derived from brain, heart, skeletal muscle, and liver collected from P0 wild type and SCOT-KO mice.

Figure 4.1

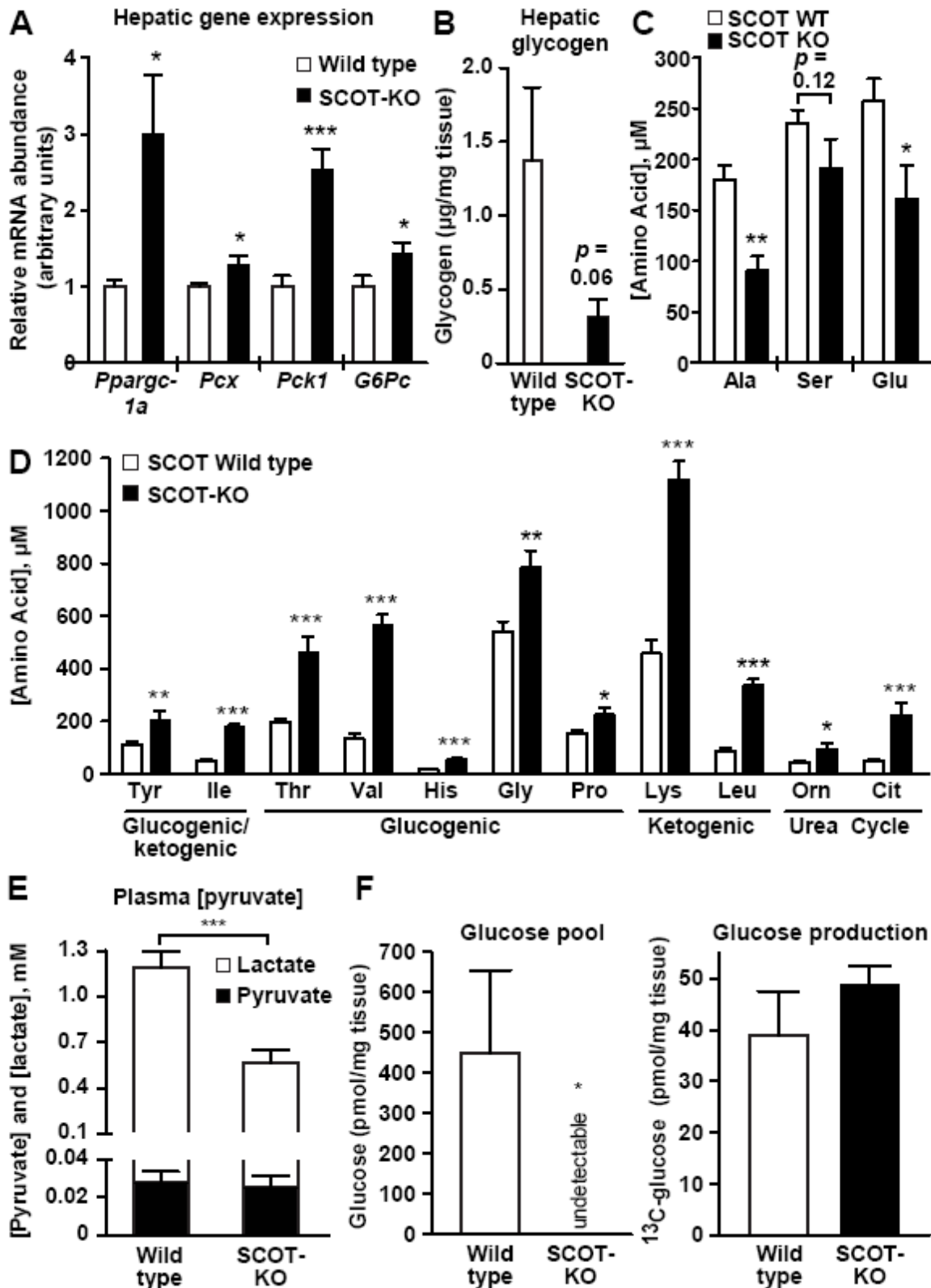


Figure 4.2

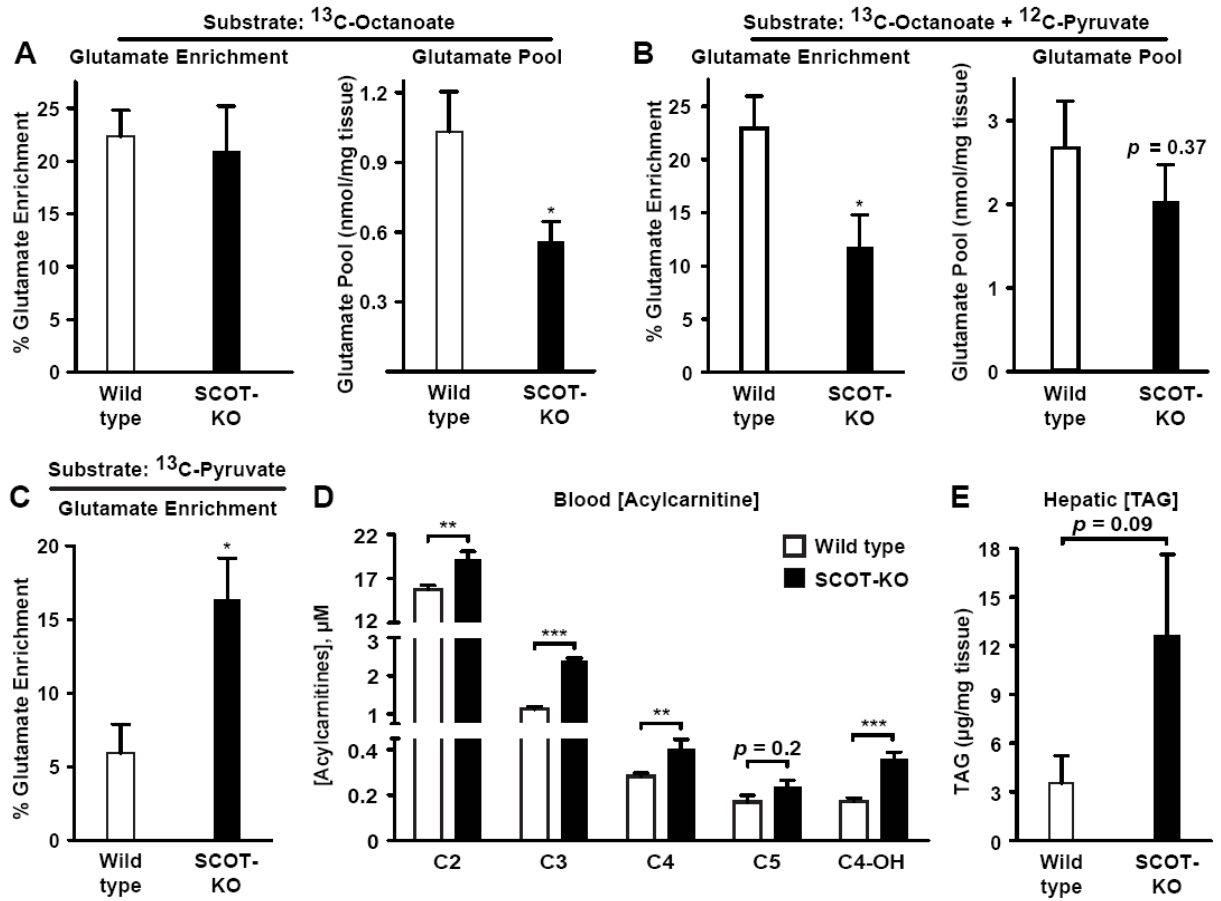


Figure 4.3

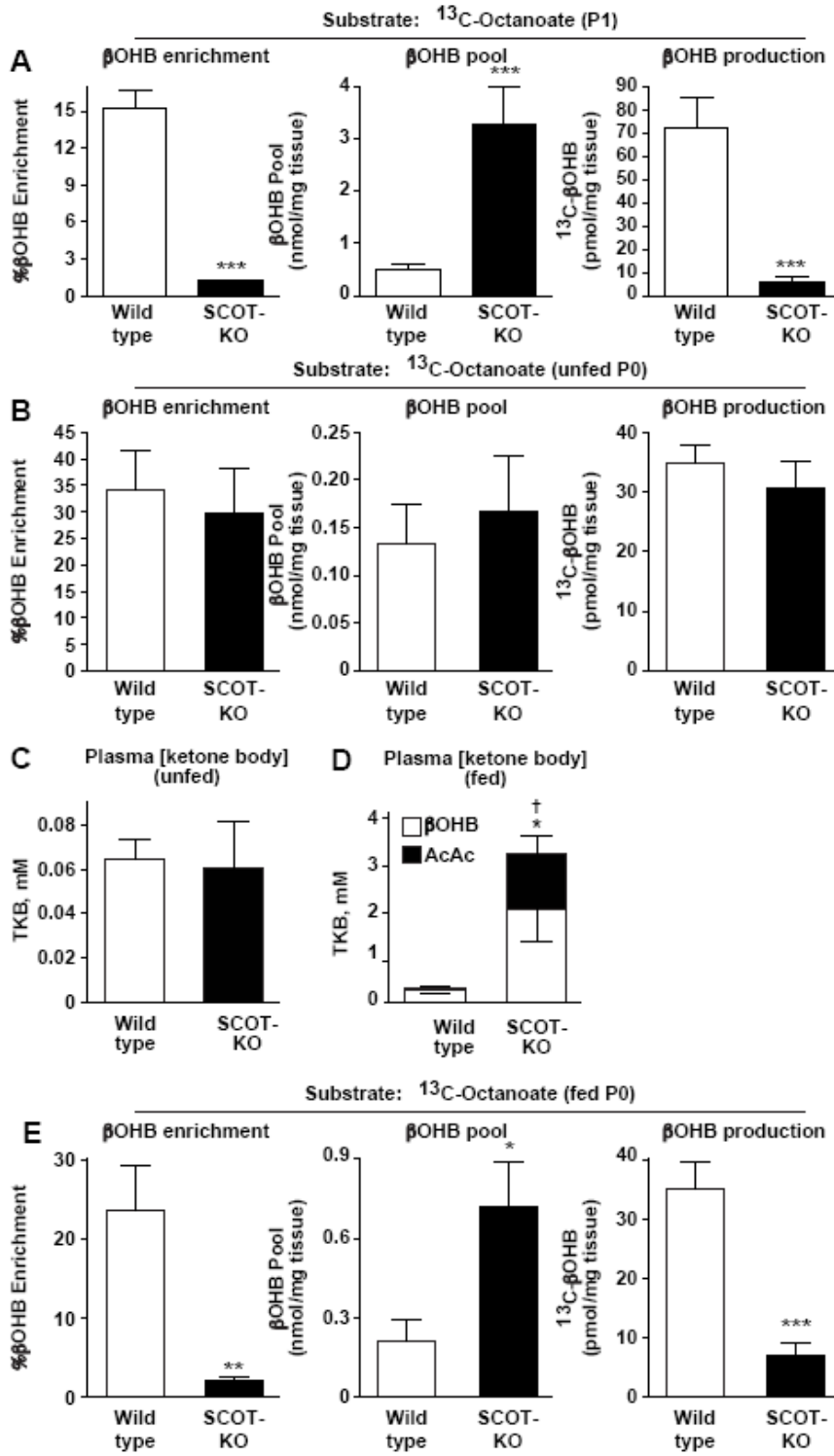


Figure 4.4

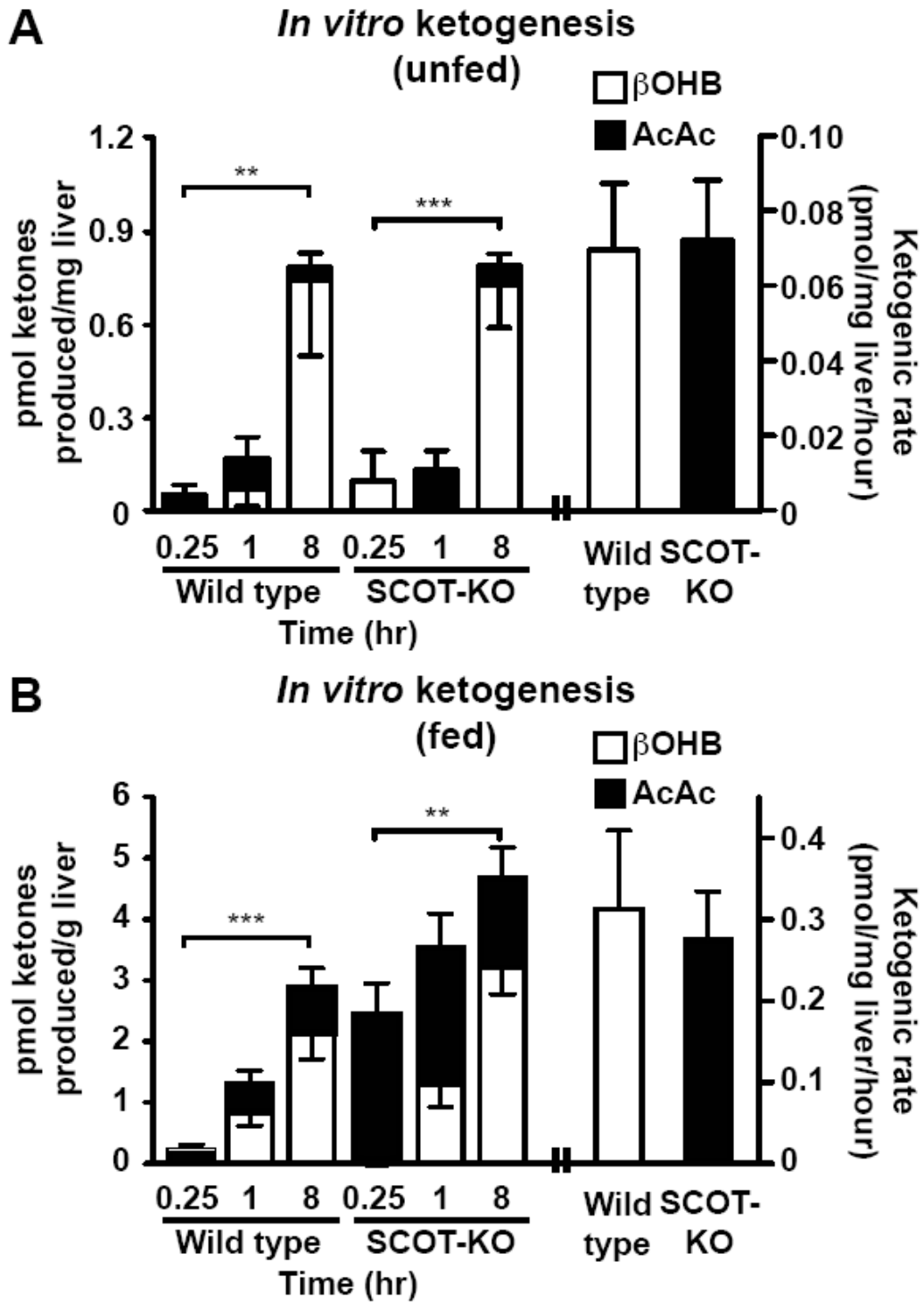


Figure 4.5

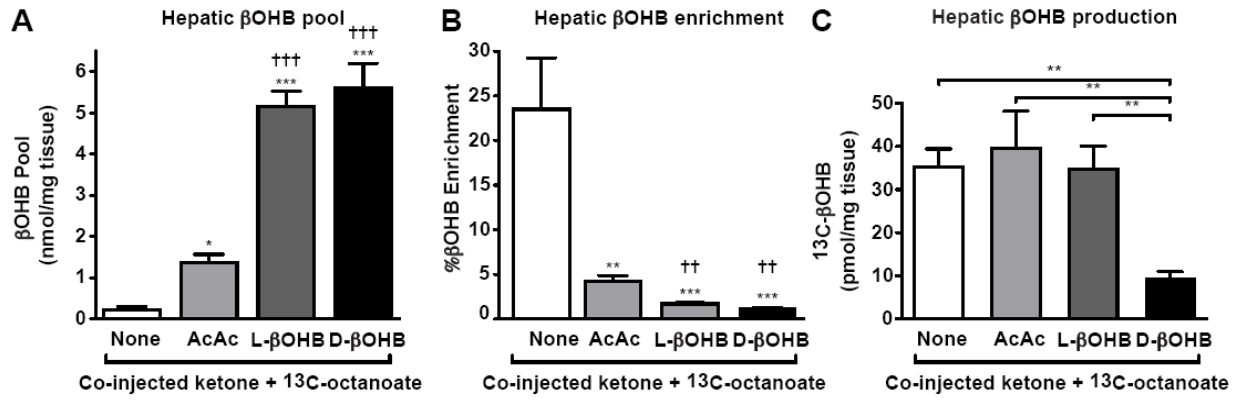


Figure 4.6

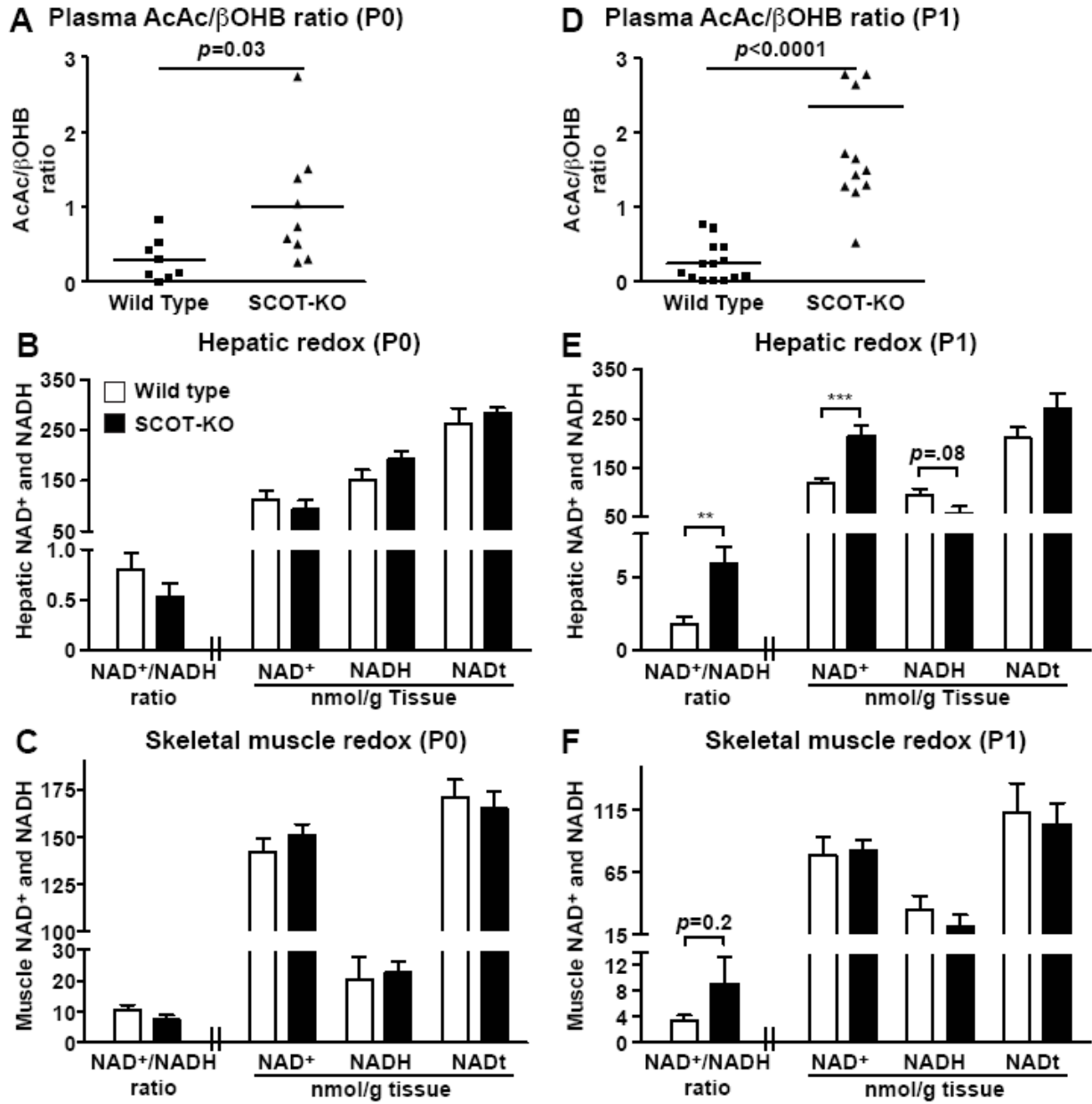


Figure S4.1

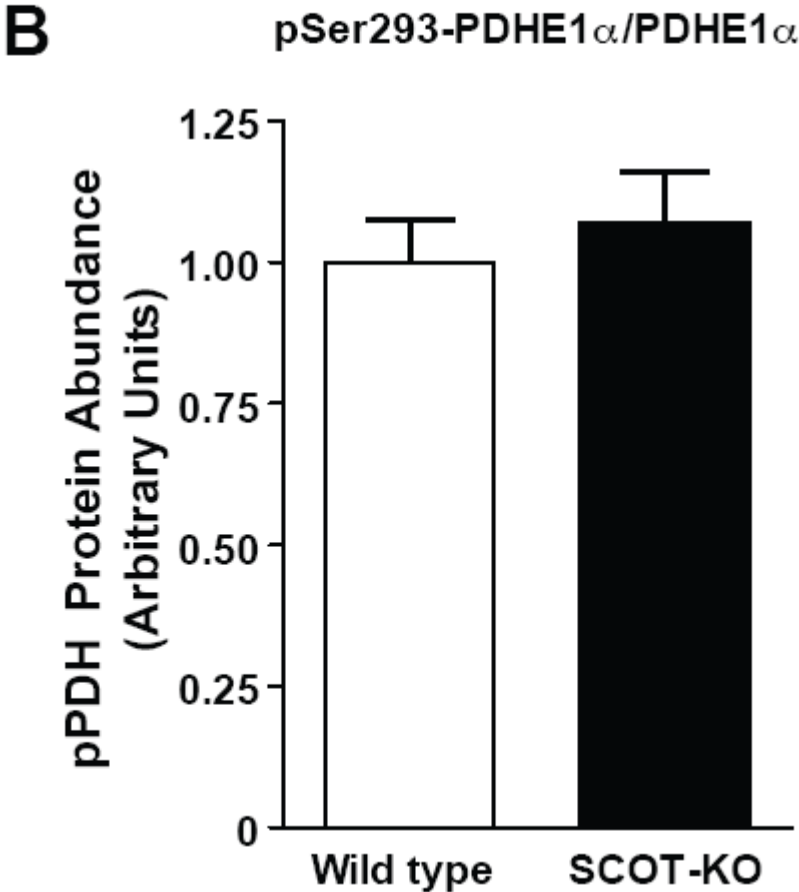
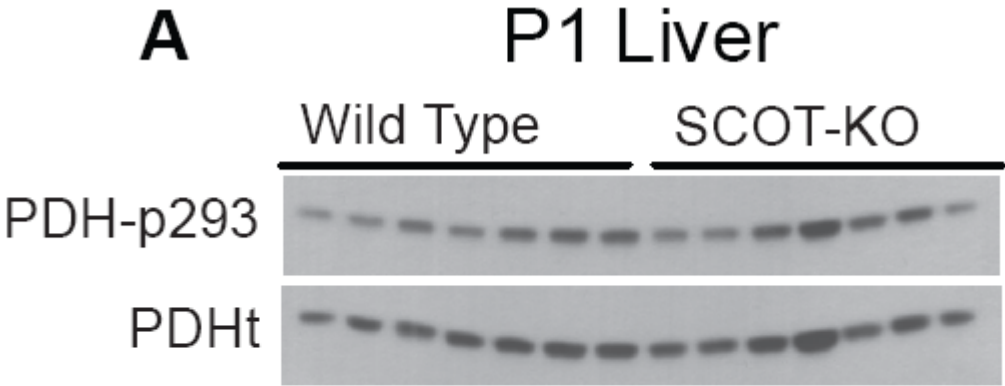


Figure S4.2

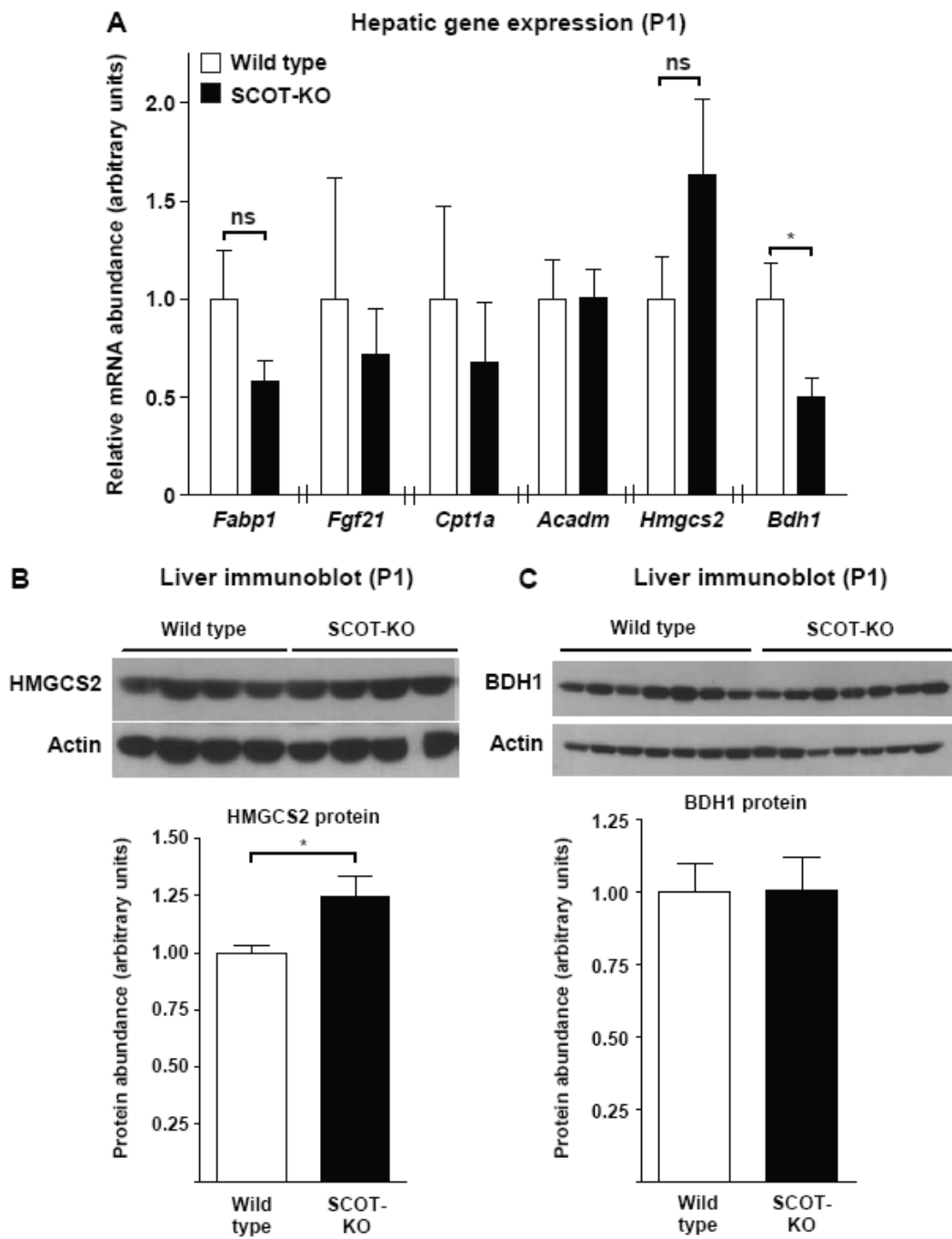


Figure S4.3

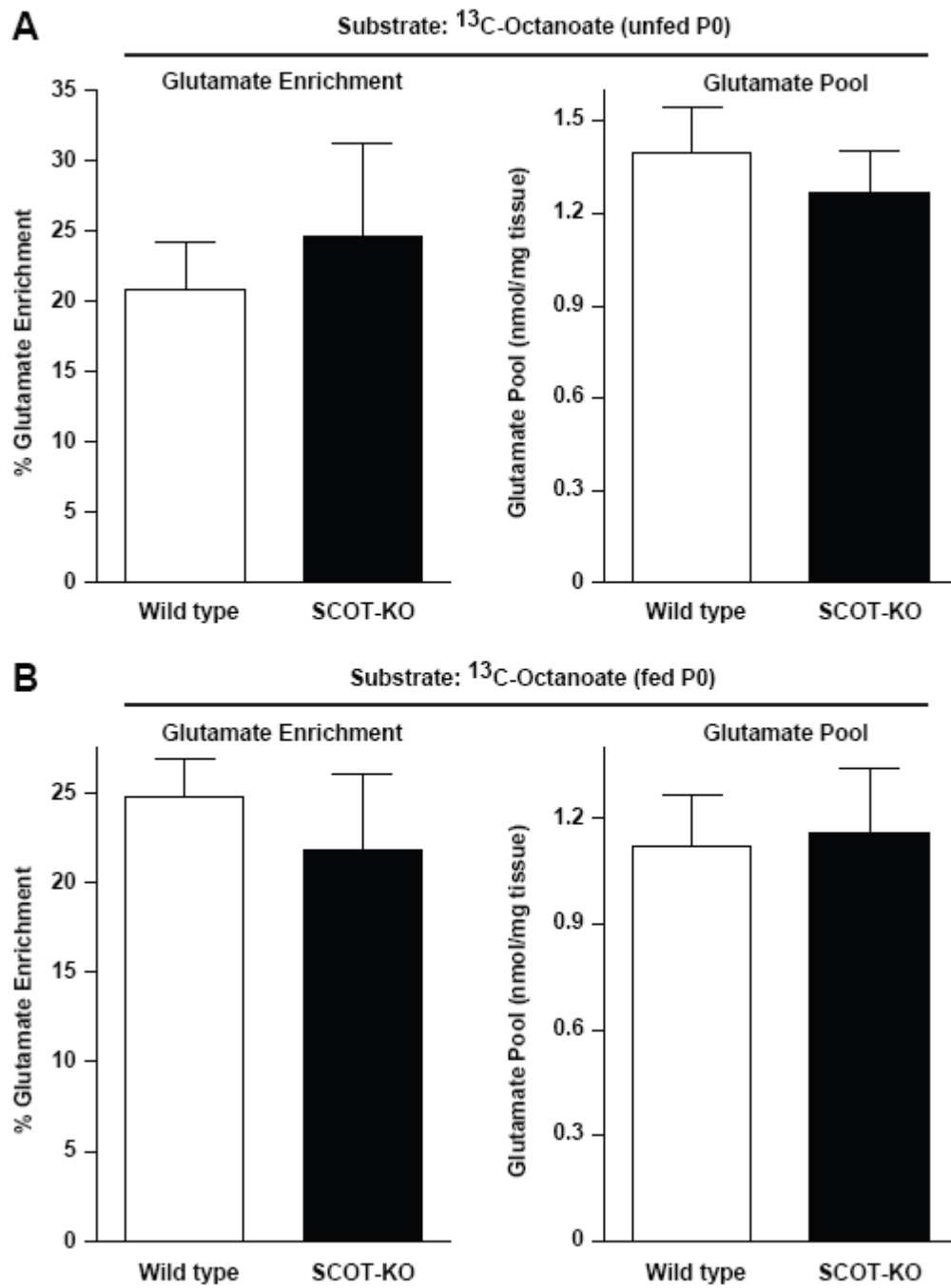


Figure S4.4

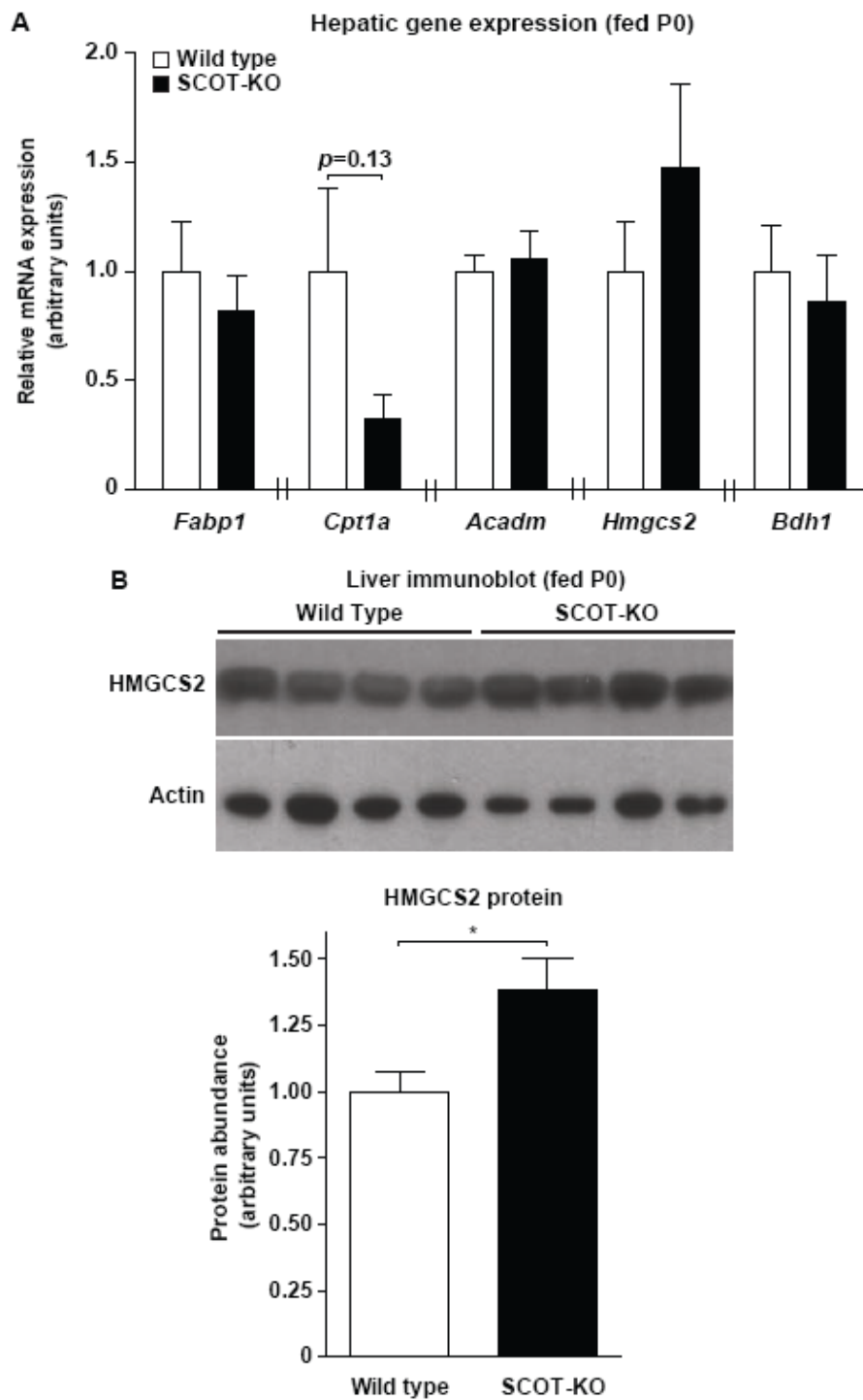


Figure S4.5

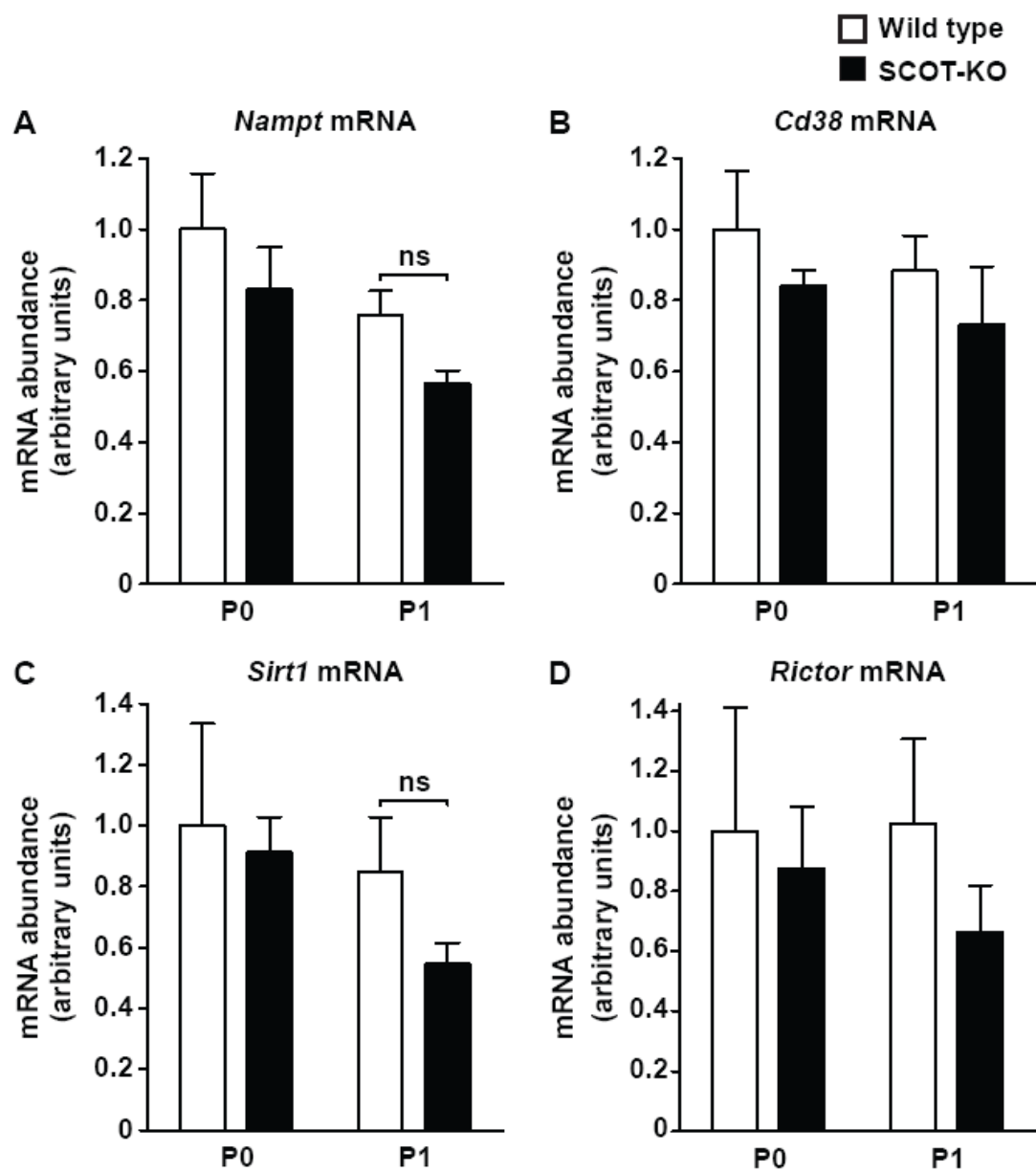


Figure S4.6

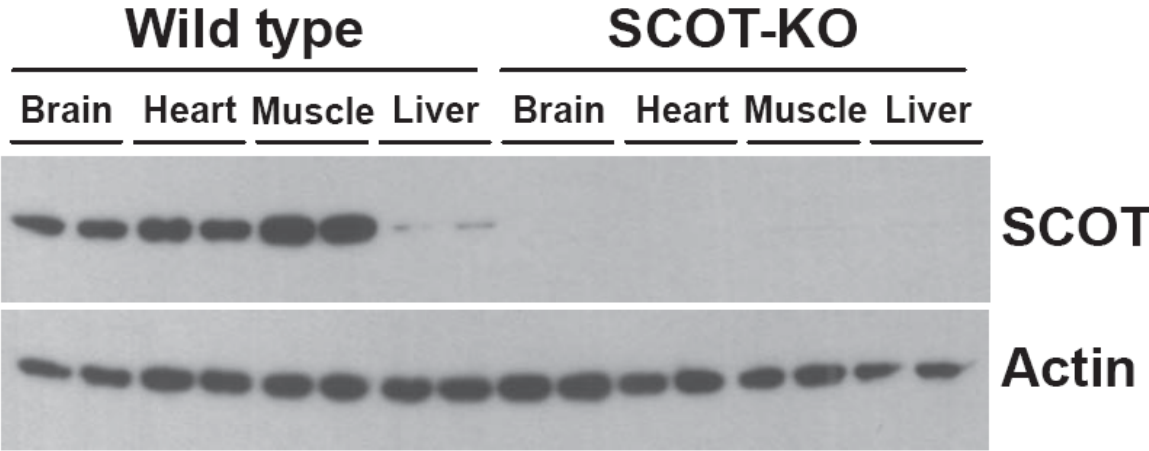


Table S4.1

RT-qPCR Primers	Sequence (5'-3')	
	Forward	Reverse
<i>Acadm</i>	GCTGGAGACATTGCCAATCA	TCTTGGCGTCCCTCATCAG
<i>Bdh1</i>	TGCAACAGTGAAGAGGTGGAGAAG	CAAACGTTGAGATGCCTGCGTTGT
<i>Cpt1a</i>	CATGTCAAGCCAGACGAAGA	TGGTAGGAGAGCAGCACCTT
<i>Fabp1</i>	AAAGTGGTCCGCAATGAGTTCACC	TTGTCACCTTCCAGCTTGACGACT
<i>Fgf21</i>	CCAGATGTGGGCTCCTCTGAC	AGAAACAGCCCTAGATTGAGGAAGAGT
<i>G6pc</i>	AAAGTCAACCGCCATGCAAAGGAC	TAGCAAAGAAAGACAGGGCTACCAG
<i>Hmgcs2</i>	TGGTTCAAGACAGGGACACAGAAC	AGAGGAATACCAGGGCCCAACAAT
<i>Rpl32</i>	CCTCTGGTGAAGCCCAAGATC	TCTGGGTTTCCGCCAGTTT
<i>Pck1</i>	GGAAGGACAAAGATGGCAAGTTC	AGGCGTTTTCTTAGGGATGTAG
<i>Pcx</i>	ACAGCACACACACTACCTGCAATG	GCAGGCCCTTATTTGGCAAGAGAT
<i>Ppargc1a</i>	CGGAAATCATATCCAACCAG	TGAGGACCGCTAGCAAGTTTG

Table S4.2

Table S2: P0 Hepatic Taurine Concentrations

Age	Genotype	Treatment	[Taurine] ± SEM	95% CI of mean	<i>p</i> value vs identically treated WT	<i>p</i> value vs unfed genotype control	<i>p</i> value vs Fed, [¹³ C]Octanoate WT
P0	Wild Type	Unfed, [¹³ C]Octanoate	9.27±1.3, n = 7	6.088-12.46	-	-	-
		Fed, [¹³ C]Octanoate	9.13±1.7, n = 7	4.959-13.3	-	* <i>p</i> > 0.05	-
		Fed, [¹³ C]Octanoate + unlabeled AcAc	7.24±0.29, n = 5	6.444-8.038	-	-	** <i>p</i> > 0.05
		Fed, [¹³ C]Octanoate + unlabeled L-βOHB	10.35±0.99, n = 5	7.613-13.09	-	-	** <i>p</i> > 0.05
		Fed, [¹³ C]Octanoate + unlabeled D-βOHB	9.90±0.71, n = 7	8.156-11.64	-	-	** <i>p</i> > 0.05
	SCOT-KO	Unfed, [¹³ C]Octanoate	9.64±1.2, n = 5	6.313-12.97	* <i>p</i> > 0.05	-	-
		Fed, [¹³ C]Octanoate	9.20±1.3, n = 6	5.862-12.53	* <i>p</i> > 0.05	* <i>p</i> > 0.05	-

*2-way ANOVA, with Bonferroni Post-tests to compare matched groups

**1-way ANOVA, with Tukey's Multiple Comparison Test

Table S4.3

Table S3: P1 Hepatic Taurine Concentrations

Age	Genotype	Treatment	[Taurine] ± SEM	95% CI of mean	p value vs identically treated WT	p value vs Fed, [¹³ C]Octanoate genotype control
P1	Wild Type	Fed, [¹³ C]Octanoate	7.13±0.61, n = 8	5.684-8.571	-	-
		Fed, [¹³ C]Octanoate + unlabeled Pyruvate	7.04±1.17, n = 6	4.019-10.05	-	*p > 0.05
		Fed, [¹³ C]Pyruvate	7.39±1.09, n = 3	2.699-12.09	-	*p > 0.05
	SCOT-KO	Fed, [¹³ C]Octanoate	5.12±0.78, n = 6	3.122-7.126	*p > 0.05	-
		Fed, [¹³ C]Octanoate + unlabeled Pyruvate	4.97±0.31, n = 7	4.2-5.74	*p > 0.05	*p > 0.05
		Fed, [¹³ C]Pyruvate	5.48±0.67, n = 3	2.608-8.361	*p > 0.05	*p > 0.05

*2-way ANOVA, with Bonferroni Post-tests to compare matched groups

Table S4.4

Table S4: P0 Blood Amino Acid Profile

Amino Acid	Wild Type							SCOT-KO					Average		
	4044	4045	4046	4049	4051	4090	4092	4047	4050	4091	4094	4093	Wild Type	SCOT-KO	t-test
Allo-Isoleucine	0	0	0	0	0	0	0	0	0	0	0	0	0.00	0.00	-
Homocystine	0	0	0	0	0	0	0	0	0	0	0	0	0.00	0.00	-
Cystathionine	2	5	3	3	7	1	2	5	2	1	2	2	3.29	2.40	0.435219394
Citrulline	65	68	74	64	63	90	64	73	72	76	63	62	69.71	69.20	0.91983894
Argininosuccinic Acid	0	0	0	0	0	0	0	0	0	0	0	0	0.00	0.00	-
Ornithine	84	94	79	120	157	115	101	104	105	120	90	84	107.14	100.60	0.629638674
Homocitrulline	5	3	3	3	3	3	3	4	3	3	2	3	3.29	3.00	0.522769653
Hydroxyproline	105	68	83	82	86	96	104	70	78	92	96	76	89.14	82.40	0.377662835
a-Amino Adipic Acid	17	21	15	21	24	21	19	22	14	17	14	17	19.71	16.80	0.139698424
B-Amino Isobutyric Acid	1	2	1	2	2	2	1	4	2	1	1	1	1.57	1.80	0.681212747
B-Alanine	43	28	33	42	45	37	37	51	45	28	26	28	37.86	35.60	0.665728987
Sarcosine	23	19	12	10	13	19	10	11	7	7	4	5	15.14	6.80	0.008162578
Gamma-Amino Butyric Acid	7	5	8	13	4	18	38	8	10	8	13	11	13.29	10.00	0.561582295
Carnosine	1	0	1	0	0	1	0	1	1	0	1	0	0.43	0.60	0.599470311
a-Amino Butyric Acid	6	6	5	5	9	8	7	6	4	8	9	6	6.57	6.60	0.977671778
Phenylalanine	151	136	163	122	126	121	85	122	133	110	111	92	129.14	113.60	0.247921683
Tyrosine	162	232	218	142	181	147	114	255	184	174	120	123	170.86	171.20	0.990481268
Isoleucine	74	92	76	67	80	84	135	102	96	104	63	61	86.86	85.20	0.900878112
Threonine	214	261	316	260	323	328	277	289	340	387	369	280	282.71	333.00	0.080636857
Valine	224	271	270	221	240	219	143	289	308	286	200	189	226.86	254.40	0.354021927
Histidine	51	91	92	66	98	66	24	93	103	54	28	26	69.71	60.80	0.629664813
Serine	258	260	291	283	256	451	305	233	294	318	362	272	300.57	295.80	0.897297763
Glycine	994	656	729	779	729	1050	1130	779	1010	1100	975	1050	866.71	982.80	0.255152912
Methionine	200	171	145	140	167	113	111	134	135	119	84	89	149.57	112.20	0.054794954
Cystine	1	1	0	0	3	1	1	5	1	2	1	1	1.05	2.00	0.246151273
Glutamine	81	195	81	50	76	561	699	219	26	544	648	557	249.00	398.80	0.359067939
Glutamic Acid	676	566	647	740	797	340	375	539	755	239	258	250	591.57	408.20	0.147941856
GLN + GLUT	757	761	728	790	873	901	1074	758	781	783	906	807	840.57	807.00	0.581285893
Arginine	643	506	495	654	319	601	654	530	790	774	560	438	553.14	618.40	0.435911217
Alanine	240	333	267	238	379	306	232	190	217	219	209	197	285.00	206.40	0.012604607
Proline	205	287	279	211	280	263	211	220	227	243	218	206	248.00	222.80	0.183189893
Lysine	1300	1090	1130	1320	1020	1130	1140	1250	1650	1580	1040	905	1161.43	1285.00	0.366499673
Leucine	147	185	158	132	152	144	61	184	190	175	129	105	139.86	156.60	0.469888583

Table S4.5

Table S5: P1 Blood Amino Acid Profile

Amino Acid	Wild Type										SCOT-KO					Average		
	3778	3779	3781	4273	4274	4275	4277	4279	4280	4282	3780	3782	3783	4276	4281	Wild Type	SCOT-KO	t-test
Allo-Isoleucine	0	0	0	0	0	0	0	0	0	0	0	0	0	0	0.00	0.00	-	
Homocystine	0	0	0	0	0	0	0	0	0	0	0	0	0	0	0.00	0.00	-	
Cystathionine	0	0	0	0	0	0	0	0	0	0	0	0	0	0	0.00	0.40	0.164823445	
Citrulline	32	31	33	65	50	67	49	64	71	51	138	265	378	196	138	51.30	223.00	0.000112041
Argininosuccinic Acid	0	0	0	0	1	0	0	1	1	1	0	0	0	1	1	0.40	0.40	1
Ornithine	26	19	23	55	54	56	37	64	53	48	75	41	64	100	180	43.50	92.00	0.017523084
Homocitrulline	1	1	1	2	2	2	1	2	2	2	5	7	7	3	3	1.60	5.00	0.000165899
Hydroxyproline	61	75	97	74	68	79	80	79	78	80	48	31	52	89	57	77.10	55.40	0.014528725
a-Amino Adipic Acid	10	7	9	11	10	8	12	12	11	13	26	16	11	16	18	10.30	17.40	0.00220857
B-Amino Isobutyric Acid	0	1	1	1	1	1	1	1	1	1	8	4	5	5	8	0.90	6.00	8.8533E-07
B-Alanine	16	28	30	21	14	20	15	19	20	24	25	18	21	28	34	20.70	25.20	0.166704481
Sarcosine	2	0	0	6	4	3	4	6	6	6	5	14	3	5	8	3.70	7.00	0.075116628
Gamma-Amino Butyric Acid	14	5	13	12	4	15	6	7	6	10	16	7	15	22	12	9.20	14.40	0.057859734
Carnosine	0	1	1	0	0	0	0	0	0	1	0	0	1	0	0	0.30	0.20	0.705338238
a-Amino Butyric Acid	3	3	3	3	2	2	3	3	5	3	21	11	14	12	14	3.00	14.40	4.96457E-07
Phenylalanine	63	60	57	93	73	164	78	103	88	71	100	80	88	153	85	85.00	101.20	0.357398664
Tyrosine	77	77	86	142	105	188	80	137	120	85	151	122	190	212	335	109.70	202.00	0.008951912
Isoleucine	21	35	23	72	42	76	41	79	60	35	190	134	205	189	165	48.40	176.60	2.12516E-07
Threonine	150	152	188	205	190	275	158	196	252	194	456	263	443	647	488	196.00	459.40	6.3605E-08
Valine	78	89	86	167	106	210	113	216	182	89	554	429	691	570	575	133.60	563.80	3.67709E-08
Histidine	11	11	11	29	17	26	13	26	17	13	52	36	57	63	66	17.40	54.80	3.06019E-06
Serine	163	191	239	274	243	294	197	255	264	237	165	114	160	243	273	235.70	191.00	0.123295735
Glycine	365	370	448	568	477	606	543	699	692	635	716	653	716	1020	811	540.30	783.20	0.004478959
Methionine	29	60	36	64	48	102	54	58	75	53	50	40	54	95	72	57.90	62.20	0.711631387
Cystine	1	0	0	1	1	1	1	0	1	1	1	1	1	2	1	0.70	1.20	0.075345501
Glutamine	261	237	269	330	262	403	257	429	493	382	494	292	297	557	482	332.30	424.40	0.117713969
Glutamic Acid	168	161	182	363	267	312	226	299	297	295	147	89	90	249	229	257.00	160.80	0.028083563
Gln + Glu	429	398	451	693	529	715	483	728	790	677	641	381	387	806	711	589.30	585.20	0.963720784
Arginine	154	135	175	503	462	354	282	496	420	448	348	329	413	678	518	342.90	457.20	0.174186768
Alanine	117	151	242	198	178	235	159	160	220	145	69	62	74	137	110	180.50	90.40	0.00100276
Proline	113	111	152	175	130	227	148	153	200	141	216	154	183	302	263	155.00	223.60	0.015702315
Lysine	278	248	242	664	538	449	440	692	505	514	891	1085	1237	1280	1100	457.00	1118.60	3.74225E-06
Leucine	40	60	49	117	68	145	73	138	101	59	351	257	378	373	324	85.00	336.60	5.61194E-08

Table S4.6

Table S6: P1 Blood Acylcarnitine Profile

Acylcarnitir	Wild Type										SCOT-KO					Average		
	3778	3779	3781	4273	4274	4275	4277	4279	4280	4282	3780	3782	3783	4276	4281	Wild Type	SCOT-KO	t-test
C2	17.72	14.89	16.57	17.48	13.75	14.75	17.18	16.77	15.38	12.77	21.16	18.51	19.17	20.94	16.09	15.73	19.18	0.004005638
C3	0.99	1.27	0.94	1.04	0.85	0.96	1.40	1.59	1.04	1.20	2.29	2.66	2.34	2.19	2.45	1.13	2.39	9.95717E-08
C4	0.21	0.25	0.23	0.33	0.33	0.33	0.24	0.33	0.27	0.31	0.35	0.29	0.44	0.38	0.55	0.28	0.40	0.007942608
C5	0.06	0.09	0.09	0.13	0.07	0.27	0.25	0.29	0.17	0.28	0.14	0.20	0.25	0.30	0.29	0.17	0.24	0.198711267
C4-OH	0.16	0.12	0.14	0.17	0.14	0.19	0.24	0.15	0.27	0.14	0.37	0.33	0.33	0.30	0.47	0.17	0.36	2.5966E-05
C6	0.11	0.15	0.12	0.17	0.12	0.22	0.15	0.16	0.11	0.20	0.17	0.07	0.08	0.22	0.13	0.15	0.13	0.521753727
C5-OH	0.11	0.21	0.15	0.09	0.16	0.10	0.18	0.11	0.08	0.14	0.14	0.13	0.11	0.15	0.13	0.13	0.13	0.983879556
C6-OH	0.06	0.08	0.07	0.07	0.07	0.14	0.06	0.07	0.14	0.10	0.10	0.05	0.06	0.06	0.09	0.09	0.07	0.422646178
C8:1	0.08	0.08	0.07	0.07	0.14	0.07	0.12	0.11	0.07	0.10	0.07	0.07	0.09	0.09	0.09	0.09	0.08	0.521978657
C8	0.14	0.16	0.20	0.35	0.18	0.21	0.15	0.21	0.25	0.24	0.27	0.20	0.21	0.16	0.14	0.21	0.19	0.637227768
C3-DC	0.13	0.21	0.07	0.10	0.14	0.15	0.18	0.11	0.07	0.14	0.10	0.15	0.13	0.15	0.14	0.13	0.13	0.883277166
C10:1	0.06	0.13	0.10	0.18	0.11	0.14	0.12	0.11	0.18	0.21	0.20	0.07	0.15	0.16	0.14	0.13	0.14	0.654451525
C10	0.14	0.27	0.20	0.18	0.14	0.17	0.21	0.21	0.14	0.21	0.17	0.12	0.36	0.22	0.23	0.19	0.22	0.334709346
C5-DC	0.04	0.09	0.09	0.07	0.05	0.05	0.08	0.05	0.08	0.11	0.05	0.07	0.08	0.10	0.10	0.07	0.08	0.567756409
C12:1	0.03	0.03	0.07	0.07	0.14	0.07	0.06	0.07	0.14	0.07	0.03	0.05	0.06	0.19	0.18	0.07	0.10	0.351586709
C12	0.25	0.24	0.61	0.46	0.25	0.31	0.21	0.25	0.36	0.17	0.27	0.32	0.21	0.19	0.32	0.31	0.26	0.454988682
C12-OH	0.08	0.11	0.07	0.07	0.11	0.10	0.06	0.07	0.11	0.10	0.03	0.05	0.09	0.06	0.09	0.09	0.07	0.079421424
C14:2	0.13	0.09	0.08	0.15	0.11	0.11	0.09	0.08	0.11	0.08	0.10	0.09	0.12	0.21	0.12	0.10	0.13	0.21613272
C14:1	0.13	0.15	0.23	0.34	0.22	0.15	0.12	0.28	0.22	0.19	0.22	0.13	0.27	0.25	0.20	0.20	0.21	0.776679216
C14	0.58	0.80	1.02	0.56	0.41	0.44	0.56	0.53	0.59	0.42	0.61	0.63	1.04	0.67	0.35	0.59	0.66	0.551167734
C14:1-OH	0.08	0.09	0.08	0.11	0.22	0.15	0.12	0.08	0.19	0.08	0.10	0.09	0.19	0.21	0.12	0.12	0.14	0.435195153
C14-OH	0.08	0.09	0.11	0.07	0.11	0.18	0.03	0.08	0.07	0.08	0.06	0.13	0.12	0.08	0.08	0.09	0.09	0.907496141
C16:1	0.23	0.19	0.30	0.23	0.27	0.23	0.30	0.26	0.33	0.20	0.25	0.16	0.46	0.29	0.16	0.25	0.27	0.781835331
C16	1.77	1.80	2.74	1.97	2.12	1.85	2.38	2.53	2.54	2.36	1.92	1.81	2.58	2.32	1.63	2.21	2.05	0.447653434
C16:1-OH	0.10	0.16	0.15	0.08	0.16	0.15	0.11	0.08	0.11	0.16	0.07	0.16	0.07	0.17	0.16	0.13	0.13	0.929752724
C16-OH	0.13	0.09	0.15	0.08	0.16	0.12	0.15	0.11	0.07	0.16	0.07	0.10	0.11	0.08	0.12	0.12	0.10	0.132382636
C18:2	0.35	0.25	0.30	0.31	0.31	0.19	0.41	0.45	0.40	0.41	0.15	0.42	0.39	0.34	0.24	0.34	0.31	0.530465147
C18:1	0.48	0.63	0.49	0.93	0.90	0.69	0.86	0.68	1.05	1.10	0.65	0.42	1.24	1.01	0.57	0.78	0.78	0.982233726
C18	0.29	0.28	0.60	0.43	0.47	0.46	0.45	0.53	0.36	0.49	0.47	0.45	0.71	0.59	0.49	0.44	0.54	0.081425519
C18:2-OH	0.06	0.03	0.04	0.08	0.04	0.08	0.07	0.00	0.07	0.04	0.04	0.06	0.07	0.08	0.04	0.05	0.06	0.566729767
C18:1-OH	0.10	0.06	0.07	0.08	0.12	0.08	0.11	0.11	0.07	0.04	0.07	0.03	0.07	0.08	0.12	0.08	0.08	0.594583376
C3:1	0.13	0.18	0.07	0.13	0.14	0.15	0.14	0.15	0.17	0.07	0.13	0.05	0.19	0.11	0.09	0.13	0.12	0.454109398
C5:1	0.04	0.03	0.06	0.07	0.05	0.22	0.10	0.11	0.08	0.09	0.05	0.07	0.06	0.05	0.16	0.08	0.08	0.780115357
C7	0.06	0.06	0.06	0.07	0.07	0.07	0.05	0.03	0.06	0.06	0.05	0.04	0.03	0.12	0.10	0.06	0.07	0.483714602
C10:2	0.06	0.16	0.10	0.07	0.18	0.10	0.09	0.14	0.14	0.07	0.07	0.15	0.24	0.16	0.14	0.11	0.15	0.171416363
C4-DC	0.24	0.17	0.26	0.25	0.17	0.25	0.21	0.24	0.22	0.31	0.15	0.17	0.22	0.22	0.35	0.23	0.22	0.764523709
C10:1-OH	0.06	0.08	0.07	0.11	0.07	0.14	0.18	0.11	0.11	0.10	0.10	0.07	0.06	0.06	0.14	0.10	0.09	0.469590854
C12:1-OH	0.08	0.11	0.13	0.07	0.11	0.14	0.06	0.07	0.07	0.03	0.10	0.07	0.12	0.22	0.14	0.09	0.13	0.083188547
C18-OH	0.06	0.06	0.04	0.08	0.08	0.19	0.07	0.08	0.07	0.08	0.04	0.13	0.07	0.08	0.08	0.08	0.08	0.947736921
C0 (PS)	43.28	36.93	46.94	49.43	41.17	49.08	59.39	59.24	53.79	45.28	51.99	50.89	66.76	41.69	51.83	48.45	52.63	0.35296229

Table S4.7

Table S7: P0 Blood Acylcarnitine Profile

Acylcarnitin	Wild Type							SCOT-KO					Average		
	4044	4045	4046	4049	4051	4090	4092	4047	4050	4091	4093	4094	Wild Type	SCOT-KO	t-test
C2	11.89	18.10	19.00	14.48	18.92	19.42	13.98	17.11	13.14	14.49	12.72	11.29	16.54	13.75	0.110271
C3	1.30	1.21	1.29	1.22	0.82	1.98	1.13	1.21	1.34	1.47	1.10	1.10	1.28	1.24	0.843921
C4	0.35	0.52	0.46	0.32	0.39	0.33	0.29	0.50	0.34	0.39	0.20	0.20	0.38	0.33	0.3925845
C5	0.19	0.30	0.34	0.23	0.27	0.23	0.12	0.34	0.22	0.17	0.14	0.14	0.24	0.20	0.3947801
C4-OH	0.07	0.14	0.18	0.07	0.09	0.15	0.08	0.18	0.12	0.15	0.11	0.10	0.11	0.13	0.3908674
C6	0.09	0.12	0.18	0.10	0.13	0.11	0.10	0.12	0.13	0.14	0.13	0.12	0.12	0.13	0.5341213
C5-OH	0.10	0.11	0.15	0.09	0.13	0.17	0.13	0.20	0.14	0.11	0.19	0.13	0.13	0.15	0.191973
C6-OH	0.03	0.05	0.08	0.07	0.07	0.09	0.05	0.08	0.05	0.05	0.04	0.06	0.06	0.06	0.6963757
C8:1	0.05	0.07	0.06	0.08	0.06	0.04	0.07	0.07	0.11	0.20	0.07	0.06	0.06	0.10	0.1040714
C8	0.17	0.20	0.26	0.21	0.14	0.11	0.18	0.15	0.20	0.19	0.12	0.15	0.18	0.16	0.4408606
C3-DC	0.09	0.11	0.13	0.11	0.11	0.09	0.12	0.14	0.09	0.15	0.12	0.07	0.11	0.11	0.7679052
C10:1	0.09	0.10	0.08	0.09	0.09	0.12	0.10	0.10	0.09	0.15	0.10	0.10	0.10	0.11	0.4189441
C10	0.06	0.24	0.15	0.15	0.10	0.10	0.12	0.21	0.14	0.09	0.11	0.11	0.13	0.13	0.976955
C5-DC	0.04	0.07	0.09	0.05	0.08	0.07	0.04	0.09	0.06	0.09	0.05	0.05	0.06	0.07	0.5562663
C12:1	0.14	0.08	0.08	0.11	0.07	0.08	0.05	0.07	0.09	0.17	0.08	0.05	0.09	0.09	0.8494803
C12	0.17	0.42	0.32	0.29	0.19	0.18	0.12	0.23	0.38	0.18	0.20	0.23	0.24	0.24	0.953781
C12-OH	0.04	0.09	0.05	0.06	0.04	0.07	0.04	0.06	0.06	0.09	0.03	0.04	0.06	0.06	0.9008834
C14:2	0.07	0.09	0.05	0.12	0.05	0.06	0.05	0.08	0.08	0.12	0.09	0.15	0.07	0.11	0.0588834
C14:1	0.21	0.27	0.23	0.17	0.17	0.16	0.15	0.15	0.30	0.23	0.25	0.19	0.20	0.23	0.3246697
C14	0.38	0.65	0.54	0.64	0.36	0.44	0.42	0.55	0.67	0.44	0.40	0.51	0.49	0.51	0.7392525
C14:1-OH	0.08	0.15	0.10	0.15	0.10	0.07	0.09	0.13	0.11	0.09	0.10	0.09	0.11	0.10	0.8638048
C14-OH	0.06	0.06	0.07	0.06	0.05	0.05	0.05	0.10	0.07	0.07	0.06	0.06	0.06	0.07	0.0819066
C16:1	0.23	0.26	0.31	0.40	0.27	0.22	0.25	0.39	0.50	0.26	0.19	0.28	0.28	0.32	0.3986522
C16	1.98	2.00	2.24	2.76	1.32	2.20	2.31	2.05	2.83	2.20	1.94	1.84	2.12	2.17	0.8271742
C16:1-OH	0.06	0.08	0.09	0.09	0.05	0.07	0.07	0.05	0.11	0.09	0.06	0.04	0.07	0.07	0.736131
C16-OH	0.07	0.07	0.08	0.05	0.05	0.06	0.06	0.09	0.09	0.11	0.09	0.07	0.06	0.09	0.0031344
C18:2	0.30	0.37	0.50	0.63	0.22	0.32	0.26	0.44	0.66	0.29	0.24	0.26	0.37	0.38	0.9652934
C18:1	1.00	0.79	1.40	2.23	0.67	0.79	0.74	1.26	1.98	0.89	0.63	0.57	1.09	1.06	0.943201
C18	0.41	0.40	0.45	0.67	0.26	0.54	0.39	0.44	0.72	0.47	0.50	0.35	0.45	0.50	0.5195411
C18:2-OH	0.05	0.02	0.03	0.06	0.03	0.06	0.03	0.04	0.07	0.08	0.03	0.02	0.04	0.05	0.5534946
C18:1-OH	0.07	0.06	0.04	0.09	0.06	0.03	0.03	0.05	0.09	0.08	0.06	0.05	0.06	0.07	0.3753727
C3:1	0.37	0.17	0.21	0.19	0.27	0.20	0.43	0.23	0.11	0.37	0.53	0.30	0.26	0.31	0.5671146
C5:1	0.09	0.06	0.04	0.03	0.05	0.04	0.06	0.08	0.07	0.08	0.07	0.08	0.05	0.08	0.0295567
C7	0.03	0.04	0.09	0.02	0.05	0.04	0.02	0.07	0.05	0.05	0.03	0.04	0.04	0.05	0.664936
C10:2	0.06	0.09	0.08	0.10	0.06	0.04	0.08	0.13	0.15	0.23	0.08	0.13	0.07	0.15	0.007564
C4-DC	0.10	0.18	0.12	0.14	0.19	0.24	0.17	0.18	0.16	0.20	0.24	0.14	0.16	0.18	0.4284734
C10:1-OH	0.08	0.12	0.07	0.08	0.11	0.08	0.05	0.06	0.09	0.18	0.08	0.07	0.08	0.10	0.5408406
C12:1-OH	0.08	0.11	0.06	0.12	0.09	0.12	0.09	0.10	0.04	0.21	0.06	0.07	0.10	0.09	0.9544801
C18-OH	0.02	0.05	0.05	0.08	0.02	0.04	0.06	0.05	0.07	0.08	0.05	0.06	0.05	0.06	0.1615676
C0 (PS)	46.92	55.73	67.17	54.57	60.31	70.25	50.30	82.58	49.33	56.12	56.28	60.15	57.89	60.89	0.6336703

Chapter 5

PPAR α -dependent ketogenesis prevents hepatic steatosis in neonatal mice

The work presented in this chapter has been adapted from:

Cotter, D. G., Ercal, B., d'Avignon, D. A., and Crawford, P. A. *Submitted.*

Abstract

Peroxisome Proliferator Activated Receptor alpha (PPAR α) is a master transcriptional regulator of hepatic intermediary metabolism. PPAR α mediates the adaptive response to fasting. Like fasting, nutrient supply is abruptly altered at birth when a transplacental supply of carbohydrates is replaced by a high-fat, low-carbohydrate milk diet. Here we use ^{13}C -labeled substrates to quantify dynamic metabolism and complimentary systems physiology approaches in neonatal mice to demonstrate a critical role for PPAR α in hepatic metabolic adaptation to birth. PPAR α -Knockout (KO) neonates exhibit hypoglycemia due to impaired conversion of glycerol to glucose. Quantitative substrate fate mapping of the medium-chain fatty acid [^{13}C]Octanoate in neonatal liver revealed normal contribution of this fatty acid to the hepatic TCA cycle in PPAR α -KO neonates. Moreover, livers of PPAR α -KO neonates showed evidence of direct contribution of octanoate-derived ^{13}C -labeled carbons to glucose. These mice also exhibited hypoketonemia, which could be mechanistically linked to a 50% decrease in hepatic ketogenesis from [^{13}C]Octanoate. Decreased ketogenesis was associated with diminished mRNA and protein abundance of the fate-committing ketogenic enzyme mitochondrial 3-hydroxymethylglutaryl-CoA synthase and decreased protein abundance of the ketogenic enzyme Beta-hydroxybutyrate dehydrogenase 1. Finally, hepatic triglyceride and free fatty acid concentrations were increased 6.9- and a 2.7-fold, respectively, in PPAR α -KO neonates. Together, these findings indicate an important role for PPAR α -dependent ketogenesis in disposal of excess hepatic fatty acids during the neonatal period.

Introduction

Nutrient supply and organismal bioenergetics shift dramatically at birth. At birth, a continuous transplacental nutrient stream replete with carbohydrates ceases and is replaced by a high-fat, low-carbohydrate milk diet (20,71). Thus, the neonatal liver must coordinate inductions of hepatic fatty acid oxidation, ketogenesis, and gluconeogenesis to meet the metabolic demands required for adaptation to extrauterine life (20,71). Fatty acid oxidation yields high-energy phosphates and reducing equivalents used to fuel the endergonic reactions of hepatic gluconeogenesis, and acetyl-CoA, which can be converted to ketone bodies through ketogenesis. While glucose produced in the liver is the primary fuel source for the neonatal brain, ketone bodies serve as an important glucose-sparing fuel source (2,4,71,301). Mice that cannot oxidize ketone bodies exhibit lethal neonatal hypoglycemia, indicating that ketone body metabolism is required for adaptation to birth (78).

Ketone body metabolism is a high capacity energy conduit between the liver and extrahepatic tissues that can dispose of up to two-thirds of the fat entering the liver (281). In liver mitochondria, a series of ketogenic reactions catalyzed by mitochondrial thiolase, mitochondrial 3-hydroxymethylglutaryl-CoA synthase (HMGCS2; fate-committing), and HMG-CoA lyase condense acetyl-CoA derived from beta-oxidation of fatty acids into the ketone body, acetoacetate (AcAc), which is reduced to beta-hydroxybutyrate (β OHB) by beta-hydroxybutyrate dehydrogenase 1 [(BDH1); reviewed in (2,4,5,301)]. Within mitochondria of extrahepatic tissues, BDH1 oxidizes β OHB to AcAc. Terminal oxidation of ketone bodies requires covalent activation of AcAc by coenzyme A (CoA), which is catalyzed by mitochondrial succinyl-CoA-3:oxoacid CoA transferase (SCOT), the fate committing enzyme of ketone body oxidation. SCOT is uniquely required for ketone body oxidation, and thus, oxidation of ketones does not occur in its absence (301).

Our past studies of germline SCOT-Knockout (KO) mice indicate that ketone body oxidation is required for life. All germline SCOT-KO mice die within the first 48 hr of life with hyperketonemia and hypoglycemia, and in a manner that phenocopies human sudden infant death syndrome (78,313). Surprisingly, ketone body oxidation is dispensable for survival of the neonatal period and starvation in

adults when individually eliminated from cardiomyocytes, skeletal myocytes, and neurons, which comprise the three greatest consumers of ketone bodies (108). Paradoxically, ketone body oxidation, an exclusively extrahepatic process (74,164), contributes to hepatic metabolic homeostasis by preventing toxic accumulation of ketone bodies, which alters pyruvate metabolism, fatty acid oxidation, inhibits ketogenesis, and oxidizes redox potential in liver (313). Thus, inter-organ coordination of ketogenesis and ketone body oxidation is critical for preservation of hepatic intermediary metabolism, which is vital during the transition to extrauterine life.

The nuclear receptor Peroxisome Proliferator Activated Receptor alpha (PPAR α) acts as a master transcriptional regulator of hepatic intermediary metabolism (314,315). Fasted PPAR α -KO mice exhibit hypoglycemia, hypoketonemia, and hepatic steatosis (316,317). In response to fatty acids, PPAR α promotes ketogenesis by inducing enzymatic mediators of fatty acid oxidation, Fibroblast growth factor 21 (*Fgf21*), and by directly stimulating *Hmgcs2* transcription (50,52,53,318,319). Significant overlap exists between the bioenergetic challenges faced during fasting and during the transition to birth. Therefore, we applied high-resolution measures of dynamic metabolism using ¹³C-labeled substrates and systems physiology approaches to neonatal mice to determine the mechanisms by which PPAR α supports adaptation to birth.

Methods

Animals. Fed postnatal day zero (P0, the first day of postnatal life) mice were collected within 4 hr of birth. All P1 mice were maintained with the dam through the first 30h after birth, and were milk fed. The presence of gastric milk spots was checked in all mice, both by visual inspection of the abdomen prior to experimentation and by gross examination of the gastric contents after sacrifice. Breeder pairs were maintained at 22°C on standard polysaccharide-rich chow diet (Lab Diet 5053) and autoclaved water ad libitum. Lights were off between 1800 and 0600. All experiments consisted of mouse pups that were harvested from at least two litters from two different breeder pairings. All experiments were conducted using protocols approved by the Animal Studies Committee at Washington University.

Plasma Metabolite Quantification. Serum total ketone bodies (TKB) were determined using standard biochemical assays coupled to colorimetric substrates as described previously (51). Blood glucose was measured in duplicate using handheld glucometers (Aviva).

Tissue Metabolite Quantification. Hepatic triacylglyceride (TAG) and free fatty acid (FFA) concentrations were quantified biochemically using a Folch extract of liver, as described previously (126).

Gene expression analysis. Quantification of gene expression was performed using real-time RT-quantitative PCR using the $\Delta\Delta C_t$ approach as described (51), normalizing to Rpl32, using primer sequences listed within **Table 5.1**.

Immunoblotting. Lysates from liver were generated in a protein lysis buffer: 20 mM Tris-HCl, 150 mM NaCl, 1 mM EDTA, 1% Triton X-100, 1% phosphatase inhibitor cocktail (Sigma), and protease inhibitor cocktail (complete mini EDTA-free, Roche), pH 7.5. Immunoblots to detect HMGCS2 (rabbit anti-mHMGCS; Santa Cruz Biotechnology), BDH1 (rabbit anti-BDH1; Proteintech Group), and actin (rabbit anti-actin, Sigma) were performed as described (78). Band intensities were quantified densitometrically using Quantity One software (Bio-Rad).

Glycerol and glucose tolerance tests. Glucose and glycerol tolerance were measured in fed P0 mice that had been removed from the dam and maintained on a heating pad for the duration of the experiment. For glucose tolerance tests, neonates were injected intraperitoneally (ip) with 4% glucose dissolved in milliQ H₂O (2g/kg body weight). Blood glucose was measured at 15 min and at 60 min after glucose administration via tail snip and decapitation, respectively. For glycerol tolerance tests, neonates were injected with 4% glycerol in phosphate buffered saline (2g/kg body weight). Blood glucose was measured prior to glycerol administration via tail snip and 45 min after glycerol administration via decapitation.

In vivo substrate utilization. P0 or P1 mice were injected ip with 10 μ mol of sodium [1,2,3,4-¹³C₄]octanoate per g of body weight (vendor for stable isotopes: Cambridge Isotope Laboratories). After intraperitoneal injections, neonatal mice were maintained on a heating pad for 20 min, killed by decapitation, and tissues were rapidly freeze-clamped in liquid N₂. Neutralized perchloric acid tissue

extracts were profiled using ^{13}C -edited proton nuclear magnetic resonance (NMR) measured at 11.75 T (Varian/Agilent Direct Drive-1) via first increment gradient heteronuclear single-quantum correlation (gHSQC). Signals were collected from extracts dissolved in 275 μL of D_2O + 1 mM trimethylsilyl propionate (TSP), loaded into high precision, thin walled 5-mm tubes (Shigemi). Quantification of signals by integration of the $^1\text{H}\{^{13}\text{C}\}$ and ^{13}C -edited (gHSQC) collections of carbon 2 for taurine, carbon 4 for βOHB , carbon 1 for glucose, and carbon 4 for glutamate were as described previously (78). Fractional enrichments of ^{13}C -labeled glucose, glutamate, and βOHB and tissue concentrations (pool size) of glucose, taurine, glutamate, and βOHB were calculated as described previously (51,313).

Results

PPAR α deficient neonates exhibit hypoglycemia due to impaired gluconeogenesis from glycerol. During fasting, the switch to a lipid-dominated nutrient supply evokes hypoglycemia in adult PPAR α -KO mice (316,317). Similarly, the shift to a high-fat, low-carbohydrate milk diet caused hypoglycemia in neonatal PPAR α -KO mice. On the first day of life, postnatal day zero (P0), glycemia did not differ between wild type and PPAR α -KO neonates (**Fig. 5.1A, left**). As expected, wild type neonates significantly increased glycemia between P0 and the second day of life [(P1); **Fig. 5.1A, white bars**]. In contrast, PPAR α -KO neonates failed to increase glycemia between P0 and P1 (**Fig. 5.1A, black bars**), and on P1, blood glucoses were significantly lower in PPAR α -KO neonates compared to control mice (**Fig. 5.1A, right**). Glucose tolerance tests in P0 mice demonstrated that glucose utilization was not different between wild type and PPAR α -KO neonates (**Fig. 5.1B**), suggesting that impaired gluconeogenesis might underlie the hypoglycemia of PPAR α -KO neonates. While hepatic mRNA abundances of the gluconeogenic mediators Phosphoenol pyruvate carboxykinase (*Pck1*), Glucose-6-phosphatase (*G6Pc*), and Glycerol Kinase (*Gyk*) did not differ between groups of mice on P0 or P1, expression of Glycerol phosphate dehydrogenase (*Gpd2*) trended lower in PPAR α -KO neonates on P0 and P1 (**Fig. 5.2A-D**). Furthermore, blood glucoses were lower in P0 PPAR α -KO neonates following intraperitoneal glycerol administration (glycerol

tolerance test), suggesting that PPAR α -KO neonates do not effectively convert glycerol to glucose (**Fig. 5.2E**). These results indicate that PPAR α supports glycemia during adaptation to birth by promoting gluconeogenesis from glycerol.

Loss of PPAR α does not disrupt oxidation of medium-chain fatty acids in neonatal liver. PPAR α influences hepatic energy metabolism through transcriptional regulation of the mediators of fatty acid oxidation, which is critical for gluconeogenesis. Surprisingly, mRNA abundances of many known PPAR α target genes involved in fatty acid oxidation, including Peroxisome proliferator activated receptor gamma coactivator 1-alpha (*Ppargc1a*), Carnitine palmitoyltransferase 1a (*Cpt1a*), and Acyl-CoA oxidase (*ACO*) were not different between groups of mice on either P0 or P1 (**Fig. 5.3A-C**). In fact, PPAR α -KO neonates significantly induced *Cpt1a* between P0 and P1 (**Fig. 5.3B**). Of the mediators of fatty acid oxidation analyzed, only medium chain acyl-CoA dehydrogenase (*Acadm*) transcript abundances were significantly decreased in PPAR α -KO neonates, and only on P1 (**Fig. 5.3D**). Next, we directly analyzed fatty acid oxidation in neonatal liver using proton edited ^{13}C -nuclear magnetic resonance (NMR) spectroscopy to quantify contribution of the medium-chain fatty acid [^{13}C]octanoate to the hepatic tricarboxylic acid (TCA) cycle. Following a 20 min incubation with [^{13}C]octanoate (10 $\mu\text{mol/g}$ body weight), neonates were sacrificed and livers were extracted for NMR profiling. ^{13}C -enrichment of glutamate, which serves as a quantitative surrogate for entry of ^{13}C -acetyl-CoA into the TCA cycle for terminal oxidation (136), and tissue glutamate concentrations (pool) did not differ between groups of mice on P0 or P1 (**Fig. 5.3E**). Concentrations of taurine, a normalizing metabolite, also did not differ between groups of mice on P0 or P1 (**Fig. 5.3F**). Moreover, ^{13}C -glucose enrichment from [^{13}C]octanoate was detected in both wild type and PPAR α -KO neonates on P0 and in PPAR α -KO neonates on P1 (**Fig. 5.3G, left**). On P1, enrichment of ^{13}C -glucose from octanoate was 3-fold greater in PPAR α -KO neonates compared to wild type mice (**Fig. 5.3G, left**). Since hepatic glucose pools did not differ between groups, increased enrichment reflects increased gluconeogenesis from octanoate in the PPAR α -KO neonates. ^{13}C –enrichments of 2-3% are very low, as 1% enrichment occurs from naturally abundant ^{13}C . Nonetheless, these results indicate preserved contribution of fatty acids to the hepatic TCA cycle in PPAR α -KO neonates.

Hepatic steatosis is linked to impaired ketogenesis in PPAR α deficient neonates. To test the hypothesis that loss of PPAR α , which is an important inducer of *Hmgcs2* and ketogenesis in adult mice, would disrupt ketone body metabolism during the highly ketogenic neonatal period (2,4,20,50,316,317), we performed a series of experiments in wild type and PPAR α deficient neonatal mice. Circulating total ketone body (TKB) concentrations were significantly lower in PPAR α -KO neonates on P1 (**Fig. 5.4A**). Blunted ketonemia was associated with a 3-fold decrease in *Hmgcs2* transcript abundance on P1 (**Fig. 5.4B**). Conversely, *Bdh1* transcript abundance increased significantly between P0 and P1 in both wild type and PPAR α -KO neonates (**Fig. 5.4C**). Immunoblots in liver demonstrated that HMGCS2 protein abundance was decreased ~25% on P0 and ~20% on P1 in PPAR α -KO neonates (**Fig. 5.4D, middle**). Despite decreased *Hmgcs2* mRNA abundance in P1 PPAR α -KO livers, HMGCS2 protein abundance increased ~25% in both genotypes. BDH1 protein abundance was decreased ~25% on P1 in PPAR α -KO neonates, and unlike wild type mice, did not increase from P0 to P1 (**Fig. 5.4D, bottom**). NMR profiling of [¹³C]Octanoate metabolism in neonatal liver revealed that blunted ketonemia was due to impaired ketogenesis. Enrichment of ¹³C- β OHB was decreased ~33% on P0 and ~50% on P1 in PPAR- α -KO livers (**Fig. 5.5A, left**). Because hepatic β OHB concentrations did not differ between genotypes on P0 or P1 (**Fig. 5.5A, right**), decreased ¹³C- β OHB enrichment reflects decreased ketogenesis. In addition, livers of PPAR- α -KO mice exhibited significantly increased concentrations of hepatic triacylglycerides (TAG) and free fatty acids (FFA) on P1 (**Fig. 5.5B-C**). Together, these results indicate an important role for PPAR α -dependent ketogenesis in prevention of hepatic steatosis in neonatal mice.

Discussion

The transition to extrauterine life incurs marked shifts in nutrient availability and energy metabolism. In contrast to the carbohydrate-replete nutrient state experienced *in utero*, the neonatal energy economy is dominated by lipid metabolism. Thus, it is surprising that mice deficient in PPAR α , a master regulator of lipid metabolism, survive the neonatal period. Using NMR to quantitatively map substrate fate in neonatal liver and systems physiology approaches, we have identified and mechanistically dissected the metabolic

defects exhibited by PPAR α -KO neonates. These mice showed hypoglycemia that was mechanistically linked to decreased gluconeogenesis from glycerol. Surprisingly, livers of PPAR α -KO mice exhibited normal expression of many mediators of fatty acid oxidation. Furthermore, terminal oxidation of the medium-chain fatty acid octanoate was normal in livers of these mice. Unlike fatty acid oxidation, ketogenesis was markedly impaired in PPAR α -KO neonates. These mice displayed hypoketonemia due to a 50% decrease in hepatic ketogenesis that was linked to decreased expression of ketogenic enzymes and was associated with hepatic steatosis. Together, our results identify a critical role for PPAR α -dependent ketogenesis in disposal of excess hepatic fatty acids in the neonatal period.

PPAR α -KO neonates exhibited hypoglycemia, hypoketonemia, and hepatic steatosis, and thus, phenocopy fasted adult PPAR α -KO mice (316,317). The mechanisms underlying fasting hypoglycemia in adult PPAR α -KO mice are controversial. Kersten and colleagues have linked hypoglycemia to decreased hepatic glucose production from glycerol (320), while Xu et al. has shown preserved gluconeogenesis from glycerol (321). Our results in neonates are most consistent with the findings of Kersten et al., as glycerol tolerance tests revealed that PPAR α -KO neonates do not effectively convert glycerol to glucose. While increased glucose utilization could drive hypoglycemia, adult PPAR α -KO mice actually exhibit decreased glucose utilization (320). Similarly, glucose tolerance did not differ between groups of neonatal mice, suggesting that increased glucose utilization was not responsible for neonatal hypoglycemia.

Since hepatic fatty acid oxidation supports gluconeogenesis, impaired fatty acid oxidation is frequently offered as a cause of hypoglycemia in PPAR α -KOs (316,317). However, due to the challenges associated with directly measuring contribution of fatty acids to the TCA cycle, ketonemia is often used as a surrogate for fatty acid oxidation. Here we used [^{13}C]Octanoate, a medium chain fatty acid avidly enters the mitochondrial matrix independently of allosterically regulated mitochondrial carnitine palmitoyltransferase 1a (5), to directly interrogate the activities of β -oxidation, fractional contribution to the TCA cycle, and ketogenesis. Our results indicate that impaired fatty acid oxidation does not contribute to hypoglycemia in PPAR α -KO neonates, since contribution of [^{13}C]Octanoate to the TCA cycle for

terminal oxidation was normal in livers of these mice. Second, our results indicate that ketogenesis is a poor surrogate for fatty acid oxidation, as ketonemia and ketogenesis are diminished in PPAR α -KO neonates (**Fig. 5.4A and 5.5A**), while contribution of fatty acid oxidation-derived Ac-CoA to the TCA cycle is preserved (**Fig. 5.3E**). In fact, contribution of [^{13}C]Octanoate to the hepatic TCA cycle is robust enough to measure its incorporation into ^{13}C -glucose (**Fig. 5.2G**). Fatty acid carbons do not normally contribute to gluconeogenesis because rates of pyruvate carboxylation (to the TCA cycle intermediate oxaloacetate) and subsequent efflux into gluconeogenesis (pyruvate cycling) greatly exceed TCA cycle flux in liver (30,322). Prospectively, impaired mitochondrial pyruvate carboxylase activity (encoded by *Pcx*, a PPAR α target gene) could permit increased incorporation of fatty-acid derived carbon into glucose and impair gluconeogenesis from pyruvate. Furthermore, ^{13}C -labeling of glucose detected in the present study does not reflect net gluconeogenesis from fatty acids. Unlike lower organisms, mammals cannot channel net acetyl-CoA carbon into glucose due to absence of the glyoxalate cycle enzymes isocitrate lyase and malate synthase (323). Ac-CoA entering the mammalian TCA cycle must instead pass through two obligatory decarboxylation reactions, catalyzed by isocitrate dehydrogenase and alpha-ketoglutarate dehydrogenase, before proceeding on to generate gluconeogenic intermediates. Because two moles of carbon are lost as CO_2 for every mole of Ac-CoA that enters the mammalian TCA cycle, net gluconeogenesis from fat does not occur.

As indicated above, PPAR α -KO neonates exhibited marked suppression of hepatic ketogenesis. On P0, ketogenesis was diminished by ~33%, and by P1, the diminution of ketogenesis reached 50%. Such ketogenic suppression seems disproportionate to the moderately decreased HMGCS2 and BDH1 protein abundances observed in livers of these mice. Prospectively, decreased activity of the NAD^+ -dependent mitochondrial deacylases Sirtuin 3 and 5, which increase HMGCS2 enzymatic activity via deacetylation and desuccinylation, respectively (64,324), could account for the apparent mismatch between low ^{13}C - βOHB enrichment and nearly normal HMGCS2 and BDH1 protein abundances. Nonetheless, ketogenic suppression was associated with massive hepatic steatosis. PPAR α -KO livers

exhibited 6.9- and 2.7-fold increases in TAG and FFA concentrations, respectively. Together, these results reveal an important role for PPAR α -dependent ketogenesis in disposal of excess hepatic fat that may be relevant to nonalcoholic fatty liver disease (NAFLD).

NAFLD and nonalcoholic steatohepatitis (NASH) affect approximately one billion individuals worldwide and incur significant morbidity and mortality (325-327). Nonetheless, effective therapies that directly target NAFLD and NASH do not currently exist (328). While PPAR α deficiency increases NASH susceptibility (329,330), treatment with the PPAR α agonist Wy-14643 protects against diet-induced steatohepatitis in mice (330). Similarly, fenofibrate treatment ameliorated NASH in mice (331). Unfortunately, fenofibrate treatment does not decrease hepatic triglyceride content in human NAFLD (332,333). One resolution for this interspecies discrepancy is offered by the finding that PPAR α agonists stimulate ketogenesis much more robustly in rodents than in humans (334-338). Thus, development and testing of direct ketogenic activators for mitigation of human NAFLD is warranted.

Figure legends:

Figure 5.1: PPAR α -KO mice exhibit neonatal hypoglycemia. **A.** Blood glucose on postnatal day zero and one (P0 and P1) in suckling wild type and PPAR α -KO mice. **B.** Glucose tolerance in P0 mice. Basal glycemia (0 min timepoint) is replicated from **A** since glycemia can only be measured twice in neonatal mice. $n > 10/\text{group}$, ***, $p < 0.001$ by 2-way ANOVA, as indicated.

Figure 5.2: PPAR α promoted gluconeogenesis from glycerol in neonatal mice. **A-D.** mRNA abundances of gluconeogenic mediators in liver. $n = 5/\text{group}$, **, $p < 0.01$ by 2-way ANOVA, as indicated.

E. Glycerol tolerance test in fed P0 mice, $n > 10/\text{group}$ **, $p < 0.01$ by Student's *t* test, as indicated.

Phosphoenolpyruvate carboxykinase 1, *Pck1*; Glucose-6-phosphatase, *G6pc*; Glycerol kinase, *Gyk*; Glycerol phosphate dehydrogenase, *Gpd2*.

Figure 5.3: Normal hepatic fatty acid oxidation in PPAR α -KO neonates. **A-D.** Hepatic mRNA abundances of mediators of fatty acid oxidation. n = 5/group, *, $p < 0.05$ by 2-way ANOVA, as indicated. **E.** Hepatic fractional ^{13}C -enrichments of glutamate (left) and total hepatic glutamate pools (right) 20 min after ip injection of sodium [1,2,3,4- $^{13}\text{C}_4$]octanoate (10 μmol per g body weight) in neonatal mice. n=3-8/group. **F.** Total hepatic taurine pools from the same mice as in **E.** **G.** Hepatic fractional ^{13}C -enrichments of glucose (left) and total hepatic glucose pools (right) from the same mice as in **E.** **, $p < 0.01$ by 2-way ANOVA, as indicated. Peroxisome proliferator activated receptor gamma coactivator 1-alpha, *Pparg1a*; Carnitine palmitoyl transferase 1a, *Cpt1a*; Acyl-CoA oxidase, *ACO*; Medium chain acyl-CoA dehydrogenase, *Acadm*.

Figure 5.4: PPAR α -KO neonates exhibit hypoketolemia due to decreased expression of ketogenic enzymes. **A.** Serum total ketone bodies (TKB) in fed neonatal mice, n > 6/group. **B-C.** Hepatic mRNA abundances of ketogenic enzymes, n = 5/group. **D.** Immunoblots for mitochondrial 3-hydroxymethylglutaryl CoA synthase 2 (HMGCS2), beta-hydroxybutyrate dehydrogenase 1 (BDH1), and actin in neonatal liver (quantification normalized to actin below). n = 4/group, *, $p < 0.05$, **, $p < 0.01$, ***, $p < 0.001$ by 2-way ANOVA, as indicated.

Figure 5.5: Ketogenic suppression is associated with neonatal hepatic steatosis. **A.** Hepatic fractional ^{13}C -enrichments of β -hydroxybutyrate (βOHB) (left) and total βOHB pools (right) 20 min after ip injection of sodium [1,2,3,4- $^{13}\text{C}_4$]octanoate (10 μmol per g body weight) in neonatal mice. n = 3-8/group, *, $p < 0.05$ by 2-way ANOVA. **B.** Hepatic triacylglyceride (TAG) and free fatty acid (FFA; **C**) concentrations in suckling mice on P1. n = 6-7/group, ***, $p < 0.001$ by Student's *t* test, as indicated.

Figure 5.1

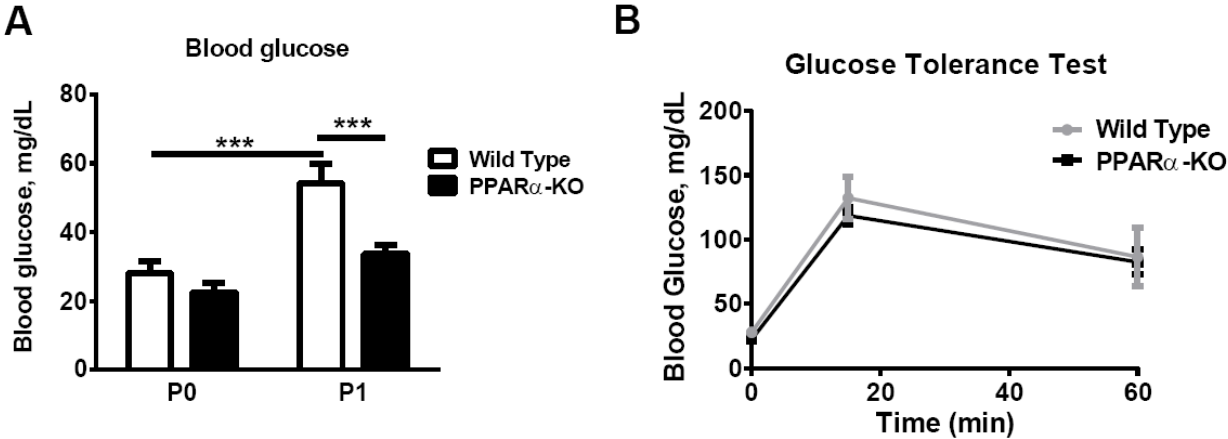


Figure 5.2

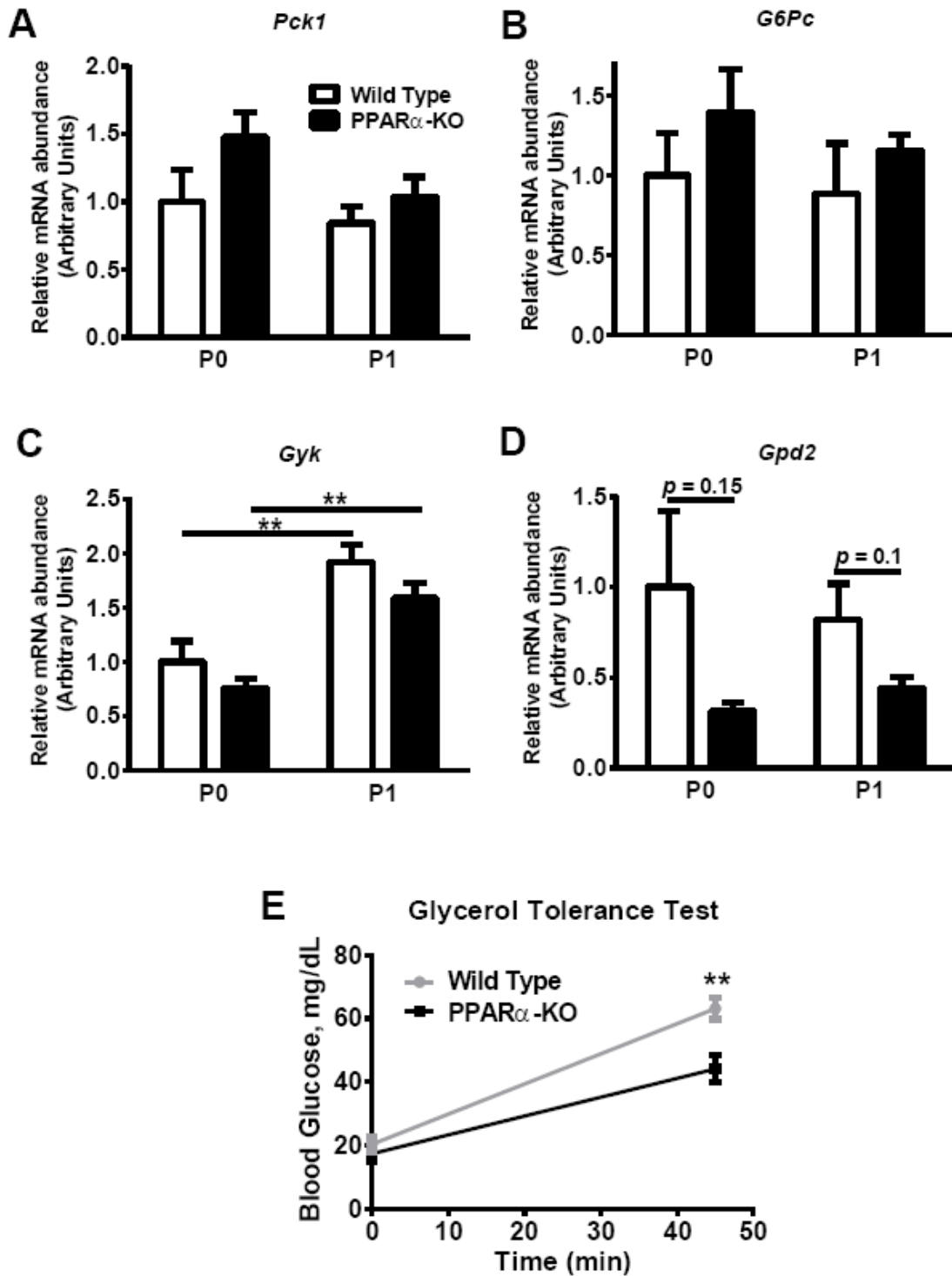


Figure 5.3

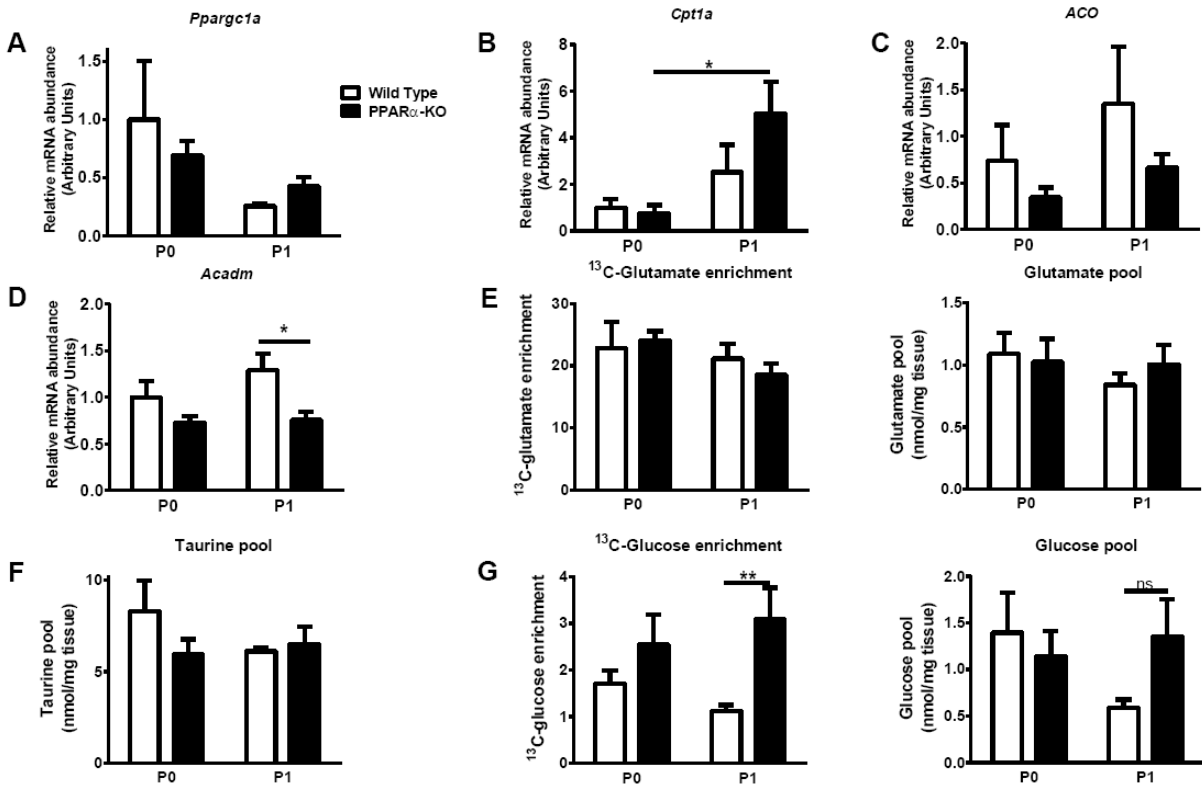


Figure 5.4

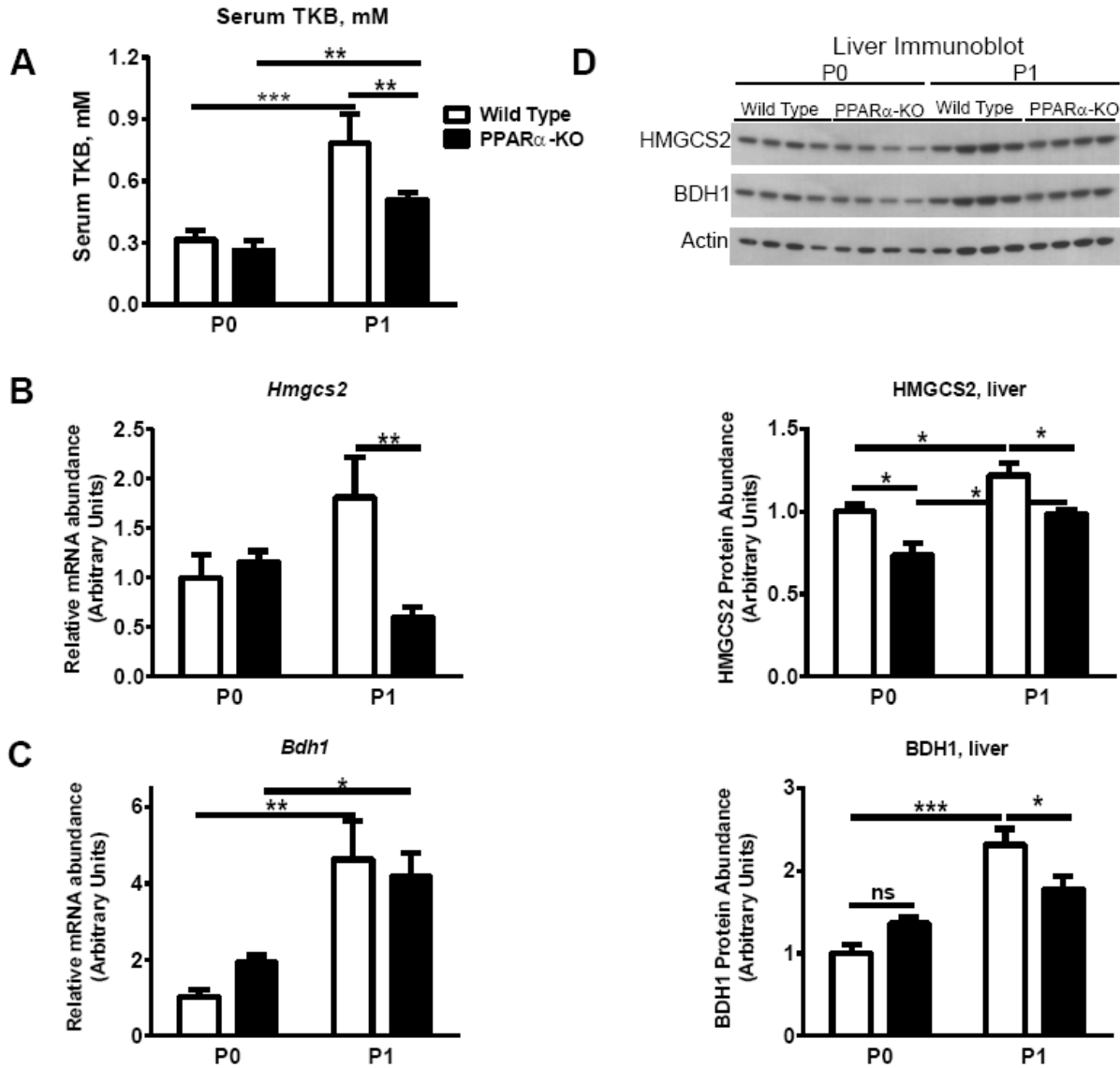


Figure 5.5

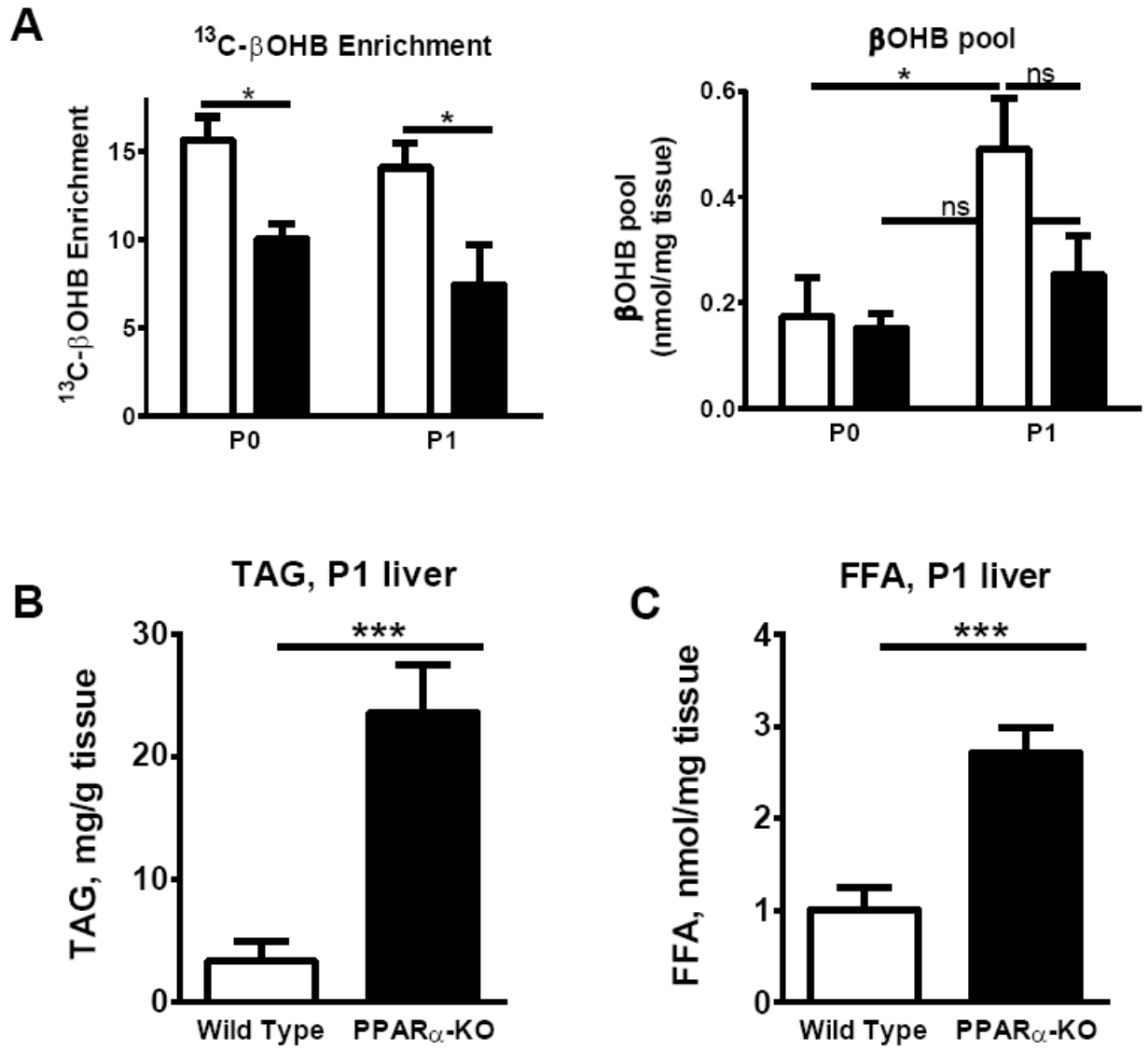


Table 5.1**Table 1**

RT-qPCR Primers	Sequence (5'-3')	
	Forward	Reverse
<i>Acadm</i>	GCTGGAGACATTGCCAATCA	TCTTGGCGTCCCTCATCAG
<i>ACO</i>	GGATGGTAGTCCGG	AGTCTGGATCGTTC
<i>Bdh1</i>	TGCAACAGTGAAGAGGTGGAGAAG	CAAACGTTGAGATGCCTGCGTTGT
<i>Cpt1a</i>	CATGTCAAGCCAGACGAAGA	TGGTAGGAGAGCAGCACCTT
<i>G6pc</i>	AAAGTCAACCGCCATGCAAAGGAC	TAGCAAAGAAAGACAGGGCTACCAG
<i>Gpd2</i>	GGACCGTAGTTGTGGAGGAT GTG	CTCTGGTTGTACATAGCGCTGGCT
<i>Gyk</i>	CCGTTACTCCACATGGAAGAAAGCTGTG	GCATCTTGGAATCCGTGAGGTGG
<i>Hmgcs2</i>	TGGTTCAAGACAGGGACACAGAAC	AGAGGAATACCAGGGCCCAACAAT
<i>Rpl32</i>	CCTCTGGTGAAGCCCAAGATC	TCTGGGTTTCCGCCAGTTT
<i>Pck1</i>	GGAAGGACAAAGATGGCAAGTTC	AGGCGTTTTCTTAGGGATGTAG
<i>Ppargc1a</i>	CGGAAATCATATCCAACCAG	TGAGGACCGCTAGCAAGTTTG

Chapter 6

Ketogenesis prevents diet-induced fatty liver injury and hyperglycemia through coenzyme A recycling

The work presented in this chapter and subchapters has been adapted from:

Cotter, D. G., Ercal, B., Leid, J. M., d'Avignon, D. A., Graham, M. J., Dietzen, D. J., Brunt, E. M., and Crawford, P. A. *Submitted*.

Summary

Nonalcoholic fatty liver disease (NAFLD) spectrum disorders affect approximately one billion individuals worldwide, and incur significant morbidity and mortality (325-327). The driver mechanisms that underlie NAFLD remain incompletely defined, impeding the development of effective treatments (328,339,340). Here we use a murine model of mitochondrial 3-hydroxymethylglutaryl CoA synthase (HMGCS2)-deficiency to demonstrate a critical role for ketogenesis in the modulation of hepatic glucose production and prevention of hepatic injury and inflammation in 'non-ketogenic' nutrient states. Using nuclear magnetic resonance spectroscopy to quantitatively map ¹³C-labeled substrate fate in perfused livers, we show that adult-onset loss of HMGCS2 increases hepatic gluconeogenesis from pyruvate and causes mild hyperglycemia in the fed state. High-fat diet feeding of ketogenesis insufficient mice causes extensive hepatocyte injury, pan-acinar inflammation, and elevated serum alanine aminotransferase activity. Hepatocellular injury in ketogenesis insufficient mice fed a high fat diet was associated with decreased glycemia, which could be mechanistically linked to fatty acid-induced sequestration of free coenzyme A (CoASH) that caused secondary derangements of hepatic tricarboxylic acid (TCA) cycle intermediate concentrations and impaired gluconeogenesis. Supplementation of the CoASH precursors pantothenic acid and cysteine normalized TCA intermediates and hepatic glucose production in ketogenesis insufficient livers. These findings identify hepatic ketogenesis as a critical regulator of hepatic glucose metabolism and TCA cycle function via coordination of CoASH homeostasis in the absorptive state and indicate that ketogenesis is a prospective modulator of fatty liver disease.

Introduction

Nonalcoholic fatty liver disease (NAFLD) and nonalcoholic steatohepatitis (NASH) are now the most common causes of liver disease in Western countries (325). NAFLD-induced liver failure is one of the most common reasons for liver transplantation. NAFLD increases the risk of developing type 2 diabetes, worsens glycemic control, and contributes to the pathogenesis of cardiovascular disease and chronic kidney disease (341-343). The pathogenic mediators that favor a NAFLD or NASH phenotype are incompletely understood, but are thought to involve abnormalities of hepatocyte metabolism, hepatocyte autophagy and endoplasmic reticulum stress, hepatic immune cell function, adipose tissue inflammation, and systemic inflammatory mediators (341,343-345). Perturbations of carbohydrate, lipid, and amino acid metabolism occur in and contribute to obesity, diabetes, and NAFLD in humans and in model organisms [reviewed in (346-350)]. While hepatocyte abnormalities in cytoplasmic lipid metabolism are commonly observed in NAFLD (335), the role of mitochondrial metabolism, which governs the oxidative and terminal ‘disposal’ of fats, in NAFLD pathogenesis is less clear. Nonetheless, most investigators agree that abnormalities of mitochondrial metabolism occur in and contribute to NAFLD [reviewed in (351-353)].

Ketogenesis can dispose of as much as two-thirds of the fat entering the liver (281), and thus dysregulation of ketone body metabolism could potentially contribute to NAFLD pathogenesis. Hepatic ketogenesis is activated in states of high fatty acid and diminished carbohydrate availability, and/or when circulating insulin concentrations are very low (2,4,5,301). Within hepatic mitochondria, ketogenic reactions condense β -oxidation-derived acetyl-CoA into the ketone bodies acetoacetate (AcAc) and beta-hydroxybutyrate (β OHB). In doing so, ketogenesis disposes of acetyl-CoA generated in excess of the liver’s own energetic needs and simultaneously recycles two moles of free CoASH per mole of ketone produced [reviewed in (4,5,301)]. Robust ketogenesis is limited to hepatocytes due to relatively restricted expression of the fate-committing ketogenic enzyme, mitochondrial 3-hydroxymethylglutaryl-CoA synthase (HMGCS2), under normal conditions (44). In contrast, oxidative disposal of ketone bodies is nearly ubiquitous, as all cells, except for hepatocytes, express the fate-committing enzyme of ketone body

oxidation, succinyl-CoA:3-oxoacid CoA transferase [SCOT; (74,164)]. Within mitochondria of extrahepatic tissues, β OHB is re-oxidized to AcAc, and via a reaction uniquely catalyzed by SCOT, is directed towards the TCA cycle for terminal oxidation (301). Despite the high capacity for disposal of hepatic fatty acids, ketone body metabolism has been overlooked as a potential therapeutic target in NAFLD.

Through incompletely defined mechanisms, obesity-associated hyperinsulinemia suppresses ketogenesis creating a state of ketogenic insufficiency and leading to relative hypoketonemia in obese animal models and humans, when compared to lean controls (12,42,238,239,354,355). To test the hypotheses that impaired ketogenesis, even in carbohydrate replete and thus ‘non-ketogenic’ states, contributes to abnormal glucose metabolism and provokes steatohepatitis, we generated a mouse model of ketogenic insufficiency, and used complementary high-resolution measures of dynamic metabolism using ^{13}C -labeled substrates with systems physiology approaches to measure the effects of ketogenic impairment.

Results

Ketogenic insufficiency causes abnormal hepatic glucose and lipid metabolism. The ability of ketogenesis to influence hepatic glucose and lipid homeostasis has only been preliminarily defined. To determine the consequences of impaired ketogenesis during the highly ketogenic neonatal period, suckling mice were injected subcutaneously (25 mg/kg) with an HMGCS2 targeted antisense oligonucleotide (ASO) daily beginning on the second day of extrauterine life. Compared to littermates injected with scrambled sequence control ASO, HMGCS2 ASO treatment decreased hepatic HMGCS2 protein abundance by 70% by postnatal day 12 (**Fig. 6.1A**). These mice exhibited normal body weights and blood glucose concentrations, and displayed mildly decreased plasma ketone body concentrations (0.9 ± 0.05 mM vs. 1.3 ± 0.17 mM in controls, $n = 4-6/\text{group}$, $p < 0.05$; **Fig. 6.1B** and **Fig. S6.1A-B**). Intriguingly, this partial loss of ketogenesis was associated with a nearly seven-fold increase in hepatic

triacylglycerol (TAG) concentrations (6.56 ± 1.2 vs. 0.96 ± 0.2 mg/g tissue in controls, $n = 4-6/\text{group}$, $p < 0.001$; **Fig. 6.1C**). To determine whether HMGCS2-mediated ketogenesis plays a role in a model of adult NAFLD, we performed intraperitoneal injections of HMGCS2 ASO (25 mg/kg biweekly for four weeks) into C57BL/6 male mice maintained on a standard low-fat chow diet. After four weeks, hepatic *Hmgcs2* transcript abundance was decreased by 88% ($n = 8-10$ per group, $p < 0.001$), without diminishing the scant *Hmgcs2* transcript abundance normally observed in subcutaneous adipose tissue [(356), (**Fig. S6.1C-D**)], and immunoreactive HMGCS2 was eliminated from liver compared to mice treated with a scrambled sequence control ASO (**Fig. 6.1D**). ASO treatment did not diminish protein abundance of cytoplasmic 3-hydroxymethylglutaryl-CoA synthase (HMGCS1), which catalyzes the penultimate reaction in mevalonate synthesis (**Fig. S6.1E**).

HMGCS2 ASO-treated mice exhibited markedly blunted ketonemia at both baseline (fed state) and in response to nutrient deprivation (**Fig. 6.1E**). To confirm the inability of HMGCS2 ASO-treated mice to effectively incorporate fatty acid-derived carbon into ketone bodies, livers from control and HMGCS2 ASO-treated mice were perfused via the portal vein with an oxygenated buffer containing [^{13}C]octanoic acid. Quantitative mapping of ^{13}C -label into the ketone body βOHB , using ^{13}C -edited proton NMR profiling (51,78,108,313), revealed markedly blunted hepatic ketogenesis in livers of HMGCS2 ASO-treated mice in both the fed and fasted state, confirming that HMGCS2 is required for effective derivation of ketone bodies from fatty acids, indicating that livers of these mice exhibit impaired ketogenesis, i.e. are ketogenesis insufficient (**Fig. S6.1F**). Despite exhibiting marked ketogenic impairment, HMGCS2 ASO-treated mice fed a standard low fat chow diet did not differ in body weights, body composition, or food intake compared to control mice (**Fig. S6.2A-C**). HMGCS2 ASO-treated mice also exhibited normal serum free fatty acid (FFA) and TAG concentrations and a normal physiologic distribution of residual βOHB and AcAc (**Fig. 6.2D-F**). Interestingly, HMGCS2 ASO-treated mice displayed mild, but very consistently elevated blood glucose concentrations (160.9 ± 3.2 vs. 145.0 ± 3.4 mg/dL in controls, $n = 28-36/\text{group}$, $p = 0.0013$) without changes in serum insulin concentrations (**Fig. S6.2G-H**).

Ketogenic insufficiency causes hepatic inflammation, injury, and reprogrammed intermediary metabolism in the setting of carbohydrate-replete overnutrition. To determine the effects of ketogenic insufficiency in the context of overnutrition, mice previously receiving ASOs for two weeks while on a standard low-fat chow diet were then maintained for eight weeks on a 60% high fat diet (HFD) that is commonly used to induce hyperglycemia and hepatic steatosis and inflammation in wild-type mice. HMGCS2 immunoblots indicated that hepatic HMGCS2 protein abundance was decreased by 93% within two weeks of ASO treatment (**Fig. S6.3A**), and continued to decrease to undetectable levels by the end of the eight week HFD-feeding interval, during which time ASO treatments were continued biweekly (**Fig. S6.3B**). While serum TAG and FFA concentrations did not differ between groups of HFD-fed mice (**Fig. S6.3C-D**), serum ketone body concentrations were significantly decreased in HFD-HMGCS2 ASO-treated mice (0.04 ± 0.02 mM vs. 0.26 ± 0.03 mM, $p < 0.0001$, $n = 8-10$ /group; **Fig. S6.3E**). After 8 weeks of HFD-feeding, control and HMGCS2 ASO-treated mice exhibited mild hepatic steatosis to an equal extent, as determined by biochemical quantification of hepatic TAG (**Fig. 6.2A**). As expected, serum alanine aminotransferase (ALT) activity, a circulating biomarker of hepatocellular injury, was not elevated in HFD-fed control mice, given the relatively brief duration of HFD maintenance (**Fig. 6.2B**). Conversely, HFD-feeding increased serum ALT activity by nearly four-fold in HMGCS2 ASO-treated mice compared to those maintained on standard chow (223.5 ± 37.65 vs. 61.2 ± 4.03 U/L in chow-fed HMGCS2 ASO-treated mice, $n = 4-5$ /group, $p < 0.0001$) and three-fold compared to HFD-fed control mice [223.5 ± 37.65 vs. 74.25 ± 6.14 U/L in controls, $n = 4$ /group, $p < 0.0001$]; (**Fig. 6.2B**). Blinded histopathologic evaluation of liver tissue from ketogenesis insufficient mice fed a HFD exhibited evidence of injury, including pan-acinar inflammatory infiltrates and acidophil bodies [(dying hepatocytes; (**Fig. 6.2C**)]. These findings were not observed in livers from HFD-fed control ASO-treated mice or chow-fed HMGCS2-deficient mice (**Fig. 6.2C**). In addition, livers of HFD-fed HMGCS2 ASO-treated mice exhibited increased numbers of sinusoidal macrophages, confirmed with F4/80 immunohistochemical staining (80.47 ± 6.09 vs. 49.33 ± 3.17 F4/80⁺ cells/20X field, $p < 0.001$, $n = 5$ fields/liver from three livers/group; **Fig. 6.2D**) and increased evidence of stellate cell activation, as

indicated by anti-smooth muscle actin immunostaining (8.19 ± 1.00 vs. 3.36 ± 0.61 SMA⁺ cells/10X field, $p < 0.001$, $n = 19$ fields/liver from three livers/group; **Fig. 6.2E**). These results indicate that ketogenic insufficiency in the setting of overnutrition accelerates a pronounced NASH-like phenotype.

To determine the metabolic effects of ketogenic insufficiency in the setting of overnutrition, we monitored blood glucose concentrations during the course of HFD administration. While blood glucose levels were higher in HMGCS2 ASO-treated mice at the onset of HFD, glycemia began to decline in these mice after five weeks of maintenance on this diet (**Fig. 6.3A-B**). HFD-fed HMGCS2 ASO-treated mice also gained significantly less weight than control mice (final weight after HFD-feeding: 26.82 ± 0.7 g vs. 30.32 ± 1.2 g in controls, $p = 0.019$, $n = 8-10$ /group) and ingested fewer calories [9.96 ± 0.3 kCal/mouse/day vs. 12.91 ± 0.3 kCal/mouse/day in controls, $p < 0.0001$, $n = 8-10$ mice/group over 16 measurements of food intake); (**Fig. S6.4A-B**)]. Furthermore, gluconeogenesis from [¹³C]pyruvate (and its redox partner [¹³C]lactate, which was also included in these perfusions in physiological proportion to maintain normal NAD⁺/NADH redox potential) was decreased four-fold in livers of HFD-fed HMGCS2 ASO-treated mice ($1.8 \pm 0.3\%$ vs. 7.3 ± 1.1 enrichment as [¹³C]glucose in controls, $p = 0.0009$, $n = 4-5$ /group; **Fig. 6.3C**). While the total hepatic glucose pool was expanded in perfused livers of HFD-fed HMGCS2 ASO-treated mice (**Fig. S6.5A**), de novo ¹³C-labeling of glucose from [¹³C]pyruvate was markedly diminished in HFD-fed HMGCS2 ASO-treated livers (3.91 ± 1.67 vs. 10.44 ± 0.9 pmol [¹³C]glucose produced/mg tissue in controls, $p = 0.0156$, $n = 4-5$ /group; **Fig. 6.**). Similar to the responses to the 60% HFD, HMGCS2 ASO-treated mice maintained on a distinct 40% fat/sucrose enriched diet for 8 weeks also exhibited decreased weight gain, decreased caloric intake, decreased body fat percentages, and decreased blood glucoses (**Fig. S6.4C-F**). Ketogenesis insufficient mice fed a 40% fat diet also exhibited equivalent hepatic steatosis to control HFD-fed mice, modestly increased serum ALT activity, and microgranuloma formation and inflammatory infiltrates in liver (**Fig. S6.6A-C**). Importantly, both the elevation of serum ALT activity and the degree of histopathologic evidence of hepatic inflammation was diminished in HMGCS2 ASO-treated mice fed a 40% fat diet compared to those fed a 60% HFD,

suggesting that chronic exposure to excess dietary fat drives the NASH-like phenotype observed in HMGCS2 ASO-treated mice.

To define the specific metabolic mechanisms leading to fatty acid induced hepatocellular dysfunction, we quantified gluconeogenesis from [¹³C]pyruvate in perfused livers of ASO-treated mice fed a standard low-fat chow diet in the presence and absence of octanoic acid, a medium chain fatty acid that enters the mitochondrial matrix independently of carnitine palmitoyltransferase 1 (CPT1), and rapidly stimulates mitochondrial β-oxidation and gluconeogenesis (5). Consistent with hyperglycemia in chow-fed HMGCS2 ASO-treated mice (**Fig. S6.2G**), basal gluconeogenesis from pyruvate was increased (15.21 ± 2.06% ¹³C-enrichment of glucose, vs. 9.04 ± 1.01% in controls, n = 7-8/group, p = 0.015, **Fig. 6.3D**). Because total hepatic glucose concentrations did not differ between groups (**Fig. S6.5C**), increased enrichment reflects increased production from pyruvate. As expected, addition of unlabeled octanoic acid to the perfusion buffer stimulated gluconeogenesis in livers of control animals (**Fig. 6.3D**, *white bars*) but in contrast, HMGCS2 ASO-treated livers perfused with octanoic acid did not increase gluconeogenesis, and in fact exhibited decreased ¹³C-glucose enrichment compared to control livers [(11.83 ± 1.70% ¹³C-enrichment of glucose vs. 17.61 ± 1.34% in controls, n=7-8/group, p = 0.018, **Fig. 6.3D**), without altering total glucose pools (**Fig. S6.5C**). The inability of octanoic acid to stimulate glucose production in HMGCS2 ASO-treated livers was observed despite increased mRNA abundances of *Ppara*, *Aco*, *Cpt1a*, *Ppargc1a*, *Pck1*, and *Me2* and normal mRNA abundances of *Acadm*, *Fgf21*, and *G6Pc* in liver (**Fig. S6.5D**), suggesting that a metabolic mechanism, rather than insufficient expression of the enzymatic mediators of fatty acid oxidation and gluconeogenesis, underlies the observed defect in fatty-acid stimulated glucose production in the setting of ketogenic insufficiency.

Ketogenic insufficiency sequesters free coenzyme A. Because induction of gluconeogenesis by fatty acids is dependent on the NADH and ATP generated through the TCA cycle (281,357,358), we hypothesized that the failure of mitochondrial fatty acids to stimulate gluconeogenesis in the absence of ketogenesis could be mechanistically linked to a failure to couple β-oxidation of fatty acids to their terminal oxidation in the TCA cycle. To determine whether there were abnormalities of TCA cycle

function in livers of HMGCS2 ASO-treated mice, we measured TCA cycle intermediate pool concentrations in perfused livers of control and HMGCS2 ASO-treated mice. While tissue α -KG concentrations were normal in livers perfused in the absence of octanoate, inclusion of this fatty acid in the perfusion buffer increased concentrations of α -KG by two-fold in HMGCS2 ASO-treated livers (0.75 ± 0.08 nmol/mg tissue vs. 0.34 ± 0.08 nmol/mg tissue in control livers perfused with octanoate, $n = 7-8$ /group, $p = 0.0032$, **Fig. 6.3E**). Perfusion with octanoic acid also increased hepatic concentrations of glutamate, an equilibrium partner of α -KG, by two-fold, and decreased hepatic succinate concentrations by 43% in HMGCS2 ASO-treated livers (99.89 ± 12.89 pmol/mg tissue vs. 162.8 ± 20.08 pmol/mg tissue in controls, $p < 0.01$, $n = 7-8$ /group; **Fig. S6.5E** and **Fig. 6.3F**). Collectively, these findings suggest a block at the TCA cycle reaction catalyzed by the α -KG dehydrogenase complex. Because the oxidative decarboxylation of α -KG to succinyl-CoA, which is subsequently converted to succinate, requires free CoASH, we quantified CoASH concentrations in unperfused and perfused livers of ASO-treated mice. While HMGCS2-ASO treatment did not alter CoASH concentrations in unperfused livers of standard chow-fed mice, or in livers perfused in the absence of octanoate, hepatic CoASH concentrations were decreased 60% in HMGCS2 ASO-treated livers perfused with octanoic acid (40.73 ± 14.35 pmol/mg tissue vs. 106.6 ± 24.31 pmol/mg tissue in controls, $p = 0.035$, $n = 8$ /group, **Fig. 6.3G**). Fatty acid-induced depletion of CoASH observed in HMGCS2 ASO-treated livers occurred despite normal expression of *Pank1a*, and increased expression of *Pank1b* (1 ± 0.022 vs. 2.5 ± 0.6 , $p = 0.04$, $n = 8-10$ /group), which phosphorylate pantothenic acid in the first step of de novo CoASH biosynthesis (**Fig. S6.5F**).

Consistent with the octanoate-induced derangements of TCA cycle intermediates and CoASH depletion in livers of standard chow-fed HMGCS2 ASO-treated mice, unperfused livers of HMGCS2 ASO-treated mice fed a 60% HFD displayed increased [glutamate] (2.56 ± 0.4 vs. 1.12 ± 0.12 nmol/mg tissue in controls, $p = 0.018$, $n = 4-5$ /group), a trend towards decreased [succinate], and decreased hepatic [CoASH] (28.40 ± 11.51 pmol CoASH/mg tissue vs. 103.10 ± 32.62 in controls, $p = 0.049$, $n = 8$ /group; **Fig. S6.5G-I**). Finally, circulating short- and medium-chain acylcarnitine concentrations, but not those of

long-chain acylcarnitines, were significantly increased in HMGCS2 ASO-treated mice fed a 40% fat diet (**Fig. S6.7**; for a full profile for chow-fed and 40% HFD-fed mice, see **Table S6.1-2**). Taken together, these results suggest that ketogenic insufficiency in the setting of high fat delivery to mitochondria depletes free CoASH and thereby impairs TCA cycle function, which inhibits entry of acetyl-CoA and thus favors increased accumulation of shorter-chain acylcarnitines.

To determine if supplementation of the CoA precursors pantothenic acid (vitamin B₅) and cysteine, could restore glucose production and normalize TCA cycle intermediate concentrations in HMGCS2 ASO-treated livers, we perfused livers of HMGCS2-deficient and control animals with exogenous octanoate and CoA precursors. While inclusion of pantothenic acid and cysteine with [¹³C]lactate, [¹³C]pyruvate, and unlabeled octanoic acid during a 15 min perfusion failed to normalize gluconeogenesis in HMGCS2 ASO-treated livers, (**Fig. 6.4A, left**), prolonged repletion of CoASH precursors by perfusing livers with pantothenic acid and cysteine for 45 min prior to perfusion with [¹³C]lactate and [¹³C]pyruvate, unlabeled octanoic acid, pantothenic acid, and cysteine for 15 min normalized ¹³C-glucose enrichment (**Fig. 6.4A, right**). Total hepatic glucose concentrations did not differ between control and HMGCS2 ASO-treated livers in either perfusion experiment (**Fig. S6.8**). Moreover, pre-perfusion with CoASH precursors attenuated the expansion of the α -KG and glutamate pools in HMGCS2 ASO-treated livers, with pre-perfused HMGCS2 ASO-treated livers exhibiting a 29% decrease in [α -KG] and a 43% decrease in [glutamate] compared to HMGCS2 ASO-treated livers that were not pre-perfused with CoASH precursors (n= 5-7/group, $p < 0.05$ for α -KG, and $p < 0.001$ for glutamate; **Fig. 6.4B-C**). Finally, inclusion of pantothenic acid and cysteine normalized succinate concentrations in livers of HMGCS2 ASO-treated mice irrespective of the length of the perfusion (**Fig. 6.4D**). Taken together, these results mechanistically link the HFD-induced hypoglycemia and fat-induced impairment of hepatic gluconeogenesis observed in ketogenesis insufficient mice to CoASH depletion and inhibition of the α -KG dehydrogenase reaction of the TCA cycle.

Discussion

Hepatic ketogenesis is activated when fatty acids are plentiful, carbohydrates are in short supply, and/or circulating insulin concentrations are low (2,4,5,44,301). This spillover pathway converts β -oxidation-derived acetyl-CoA, produced in excess of the hepatocyte's own energy needs, into ketone body intermediates, thus diverting carbon away from the hepatic TCA cycle and providing extrahepatic tissues with an avidly oxidized fuel source. This paradigm forms an 'altruistic' model of ketone body metabolism, in which the hepatocyte shares 'pre-catabolized' energy stored in fatty acids with other organs that may require it, particularly in states of diminished carbohydrate availability. However, this model neither accounts for the hepatocyte's need to support ketogenesis for its own metabolic homeostasis, nor considers the importance of basal hepatic ketogenesis in physiological states that are not considered 'ketogenic' (*i.e.*, carbohydrate restricted). These are the first studies to demonstrate a critical role for hepatic ketogenesis in the normal absorptive state and in prevention of metabolic decompensation in the setting of overnutrition, which triggers a cascade of events that culminates in hepatic injury and hepatic inflammation when ketogenic capacity is markedly impaired.

Our data are consistent with a model in which ketogenesis that is inadequately matched to the supply and availability of fat (ketogenic insufficient) in the normal fed state will channel β -oxidation-derived acetyl-CoA into the TCA cycle, generating the ATP and NADH to support increased gluconeogenesis from pyruvate, predisposing to hyperglycemia (**Fig. 6.4E**). Therefore, even in the non-lipolytic absorptive state, in which dietary carbohydrates are abundant, hepatic ketogenesis serves a critical role in regulating glycemia. When ketogenesis is insufficient, acute delivery of fatty acids and chronic exposure to a 'non-ketogenic' (not carbohydrate restricted) high-fat diet both result in the inability to couple increased fat availability to increased gluconeogenesis through mechanisms that can be linked to sequestration of free CoASH, a critical by-product yielded by ketogenesis. Our data are most consistent with a model in which the CoASH liberated by ketogenesis is critical in states of high fat delivery, supporting the α -KG dehydrogenase reaction and therefore effective TCA cycle function. Taken

together, these results mechanistically link ketogenesis to hepatic CoASH homeostasis and gluconeogenesis, and provide strong evidence for a previously unknown role of ketogenesis in prevention of hyperglycemia and hepatic injury. These findings are underscored by our recent studies of germline SCOT-knockout (KO) mice, which cannot terminally oxidize ketone bodies in any tissue. These mice exhibit hyperketonemic hypoglycemia and die within 48 hr of birth in a manner that phenocopies human sudden infant death syndrome [SIDS, (78)]. Despite the fact that SCOT is normally excluded from hepatocytes, livers of SCOT-KO mice develop abnormalities of hepatic fatty acid oxidation, pyruvate metabolism, redox potential, and even ketogenesis (164,313). In stark contrast to the severe metabolic derangements and SIDS-like phenotype observed in neonatal SCOT-KO mice, mice that cannot oxidize ketone bodies selectively within neurons, cardiomyocytes, or skeletal myocytes, which comprise the three greatest consumers of ketone bodies, survive the neonatal period and starvation as adults (108). Together, these results indicate that coordination of ketogenesis and ketone body oxidation may be of even greater importance to preserve the dynamic intermediary metabolic network in the liver than it is to provide energy to extrahepatic tissues.

Genome-wide association and exome sequencing studies have revealed associations between numerous genes encoding mediators of lipid metabolism and NAFLD/NASH (327,359). Variations in the genes encoding ketogenic mediators, including HMGCS2, HMG-CoA lyase, and β OHB dehydrogenase have not yet been unveiled as independent predictors of liver pathology or diabetes. While complete HMGCS2-deficiency is very rare in humans, case reports indicate that encoded variation in ketogenic capacity exists in populations worldwide. Total HMGCS2 enzymatic deficiency is associated with pediatric hypoketonemic hypoglycemia and hepatic steatosis (66-68,360-362). Importantly, our studies of neonatal mice revealed that partial loss of HMGCS2 activity caused marked hepatic steatosis vastly out of proportion to the diminution in neonatal ketosis, but did not result in neonatal hypoglycemia or failure to thrive. These findings raise the possibility that insidious genetic polymorphisms yielding very subtle ketogenic defects could latently predispose to fatty liver disease, and attest to the critical fine-tuning role that hepatic ketogenesis plays in the regulation of hepatic glucose and lipid metabolism.

In the setting of ketogenic insufficiency, perfusion with octanoate depletes CoASH, inhibiting the α -KG dehydrogenase reaction of the TCA cycle, which manifests as increased α -KG and decreased succinate concentrations. Similarly, perfused livers of HFD-fed HMGCS2 ASO-treated mice exhibit decreased hepatic glucose production from pyruvate, and unperfused livers of HFD-fed HMGCS2 ASO-treated mice demonstrate a trend towards decreased [CoASH]. Only longer-term replenishment of the CoA precursors pantothenic acid and cysteine prevented the octanoate-induced impairment of glucose production in livers of ketogenesis-insufficient mice, diminished the increase in [α -KG], and mitigated the decrease in [succinate]. The findings suggest severe depletion of CoASH precursors in HMGCS2 ASO-treated livers or that the kinetics of CoASH biosynthesis and mitochondrial import [(CoASH biosynthesis and transport reviewed in (363)] occur too slowly to mitigate these metabolic abnormalities. Together, these findings identify ketogenesis as a significant modifier of the TCA cycle and gluconeogenesis through modulation of acetyl-CoA pools and CoASH homeostasis.

Unlike many tissues that must synthesize CoASH *de novo* or regenerate it via acyl-CoA thioesterases (363,364), hepatocytes can robustly engage ketogenesis to regenerate CoASH (4,5,301). After a brief eight week interval of HFD-feeding that is insufficient to cause hepatic injury in control mice [(42) and **Fig. 6.2B-C**], mice that cannot effectively liberate CoASH from acetate through ketogenesis exhibit significantly elevated serum ALT activity and histopathologic evidence of hepatic injury and inflammation. The severity of hepatic injury positively correlates with dietary fat content, indicating an important postprandial role for ketogenesis in (i) disposal of excess dietary fat and (ii) liberation of CoASH from acetyl-CoA. Furthermore, ASO-treated mice fed a HFD developed equivalent steatosis, but only ketogenic insufficient mice developed severe inflammation, suggesting that of the two major NAFLD subtypes, simple steatosis and NASH, impaired ketogenesis is an important determinant of NASH (325). Other forms of hepatocellular injury are also associated with decreased CoASH concentrations. In acute acetaminophen toxicity, CoASH levels decrease simultaneously with decreasing HMGCS2 enzymatic activity (365,366). Potentially fatal valproic acid therapy-induced hepatic dysfunction, which is associated with impaired β -oxidation of fatty acids and ketogenesis due to

sequestration of CoASH into poorly metabolized valproyl CoA, can be prevented by administration of CoA precursors (367,368). In rodents, hepatic CoASH concentrations decrease in response to HFD (369), while the concentration of pantothenic acid actually increases (370), suggesting that hepatic CoASH homeostasis is dysregulated in obesity. De novo CoASH synthesis is required for life in mice and impaired CoASH synthesis is associated with fasting induced hepatic steatosis (371,372). Nonetheless, the importance of de novo CoASH synthesis in obesity and its relation to NAFLD remain relatively unexplored.

No current pharmacological therapies directly treat NAFLD or NASH. These diseases are currently addressed through lifestyle modifications such as weight loss and treatment of dyslipidemia and hyperglycemia (328). A variety of agents are at various stages of investigation, including compounds targeting oxidative stress, nuclear receptor activators, insulin sensitizers, modifiers of dyslipidemias, and immunomodulatory agents (342,345). Ketogenesis has not yet been considered as a metabolic target. Obese humans and mice exhibit diminished whole body ketone body turnover (12,42). Furthermore, circulating ketone body concentrations are generally decreased in obese humans (238,239,354), and serve as predictive biomarkers for conversion to type 2 diabetes in patients with impaired fasting glucose (373). Furthermore, compared to BMI-matched individuals, obese patients with NAFLD exhibit increased hepatic glucose production and TCA cycle flux, but not ketogenesis (355). DNA methylation, nuclear receptor-mediated transcriptional activation, and reversible succinylation, acetylation, and phosphorylation all exert multi-tiered transcriptional and post-translational regulation of *Hmgcs2* expression and HMGCS2 enzymatic activity to coordinate ketogenesis during diverse physiologic contexts [(11,47,64,65,324) and reviewed in (301)]. Therefore, HMGCS2 and other enzymatic mediators of ketogenesis may be considered in future investigations of metabolic regulation of abnormal hepatic metabolism in the setting of fatty liver disease and obesity.

Methods

Animals. All adult mice studied were males on a C57BL/6N X C57BL/6J hybrid background. For neonatal experiments, both sexes were studied. Unless otherwise noted, mice were maintained on standard low fat chow diet in which 13% of the calories are from fat, 25% from protein, and 62% from carbohydrates (Lab Diet 5053) and autoclaved water *ad libitum*. Lights were off between 1800 and 0600 in a room maintained at 22°C. For all adult mouse experiments, mice were housed in groups of 4-5 on sawdust bedding. ASO treatment was initiated in six week-old mice by intraperitoneal injection (25 mg/kg) with HMGCS2 targeted ASOs (ISIS 191229; CTGTTTGTCCTGCTGGATG) or with scrambled sequence control ASOs (ISIS 141923; 5'-CCTTCCCTGAAGGTTCCCTCC-3') biweekly for four weeks. For HFD studies, after two weeks of ASO treatment, mice were maintained for eight weeks on either a high fat diet in which 60% of calories are from fat, 20% from protein, and 20% from carbohydrates (D12492, Research Diets) or, in separate cohorts, a diet in which 40.7% of calories are from fat, 19% from protein, and 40.3% from carbohydrates (TD 110290, Harlan Teklad), during which time biweekly ASO administration continued. For the neonatal experiments, ASOs were administered (25 mg/kg) subcutaneously daily, beginning on the second day of life and until postnatal day 12 (P12). Pups were marked on the abdomen daily with a permanent marker to enable longitudinal monitoring of body weight and blood glucose. Marking also enabled control and HMGCS2 ASOs to be administered to different pups within the same litter, thus, minimizing inter-litter variance in metabolic parameters. All experiments were conducted using protocols approved by the Animal Studies Committee at Washington University.

Measurements of food intake, body weight, and body composition. Food intake was monitored beginning on day 1 of ASO treatment for each cage of mice. Food intake was measured biweekly for the duration of each experiment and normalized to the number of mice per cage and the number of days between measurements, which was always three or four days. Mice were also weighed biweekly at the onset of all experiments. Body weights and body composition were recorded following a four-hour fast (1000-1400),

after which food was returned immediately. Percent body fat and lean body mass were determined in awake adult animals using an EchoMRI instrument (Echo Medical Systems, Houston, TX).

Plasma Metabolite Quantification. Serum triacylglycerol (TAG), free fatty acids (FFAs), total ketone bodies (TKB), beta-hydroxybutyrate (β OHB), and acetoactate (AcAc) were determined using standard biochemical assays coupled to colorimetric substrates as described previously (51). Blood glucose was measured in duplicate using handheld glucometers (Aviva). Serum insulin was measured using an enzyme-linked immunosorbent assay (Millipore) and serum alanine aminotransferase (ALT) was measured using an assay from Teco Diagnostics, according to manufacturer's instructions.

Tissue Metabolite Quantification. Hepatic [TAG] were quantified biochemically using a Folch extract of liver, as described previously (126). Tissue CoASH concentrations were measured in freeze-clamped and bio-pulverized liver tissue. Approximately 75 mg of tissue were homogenized using a glass on glass dounce in 10x-volume of ice-cold deionized water. Homogenates were spun at 4°C and 15,000 x g for 20 min. Supernatants were transferred to clean tubes on ice and were then dehydrated using a rotary speed-vacuum. Tissue pellets were resuspended to 2 mg/ μ l and 20 mg of tissue (10 μ l) were loaded into a 96 well plate for CoASH detection using an enzyme linked colorimetric assay (Biovision).

Histology. Immediately following sacrifice, liver specimens were collected and fixed in 10% neutral buffered formalin (Fisher, Wilmington, DE) or cryopreserved in Optimal Cutting Temperature Compound (O.C.T. Tissue Tek). For hematoxylin and eosin stained sections, paraffin-embedded tissue was microtome-sectioned, stained and photographed using standard methods. For F4/80 immunostains, rat anti-F4/80 (Abcam, ab6640) was incubated for 1 h at room temperature on liver cryosections (diluted 1:200 in 1% bovine serum albumin/0.1% Triton X-100 in phosphate buffered saline), followed by Alexa Fluor 594 conjugated goat anti-rat IgG (Invitrogen, Carlsbad, CA; diluted 1:250 in 1% bovine serum albumin/0.1% Triton X-100 in phosphate-buffered saline) and coverslip application as previously described (1). For smooth muscle actin (SMA) immunostains, mouse monoclonal anti-SMA-Cy3 conjugate (Sigma C-6198) was incubated for 1 h at room temperature on liver cryosections (diluted 1:100 in 1% bovine serum albumin/0.1% Triton X-100 in phosphate buffered saline), followed by coverslip

application. 4',6-Diamidino-2-phenylindole (DAPI) was used as a cell nuclear counterstain (40 ng/ml in phosphate buffered saline for 5 min). All immunofluorescence images were acquired at 0.5 μ m slice thickness using a Zeiss LSM 700 confocal microscope and Zeiss Zen software. For F4/80 and SMA immunostains, five random 20X fields and nineteen random 10X fields per liver, respectively (n = 3 animals/group), were quantified manually. In each case, only staining that was clearly associated with nuclei were counted, and for SMA, only cells outside of vessel walls were counted as activated stellate cells.

Gene expression analysis. Quantification of gene expression was performed using real-time RT-quantitative PCR using the $\Delta\Delta$ Ct approach as described (51), normalizing to Rpl32, using primer sequences listed within **Supplemental Table 6.2**.

Immunoblotting. Lysates from liver were generated in a protein lysis buffer: 20 mM Tris-HCl, 150 mM NaCl, 1 mM EDTA, 1% Triton X-100, 1% phosphatase inhibitor cocktail (Sigma), and protease inhibitor cocktail (complete mini EDTA-free, Roche), pH 7.5. Immunoblots to detect HMGCS2 (rabbit anti-mHMGCS; Santa Cruz Biotechnology), HMGCS1 (rabbit anti-HMGCS1; Thermo Scientific), and actin (rabbit anti-actin, Sigma) were performed as described (78). Band intensities were quantified densitometrically using Quantity One software (Bio-Rad).

Liver perfusions. Ten minutes prior to each liver perfusion, mice received an intramuscular injection of heparin (100 Units). Mice were then anesthetized with 10 μ l of sodium pentobarbital (Fatal Plus, 390 mg/ml) administered IP. Once fully anesthetized, the abdomen was sprayed with 70% ethanol, and the mouse was placed on a surgical platform within a large reservoir to contain run-off buffer and body fluids. A transverse incision was made through the skin, fascia, and muscular layers of the lower abdomen. A lateral sagittal incision was made on each side of the body, exposing the abdominal contents. A second transverse incision was made inferior to the right kidney and towards the dorsal aspect of the mouse to allow for perfusion buffer and body fluids to drain from the abdomen. The portal vein was then exposed by gently moving the intestines laterally towards the left body wall. A suture needle was threaded under the portal vein and tied loosely. Next, the portal vein was cannulated with a 24 gauge

catheter needle, the needle was withdrawn, and tubing with buffer was reconnected to the catheter. The abdominal aorta and inferior vena cava were cut and the catheter was firmly tied into the portal vein. Finally, the heart was exposed by cutting through the diaphragm and thorax. The right atrium was cut to prevent recirculation of buffer to the liver and to terminate perfusion to the brain. All livers were perfused with an oxygenated Krebs-Henseleit bicarbonate buffer (118 mM NaCl, 25 mM NaHCO₃, 4.7 mM KCl, 0.4 mM KH₂PO₄, 2.5 mM CaCl₂, 1.22 mM MgSO₄·7·H₂O, pH 7.4), warmed to 37°C using a counter-current heat exchange circuit and a recirculating water bath, at a rate of 8 ml/min using a peristaltic pump for 15 min, unless otherwise noted. At the end of the perfusion, the liver was freeze-clamped and rapidly frozen in a bath of liquid nitrogen. Tissue was stored at -80°C until further processing. For measurements of ketogenesis in perfused livers, buffers contained sodium [1,2,3,4-¹³C₄]octanoate (0.2 mM), sodium lactate (1.5 mM), and sodium pyruvate (0.15 mM). For all measurements of gluconeogenesis, livers were perfused with sodium [3-¹³C]lactate (1.5 mM) and sodium [3-¹³C]pyruvate (0.15 mM), and in a subset of these experiments, unlabeled sodium octanoate (0.2 mM) was included in the buffer (vendor for stable isotopes: Cambridge Isotope Laboratories). For the CoASH repletion experiments, unlabeled pantothenic acid and L-cysteine were included in the perfusion buffer at 0.15 mM and 0.1 mM, respectively, in addition to sodium [3-¹³C]lactate (1.5 mM), sodium [3-¹³C]pyruvate (0.15 mM), and unlabeled sodium octanoate (0.2mM). Livers pre-perfused with CoASH precursors received unlabeled pantothenic acid (0.15 mM), Cys (0.1 mM), sodium lactate (1.5 mM), and sodium pyruvate (0.15mM) for 45 min before being switched to a buffer containing pantothenic acid (0.15 mM), cysteine (0.1 mM), sodium [3-¹³C]lactate (1.5 mM), sodium [3-¹³C]pyruvate (0.15 mM), and unlabeled sodium octanoate (0.2 mM) for 15 min.

NMR-based quantitative substrate fate mapping. Neutralized perchloric acid tissue extracts were prepared and profiled using ¹³C-edited proton nuclear magnetic resonance (NMR) measured at 11.75 T (Varian/Agilent Direct Drive-1) via first increment gradient heteronuclear single-quantum correlation (gHSQC). Signals were collected from extracts dissolved in 275 µL of D₂O + 1 mM trimethylsilyl propionate (TSP), loaded into high precision, thin walled 5-mm tubes (Shigemi). Tissue

concentrations and fractional enrichments of metabolites were determined from quantification of signals by integration from the $^1\text{H}\{^{13}\text{C}\}$ and ^{13}C -edited (gHSQC) collections of carbon 2 for taurine, carbon 4 for βOHB , carbon 1 for glucose, carbon 4 for glutamate, and $^1\text{H}\{^{13}\text{C}\}$ of carbon 3 for α -ketoglutarate and carbon 2/3 for succinate as described previously (78,313).

Tandem Mass Spectrometry (MS/MS) Analysis of Blood Amino Acids and Acylcarnitines. Blood was spotted onto 1.3-cm spots on Whatman 903 filter paper. Amino acids were quantified as butyl ester derivatives using multiple precursor/product combinations in a reversed-phase liquid chromatography protocol coupled to MS/MS (22). Carnitine esters were measured by scanning for the precursors of the common m/z 85 carnitine fragment. Quantification was achieved in all cases using stable isotope ^2H -labeled internal standards using an electrospray ionization source coupled to an API 3200-Qtrap tandem mass spectrometer (Applied Biosystems).

Acknowledgements

We thank Jeffrey Gordon, Clay Semenkovich, David Rudnick, Shin-ichiro Imai, and Rebecca Schugar, for helpful discussions, Xia Ge for assistance with NMR, Laura Kyro for assistance with graphics, and Debra Whorms and Ashley Moll for technical assistance. This work was supported by National Institutes of Health, DK091538 (to PAC), the Diabetic Research Center (DK020579), the Nutrition and Obesity Research Center (DK056341), and Training Grant HL007873 (for DGC); and the Children's Discovery Institute through St. Louis Children's Hospital (to PAC).

FIGURE LEGENDS

Fig. 6.1. Ketogenic insufficiency in mice treated with *Hmgcs2* ASO. (A) Immunoblot for HMGCS2 and actin using protein lysates derived from livers of neonatal mice treated with either a scrambled sequence control ASO or HMGCS2 ASO. Mice were treated with ASO daily for 11 days, beginning on the second day of life, and tissues and serum were collected on postnatal day 12 (P12). Protein abundance is quantified below. (B) Serum total ketone body (TKB, mM) and (C) hepatic TAG (mg/g tissue) concentrations on P12 in ASO-treated mice. (D) Immunoblot for HMGCS2 and actin using protein lysates derived from livers of adult mice treated with control or HMGCS2 ASO biweekly for four weeks beginning at six weeks of age. (E) Serum [TKB] (mM) during fasting in adult mice treated with ASO for four weeks, n = 3-5/group. *, $p < 0.05$, ***, $p < 0.001$ by Student's *t* test vs. HMGCS2-ASO treated mice, or as indicated.

Fig. 6.2. Hepatic injury in ketogenesis insufficient HFD-fed mice. (A) Hepatic [TAG] (mg/g tissue) and (B) serum ALT activity (U/L) in ASO-treated mice fed a standard chow diet fed a low fat diet (standard chow diet) for four weeks or a high fat diet for eight weeks, n = 4-5/group. (C) Representative hematoxylin and eosin stained sections of liver from ASO treated mice fed the indicated diet. Arrowheads indicate dying hepatocytes (acidophil bodies). (D) Representative 20X fields showing immunostaining for F4/80- and (E) smooth muscle actin (SMA)-positive cells in cryosections of liver from ASO treated mice fed HFD for eight weeks. Quantification for each is on right. **, $p < 0.01$, ***, $p < 0.001$ by Student's *t* test or 2-way ANOVA as appropriate, as indicated.

Fig. 6.3. Hepatic metabolic reprogramming in ketogenesis insufficient mice. (A) Blood glucose (mg/dL) and (B) the percent of basal blood glucose in ASO-treated mice beginning at the onset of 60% HFD-feeding, n = 8-10/group. (C) Quantification of ^{13}C -enrichment of glucose from [^{13}C]pyruvate (a surrogate for gluconeogenesis) determined by ^{13}C -edited proton NMR spectroscopy in liver extracts of 60% HFD-fed ASO-treated mice perfused via the portal vein with [^{13}C]lactate and [^{13}C]pyruvate in a

physiological ratio, n =4-5/group. **(D)** ^{13}C -enrichment of glucose from [^{13}C]pyruvate, **(E)** total alpha-ketoglutarate (α -KG, nmol/mg tissue), and **(F)** succinate concentrations (pmol/mg tissue) determined by NMR in liver extracts of standard chow diet-fed ASO-treated mice perfused with the indicated substrates, n = 7-8/group. **(G)** Free coenzyme A (CoASH, pmol/mg tissue) concentrations in livers of unperfused standard chow diet-fed ASO-treated mice or livers perfused with the indicated substrates, n = 3-8/group. *, $p < 0.05$, **, $p < 0.01$, ***, $p < 0.001$ by Student's *t* test or 2-way ANOVA as appropriate, vs. HMGCS2-ASO treated mice, or as indicated.

Fig. 6.4. Replenishing CoA precursors restores gluconeogenesis and TCA cycle intermediate abnormalities in livers of ketogenesis insufficient mice. **(A)** Gluconeogenesis in perfused livers of standard chow diet-fed ASO-treated mice perfused with either [^{13}C]lactate, [^{13}C]pyruvate, octanoic acid, cysteine, and pantothenic acid for 15 min [Pre-perfusion (-)] or Pre-perfused with for 45 min with unlabeled lactate, pyruvate, cysteine, and pantothenic acid followed by 15 min of perfusion with [^{13}C]lactate, [^{13}C]pyruvate, octanoic acid, cysteine, and pantothenic acid. **(B)** [α -KG] (nmol/mg tissue), **(C)** [glutamate] (nmol/mg tissue), and **(D)** [succinate] (pmol/mg tissue) in the same livers as in **(A)**. n = 5-7/group, *, $p < 0.05$, **, $p < 0.01$, ***, $p < 0.001$ by 2-way ANOVA as indicated. **(E)** Schematic model of fatty acid handling in normal liver and in fatty liver disease. NAFLD livers exhibit increased esterification to and lipolysis from lipid droplets, increased β -oxidation of fatty acids, increased terminal oxidation, increased gluconeogenesis, and diminished ketogenesis, relative to the availability of fat. Our studies demonstrate that severe ketogenic suppression sequesters CoASH due to impaired CoASH recycling, disrupts the tricarboxylic acid (TCA) cycle, and is associated with hepatic injury and inflammation.

Fig. S6.1. Metabolic parameters of ketogenesis insufficient neonatal mice, specificity of HMGCS2 ASO treatment in adult mice, and quantification of ketogenesis in perfused livers. **(A)** Body weight (g) and **(B)** blood glucose levels (mg/dL) in neonatal mice treated with ASO daily for 11 days, beginning on the second day of life (P1), n > 4/group. **(C)** *Hmgcs2* transcript abundance in liver (n = 8-10/group)

and **(D)** in subcutaneous adipose tissue ($n = 4/\text{group}$) of adult mice treated with control or HMGCS2 ASO biweekly for four weeks beginning at six weeks of age. **(E)** Cytoplasmic 3-hydroxymethylglutaryl-CoA synthase (HMGCS1) protein content in livers of adult mice treated with ASOs for four weeks. **(F)** ^{13}C - βOHB enrichment in perfused livers of ASO treated mice, demonstrating diminished production of ketone bodies from ^{13}C octanoic acid. Decreased ^{13}C - βOHB enrichment in fasted control livers compared to fed control livers is likely due to increased competition from endogenous fatty acids, which are mobilized to the liver from adipose stores during the fast, preceding the perfusion. $n = 4\text{-}8/\text{group}$. **, $p < 0.01$, ***, $p < 0.001$ by Student's t test or 2-way ANOVA as appropriate, as indicated.

Fig. S6.2. Metabolic parameters of ketogenesis insufficient adult mice fed a standard chow diet. **(A)** Body weight (g), **(B)** average food intake (kCal/mouse/day), and **(C)** body composition (g) in ASO treated mice fed a low fat diet (standard chow diet) for four weeks. **(D)** Serum free fatty acids (FFAs, mM; $n = 20/\text{group}$), **(E)** triacylglyceride (TAG, mg/dL; $n = 15\text{-}19$) **(F)** acetoacetate (AcAc) and βOHB (mM, $n = 7$ group for each ketone body), **(G)** blood glucose (mg/dL, $n = 28\text{-}36/\text{group}$), and **(H)** serum insulin (ng/ml, $n = 20\text{-}23/\text{group}$) concentrations in standard chow diet-fed ASO treated mice. **, $p < 0.01$ by Student's t test as indicated.

Fig. S6.3. Serum metabolites of ASO-treated mice fed a 60% HFD. **(A)** Immunoblot for HMGCS2 and actin using protein lysates derived from livers of adult mice treated with control or HMGCS2 ASO biweekly for two weeks beginning at six weeks of age, during which time mice were maintained on a standard chow diet (quantification on right) and **(B)** following an additional eight weeks of 60% high fat diet (HFD). **(C)** Serum [TAG] (mg/dL), **(D)** [FFA] (mM), and **(E)** [TKB] (mM) in ASO-treated mice fed a HFD for eight weeks, $n = 8\text{-}10/\text{group}$. ***, $p < 0.001$ by Student's t test as indicated.

Fig. S6.4. Body weight, energy intake, and body composition of ketogenesis insufficient mice fed either a 60% HFD or a 40% fat diet. (A) Body weight (g) and **(B)** caloric intake (kCal/mouse/day) during 60% HFD and 40% fat diet **(C-D)** maintenance and ASO treatment, n = 8-10/group, ***, $p < 0.001$ by linear regression t test. **(E)** Body composition (g) pre- and post 40% fat diet feeding. n = 10/group, *, $p < 0.05$, **, $p < 0.01$ ***, $p < 0.001$ by 2-way ANOVA as indicated. **(F)** Blood glucose concentration (mg/dL) in mice fed a 40% fat diet for eight weeks. n = 10-15, *, $p < 0.05$, by Student's t test.

Fig. S6.5. Metabolite concentrations and gene expression in livers of ketogenesis insufficient mice. (A) Total hepatic glucose concentration (pmol/mg tissue) and **(B)** moles of ^{13}C -glucose produced from ^{13}C lactate and ^{13}C pyruvate, quantified by NMR profiling of perfused liver extracts from ASO-treated mice fed a 60% HFD for eight weeks, n = 4-5/group. **(C)** Total [glucose] (pmol/mg tissue) in livers from standard chow diet-fed ASO-treated mice perfused with the indicated substrates, n = 7-8/group. **(D)** Relative transcript abundances of key mediators of fatty acid oxidation and gluconeogenesis in livers from standard chow diet-fed ASO-treated mice, n = 8-10/group. peroxisome proliferator activated receptor alpha, *Ppara*; peroxisome proliferator activated receptor gamma coactivator 1-alpha, *Pgc1a*; acyl-CoA oxidase, *Acox1*; carnitine palmitoyl transferase 1a, *Cpt1a*; medium chain acyl-CoA dehydrogenase, *Acadm*; fibroblast growth factor 21, *Fgf21*; malic enzyme 2; *Me2*; phosphoenol pyruvate carboxykinase, *Pck1*; glucose-6-phosphatase, *G6pc*. **(E)** Total [glutamate] (nmol/mg tissue) in livers from standard chow diet-fed ASO-treated mice perfused with the indicated substrates, n = 7-8/group. **(F)** Pantothenate kinase 1a and 1b (*Pank1a* and *Pank1b*) relative mRNA abundance in livers of standard chow diet-fed ASO-treated mice, n = 8-10/group. **(G)** [Glutamate] (nmol/mg tissue) and **(H)** [succinate] (nmol/mg tissue) in unperfused livers of 60% HFD-fed ASO-treated mice n = 4-5/group. **(I)** Free coenzyme A (CoASH, pmol/mg tissue) concentrations in unperfused livers of 60% HFD-fed ASO-treated mice, n = 8/group. *, $p < 0.05$, **, $p < 0.01$, ***, $p < 0.001$ by Student's t test or 2-way ANOVA as appropriate, as indicated.

Fig. S6.6. Hepatic injury in ketogenesis insufficient mice fed a 40% HFD. (A) Hepatic [TAG] (mg/g tissue) and **(B)** serum alanine aminotransferase (ALT, U/L) activity in ASO-treated mice fed a 40% fat diet for eight weeks, $n = 9/\text{group}$ for [TAG] and $n = 4\text{-}5/\text{group}$ for ALT. **(C)** Representative hematoxylin and eosin stained sections of liver from ASO treated mice fed the indicated diet. Black arrowheads indicate microgranulomas comprised of lipid laden Kupffer cells and grey arrowheads indicate nests of inflammatory cells. *, $p < 0.05$, by Student's t test as indicated.

Fig. S6.7. Elevation of short- and medium-chain blood acylcarnitines in ketogenesis insufficient mice fed a 40% fat diet. Blood acylcarnitines (μM) in 40% fat diet-fed ASO treated mice, determined by tandem mass spectrometry from blood spotted onto 1.3-cm spots on Whatman 903 filter paper. *, $p < 0.05$, **, $p < 0.01$ by Student's t test, as indicated. $n = 9\text{-}10/\text{group}$.

Fig. S6.8. Hepatic glucose pools in livers perfused with supplemental CoASH precursors. (A) Total hepatic glucose concentrations (pmol/mg tissue) in livers of standard chow diet-fed ASO-treated mice perfused with [^{13}C]lactate, [^{13}C]pyruvate, octanoic acid, cysteine, and pantothenic acid for 15 min, $n = 6\text{-}7/\text{group}$. **(B)** Total hepatic glucose concentrations (pmol/mg tissue) in livers of standard chow diet-fed ASO-treated mice perfused for 45 min with unlabeled lactate, pyruvate, cysteine, and pantothenic acid, followed by 15 min of perfusion with [^{13}C]lactate, [^{13}C]pyruvate, octanoic acid, cysteine, and pantothenic acid, $n = 5\text{-}6/\text{group}$.

Figure 6.1

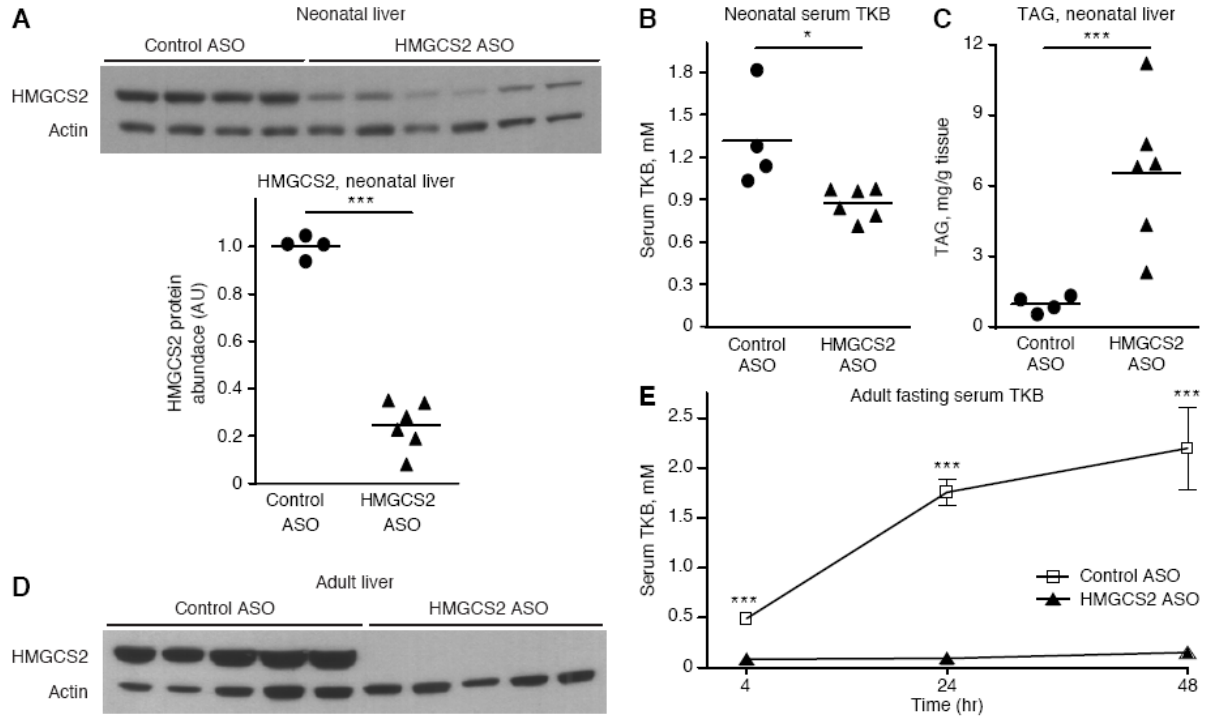


Figure 6.2

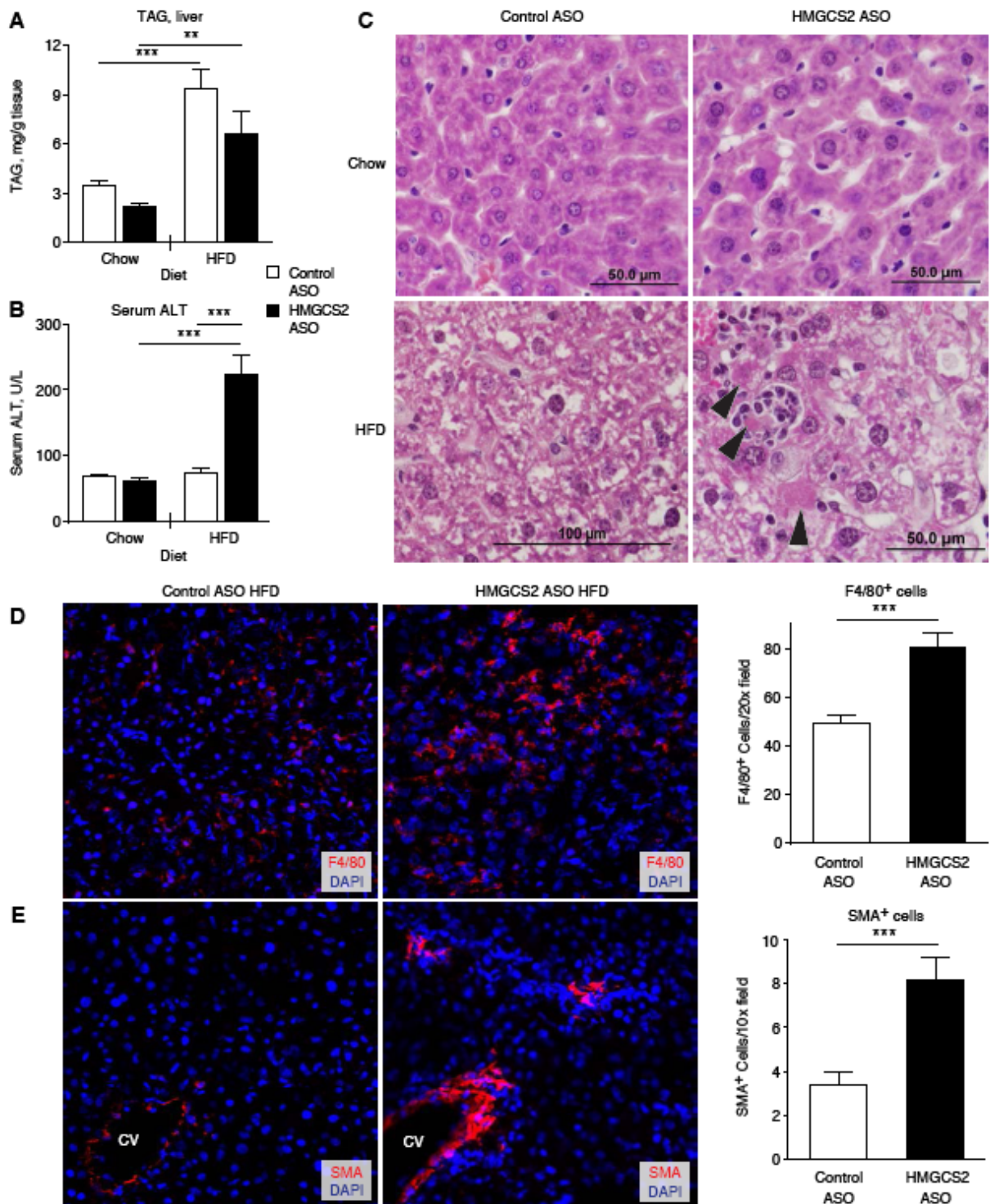


Figure 6.3

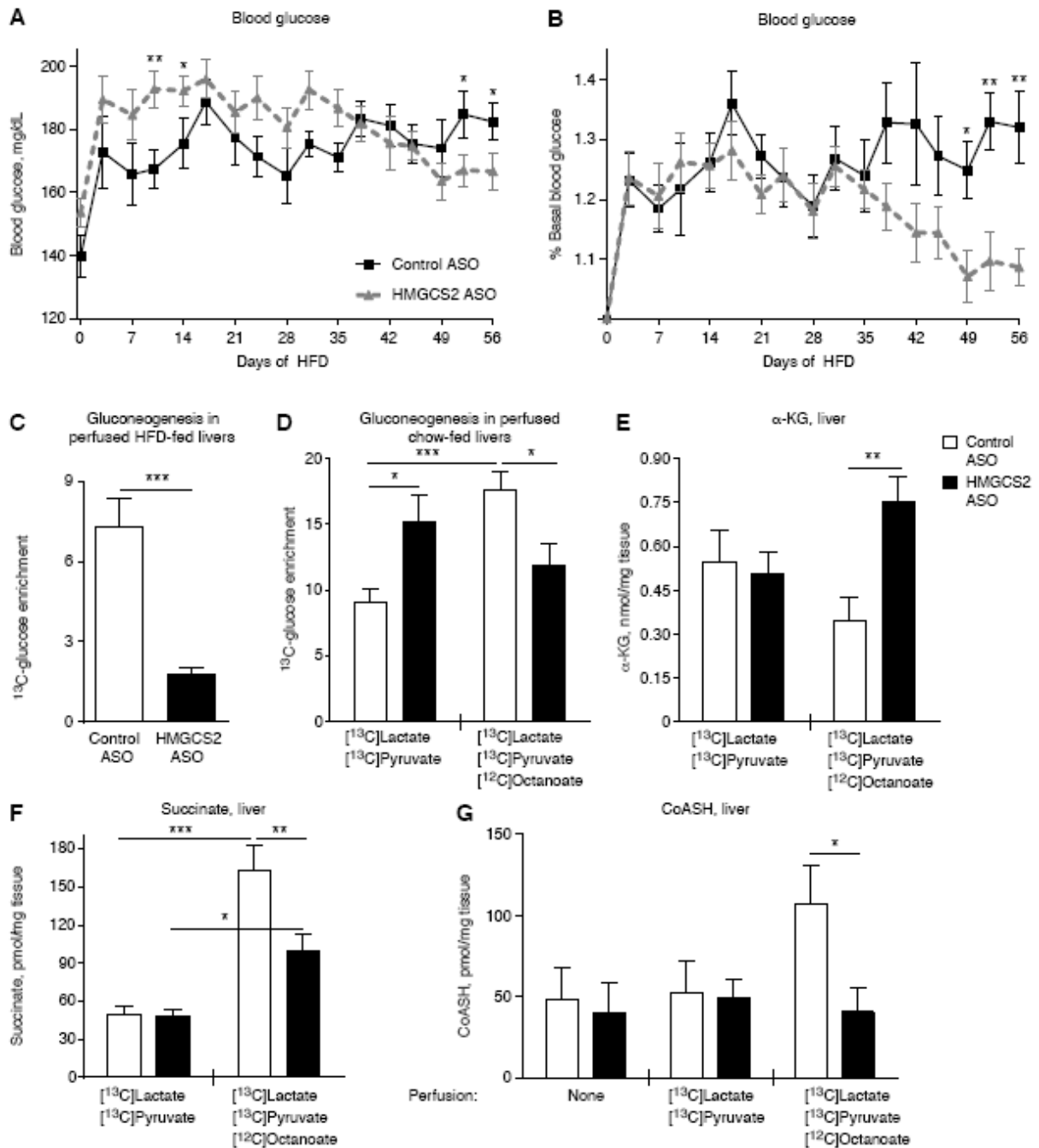


Figure 6.4

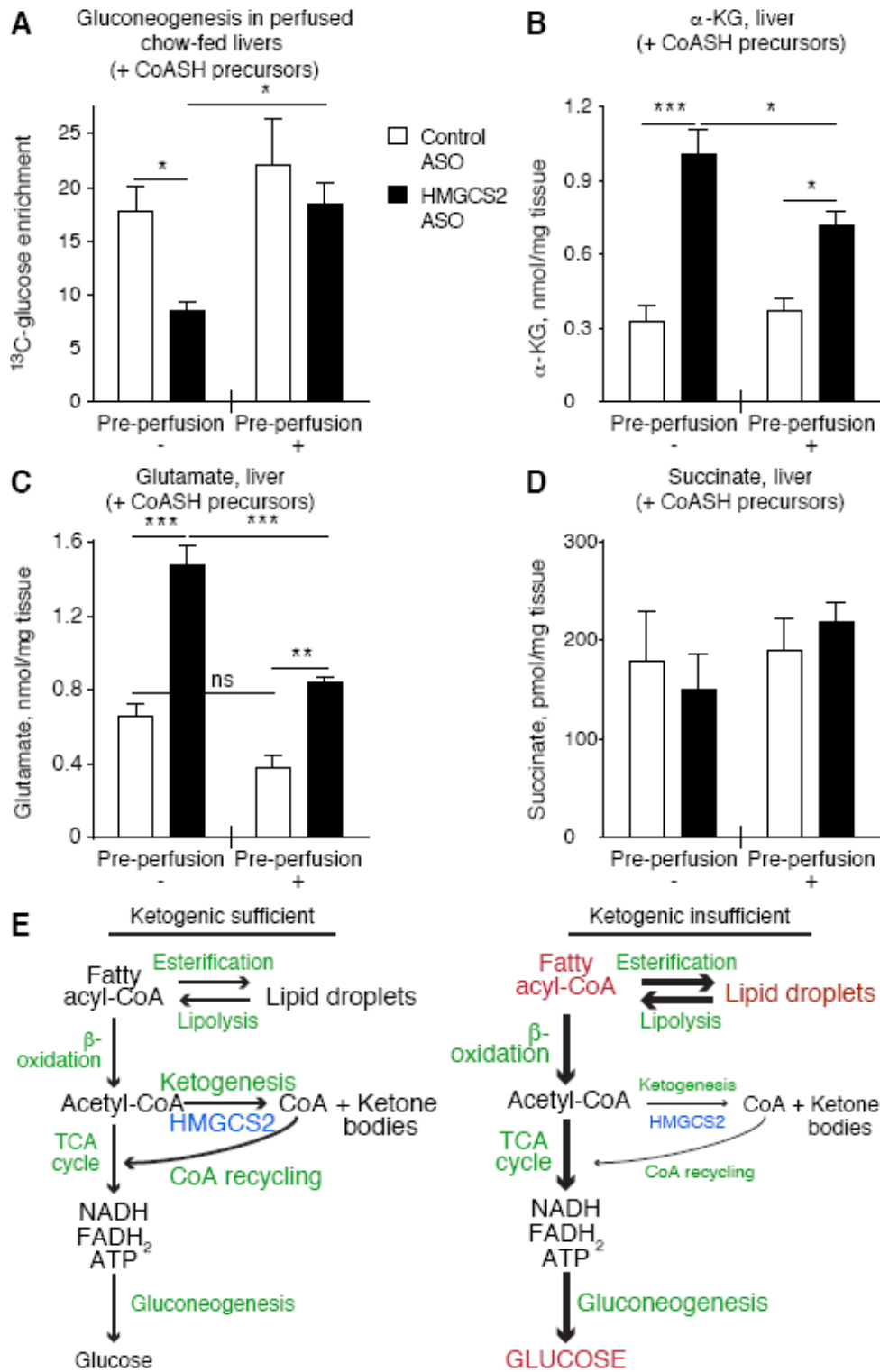


Figure S6.1

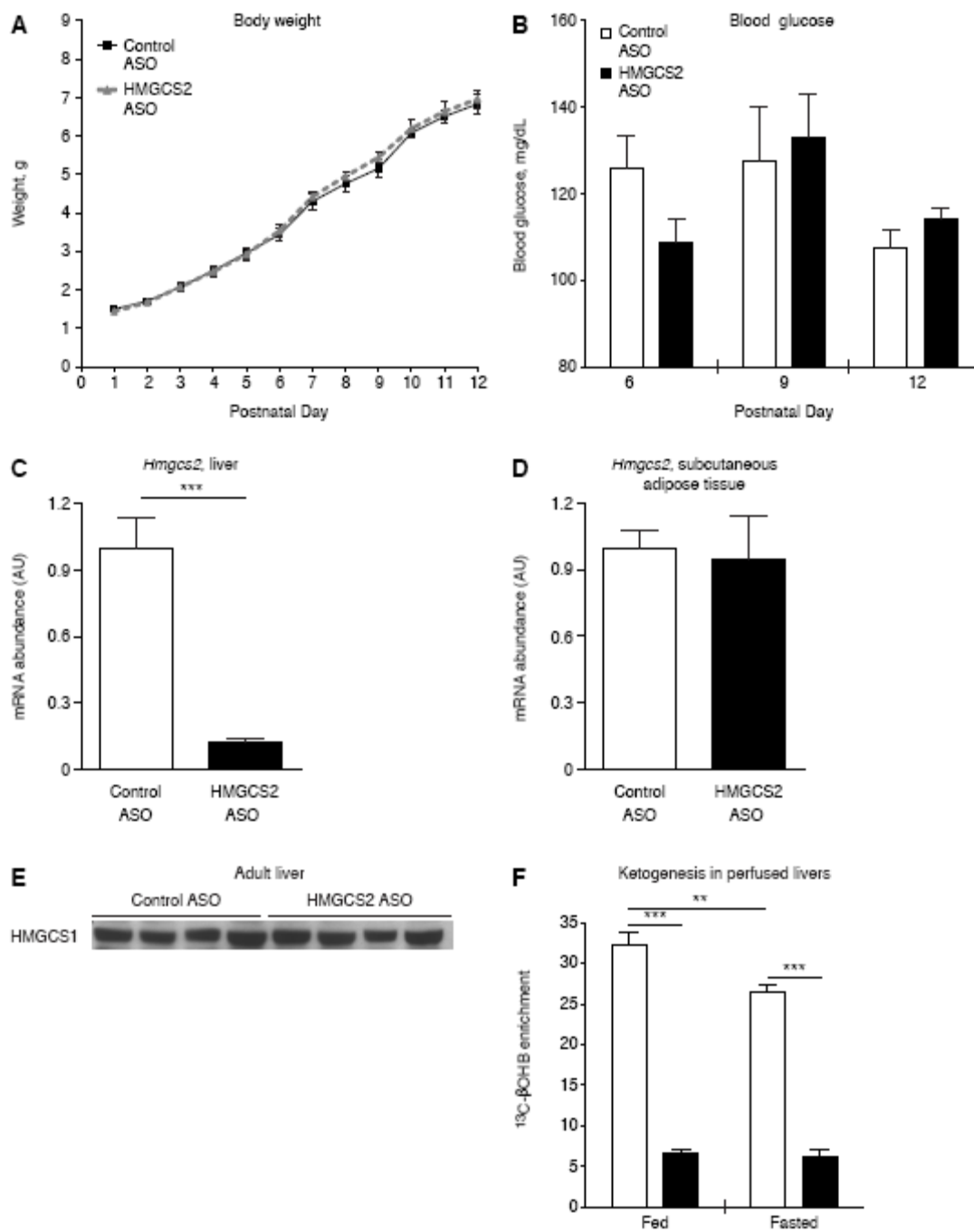


Figure S6.2

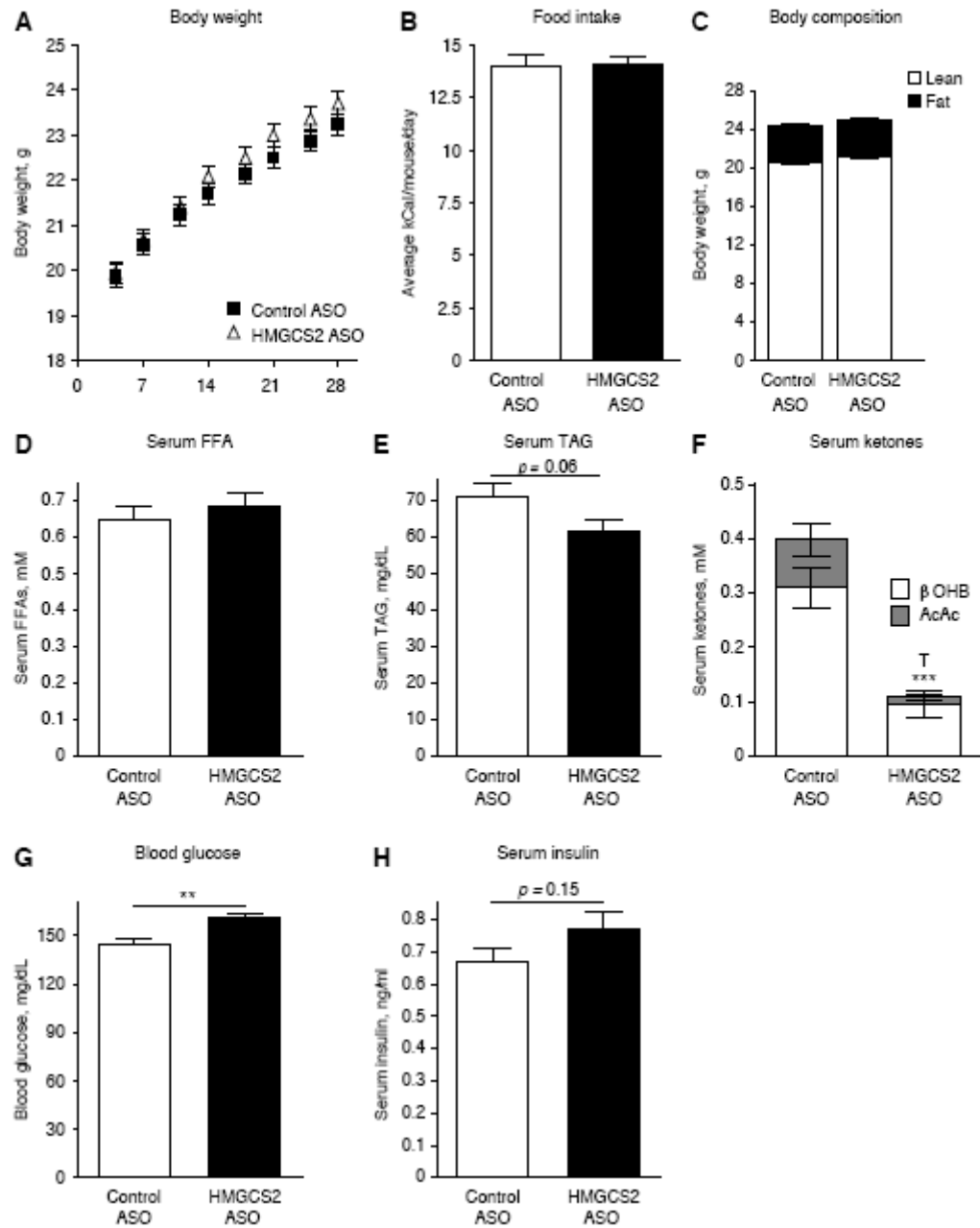


Figure S6.3

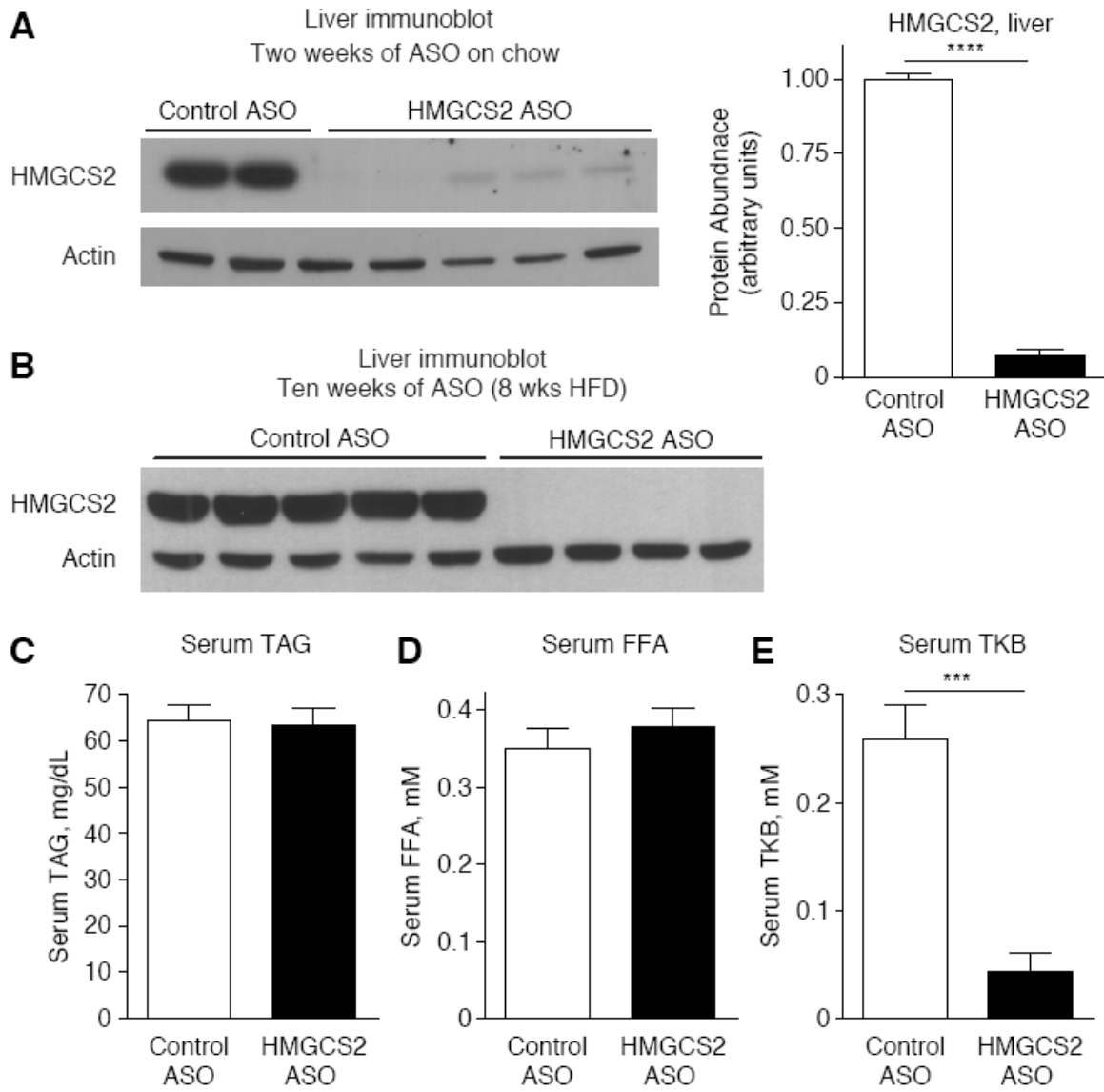


Figure S6.4

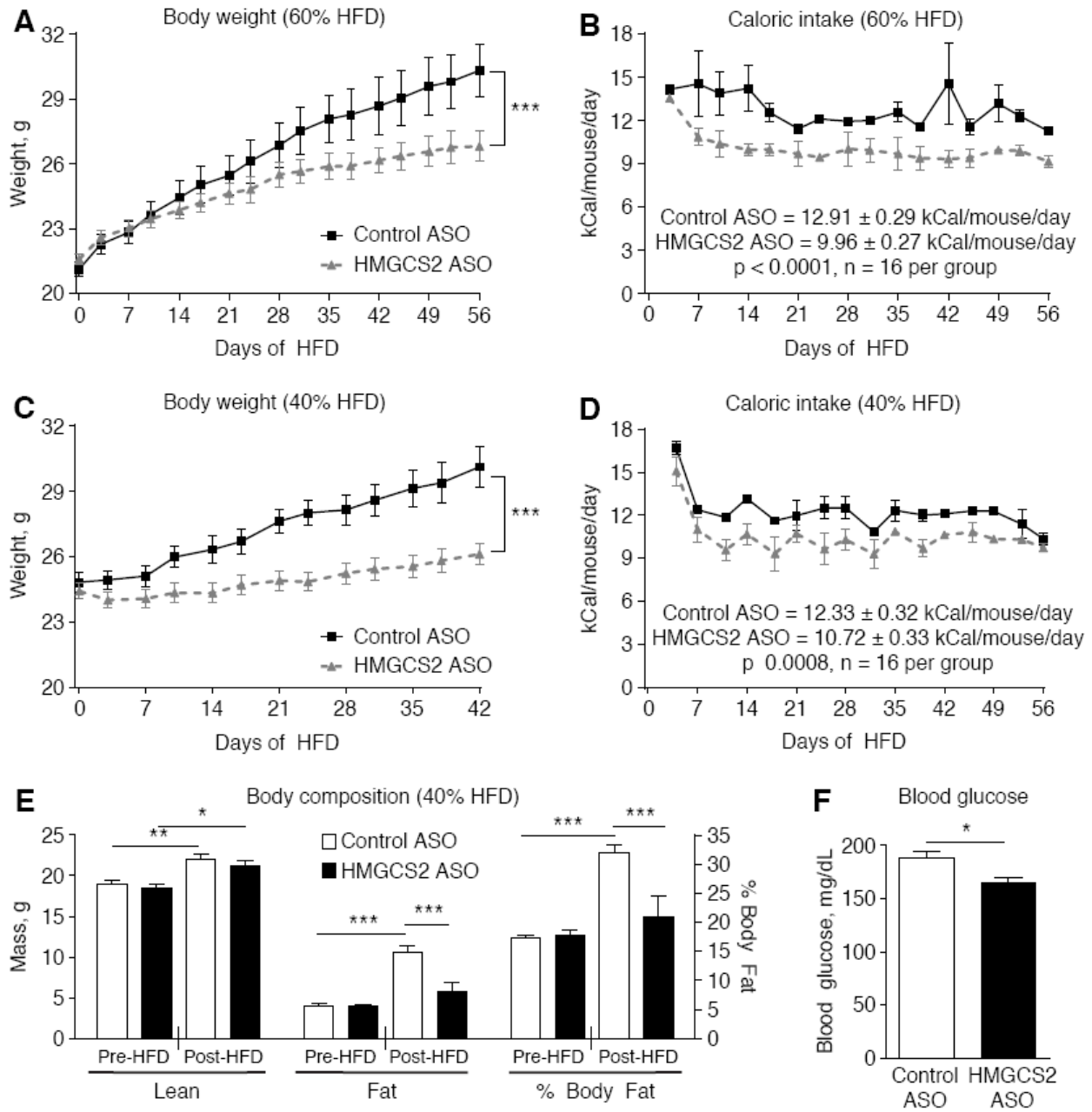


Figure S6.5

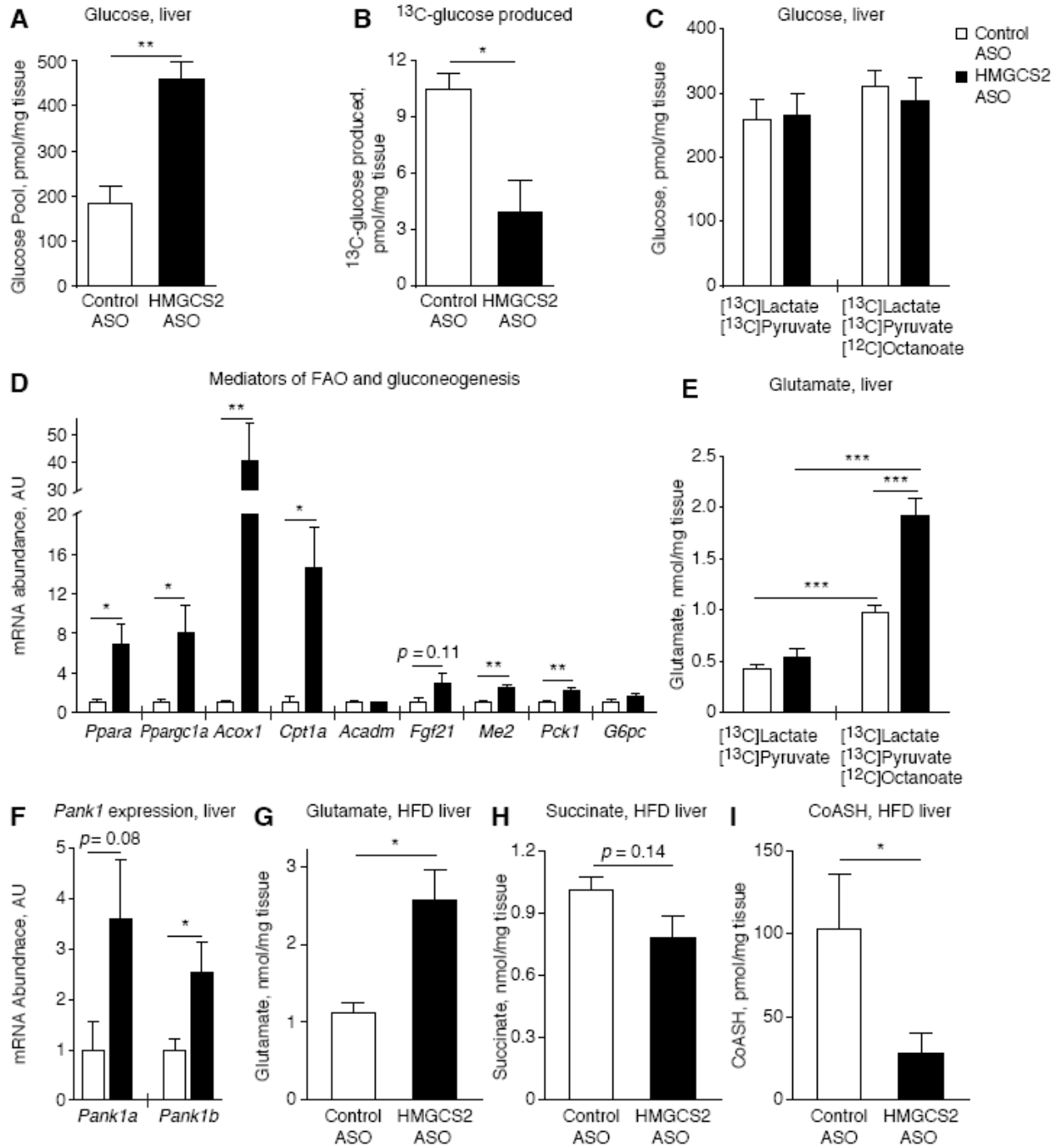


Figure S6.6

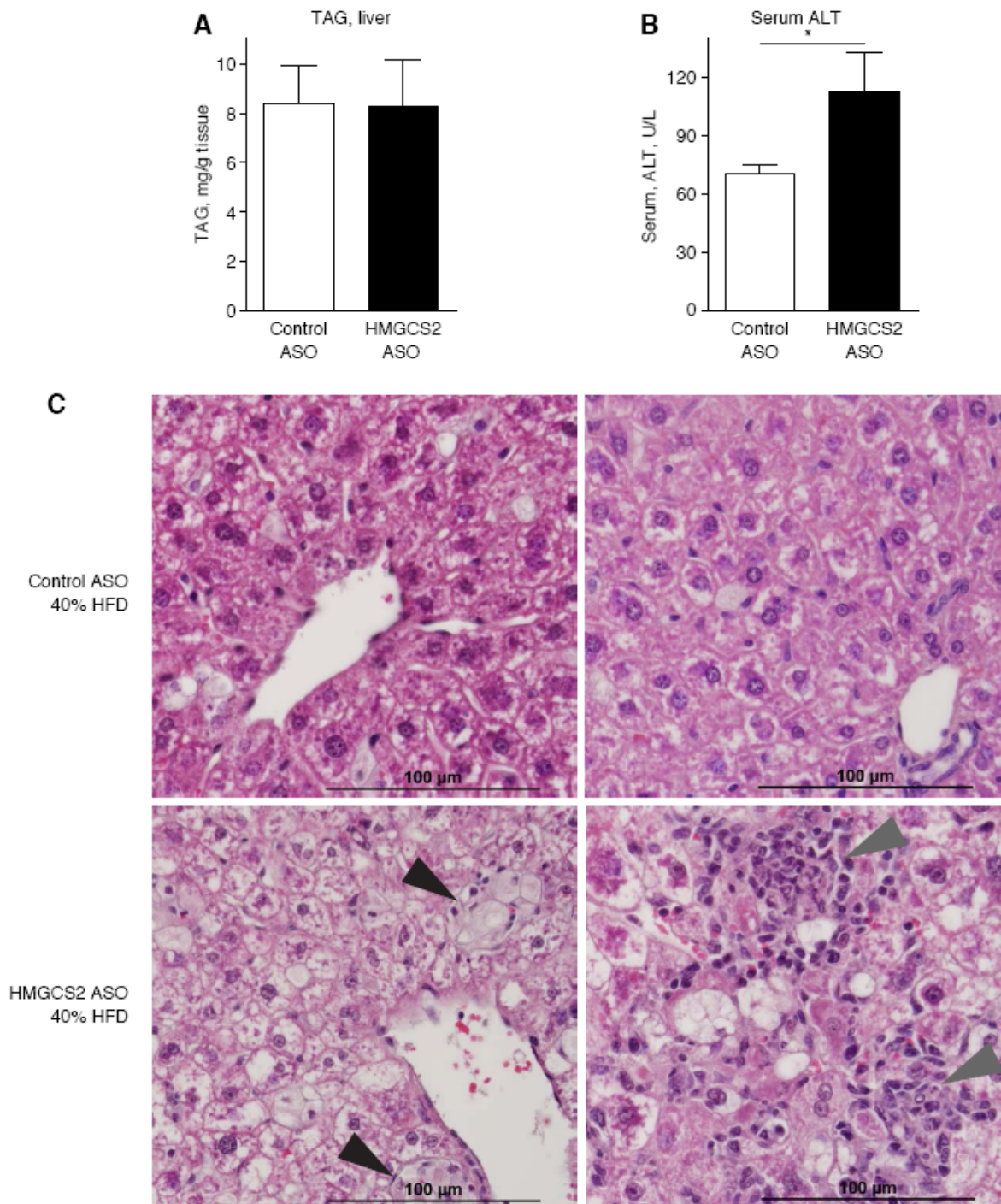


Figure S6.7

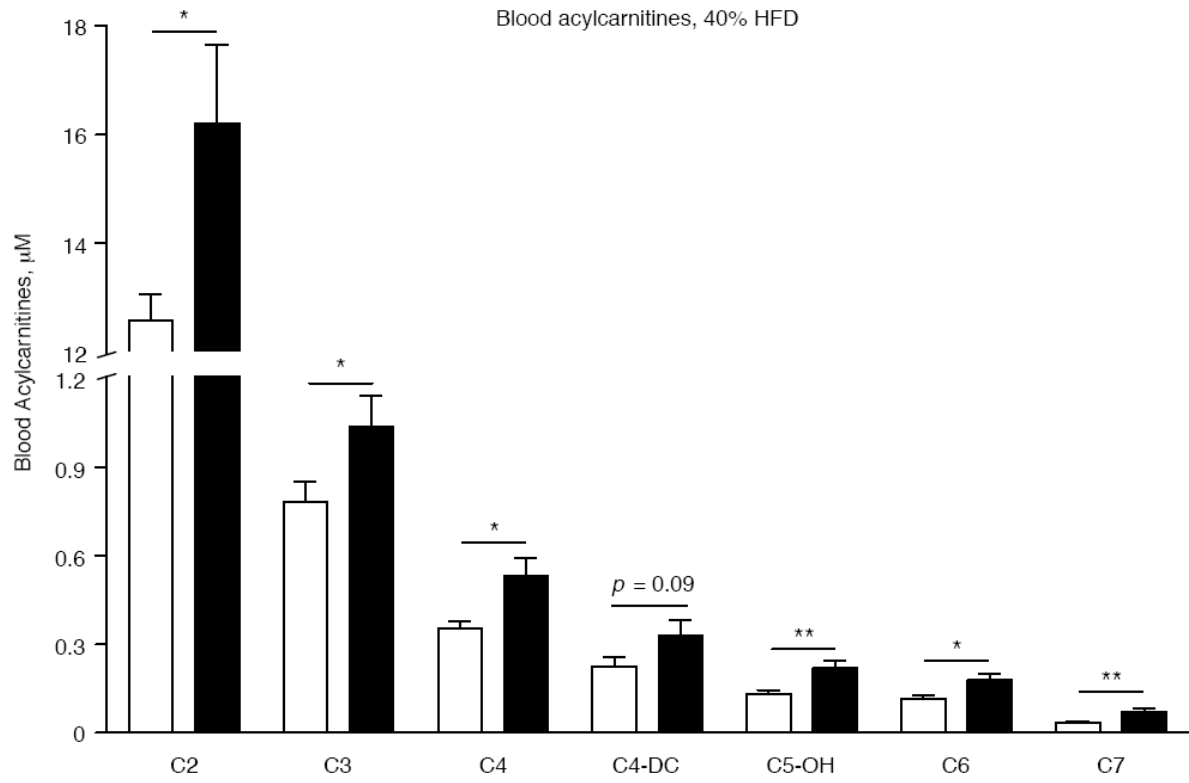


Figure S6.8

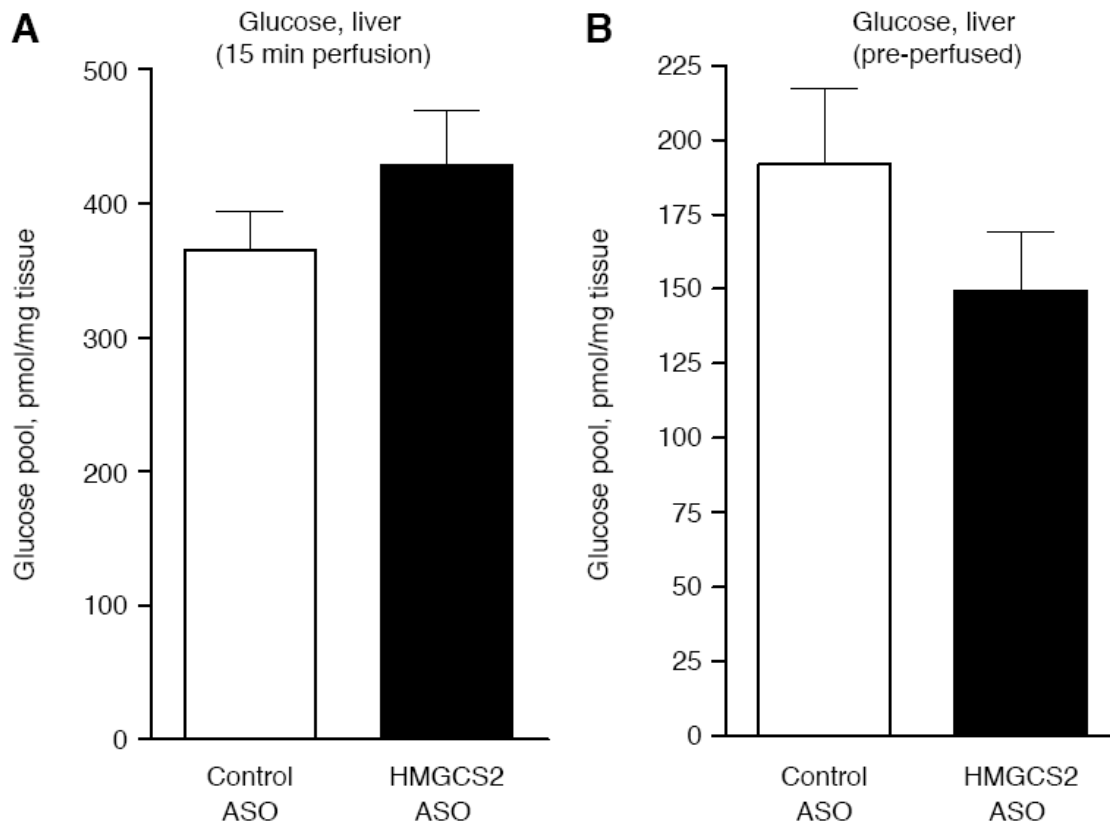


Table S6.1

Supplemental Table 1: Blood acylcarnitine profile of ASO-treated mice fed a chow diet

Acylcarnitine	Control ASO																HMGS2 ASO																t-test
	5198	5199	5200	5201	5202	5269	5270	5271	5272	5273	5203	5204	5205	5206	5207	5250	5251	5252	5253	5254	Control ASO	HMGS2 ASO											
C2	20.16	20.82	22.86	12.85	22.99	25.68	29.82	27.08	29.54	35.95	25.89	17.95	27.79	16.96	17.93	19.91	29.01	20.57	14.22	37.58	24.77	22.78											
C3	0.65	0.90	0.62	0.53	0.76	1.12	1.02	1.07	1.17	1.39	0.86	0.89	1.32	0.75	0.53	0.90	1.20	1.14	0.88	1.77	0.82	1.03											
C4	0.36	0.38	0.38	0.17	0.32	0.49	0.60	0.41	0.70	0.78	0.51	0.27	0.24	0.16	0.20	0.34	0.32	0.54	0.43	0.58	0.46	0.36											
C5	0.18	0.15	0.08	0.07	0.11	0.11	0.15	0.21	0.11	0.24	0.25	0.13	0.24	0.13	0.11	0.25	0.18	0.30	0.19	0.22	0.14	0.20											
C4-OH	0.10	0.23	0.24	0.11	0.17	0.26	0.37	0.17	0.34	0.57	0.22	0.18	0.25	0.12	0.09	0.18	0.23	0.09	0.09	0.37	0.25	0.17											
C6	0.18	0.22	0.19	0.13	0.14	0.14	0.20	0.27	0.15	0.15	0.15	0.19	0.21	0.15	0.16	0.27	0.14	0.18	0.11	0.19	0.18	0.18											
C5-OH	0.13	0.17	0.15	0.11	0.16	0.17	0.10	0.18	0.17	0.24	0.11	0.17	0.15	0.17	0.11	0.12	0.18	0.18	0.18	0.22	0.16	0.16											
C6-OH	0.06	0.08	0.03	0.03	0.07	0.07	0.08	0.07	0.08	0.13	0.05	0.05	0.11	0.07	0.04	0.02	0.06	0.06	0.06	0.11	0.07	0.06											
C7	0.05	0.04	0.06	0.04	0.07	0.09	0.03	0.03	0.06	0.04	0.06	0.02	0.04	0.04	0.05	0.08	0.05	0.09	0.05	0.10	0.05	0.06											
C8:1	0.09	0.10	0.05	0.11	0.10	0.10	0.13	0.18	0.08	0.10	0.09	0.07	0.08	0.11	0.11	0.12	0.09	0.09	0.06	0.14	0.11	0.10											
C8	0.09	0.10	0.13	0.08	0.12	0.10	0.10	0.11	0.11	0.16	0.09	0.07	0.27	0.09	0.15	0.12	0.09	0.09	0.09	0.18	0.11	0.13											
C3-DC	0.14	0.14	0.17	0.06	0.09	0.09	0.08	0.26	0.15	0.19	0.08	0.17	0.09	0.13	0.07	0.10	0.18	0.08	0.11	0.20	0.14	0.12											
C10:1	0.09	0.10	0.08	0.14	0.07	0.17	0.08	0.21	0.13	0.16	0.07	0.12	0.27	0.07	0.09	0.15	0.09	0.15	0.15	0.28	0.12	0.14											
C10	0.09	0.08	0.08	0.08	0.07	0.10	0.08	0.11	0.05	0.13	0.07	0.10	0.08	0.07	0.09	0.12	0.06	0.06	0.09	0.14	0.09	0.09											
C5-DC	0.08	0.02	0.06	0.07	0.05	0.11	0.08	0.12	0.04	0.07	0.04	0.11	0.09	0.04	0.07	0.08	0.05	0.06	0.05	0.06	0.07	0.06											
C12:1	0.12	0.08	0.05	0.03	0.05	0.07	0.08	0.11	0.03	0.05	0.09	0.05	0.08	0.05	0.11	0.07	0.03	0.12	0.06	0.11	0.07	0.08											
C12	0.12	0.08	0.16	0.11	0.10	0.17	0.16	0.11	0.13	0.18	0.11	0.07	0.22	0.09	0.15	0.07	0.09	0.12	0.06	0.14	0.13	0.11											
C12-OH	0.03	0.05	0.03	0.08	0.02	0.03	0.08	0.11	0.05	0.03	0.02	0.02	0.05	0.02	0.04	0.10	0.03	0.03	0.03	0.07	0.05	0.05											
C14:2	0.06	0.08	0.12	0.14	0.06	0.13	0.06	0.11	0.09	0.08	0.10	0.05	0.08	0.07	0.15	0.07	0.06	0.12	0.09	0.11	0.09	0.09											
C14:1	0.12	0.05	0.12	0.17	0.09	0.10	0.16	0.39	0.14	0.17	0.08	0.09	0.15	0.14	0.13	0.17	0.19	0.24	0.12	0.11	0.15	0.14											
C14	0.35	0.26	0.30	0.26	0.27	0.39	0.19	0.39	0.26	0.33	0.26	0.21	0.23	0.20	0.28	0.24	0.22	0.44	0.29	0.32	0.30	0.27											
C14:1-OH	0.12	0.05	0.06	0.06	0.12	0.06	0.09	0.11	0.06	0.11	0.05	0.09	0.06	0.07	0.08	0.07	0.03	0.12	0.09	0.07	0.08	0.07											
C14-OH	0.03	0.08	0.06	0.09	0.03	0.06	0.06	0.14	0.03	0.06	0.05	0.07	0.04	0.09	0.03	0.05	0.03	0.04	0.03	0.04	0.06	0.06											
C16:1	0.15	0.15	0.12	0.30	0.14	0.10	0.12	0.20	0.23	0.19	0.16	0.12	0.21	0.10	0.09	0.18	0.24	0.18	0.11	0.10	0.17	0.15											
C16	0.88	1.24	1.59	1.39	1.20	1.69	1.38	1.60	1.47	2.05	1.30	1.29	2.16	1.21	1.41	1.60	1.77	1.65	1.68	1.60	1.45	1.57											
C16:1-OH	0.09	0.03	0.06	0.10	0.09	0.06	0.06	0.12	0.09	0.06	0.05	0.12	0.05	0.05	0.07	0.03	0.03	0.11	0.07	0.10	0.08	0.07											
C16-OH	0.12	0.15	0.06	0.10	0.11	0.06	0.06	0.08	0.06	0.10	0.03	0.07	0.10	0.10	0.07	0.05	0.07	0.07	0.07	0.03	0.09	0.07											
C18:2	0.18	0.15	0.27	0.27	0.14	0.45	0.29	0.40	0.23	0.32	0.26	0.34	0.42	0.18	0.15	0.28	0.24	0.28	0.21	0.24	0.27	0.26											
C18:1	0.50	0.42	0.59	0.68	0.43	0.48	0.50	0.64	0.69	0.74	0.34	0.49	0.62	0.42	0.33	0.48	0.61	0.63	0.47	0.44	0.55	0.48											
C18	0.18	0.21	0.35	0.44	0.26	0.35	0.35	0.56	0.35	0.42	0.36	0.32	0.34	0.26	0.26	0.41	0.51	0.46	0.50	0.48	0.35	0.39											
C18:2-OH	0.03	0.03	0.00	0.03	0.00	0.00	0.06	0.04	0.00	0.03	0.03	0.02	0.03	0.03	0.04	0.05	0.03	0.04	0.04	0.03	0.02	0.03											
C18:1-OH	0.09	0.06	0.06	0.07	0.06	0.03	0.06	0.08	0.06	0.10	0.03	0.05	0.10	0.08	0.07	0.05	0.03	0.04	0.04	0.07	0.07	0.07											
C3:1	0.03	0.03	0.03	0.03	0.12	0.04	0.03	0.04	0.06	0.03	0.08	0.03	0.06	0.05	0.02	0.03	0.04	0.04	0.07	0.12	0.04	0.05											
C5:1	0.03	0.04	0.04	0.02	0.02	0.06	0.03	0.03	0.02	0.04	0.02	0.04	0.02	0.02	0.05	0.04	0.05	0.06	0.02	0.06	0.03	0.04											
C10:2	0.06	0.08	0.03	0.08	0.02	0.03	0.08	0.07	0.05	0.05	0.02	0.02	0.05	0.05	0.04	0.02	0.09	0.06	0.03	0.04	0.06	0.06											
C4-DC	0.18	0.18	0.31	0.15	0.25	0.23	0.30	0.26	0.44	0.26	0.29	0.24	0.14	0.16	0.17	0.20	0.35	0.28	0.24	0.34	0.25	0.24											
C10:1-OH	0.09	0.05	0.13	0.06	0.05	0.20	0.29	0.21	0.16	0.16	0.11	0.12	0.16	0.09	0.13	0.37	0.30	0.24	0.15	0.25	0.14	0.18											
C12:1-OH	0.06	0.08	0.03	0.08	0.15	0.10	0.08	0.07	0.11	0.10	0.07	0.07	0.11	0.09	0.04	0.07	0.06	0.09	0.09	0.07	0.09	0.08											
C18-OH	0.03	0.03	0.03	0.03	0.07	0.03	0.06	0.06	0.08	0.03	0.06	0.03	0.05	0.03	0.05	0.04	0.03	0.07	0.04	0.04	0.05	0.04											

Table S6.2

Supplemental Table 2: Blood acylcarnitine profile of ASO-treated mice fed a 40% fat diet

	Control ASO										HMGSZ ASO										Average		t-test
	5055	5056	5057	5058	5059	4791	4792	4793	4794	4795	5065	5066	5067	5068	5069	4797	4798	4799	4800	Control ASO	HMGSZ ASO		
Acylcarnitine	12.43	13.37	13.65	11.74	11.40	10.58	10.35	14.20	13.05	14.98	10.97	19.11	21.57	20.56	11.54	13.90	14.38	21.24	12.58	12.57	16.21	0.0244	
C2	0.64	0.66	1.31	0.82	0.61	0.63	0.86	0.87	0.59	0.87	0.89	1.54	1.35	1.25	0.49	1.00	0.92	1.16	0.74	0.78	1.04	0.0585	
C3	0.42	0.39	0.40	0.39	0.27	0.25	0.25	0.49	0.29	0.34	0.40	0.58	0.63	0.53	0.30	0.29	0.54	0.64	0.87	0.35	0.53	0.0133	
C4	0.13	0.15	0.18	0.19	0.19	0.15	0.12	0.23	0.21	0.15	0.10	0.20	0.19	0.28	0.26	0.14	0.10	0.31	0.11	0.17	0.19	0.5339	
C4-OH	0.19	0.16	0.13	0.13	0.09	0.08	0.15	0.27	0.11	0.14	0.16	0.16	0.17	0.20	0.07	0.15	0.20	0.20	0.10	0.15	0.16	0.6368	
C6	0.19	0.15	0.07	0.11	0.08	0.15	0.10	0.11	0.09	0.11	0.14	0.20	0.19	0.22	0.19	0.21	0.08	0.29	0.09	0.12	0.18	0.0228	
C5-OH	0.10	0.20	0.18	0.13	0.08	0.13	0.15	0.09	0.14	0.13	0.10	0.17	0.27	0.31	0.23	0.18	0.29	0.31	0.12	0.13	0.22	0.0062	
C6-OH	0.04	0.09	0.04	0.06	0.05	0.08	0.06	0.06	0.08	0.06	0.04	0.07	0.07	0.13	0.04	0.06	0.08	0.07	0.02	0.06	0.06	0.8210	
C7	0.03	0.05	0.04	0.03	0.04	0.06	0.02	0.05	0.00	0.02	0.03	0.03	0.11	0.09	0.11	0.07	0.06	0.10	0.05	0.03	0.07	0.0021	
C8:1	0.08	0.06	0.04	0.06	0.10	0.08	0.08	0.17	0.08	0.11	0.07	0.07	0.03	0.13	0.07	0.14	0.10	0.17	0.10	0.09	0.10	0.4784	
C8	0.16	0.15	0.12	0.06	0.10	0.17	0.23	0.19	0.20	0.11	0.11	0.14	0.14	0.35	0.14	0.19	0.13	0.14	0.12	0.15	0.16	0.6567	
C3-DC	0.11	0.15	0.16	0.22	0.25	0.11	0.10	0.20	0.11	0.10	0.15	0.24	0.18	0.30	0.09	0.27	0.09	0.31	0.05	0.15	0.19	0.3419	
C10:1	0.16	0.09	0.08	0.06	0.10	0.08	0.08	0.14	0.08	0.06	0.11	0.11	0.10	0.13	0.07	0.11	0.13	0.10	0.10	0.09	0.11	0.2680	
C10	0.16	0.17	0.04	0.09	0.19	0.11	0.14	0.08	0.08	0.11	0.14	0.18	0.14	0.35	0.11	0.17	0.10	0.27	0.10	0.12	0.17	0.1000	
C5-DC	0.06	0.07	0.11	0.05	0.08	0.04	0.05	0.05	0.05	0.07	0.10	0.07	0.08	0.12	0.08	0.05	0.06	0.08	0.04	0.06	0.07	0.2975	
C12:1	0.12	0.12	0.12	0.09	0.10	0.08	0.06	0.11	0.10	0.14	0.04	0.07	0.03	0.17	0.07	0.08	0.10	0.20	0.10	0.10	0.10	0.7432	
C12	0.12	0.15	0.12	0.18	0.14	0.22	0.14	0.22	0.18	0.17	0.21	0.14	0.14	0.22	0.07	0.22	0.15	0.20	0.12	0.16	0.16	0.9818	
C12-OH	0.04	0.06	0.08	0.03	0.10	0.06	0.11	0.06	0.05	0.03	0.04	0.11	0.07	0.09	0.07	0.06	0.10	0.07	0.05	0.06	0.07	0.3839	
C14:2	0.07	0.05	0.07	0.03	0.04	0.14	0.14	0.19	0.11	0.17	0.03	0.06	0.07	0.04	0.08	0.09	0.13	0.21	0.17	0.10	0.10	0.9671	
C14:1	0.11	0.13	0.20	0.18	0.14	0.25	0.25	0.19	0.11	0.13	0.24	0.22	0.21	0.30	0.21	0.18	0.24	0.24	0.17	0.17	0.22	0.0214	
C14	0.26	0.40	0.23	0.40	0.22	0.28	0.47	0.45	0.34	0.33	0.21	0.45	0.49	0.60	0.29	0.42	0.27	0.33	0.29	0.34	0.37	0.4761	
C14:1-OH	0.11	0.08	0.10	0.09	0.07	0.14	0.11	0.22	0.11	0.07	0.14	0.16	0.11	0.13	0.13	0.12	0.11	0.09	0.07	0.11	0.12	0.7261	
C14-OH	0.04	0.05	0.07	0.12	0.11	0.08	0.04	0.03	0.06	0.07	0.03	0.03	0.04	0.04	0.04	0.03	0.05	0.06	0.05	0.07	0.04	0.0394	
C16:1	0.17	0.15	0.15	0.21	0.16	0.32	0.30	0.23	0.20	0.21	0.15	0.19	0.26	0.24	0.13	0.30	0.26	0.24	0.22	0.21	0.22	0.8564	
C16	1.01	0.92	0.98	1.03	0.74	1.29	1.27	1.25	0.86	1.10	0.73	1.38	1.09	1.63	0.74	1.71	1.21	1.72	0.97	1.04	1.24	0.1677	
C16:1-OH	0.07	0.07	0.19	0.06	0.08	0.06	0.07	0.10	0.14	0.10	0.03	0.13	0.15	0.08	0.09	0.15	0.18	0.13	0.07	0.10	0.11	0.4079	
C16-OH	0.07	0.10	0.11	0.09	0.08	0.13	0.22	0.10	0.06	0.07	0.09	0.09	0.11	0.08	0.13	0.09	0.10	0.10	0.05	0.10	0.09	0.6693	
C18:2	0.17	0.10	0.11	0.15	0.16	0.16	0.11	0.26	0.09	0.14	0.12	0.16	0.11	0.12	0.09	0.32	0.08	0.20	0.10	0.14	0.14	0.9880	
C18:1	0.61	0.52	0.53	0.53	0.43	0.84	0.90	0.79	0.72	0.48	0.40	0.78	0.75	0.69	0.79	0.89	0.77	1.05	0.63	0.63	0.75	0.1560	
C18	0.24	0.32	0.53	0.29	0.19	0.39	0.37	0.46	0.40	0.55	0.43	0.56	0.41	0.65	0.48	0.59	0.36	0.61	0.24	0.37	0.48	0.0791	
C18:2-OH	0.10	0.07	0.04	0.06	0.00	0.03	0.15	0.03	0.06	0.00	0.03	0.06	0.04	0.04	0.00	0.06	0.05	0.07	0.05	0.05	0.04	0.5492	
C18:1-OH	0.13	0.12	0.08	0.12	0.04	0.06	0.07	0.07	0.03	0.07	0.06	0.09	0.11	0.08	0.04	0.12	0.10	0.07	0.12	0.08	0.09	0.5084	
C3:1	0.32	0.04	0.00	0.04	0.05	0.03	0.10	0.06	0.03	0.10	0.05	0.00	0.04	0.06	0.04	0.03	0.06	0.08	0.02	0.04	0.04	0.3079	
C5:1	0.06	0.02	0.04	0.03	0.00	0.04	0.07	0.07	0.09	0.02	0.03	0.07	0.04	0.06	0.04	0.07	0.04	0.05	0.05	0.04	0.05	0.6086	
C10:2	0.08	0.03	0.00	0.06	0.10	0.06	0.03	0.03	0.08	0.08	0.04	0.07	0.03	0.04	0.04	0.08	0.05	0.07	0.14	0.05	0.06	0.5418	
C4-DC	0.23	0.26	0.36	0.43	0.13	0.15	0.15	0.20	0.15	0.19	0.20	0.49	0.66	0.36	0.30	0.23	0.20	0.32	0.20	0.22	0.33	0.0947	
C10:1-OH	0.12	0.17	0.12	0.21	0.14	0.03	0.08	0.08	0.08	0.14	0.14	0.14	0.14	0.09	0.18	0.11	0.13	0.14	0.14	0.12	0.13	0.4185	
C12:1-OH	0.16	0.09	0.04	0.12	0.14	0.11	0.11	0.14	0.08	0.06	0.07	0.11	0.10	0.09	0.07	0.14	0.10	0.07	0.10	0.10	0.09	0.4829	
C18-OH	0.07	0.07	0.11	0.03	0.04	0.06	0.07	0.03	0.09	0.07	0.03	0.03	0.07	0.04	0.00	0.12	0.10	0.07	0.05	0.06	0.06	0.6012	

Table S6.3**Supplemental Table 1**

RT-qPCR Primers	Sequence (5'-3')	
	Forward	Reverse
<i>Hmgcs2</i>	TGGTTCAAGACAGGGACACAGAAC	AGAGGAATACCAGGGCCCAACAAT
<i>PPAR α</i>	TCGGCCTGGCCTTCTAAACATAG	TCTTGCAACAGTGGGTGCAGCG
<i>Ppargc1 α</i>	CGGAAATCATATCCAACCAG	TGAGGACCGCTAGCAAGTTTG
<i>ACO</i>	GGATGGTAGTCCGG	AGTCTGGATCGTTC
<i>Cpt1a</i>	CATGTCAAGCCAGACGAAGA	TGGTAGGAGAGCAGCACCTT
<i>Acadm</i>	GCTGGAGACATTGCCAATCA	TCTTGGCGTCCCTCATCAG
<i>Fgf21</i>	CCAGATGTGGGCTCCTCTGAC	AGAAACAGCCCTAGATTGAGGAAGAGT
<i>ME2</i>	AGAAGGAGTGAGTGCTCACCGAAT	ACTACAAAGGGACGTCAGAGCAGA
<i>Pck1</i>	GGAAGGACAAAGATGGCAAGTTC	AGGCGTTTTCTTAGGGATGTAG
<i>G6pc</i>	AAAGTCAACCGCCATGCAAAGGAC	TAGCAAAGAAAGACAGGGCTACCAG
<i>L32</i>	CCTCTGGTGAAGCCCAAGATC	TCTGGGTTTCCGCCAGTTT

Chapter 7

¹³C-edited proton NMR spectroscopy method for measurement of gluconeogenesis from pyruvate in the perfused mouse liver

Abstract

Measurement of hepatic glucose production (HGP) in rodent models is integral to obesity and diabetes research. Nonetheless, HGP is not routinely measured due to the challenges associated with clamp techniques, *in vivo* tracer studies, and *ex vivo* carbon NMR methods. Thus, we have developed a simple proton-edited ¹³C-NMR method to measure HGP from pyruvate *in situ* in the mouse. Here we demonstrate the validity of this method in cohorts of chow-fed and 24 hr fasted wild type male mice. Contribution of [¹³C]pyruvate, delivered via the portal vein in a euthermic oxygenated buffer, to the TCA cycle for terminal oxidation and to gluconeogenesis was quantified by NMR in mouse liver extracts. As expected, contribution of [¹³C]pyruvate to hepatic gluconeogenesis increased and hepatic pyruvate oxidation decreased with fasting. The methods contained here provide a relatively simple means of measuring hepatic gluconeogenesis from pyruvate using proton edited ¹³C-NMR and can easily be adapted to map the fate of various substrates.

Methods

Animals. All adult mice studied were males on a C57BL/6N X C57BL/6J hybrid background. Mice were maintained on standard low fat chow diet in which 13% of the calories are from fat, 25% from protein, and 62% from carbohydrates (Lab Diet 5053) and autoclaved water *ad libitum*. Lights were off between 1800 and 0600 in a room maintained at 22°C. For all experiments, mice were housed in groups of 4-5 on sawdust bedding. All experiments were conducted using protocols approved by the Animal Studies Committee at Washington University.

Liver perfusions. Ten minutes prior to each liver perfusion, mice received an intramuscular injection of heparin (100 Units). Mice were then anesthetized with 10μl of sodium pentobarbital (Fatal Plus, 390

mg/ml) administered IP. Once fully anesthetized, the abdomen was sprayed with 70% ethanol, and the mouse was placed on a surgical platform within a large reservoir to contain run-off buffer and body fluids. A transverse incision was made through the skin, fascia, and muscular layers of the lower abdomen. A lateral sagittal incision was made on each side of the body, exposing the abdominal contents. A second transverse incision was made inferior to the right kidney and towards the dorsal aspect of the mouse to allow for perfusion buffer and body fluids to drain from the abdomen. The portal vein was then exposed by gently moving the intestines laterally towards the left body wall. A suture needle was threaded under the portal vein and tied loosely. Next, the portal vein was cannulated with a 24 gauge catheter needle, the needle was withdrawn, and tubing with buffer was reconnected to the catheter. The abdominal aorta and inferior vena cava were cut and the catheter was firmly tied into the portal vein. Finally, the heart was exposed by cutting through the diaphragm and thorax. The right atrium was cut to prevent recirculation of buffer to the liver and to terminate perfusion to the brain. All livers were perfused with an oxygenated Krebs-Henseleit bicarbonate buffer (118 mM NaCl, 25 mM NaHCO₃, 4.7 mM KCl, 0.4 mM KH₂PO₄, 2.5 mM CaCl₂, 1.22 mM MgSO₄·7·H₂O, pH 7.4), warmed to 37°C using a counter-current heat exchange circuit and a recirculating water bath, at a rate of 8 ml/min using a peristaltic pump for 15 min. At the end of the perfusion, the liver was freeze-clamped and rapidly frozen in a bath of liquid nitrogen. Tissue was stored at -80°C until further processing. For measurements of gluconeogenesis in perfused livers, buffers contained sodium [3-¹³C]lactate (1.5 mM), sodium [3-¹³C]pyruvate (0.15 mM), and unlabeled sodium octanoate (0.2 mM; vendor for stable isotopes: Cambridge Isotope Laboratories).

NMR-based quantitative substrate fate mapping. Neutralized perchloric acid tissue extracts were prepared and profiled using ¹³C-edited proton nuclear magnetic resonance (NMR) measured at 11.75 T (Varian/Agilent Direct Drive-1) via first increment gradient heteronuclear single-quantum correlation (gHSQC). Signals were collected from extracts dissolved in 275 µL of D₂O + 1 mM trimethylsilyl propionate (TSP), loaded into high precision, thin walled 5-mm tubes (Shigemi). Tissue concentrations and fractional enrichments of metabolites were determined from quantification of signals

by integration from the $^1\text{H}\{^{13}\text{C}\}$ and ^{13}C -edited (gHSQC) collections of carbon 2 for taurine, carbon 1 for glucose, and carbon 4 for glutamate, as described previously (78,313).

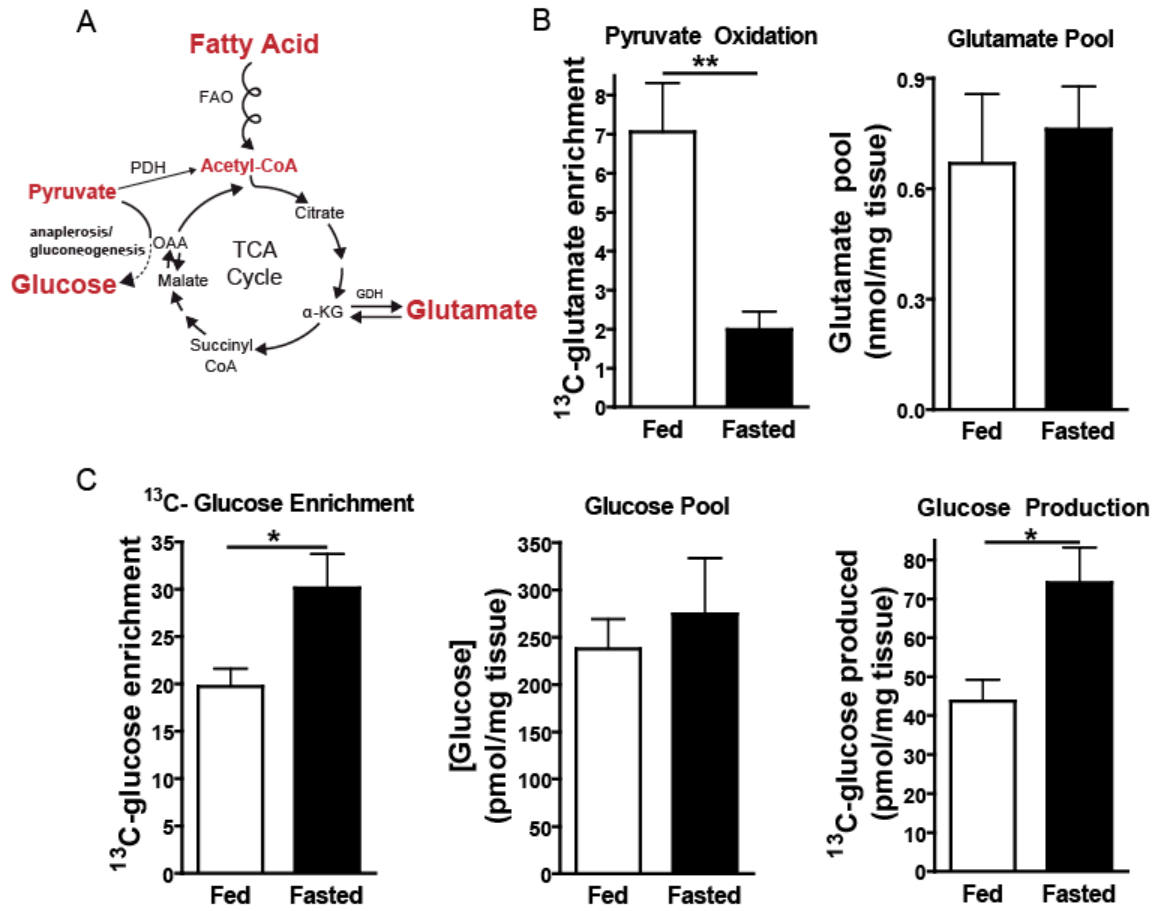
Results and Discussion

Pyruvate oxidation decreases during fasting and gluconeogenesis from pyruvate increases. Numerous metabolic, allosteric, and molecular mechanisms ensure pyruvate oxidation decreases and hepatic glucose production (HGP) increases during fasting. Thus, the fed-fasted transition provides an optimal paradigm in which to test the validity of new approaches that quantify HGP. In liver, pyruvate can enter the TCA cycle either through oxidation to acetyl-CoA in a reaction catalyzed by pyruvate dehydrogenase (PDH) or via carboxylation to OAA (oxaloacetate), which is catalyzed by phosphoenolpyruvate carboxykinase (PEPCK, encoded by *Pck1*). Oxidative entry of pyruvate to the TCA cycle via PDH destines the pyruvate for terminal oxidation, while anaplerotic entry as OAA replenishes TCA intermediates and supports gluconeogenesis (**Fig. 7.1A**). As expected, ^{13}C -glutamate enrichment, which serves as a quantitative surrogate for carbon entry into the TCA cycle for terminal oxidation, was decreased significantly in perfused livers of fasted mice (**Fig. 7.1B, left**). Since total hepatic glutamate concentrations (pools) were not different between fed and fasted mice (**Fig. 7.1B, right**), these results indicated that pyruvate oxidation decreased during fasting. In addition, ^{13}C -glucose enrichment was increased in perfused livers of fasted mice (**Fig. 7.1C, left**), which reflected increased HGP, as total hepatic glucose pools did not differ between fed and fasted mice (**Fig. 7.1C, middle**). Moreover, fasted livers produced more total moles of ^{13}C -labeled glucose (**Fig. 7.1C, right**). Our results are consistent with published findings that indicate that pyruvate oxidation decreases and pyruvate carboxylation increases during fasting to support HGP, and thus, validate our NMR method.

Figure legends

Figure 7.1: Fasting alters pyruvate fate in perfused livers. **A.** Schematic of mitochondrial pyruvate and fatty acid fates. **B.** ^{13}C -glutamate enrichment (pyruvate oxidation) in extracts of perfused livers of chow-fed and 24 hr fasted mice (left) and total hepatic glutamate concentration (pool; right). **C.** ^{13}C -glucose enrichment in extracts of perfused livers of chow-fed and 24 hr fasted mice (left) and total hepatic glucose pool (middle), and moles of ^{13}C -glucose produced per mg tissue (right). FAO, fatty acid oxidation; PDH, pyruvate dehydrogenase; OAA, oxaloacetate; α -KG, alpha-ketoglutarate; GDH, glutamate dehydrogenase. *, $p < 0.05$, **, $p < 0.01$ by Student's t test, as indicated.

Figure 7.1



Chapter 8

Ketogenesis insufficient mice exhibit impaired fasting glucose and hepatic steatosis

Main findings:

Fasted ketogenesis insufficient mice exhibited hyperglycemia and hepatic steatosis.

¹³C-pyruvate oxidation was decreased in perfused livers of ketogenesis insufficient mice, both in the presence and absence of exogenous unlabeled fatty acids.

Exogenous fatty acids increased anaplerosis from pyruvate in perfused ketogenesis insufficient livers.

Conclusion:

Ketogenesis supports disposal of excess hepatic fat.

Decreased pyruvate oxidation is likely due to increased competition from fatty acids that cannot be disposed of through ketogenesis.

Accumulation of Ac-CoA, due to insufficient ketogenesis, may allosterically activate pyruvate carboxylase, and thus, stimulate anaplerosis.

Future Direction:

Determine if increased terminal fatty acid oxidation and increased pyruvate cycling support increased hepatic glucose production in fasted HMGCS2-deficient mice.

Figure legends

Figure 8.1: Fasting-induced hyperglycemia is associated with hepatic steatosis in ketogenesis insufficient mice. **A.** Blood glucose during fasting in ASO treated mice. **B.** Hepatic triacylglyceride (TAG) concentrations in fasted ASO treated mice. $n > 5/\text{group}$, **, $p < 0.01$, ***, $p < 0.001$ by Student's *t* test, as indicated.

Figure 8.2: Altered hepatic pyruvate fate in ketogenesis insufficient mice. **A.** Schematized pyruvate fate within hepatic mitochondria. PDH, pyruvate dehydrogenase; PCx, pyruvate carboxylase; ME, malic enzyme; OAA, oxaloacetate; α -KG, alpha-ketoglutarate. **B.** ¹³C-enrichment of glutamate carbon 4 (pyruvate oxidation) in livers of ASO-treated mice perfused with the indicated substrates. **C.** Immunoblot for phosphoserine 293 PDH-E1 α and total PDH-E1 α in livers of chow-fed ASO-treated mice. **D.** ¹³C-enrichment of α -KG carbon 3 (pyruvate anaplerosis) in livers of ASO-treated mice perfused with the indicated substrates. $n \geq 5/\text{group}$, *, $p < 0.05$, **, $p < 0.01$, ***, $p < 0.001$ by 2-way ANOVA, as indicated.

Figure 8.1

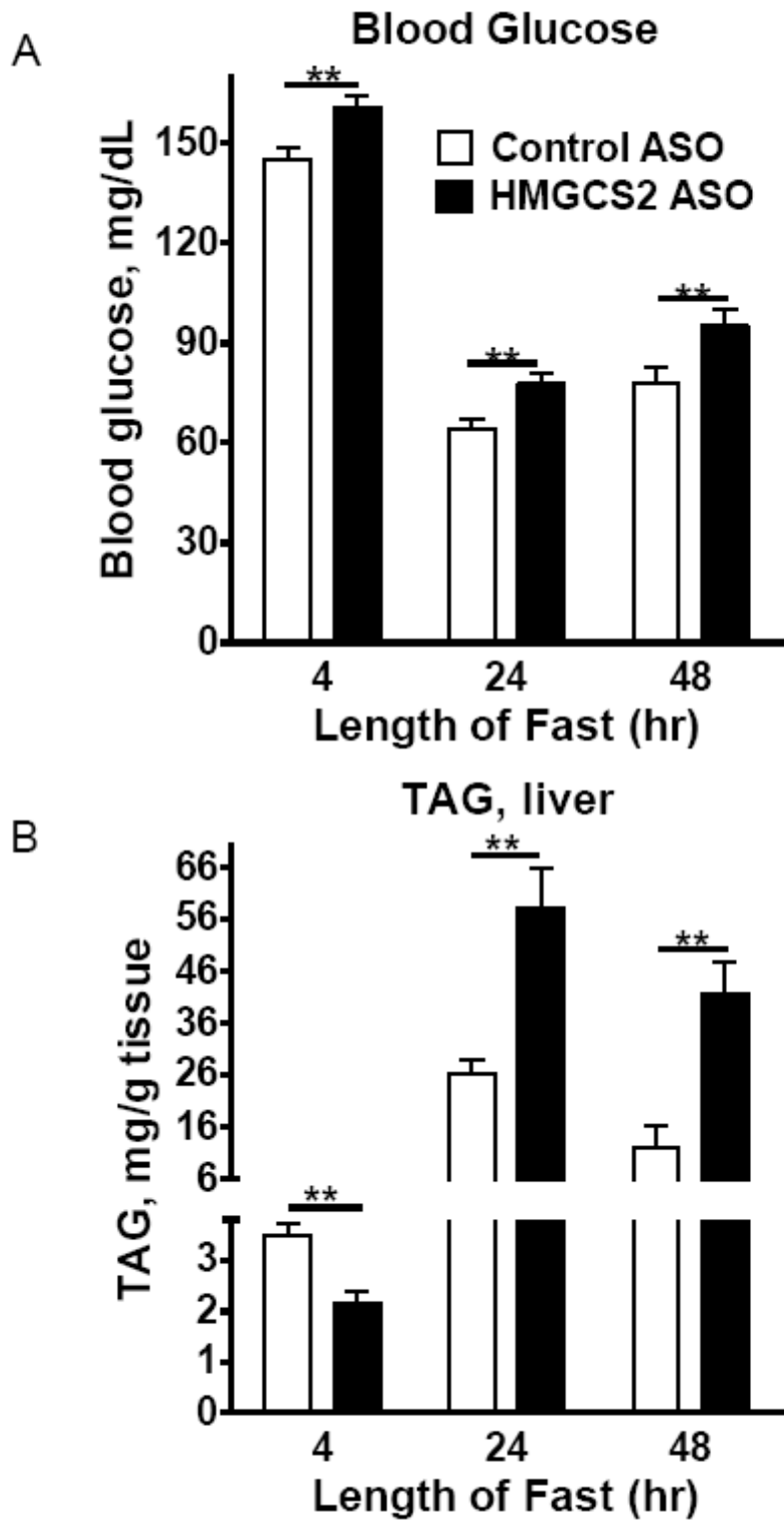
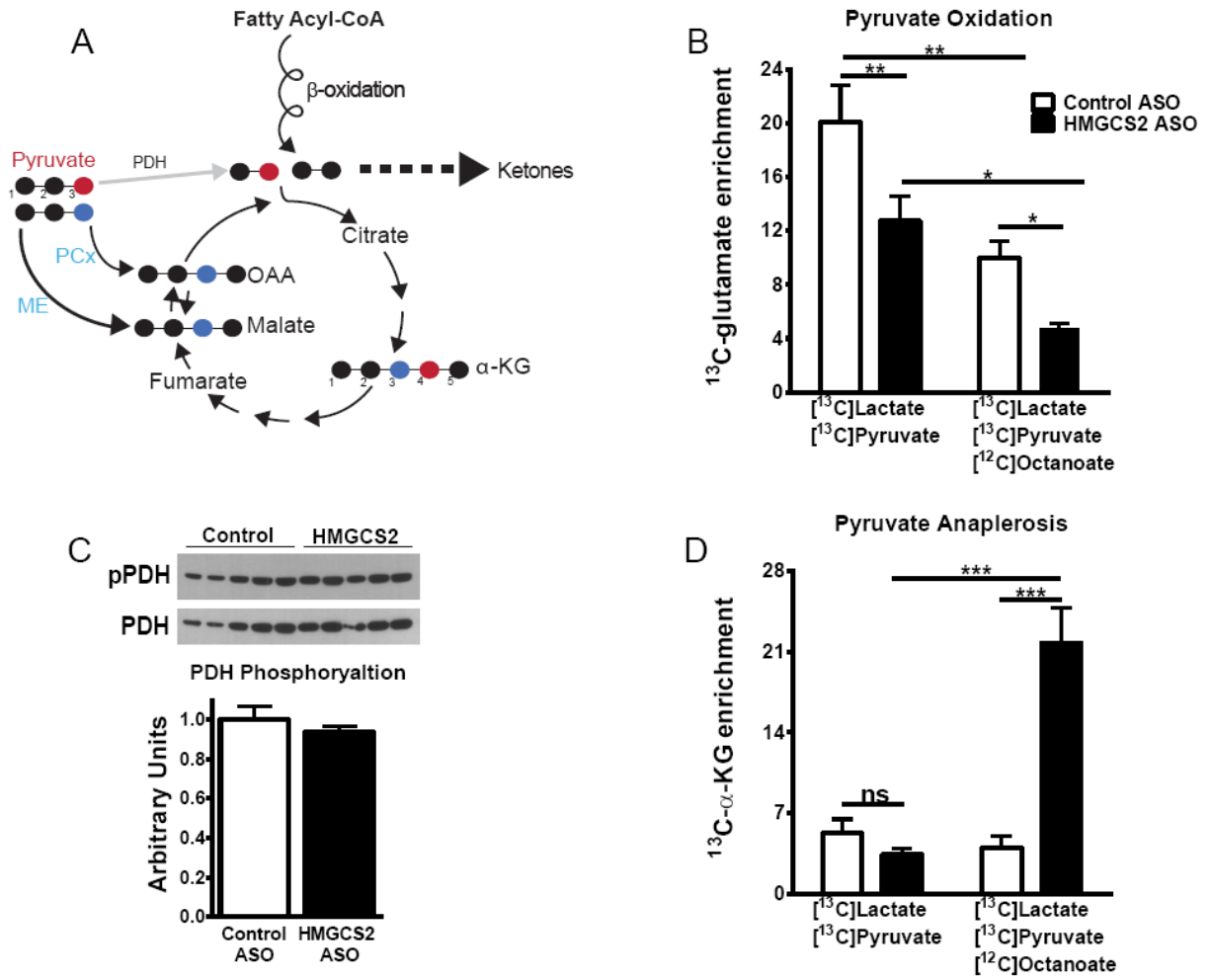


Figure 8.2



Concluding Remarks

Ketone body metabolism is classically described as a two-compartment metabolic pathway wherein an altruistic liver provisions extrahepatic tissues with avidly oxidized ketone bodies during states characterized by limited carbohydrate availability. Up to two-thirds of the fat entering the liver is channeled into ketogenesis (281). During human starvation in humans, ketogenic rates approach 150 g ketone produced/day, which exceeds hepatic glucose production during starvation by 50% (84,374). The bioenergetic benefits of extrahepatic ketone body oxidation are manifold (reviewed in Ch. 1). Ketone bodies supplant glucose as the primary fuel source in the brain during starvation and can support up to 25% of the neonate's basal energy requirements (2,71,82). While ketone bodies undoubtedly comprise a significant and quantifiable metabolic fuel, an energetic requirement for ketone body oxidation has never been demonstrated experimentally. Moreover, the mechanisms by which hepatic ketogenesis coordinates intermediary metabolic homeostasis in liver has never been considered. Thus, my work has sought to mechanistically determine i) if ketone bodies comprise an essential fuel class, ii) which tissues, if any, energetically require ketone bodies for adaptation to birth and during starvation in the adult, and iii) novel roles for hepatic ketogenesis in preservation of the dynamic intermediary metabolic network in liver.

Biochemistry of ketone body metabolism. Pioneering investigators, including John McGarry, Daniel Foster, Dermot Williamson, John Williamson, and Hans Krebs originally defined the biochemistry of ketone body metabolism [(4,5,375) and reviewed in Ch. 1]. Briefly, ketogenesis is restricted to liver due to absence of the fate committing ketogenic enzyme mitochondrial 3-hydroxymethylglutaryl-CoA Synthase (HMGCS2) from most tissues under normal conditions. In liver mitochondria, a series of ketogenic reactions condense acetyl-CoA derived from beta-oxidation of fatty acids into the circulating ketone bodies, acetoacetate (AcAc) and beta-hydroxybutyrate (β OHB). In mitochondria of extrahepatic tissues, beta-hydroxybutyrate dehydrogenase 1 (BDH1) re-oxidizes β OHB to AcAc, which is directed towards the tricarboxylic acid (TCA) cycle for terminal oxidation by mitochondrial succinyl-CoA-3:oxoacid CoA transferase (SCOT), the fate committing enzyme of ketone body oxidation.

Human inborn errors of ketone body metabolism. Ketone body metabolism is required for normal fitness in humans. Individuals with genetic defects in either the ketogenic or ketolytic arms of this metabolic pathway typically present early life. Nine cases of human HMGCS2-deficiency have been described. These patients classically present with hypoketotic hypoglycemia (66-68,360-362,376). SCOT-deficient patients, of which there have been ~30 described cases, typically present with spontaneous ketoacidosis with or without hypoglycemia. Viral illness or brief periods of nutrient deprivation can also trigger ketoacidosis in these patients (77,79-81,97,98,100,101,148,149,290,377,378). Acute ketoacidotic episodes of SCOT-deficiency can rapidly progress to vomiting, coma, and even death, if intravenous glucose, insulin, and NaHCO_3 therapy is not initiated rapidly. Diagnosis of HMGCS2- and SCOT-deficiency is difficult due to the need for genetic testing, enzymatic assays, and liver biopsy in the case of HMGCS2-deficiency. Avoidance of fasting and ingestion of carbohydrate-replete diets are primary treatments of both of these diseases (66-68,77,79-81,97,98,100,101,148,149,290,360-362,376-378).

Latent defects in either ketogenesis or ketone body oxidation could predispose to metabolic disease later in life. Encoded variation in both ketogenesis and ketone body oxidation occur in humans (see case reports above) and both of these pathways are susceptible to down-regulation in response to a variety of stimuli (Reviewed in Ch. 1). Prospectively, latent defects in ketone body metabolism may emerge in genetically susceptible individuals and exacerbate common pathophysiological states, including obesity, diabetes, fatty liver disease, and heart failure.

Ketone body oxidation is required for life in neonatal mice. To mechanistically dissect the bioenergetic roles of ketone body metabolism during the transition to extrauterine life, our lab generated novel germline and tissue-specific SCOT-Knockout (KO) mice. SCOT catalyzes the fate committing reaction of ketone body oxidation, is expressed in all tissues except liver, and is uniquely required for ketone body oxidation (reviewed in Ch. 1). My studies of germline SCOT-KO mice revealed that ketone body oxidation is required to prevent lethal hyperketonemia and hypoglycemia. SCOT-KO mice are indistinguishable from wild littermates at birth, but die within the first 48 hr of life in a manner that

phenocopies human sudden infant death syndrome (SIDS). During ketosis, serum β OHB concentrations typically increase, such that the serum AcAc/ β OHB ratio falls. In contrast, hyperketonemia in germline SCOT-KO neonates is marked by a pathological increase in the serum AcAc concentration that drives an increased serum AcAc/ β OHB ratio (presented in Ch. 2). Because AcAc and β OHB are members of an NAD^+ / NADH -linked redox couple, the metabolic consequences of an increased AcAc/ β OHB were investigated (presented in Ch. 4 and see below).

Ketone bodies do not comprise an essential fuel source in mice. In stark contrast to the neonatal lethality exhibited by germline SCOT-KO mice, tissue-specific SCOT-KO mouse strains survive the neonatal period and starvation as adults with few metabolic abnormalities. Selective genetic targeting of SCOT in neurons, cardiomyocytes, and skeletal myocytes, which comprise the three greatest consumers of ketone bodies, resulted in specific and complete loss of SCOT protein and enzymatic activity within each of the targeted tissues. Of the tissue-specific SCOT-KO strains generated, only neonatal SCOT-neuron-KO mice exhibited mildly elevated ketonemia, suggesting that neurons comprise a large ketolytic sink in neonatal mice. Furthermore, compound germline SCOT-heterozygous; SCOT-neuron-KO mice (which exhibit a 50% decrease in SCOT protein abundance in all tissues and also completely lack SCOT in all neurons), were viable and indistinguishable from SCOT-neuron-KO mice. Adult tissue-specific SCOT-KO strains adapted well to starvation. SCOT-Neuron-KO and SCOT-Muscle-KO mice exhibit hyperketonemia during fasting, but maintained glycemia and body weight normally during fasting. Moreover, all tissue-specific SCOT-KO strains exhibited the physiologic ratio of AcAc/ β OHB during the neonatal period and during starvation as adults. Together, these results demonstrated that ketone body oxidation is not required in any single tissue for survival of the neonatal period or starvation in the adult, and suggested that minimal ketolytic reserve is required to prevent toxic accumulation of ketone bodies (presented in Ch. 3).

Extrahepatic disposal of ketone bodies preserves hepatic metabolic function in neonatal mice.

SCOT-KO mice die with hypoglycemia and hyperketonemia that is marked by a pathological increase in the ratio of AcAc/ β OHB in serum. Incredibly, total loss of ketone body oxidation, an exclusively extrahepatic process, deranged hepatic metabolism in neonatal SCOT-KO mice. β OHB accumulation in blood impaired de novo hepatic β OHB synthesis, but permitted continued production of AcAc, which selectively oxidized hepatic redox potential and increased the serum AcAc/ β OHB ratio. Oxidized hepatic redox potential drove a maladaptive increase in pyruvate oxidation, which contributed to depletion of the neonate's gluconeogenic precursor pool, and thus, limited hepatic glucose production *in vivo*. Together, these results indicated that a primary role for extrahepatic ketone body oxidation is to prevent toxic accumulation of ketone bodies, which provokes hepatic metabolic abnormalities (presented in Ch. 4).

PPAR α -dependent ketogenesis prevents neonatal hepatic steatosis. Peroxisome Proliferator Activated Receptor alpha (PPAR α) is a master transcriptional regulator of hepatic intermediary metabolism. PPAR α mediates the adaptive response to fasting. Like fasting, nutrient supply is abruptly altered at birth when a transplacental supply of carbohydrates is replaced by a high-fat, low-carbohydrate milk diet. Using ^{13}C -labeled substrates to quantify dynamic metabolism and complimentary systems physiology approaches in neonatal mice, I demonstrated a critical role for PPAR α in hepatic metabolic adaptation to birth. PPAR α -KO neonates exhibited hypoglycemia, hypoketonemia, and hepatic steatosis. Hypoketonemia was mechanistically linked to a 50% decrease in hepatic ketogenesis and was associated with neonatal fatty liver. These findings indicated an important role for PPAR α -dependent ketogenesis in disposal of excess hepatic fatty acids during the neonatal period, and prospectively, could extend to pathological nonalcoholic fatty liver disease (NAFLD) in adults (presented in Ch. 5).

Ketogenesis prevents diet-induced fatty liver injury and hyperglycemia through coenzyme A recycling. NAFLD spectrum disorders affect approximately one billion individuals worldwide. The mechanisms driving progressive steatohepatitis remain incompletely defined, impeding the development of effective treatments. Thus, we developed a murine model of HMGCS2-deficiency to determine if

ketogenesis plays a critical role in prevention of diet-induced steatohepatitis. To permit mechanistic dissection of the phenotypes offered by HMGCS2-deficient mice, I developed an *in situ* method to quantify hepatic energy metabolism in the perfused mouse liver using ^{13}C -edited proton NMR spectroscopy (presented in Ch. 6a). HMGCS2 deficient mice could not effectively convert fatty acids into ketone bodies, and were thus ketogenic insufficient. Adult-onset loss of HMGCS2 caused mild hyperglycemia and increased hepatic gluconeogenesis from pyruvate in chow-fed mice. Ketogenesis insufficient mice also exhibited impaired fasting glucose and fasting-induced hepatic steatosis (presented in Ch. 6b). High-fat diet (HFD) feeding of ketogenesis insufficient mice caused extensive hepatocyte injury and inflammation, decreased glycemia, deranged hepatic TCA cycle intermediate concentrations, and impaired hepatic gluconeogenesis due to fatty acid-induced sequestration of free coenzyme A (CoASH). Supplementation of the CoASH precursors pantothenic acid and cysteine normalized TCA intermediates and gluconeogenesis in ketogenesis insufficient livers. These findings identify ketogenesis as a critical regulator of hepatic glucose metabolism and TCA cycle function via coordination of CoASH homeostasis in the absorptive state and indicate that ketogenesis modulates fatty liver disease (presented in Ch. 6).

Future directions.

Neonatal hypoglycemia has an incidence of 10% and pathological neonatal hypoglycemia occurs in 2/1000 live births. Neonates born preterm, with intrauterine growth restriction, that are small for gestational age, with congenital anomalies or inborn errors of metabolism, and those born to diabetic mothers are at risk of developing neonatal hypoglycemia. Nonetheless, epidemiologic factors only identify 50% of at risk neonates and cannot predict which individuals will spontaneously recover from transient neonatal hypoglycemia and which will develop pathological hypoglycemia. Thus, guidelines that direct when and in which patients to intervene are lacking. My findings in neonatal mice have been leveraged into a clinical study designed to risk-stratify neonates for hypoglycemia using metabolite profiles. Current statewide screening protocols identify inborn errors of metabolism using tandem mass

spectrometric (MS/MS) quantification of blood amino acids and acylcarnitines in heel stick blood that is collected from neonates shortly after birth. Unfortunately, these screening regimens do not identify patients at risk of developing hypoglycemia that is not due to an underlying enzymatic deficiency, nor do they identify inborn errors of ketone body metabolism. Our current clinical study expands upon my findings in neonatal mice by using MS/MS to quantify circulating concentrations of ketone bodies, lactate, pyruvate, amino acids, and acylcarnitines, as well as blood AcAc/ β OHB and pyruvate/lactate ratios as reporters of hepatic redox potential, in neonatal blood collected 6-12 and 24-48 hr after birth. Blinded statistical analyses of metabolic profiles, epidemiologic factors, and clinical course will be used to risk-stratify individuals for neonatal hypoglycemia.

Inborn errors of ketone body metabolism are rarely diagnosed. These diseases may truly be rare. Alternatively, because they are difficult to diagnose, many cases may go undetected and could contribute to a subset of SIDS cases. In fact, one recent retrospective study that performed metabolic autopsies on 255 SIDS patients identified 3 individuals with underlying defects in ketone body metabolism. Finally, identification of patients with partial loss of function within ketone body metabolism may have prognostic value, as abnormalities of ketone body metabolism occur in and may directly contribute to metabolic diseases, such as heart failure, diabetes, obesity, and fatty liver disease.

My work has mechanistically defined a critical and novel role for ketogenesis in regulation of hepatic glucose production, glycemia, and prevention of diet-induced steatohepatitis. These findings warrant follow-up studies to determine if therapeutic activation of ketogenesis can ameliorate hyperglycemia and mitigate fatty liver disease. Genetic and viral approaches designed to augment ketogenesis can be employed in mouse models to determine if ketogenic activation can ameliorate hyperglycemia in diabetes models and prevent diet-induced NAFLD and NASH. Simultaneously, small molecule screens in primary hepatocytes to identify non-toxic, specific, and potent ketogenic activators, followed by subsequent compound optimization and validation in perfused livers and *in vivo* should be performed. Hepatic injury in HFD-fed ketogenesis insufficient mice is prospectively linked to pancellular metabolic dysfunction due to CoASH depletion. Therefore, we are currently performing interventions

designed to replenish hepatocellular CoASH pools *in vivo* in HFD-fed control and ketogenesis insufficient mice. These experiments include dietary supplementation of CoASH precursors (pantothenic acid and L-cysteine) and genetic, viral, and pharmacologic approaches to augment CoASH biosynthesis and/or increase CoASH liberation from acyl-CoAs. Because ketogenesis supports noncombustive and thus 'safe' disposal of mitochondrial fat, we are also performing studies to determine if excessive mitochondrial reactive oxygen species (ROS) production contributes to hepatic injury in HFD-fed ketogenesis insufficient mice. Furthermore, studies of mitochondrial biogenesis, mitochondrial respiration, mitochondrial Ca^{++} buffering, mitochondrial permeability transition pore opening, and mitochondrial ultrastructure are underway. We are working to characterize and to deconstruct the hepatic inflammation in HFD-fed ketogenesis insufficient mice using immunocompromised mouse models. Finally, because ketogenic capacity decreases with increasing age, we are studying aged control and ketogenesis insufficient mice fed a low-fat chow diet to determine if suppressed ketogenesis is sufficient to drive fatty liver disease in mice.

Abnormal lipid and carbohydrate metabolism occur in and contribute to obesity, diabetes, and NAFLD. In liver, fluxes of carbohydrate and fatty acid metabolism are tightly linked to ketogenic flux. Nonetheless, ketogenesis has largely been overlooked as both a driver and as a modifier of metabolic disease states. My work is the first to mechanistically identify insufficient ketogenesis as a driver of hyperglycemia and NASH. Prospectively, ketonemia may serve as a predictive biomarker of fatty liver disease and diabetes progression. Future studies may reveal that therapeutic augmentation of hepatic ketogenesis can mitigate hyperglycemia and ameliorate fatty liver disease.

Final thought.

My most sincere hope is that this body of work will vitalize interest in ketone body metabolism as a prospective diagnostic biomarker and therapeutic target in metabolic disease states.

Literature Cited

1. Aneja, P., Dziak, R., Cai, G. Q., and Charles, T. C. (2002) Identification of an acetoacetyl coenzyme A synthetase-dependent pathway for utilization of L-(+)-3-hydroxybutyrate in *Sinorhizobium meliloti*. *J Bacteriol* **184**, 1571-1577
2. Cahill, G. F., Jr. (2006) Fuel metabolism in starvation. *Annu Rev Nutr* **26**, 1-22
3. Krishnakumar, A. M., Sliwa, D., Endrizzi, J. A., Boyd, E. S., Ensign, S. A., and Peters, J. W. (2008) Getting a handle on the role of coenzyme M in alkene metabolism. *Microbiol Mol Biol Rev* **72**, 445-456
4. Robinson, A. M., and Williamson, D. H. (1980) Physiological roles of ketone bodies as substrates and signals in mammalian tissues. *Physiol Rev* **60**, 143-187
5. McGarry, J. D., and Foster, D. W. (1980) Regulation of hepatic fatty acid oxidation and ketone body production. *Annu Rev Biochem* **49**, 395-420
6. Johnson, R. H., Walton, J. L., Krebs, H. A., and Williamson, D. H. (1969) Post-exercise ketosis. *Lancet* **2**, 1383-1385
7. Freed, L. E., Endemann, G., Tomera, J. F., Gavino, V. C., and Brunengraber, H. (1988) Lipogenesis from ketone bodies in perfused livers from streptozocin-induced diabetic rats. *Diabetes* **37**, 50-55
8. Endemann, G., Goetz, P. G., Edmond, J., and Brunengraber, H. (1982) Lipogenesis from ketone bodies in the isolated perfused rat liver. Evidence for the cytosolic activation of acetoacetate. *J Biol Chem* **257**, 3434-3440
9. Morris, A. A. M. (2005) Cerebral ketone body metabolism. *J. Inherit. Metab. Dis.* **28**, 109-121
10. Robinson, A. M., and Williamson, D. H. (1978) Utilization of D-3-hydroxy[3-14C]butyrate for lipogenesis in vivo in lactating rat mammary gland. *Biochem J* **176**, 635-638
11. Sengupta, S., Peterson, T., Laplante, M., Oh, S., and Sabatini, D. (2010) mTORC1 controls fasting-induced ketogenesis and its modulation by ageing. *Nature* **468**, 1100-1104
12. Soeters, M. R., Sauerwein, H. P., Faas, L., Smeenge, M., Duran, M., Wanders, R. J., Ruiten, A. F., Ackermans, M. T., Fliers, E., Houten, S. M., and Serlie, M. J. (2009) Effects of Insulin on Ketogenesis Following Fasting in Lean and Obese Men. *Obesity (Silver Spring)* **17**, 1326-1331
13. Neely, J. R., Rovetto, M. J., and Oram, J. F. (1972) Myocardial utilization of carbohydrate and lipids. *Prog Cardiovasc Dis* **15**, 289-329
14. Lommi, J., Kupari, M., Koskinen, P., Naveri, H., Leinonen, H., Pulkki, K., and Harkonen, M. (1996) Blood ketone bodies in congestive heart failure. *J Am Coll Cardiol* **28**, 665-672
15. Kupari, M., Lommi, J., Ventila, M., and Karjalainen, U. (1995) Breath acetone in congestive heart failure. *The American journal of cardiology* **76**, 1076-1078
16. Lommi, J., Koskinen, P., Naveri, H., Harkonen, M., and Kupari, M. (1997) Heart failure ketosis. *J Intern Med* **242**, 231-238
17. Pittman, J. G., and Cohen, P. (1964) The Pathogenesis of Cardiac Cachexia. *N Engl J Med* **271**, 403-409
18. Fery, F., and Balasse, E. O. (1985) Ketone body production and disposal in diabetic ketosis. A comparison with fasting ketosis. *Diabetes* **34**, 326-332
19. Hall, S. E., Wastney, M. E., Bolton, T. M., Braaten, J. T., and Berman, M. (1984) Ketone body kinetics in humans: the effects of insulin-dependent diabetes, obesity, and starvation. *J Lipid Res* **25**, 1184-1194
20. Girard, J., Ferre, P., Pegorier, J. P., and Duee, P. H. (1992) Adaptations of glucose and fatty acid metabolism during perinatal period and suckling-weaning transition. *Physiol Rev* **72**, 507-562
21. Bock, H., and Fleischer, S. (1975) Preparation of a homogeneous soluble D-beta-hydroxybutyrate apodehydrogenase from mitochondria. *J Biol Chem* **250**, 5774-5761
22. Lehninger, A. L., Sudduth, H. C., and Wise, J. B. (1960) D-beta-Hydroxybutyric dehydrogenase of mitochondria. *J Biol Chem* **235**, 2450-2455

23. Sandermann, H. J., McIntyre, J. O., and Fleischer, S. (1986) Site-site interaction in the phospholipid activation of D-beta-hydroxybutyrate dehydrogenase. *J Biol Chem* **261**, 6201-6208.
24. Williamson, D. H., Lund, P., and Krebs, H. A. (1967) The redox state of free nicotinamide-adenine dinucleotide in the cytoplasm and mitochondria of rat liver. *Biochem J* **103**, 514-527
25. Guo, K., Lukacik, P., Papagrigoriou, E., Meier, M., Lee, W. H., Adamski, J., and Oppermann, U. (2006) Characterization of human DHRS6, an orphan short chain dehydrogenase/reductase enzyme: a novel, cytosolic type 2 R-beta-hydroxybutyrate dehydrogenase. *J Biol Chem* **281**, 10291-10297
26. Halestrap, A. P. (2012) The monocarboxylate transporter family--Structure and functional characterization. *IUBMB Life* **64**, 1-9
27. Hugo, S. E., Cruz-Garcia, L., Karanth, S., Anderson, R. M., Stainier, D. Y., and Schlegel, A. (2012) A monocarboxylate transporter required for hepatocyte secretion of ketone bodies during fasting. *Genes Dev* **26** 282-293
28. Jeoung, N. H., Rahimi, Y., Wu, P., Lee, W. N., and Harris, R. A. (2012) Fasting induces ketoacidosis and hypothermia in PDHK2/PDHK4-double-knockout mice. *Biochem J* **443**, 829-839
29. Merritt, M. E., Harrison, C., Sherry, A. D., Malloy, C. R., and Burgess, S. C. (2011) Flux through hepatic pyruvate carboxylase and phosphoenolpyruvate carboxykinase detected by hyperpolarized ¹³C magnetic resonance. *Proc Natl Acad Sci U S A* **108**, 19084-19089
30. Magnusson, I., Schumann, W. C., Bartsch, G. E., Chandramouli, V., Kumaran, K., Wahren, J., and Landau, B. R. (1991) Noninvasive Tracing of Krebs Cycle Metabolism in Liver. *J Biol Chem* **266**, 6975-6984
31. Thomas, L. K., Ittmann, M., and Cooper, C. (1982) The role of leucine in ketogenesis in starved rats. *Biochem J* **204**, 399-403
32. McGarry, J. D., Stark, M. J., and Foster, D. W. (1978) Hepatic malonyl-CoA levels of fed, fasted and diabetic rats as measured using a simple radioisotopic assay. *J Biol Chem* **253**, 8291-8293
33. Srere, P. A., and Foster, D. W. (1967) On the proposed relation of citrate enzymes to fatty acid synthesis and ketosis in starvation. *Biochemical and Biophysical Research Communications* **26**, 556-561
34. Ferre, P., Satabin, P., Decaux, J., Escriva, F., and Girard, J. (1983) Development and regulation of ketogenesis in hepatocytes isolated from newborn rats. *Biochem. J.* **214**, 937-942
35. Scrutton, M. C., and Utter, M. F. (1967) Pyruvate carboxylase. IX. Some properties of the activation by certain acyl derivatives of coenzyme A. *J Biol Chem* **242**, 1723-1735
36. Owen, O. E., Kalhan, S. C., and Hanson, R. W. (2002) The key role of anaplerosis and cataplerosis for citric acid cycle function. *J Biol Chem* **277**, 30409-30412
37. Cooper, R. H., Randle, P. J., and Denton, R. M. (1975) Stimulation of phosphorylation and inactivation of pyruvate dehydrogenase by physiological inhibitors of the pyruvate dehydrogenase reaction. *Nature* **257**, 808-809
38. Kahn, B. B., Alquier, T., Carling, D., and Hardie, D. G. (2005) AMP-activated protein kinase: ancient energy gauge provides clues to modern understanding of metabolism. *Cell Metab* **1**, 15-25
39. Quant, P. A., Robin, D., Robin, P., Girard, J., and Brand, M. D. (1993) A top-down control analysis in isolated rat liver mitochondria: can the 3-hydroxy-3-methylglutaryl-CoA pathway be rate-controlling for ketogenesis? *Biochim Biophys Acta* **1156**, 135-143
40. Boukaftane, Y., Duncan, A., Wang, S., Labuda, D., Robert, M.-F., Sarrazin, J., Schappert, K., and Mitchell, G. A. (1994) Human Mitochondrial HMG CoA Synthase: Liver cDNA and Partial Genomic Cloning, Chromosome Mapping to 1p12-p13, and Possible Role in Vertebrate Evolution. *Genomics* **23** 552-559
41. Cunnane, S. C., and Crawford, M. A. (2003) Survival of the fattest: fat babies were the key to evolution of the large human brain. *Comparative Biochemistry and Physiology Part A* **136** 17-26

42. Satapati, S., Sunny, N. E., Kucejova, B., Fu, X., He, T., Mendez-Lucas, A., Shelton, J. M., Perales, J. C., Browning, J. D., and Burgess, S. C. (2012) Elevated TCA cycle function in the pathology of diet induced hepatic insulin resistance and fatty liver. *J Lipid Res* **53**, 1080-1092
43. Balasse, E. O., and Fery, F. (1989) Ketone body production and disposal: effects of fasting, diabetes, and exercise. *Diabetes Metab Rev* **5**, 247-270
44. Hegardt, F. G. (1999) Mitochondrial 3-hydroxy-3-methylglutaryl-CoA synthase: a control enzyme in ketogenesis. *Biochem J* **338** (Pt 3), 569-582
45. Ayté, J., Gil-Gómez, G., and Hegardt, F. G. (1993) Methylation of the regulatory region of the mitochondrial 3-hydroxy-3-methylglutaryl-CoA synthase gene leads to its transcriptional inactivation. *Biochem. J.* **295** 807–812
46. Arias, G., Matas, R., Asins, G., Hegardt, F. G., and Serra, D. (1995) The effect of fasting and insulin treatment on carnitine palmitoyl transferase I and mitochondrial 3-hydroxy-3-methylglutaryl coenzyme A synthase mRNA levels in liver from suckling rats. *Biochem Soc Trans.* **3**, 493S.
47. Quant, P. A., Tubbs, P. K., and Brand, M. D. (1990) Glucagon activates mitochondrial 3-hydroxy-3-methylglutaryl-CoA synthase in vivo by decreasing the extent of succinylation of the enzyme. *Eur J Biochem* **187**, 169-174
48. Thumelin S, F. M., Girard J, Pegorier JP. (1993) Developmental changes in mitochondrial 3-hydroxy-3-methylglutaryl-CoA synthase gene expression in rat liver, intestine and kidney. *Biochem J* **292** 493-496.
49. Wolfrum, C., Asilmaz, E., Luca, E., Friedman, J. M., and Stoffel, M. (2004) Foxa2 regulates lipid metabolism and ketogenesis in the liver during fasting and in diabetes. *Nature* **432**, 1027-1032
50. Rodriguez, J. C., Gil-Gomez, G., Hegardt, F. G., and Haro, D. (1994) Peroxisome proliferator-activated receptor mediates induction of the mitochondrial 3-hydroxy-3-methylglutaryl-CoA synthase gene by fatty acids. *J Biol Chem* **269**, 18767-18772
51. Wentz, A. E., d'Avignon, D. A., Weber, M. L., Cotter, D. G., Doherty, J. M., Kerns, R., Nagarajan, R., Sambandam, N., and Crawford, P. A. (2010) Adaptation of myocardial substrate metabolism to a ketogenic nutrient environment. *J Biol Chem* **285**, 24447-24456
52. Inagaki, T., Dutchak, P., Zhao, G., Ding, X., Gautron, L., Parameswara, V., Li, Y., Goetz, R., Mohammadi, M., Esser, V., Elmquist, J. K., Gerard, R. D., Burgess, S. C., Hammer, R. E., Mangelsdorf, D. J., and Kliewer, S. A. (2007) Endocrine regulation of the fasting response by PPARalpha-mediated induction of fibroblast growth factor 21. *Cell Metab* **5**, 415-425
53. Badman, M. K., Pissios, P., Kennedy, A. R., Koukos, G., Flier, J. S., and Maratos-Flier, E. (2007) Hepatic fibroblast growth factor 21 is regulated by PPARalpha and is a key mediator of hepatic lipid metabolism in ketotic states. *Cell Metab* **5**, 426-437
54. Vila`-Brau, A., Sousa-Coelho, A. L. D., Mayordomo, C., Haro, D., and Marrero, P. F. (2011) Human HMGCS2 Regulates Mitochondrial Fatty Acid Oxidation and FGF21 Expression in HepG2 Cell Line. *J Biol Chem* **286**, 20423–20430
55. Meertens, L. M., Miyata, K. S., Cechetto, J. D., Rachubinski, R. A., and Capone, J. P. (1998) A mitochondrial ketogenic enzyme regulates its gene expression by association with the nuclear hormone receptor PPARalpha. *Embo J* **17**, 6972-6978
56. Kostiuik, M. A., Keller, B. O., and Berthiaume, L. G. (2010) Palmitoylation of ketogenic enzyme HMGCS2 enhances its interaction with PPAR{alpha} and transcription at the Hmgcs2 PPRE. *Faseb J*
57. Haas JT, M. J., Chanda D, Wang Y, Zhao E, Haas ME, Hirschey M, Vaitheesvaran B, Farese RV Jr, Kurland IJ, Graham M, Crooke R, Fougelle F, Biddinger SB. (2012) Hepatic Insulin Signaling Is Required for Obesity-Dependent Expression of SREBP-1c mRNA but Not for Feeding-Dependent Expression. *Cell Metab.* **15**, 873-884.
58. Zhang, W.-W., Churchill, S., and Churchill, P. (1989) Developmental regulation of D-P-hydroxybutyrate dehydrogenase in rat liver and brain. *Federation of European Biochemical Societies* **256**, 71-74

59. Reed, W. D., Clinkenbeard, D., and Lane, M. D. (1975) Molecular and catalytic properties of mitochondrial (ketogenic) 3-hydroxy-3-methylglutaryl coenzyme A synthase of liver. *J Biol Chem* **250**, 3117-3123
60. Lowe, D. M., and Tubbs, P. K. (1985) 3-Hydroxy-3-methylglutaryl-coenzyme A synthase from ox liver. Purification, molecular and catalytic properties. *Biochem J* **227**, 591-599
61. Thumelin, S., Forestier, M., Girard, J., and Pegorier, J. P. (1993) Developmental changes in mitochondrial 3-hydroxy-3-methylglutaryl-CoA synthase gene expression in rat liver, intestine and kidney. *Biochem J* **292** 493-496.
62. Zhang, Z., Tan, M., Xie, Z., Dai, L., Chen, Y., and Zhao, Y. (2011) Identification of lysine succinylation as a new post-translational modification. *Nat Chem Biol.* **7**, 58-63
63. Du, J., Zhou, Y., Su, X., Yu, J., Khan, S., Jiang, H., Kim, J., Woo, J., Kim JH, Choi, B., He, B., Chen, W., Zhang, S., Cerione, R., Auwerx, J., Hao, Q., and Lin, H. (2011) Sirt5 is a NAD-dependent protein lysine demalonylase and desuccinylase. *Science* **334**, 806-809
64. Shimazu, T., Hirschey, M. D., Hua, L., Dittenhafer-Reed, K. E., Schwer, B., Lombard, D. B., Li, Y., Bunkenborg, J., Alt, F. W., Denu, J. M., Jacobson, M. P., and Verdin, E. (2010) SIRT3 Deacetylates Mitochondrial 3-Hydroxy-3-Methylglutaryl CoA Synthase 2 and Regulates Ketone Body Production. *Cell Metab* **12**, 654-661
65. Grimsrud, P. A., Carson, J. J., Hebert, A. S., Hubler, S. L., Niemi, N. M., Bailey, D. J., Jochem, A., Stapleton, D. S., Keller, M. P., Westphall, M. S., Yandell, B. S., Attie, A. D., Coon, J. J., and Pagliarini, D. J. (2012) A Quantitative Map of the Liver Mitochondrial Phosphoproteome Reveals Posttranslational Control of Ketogenesis. *Cell metabolism* **16**, 672-683
66. Thompson, G. N., Hsu, B. Y., Pitt, J. J., Treacy, E., and Stanley, C. A. (1997) Fasting hypoketotic coma in a child with deficiency of mitochondrial 3-hydroxy-3-methylglutaryl-CoA synthase. *N Engl J Med* **337**, 1203-1207
67. Bouchard, L., Robert, M. F., Vinarov, D., Stanley, C. A., Thompson, G. N., Morris, A., Leonard, J. V., Quant, P., Hsu, B. Y., Boneh, A., Boukaftane, Y., Ashmarina, L., Wang, S., Miziorko, H., and Mitchell, G. A. (2001) Mitochondrial 3-hydroxy-3-methylglutaryl-CoA synthase deficiency: clinical course and description of causal mutations in two patients. *Pediatric research* **49**, 326-331
68. Aledo, R., Zschocke, J., Pie, J., Mir, C., Fiesel, S., Mayatepek, E., Hoffmann, G. F., Casals, N., and Hegardt, F. G. (2001) Genetic basis of mitochondrial HMG-CoA synthase deficiency. *Hum Genet* **109**, 19-23
69. Yang, S. Y., He, X. Y., and Schulz, H. (1987) Fatty acid oxidation in rat brain is limited by the low activity of 3-ketoacyl-coenzyme A thiolase. *J Biol Chem* **262**, 13027-13032
70. Edmond, J., Robbins, R. A., Bergstrom, J. D., Cole, R. A., and de Vellis, J. (1987) Capacity for substrate utilization in oxidative metabolism by neurons, astrocytes, and oligodendrocytes from developing brain in primary culture. *Journal of neuroscience research* **18**, 551-561
71. Ward Platt, M., and Deshpande, S. (2005) Metabolic adaptation at birth. *Seminars in fetal & neonatal medicine* **10**, 341-350
72. Stern, J. R., Coon, M. J., Del Campillo, A., and Schneider, M. C. (1956) Enzymes of fatty acid metabolism. IV. Preparation and properties of coenzyme A transferase. *J Biol Chem* **221**, 15-31
73. Halestrap, A. P., and Wilson, M. C. (2012) The monocarboxylate transporter family--role and regulation. *IUBMB Life.* **64**, 109-119
74. Williamson, D. H., Bates, M. W., Page, M. A., and Krebs, H. A. (1971) Activities of enzymes involved in acetoacetate utilization in adult mammalian tissues. *Biochem J* **121**, 41-47
75. Garland, P. B., Randle, P. J., and Newsholme, E. A. (1963) Citrate as an Intermediary in the Inhibition of Phosphofructokinase in Rat Heart Muscle by Fatty Acids, Ketone Bodies, Pyruvate, Diabetes, and Starvation. *Nature* **200**, 169-170
76. Fukao, T., Lopaschuk, G. D., and Mitchell, G. A. (2004) Pathways and control of ketone body metabolism: on the fringe of lipid biochemistry. *Prostaglandins Leukot Essent Fatty Acids* **70**, 243-251

77. Fukao, T. (2001) 3-ketoacid CoA transferase (SCOT) deficiency. *Orphanet encyclopedia*
78. Cotter, D. G., d'Avignon, D. A., Wentz, A. E., Weber, M. L., and Crawford, P. A. (2011) Obligat role for ketone body oxidation in neonatal metabolic homeostasis. *J Biol Chem* **286**, 6902-6910
79. Berry, G. T., Fukao, T., Mitchell, G. A., Mazur, A., Ciafre, M., Gibson, J., Kondo, N., and Palmieri, M. J. (2001) Neonatal hypoglycaemia in severe succinyl-CoA: 3-oxoacid CoA-transferase deficiency. *Journal of inherited metabolic disease* **24**, 587-595
80. Fukao, T., Mitchell, G. A., Song, X. Q., Nakamura, H., Kassovska-Bratinova, S., Orii, K. E., Wraith, J. E., Besley, G., Wanders, R. J., Niezen-Koning, K. E., Berry, G. T., Palmieri, M., and Kondo, N. (2000) Succinyl-CoA:3-ketoacid CoA transferase (SCOT): cloning of the human SCOT gene, tertiary structural modeling of the human SCOT monomer, and characterization of three pathogenic mutations. *Genomics* **68**, 144-151
81. Kassovska-Bratinova, S., Fukao, T., Song, X. Q., Duncan, A. M., Chen, H. S., Robert, M. F., Perez-Cerda, C., Ugarte, M., Chartrand, C., Vobecky, S., Kondo, N., and Mitchell, G. A. (1996) Succinyl CoA: 3-oxoacid CoA transferase (SCOT): human cDNA cloning, human chromosomal mapping to 5p13, and mutation detection in a SCOT-deficient patient. *Am J Hum Genet* **59**, 519-528
82. Owen, O. E., Morgan, A. P., Kemp, H. G., Sullivan, J. M., Herrera, M. G., and Cahill, G. F., Jr. (1967) Brain metabolism during fasting. *J Clin Invest* **46**, 1589-1595
83. Sultan, A. M. (1988) D-3-hydroxybutyrate metabolism in the perfused rat heart. *Mol Cell Biochem* **79**, 113-118
84. Reichard, G. A., Jr., Owen, O. E., Haff, A. C., Paul, P., and Bortz, W. M. (1974) Ketone-body production and oxidation in fasting obese humans. *J Clin Invest* **53**, 508-515
85. Okuda, Y., Kawai, K., Ohmori, H., and Yamashita, K. (1991) Ketone body utilization and its metabolic effect in resting muscles of normal and streptozotocin-diabetic rats. *Endocrinol Jpn* **38**, 245-251
86. Turko, I. V., Marcondes, S., and Murad, F. (2001) Diabetes-associated nitration of tyrosine and inactivation of succinyl-CoA:3-oxoacid CoA-transferase. *Am J Physiol Heart Circ Physiol* **281**, H2289-2294
87. Fenselau, A., and Wallis, K. (1976) 3-oxo acid coenzyme A-transferase in normal and diabetic rat muscle. *Biochem J* **158**, 509-512
88. Grinblat, L., Pacheco Bolanos, L. F., and Stoppani, A. O. (1986) Decreased rate of ketone-body oxidation and decreased activity of D-3-hydroxybutyrate dehydrogenase and succinyl-CoA:3-oxo-acid CoA-transferase in heart mitochondria of diabetic rats. *Biochem J* **240**, 49-56
89. Fenselau, A., and Wallis, K. (1974) Substrate specificity and mechanism of action of acetoacetate coenzyme A transferase from rat heart. *Biochemistry* **13**, 3884-3888
90. Yan, J., Young, M. E., Cui, L., Lopaschuk, G. D., Liao, R., and Tian, R. (2009) Increased glucose uptake and oxidation in mouse hearts prevent high fatty acid oxidation but cause cardiac dysfunction in diet-induced obesity. *Circulation* **119**, 2818-2828
91. Wang, Y., Peng, F., Tong, W., Sun, H., Xu, N., and Liu, S. (2010) The nitrated proteome in heart mitochondria of the db/db mouse model: Characterization of nitrated tyrosine residues in SCOT. *J Proteome Res*
92. Marcondes, S., Turko, I. V., and Murad, F. (2001) Nitration of succinyl-CoA:3-oxoacid CoA-transferase in rats after endotoxin administration. *Proc Natl Acad Sci U S A* **98**, 7146-7151
93. Rebrin, I., Bregere, C., Kamzalov, S., Gallaher, T. K., and Sohal, R. S. (2007) Nitration of tryptophan 372 in succinyl-CoA:3-ketoacid CoA transferase during aging in rat heart mitochondria. *Biochemistry* **46**, 10130-10144
94. Bregere, C., Rebrin, I., Gallaher, T. K., and Sohal, R. S. (2010) Effects of age and calorie restriction on tryptophan nitration, protein content, and activity of succinyl-CoA:3-ketoacid CoA transferase in rat kidney mitochondria. *Free Radic Biol Med* **48**, 609-618

95. Sato, K., Kashiwaya, Y., Keon, C. A., Tsuchiya, N., King, M. T., Radda, G. K., Chance, B., Clarke, K., and Veech, R. L. (1995) Insulin, ketone bodies, and mitochondrial energy transduction. *FASEB J* **9**, 651-658
96. Veech, R. L. (2004) The therapeutic implications of ketone bodies: the effects of ketone bodies in pathological conditions: ketosis, ketogenic diet, redox states, insulin resistance, and mitochondrial metabolism. *Prostaglandins Leukot Essent Fatty Acids* **70**, 309-319
97. Niezen-Koning, K. E., Wanders, R. J. A., Ruiten, J. P. N., Ijlst, L., Visser, G., Reitsma-Bierens, W. C. C., Heymans, H. S. A., Reijngoud, D. J., and Smit, G. P. A. (1997) Succinyl-CoA:acetoacetate transferase deficiency: identification of a new patient with a neonatal onset and review of the literature. *Eur J Pediatr* **156**, 870-873
98. Tildon, J. T., and Cornblath, M. (1972) Succinyl-CoA: 3-ketoacid CoA-transferase deficiency. A cause for ketoacidosis in infancy. *J Clin Invest* **51**, 493-498
99. Mitchell, G. A., and Fukao, T. (2000) Inborn Errors of Ketone Body Metabolism. in *The Online Metabolic and Molecular Bases of Inherited Diseases (OMMBID)* (Beaudet, A., Vogelstein, B., Kinzler, K. W., Antonarakis, S., and Ballabio, A. eds.), The McGraw-Hill Companies, Inc, Columbus, OH. pp
100. Saudubray, J. M., Specola, N., Middleton, B., Lombes, A., Bonnefont, J. P., Jakobs, C., Vassault, A., Charpentier, C., and Day, R. (1987) Hyperketotic states due to inherited defects of ketolysis. *Enzyme* **38**, 80-90
101. Snyderman, S. E., Sansaricq, C., and Middleton, B. (1998) Succinyl-CoA:3-ketoacid CoA-transferase deficiency. *Pediatrics* **101**, 709-711
102. Huidekoper, H. H., Duran, M., Turkenburg, M., Ackermans, M. T., Sauerwein, H. P., and Wijburg, F. A. (2008) Fasting adaptation in idiopathic ketotic hypoglycemia: a mismatch between glucose production and demand. *Eur J Pediatr*. **167**, 859-865.
103. Kochar, I. S., and Hussain, K. (2007) From hyperinsulinaemic hypoglycaemia to ketotic hypoglycaemia: the range of glucose abnormalities in patients born with intrauterine growth retardation. *Eur J Pediatr*. **166**, 1003-1007.
104. Bodamer, O. A., Hussein, K., Morris, A. A., Langhans, C. D., Rating, D., Mayatepek, E., and Leonard, J. V. (2006) Glucose and leucine kinetics in idiopathic ketotic hypoglycaemia. *Arch Dis Child*. **91**, 483-486
105. Hawdon, J. (1999) Hypoglycaemia and the neonatal brain. *Eur J Pediatr*. **158** S9-S12.
106. Fellman, V., and Kotarsky, H. (2011) Mitochondrial hepatopathies in the newborn period. *Semin Fetal Neonatal Med*. **16**, 222-228.
107. Fukao, T., Song, X. Q., Mitchell, G. A., Yamaguchi, S., Sukegawa, K., Orii, T., and Kondo, N. (1997) Enzymes of ketone body utilization in human tissues: protein and messenger RNA levels of succinyl-coenzyme A (CoA):3-ketoacid CoA transferase and mitochondrial and cytosolic acetoacetyl-CoA thiolases. *Pediatr Res* **42**, 498-502
108. Cotter, D. G., Schugar, R. C., Wentz, A. E., d'Avignon, D. A., and Crawford, P. A. (2013) Successful adaptation to ketosis by mice with tissue-specific deficiency of ketone body oxidation. *Am J Physiol Endocrinol Metab* **304**, E363-374
109. Edmond, J. (1974) Ketone bodies as precursors of sterols and fatty acids in the developing rat. *J Biol Chem* **249**, 72-80
110. Geelen, M. J., Lopes-Cardozo, M., and Edmond, J. (1983) Acetoacetate: a major substrate for the synthesis of cholesterol and fatty acids by isolated rat hepatocytes. *FEBS Lett* **163**, 269-273
111. Bergstrom, J. D., Wong, G. A., Edwards, P. A., and Edmond, J. (1984) The regulation of acetoacetyl-CoA synthetase activity by modulators of cholesterol synthesis in vivo and the utilization of acetoacetate for cholesterol synthesis. *J Biol Chem* **259**, 14548-14553
112. Webber, R. J., and Edmond, J. (1977) Utilization of L(+)-3-hydroxybutyrate, D(-)-3-hydroxybutyrate, acetoacetate, and glucose for respiration and lipid synthesis in the 18-day-old rat. *J Biol Chem* **252**, 5222-5226

113. Hasegawa, S., Noda, K., Maeda, A., Matsuoka, M., Yamasaki, M., and Fukui, T. (2012) Acetoacetyl-CoA synthetase, a ketone body-utilizing enzyme, is controlled by SREBP-2 and affects serum cholesterol levels. *Mol Genet Metab* **107**, 553-560
114. Hasegawa, S., Ikeda, Y., Yamasaki, M., and Fukui, T. (2012) The role of acetoacetyl-CoA synthetase, a ketone body-utilizing enzyme, in 3T3-L1 adipocyte differentiation. *Biol Pharm Bull* **35**, 1980-1985
115. Hasegawa, S., Kume, H., Inuma, S., Yamasaki, M., Takahashi, N., and Fukui, T. (2012) Acetoacetyl-CoA synthetase is essential for normal neuronal development. *Biochem Biophys Res Commun* **427**, 398-403
116. Lopaschuk, G. D., Ussher, J. R., Folmes, C. D., Jaswal, J. S., and Stanley, W. C. (2010) Myocardial fatty acid metabolism in health and disease. *Physiol Rev* **90**, 207-258
117. Bing, R. J. (1955) The metabolism of the heart. *Harvey Lect.* **50**, 27-70
118. Taegtmeier, H., Hems, R., and Krebs, H. A. (1980) Utilization of energy-providing substrates in the isolated working rat heart. *Biochem J* **186**, 701-711
119. Taegtmeier, H., McNulty, P., and Young, M. E. (2002) Adaptation and maladaptation of the heart in diabetes: Part I: general concepts. *Circulation* **105**, 1727-1733
120. Young, M. E., McNulty, P., and Taegtmeier, H. (2002) Adaptation and maladaptation of the heart in diabetes: Part II: potential mechanisms. *Circulation* **105**, 1861-1870
121. Garland, P. B., Newsholme, E. A., and Randle, P. J. (1962) Effect of fatty acids, ketone bodies, diabetes and starvation on pyruvate metabolism in rat heart and diaphragm muscle. *Nature* **195**, 381-383
122. Jeffrey, F. M., Diczku, V., Sherry, A. D., and Malloy, C. R. (1995) Substrate selection in the isolated working rat heart: effects of reperfusion, afterload, and concentration. *Basic Res Cardiol* **90**, 388-396
123. Tardif, A., Julien, N., Pelletier, A., Thibault, G., Srivastava, A. K., Chiasson, J. L., and Coderre, L. (2001) Chronic exposure to beta-hydroxybutyrate impairs insulin action in primary cultures of adult cardiomyocytes. *Am J Physiol Endocrinol Metab* **281**, E1205-1212
124. Hasselbaink, D. M., Glatz, J. F., Luiken, J. J., Roemen, T. H., and Van der Vusse, G. J. (2003) Ketone bodies disturb fatty acid handling in isolated cardiomyocytes derived from control and diabetic rats. *Biochem J* **371**, 753-760
125. Pelletier, A., Tardif, A., Gingras, M. H., Chiasson, J. L., and Coderre, L. (2007) Chronic exposure to ketone bodies impairs glucose uptake in adult cardiomyocytes in response to insulin but not vanadate: the role of PI3-K. *Mol Cell Biochem* **296**, 97-108
126. Crawford, P. A., Crowley, J. R., Sambandam, N., Muegge, B. D., Costello, E. K., Hamady, M., Knight, R., and Gordon, J. I. (2009) Regulation of myocardial ketone body metabolism by the gut microbiota during nutrient deprivation. *Proc Natl Acad Sci U S A* **106**, 11276-11281
127. Stanley, W. C., Meadows, S. R., Kivilo, K. M., Roth, B. A., and Lopaschuk, G. D. (2003) beta-Hydroxybutyrate inhibits myocardial fatty acid oxidation in vivo independent of changes in malonyl-CoA content. *Am J Physiol Heart Circ Physiol* **285**, H1626-1631
128. Kashiwaya, Y., Sato, K., Tsuchiya, N., Thomas, S., Fell, D. A., Veech, R. L., and Passonneau, J. V. (1994) Control of glucose utilization in working perfused rat heart. *J Biol Chem* **269**, 25502-25514
129. Maalouf, M., Sullivan, P. G., Davis, L., Kim, D. Y., and Rho, J. M. (2007) Ketones inhibit mitochondrial production of reactive oxygen species production following glutamate excitotoxicity by increasing NADH oxidation. *Neuroscience* **145**, 256-264
130. Haces, M. L., Hernandez-Fonseca, K., Medina-Campos, O. N., Montiel, T., Pedraza-Chaverri, J., and Massieu, L. (2008) Antioxidant capacity contributes to protection of ketone bodies against oxidative damage induced during hypoglycemic conditions. *Exp Neurol* **211**, 85-96
131. Huelsmann, W. C., Siliprandi, D., Ciman, M., and Siliprandi, N. (1964) Effect of Carnitine on the Oxidation of Alpha-Oxoglutarate to Succinate in the Presence of Acetoacetate or Pyruvate. *Biochim Biophys Acta* **93**, 166-168

132. Russell, R. R., 3rd, and Taegtmeyer, H. (1992) Coenzyme A sequestration in rat hearts oxidizing ketone bodies. *J Clin Invest* **89**, 968-973
133. Russell, R. R., 3rd, and Taegtmeyer, H. (1991) Pyruvate carboxylation prevents the decline in contractile function of rat hearts oxidizing acetoacetate. *Am J Physiol* **261**, H1756-1762
134. Russell, R. R., 3rd, and Taegtmeyer, H. (1991) Changes in citric acid cycle flux and anaplerosis antedate the functional decline in isolated rat hearts utilizing acetoacetate. *J Clin Invest* **87**, 384-390
135. Des Rosiers, C., Labarthe, F., Lloyd, S. G., and Chatham, J. C. (2011) Cardiac anaplerosis in health and disease: Food for thought. *Cardiovascular research* **90**, 210-219
136. Jones, J. G., Hansen, J., Sherry, A. D., Malloy, C. R., and Victor, R. G. (1997) Determination of acetyl-CoA enrichment in rat heart and skeletal muscle by ¹H nuclear magnetic resonance analysis of glutamate in tissue extracts. *Anal Biochem* **249**, 201-206
137. Laing, S. P., Swerdlow, A. J., Slater, S. D., Burden, A. C., Morris, A., Waugh, N. R., Gatling, W., Bingley, P. J., and Patterson, C. C. (2003) Mortality from heart disease in a cohort of 23,000 patients with insulin-treated diabetes. *Diabetologia* **46**, 760-765
138. Hue, L., and Taegtmeyer, H. (2009) The Randle cycle revisited: a new head for an old hat. *Am J Physiol Endocrinol Metab* **297**, E578-591
139. Kolwicz, S. C., Jr., and Tian, R. (2011) Glucose metabolism and cardiac hypertrophy. *Cardiovasc Res* **90**, 194-201
140. Ingwall, J. S., and Weiss, R. G. (2004) Is the failing heart energy starved? On using chemical energy to support cardiac function. *Circ Res* **95**, 135-145
141. Ashrafian, H., Frenneaux, M. P., and Opie, L. H. (2007) Metabolic mechanisms in heart failure. *Circulation* **116**, 434-448
142. Jaswal, J. S., Keung, W., Wang, W., Ussher, J. R., and Lopaschuk, G. D. (2011) Targeting fatty acid and carbohydrate oxidation - a novel therapeutic intervention in the ischemic and failing heart. *Biochim Biophys Acta* **1813**, 1333-1350
143. Boudina, S., and Abel, E. D. (2010) Diabetic cardiomyopathy, causes and effects. *Rev Endocr Metab Disord* **11**, 31-39
144. Abel, E. D., and Doenst, T. (2011) Mitochondrial Adaptations to Physiological versus Pathological Cardiac Hypertrophy. *Cardiovascular research* **90**, 230-242
145. Vanoverschelde, J. L., Wijns, W., Kolanowski, J., Bol, A., Decoster, P. M., Michel, C., Cogneau, M., Heyndrickx, G. R., Essamri, B., and Melin, J. A. (1993) Competition between palmitate and ketone bodies as fuels for the heart: study with positron emission tomography. *Am J Physiol* **264**, H701-707
146. Janardhan, A., Chen, J., and Crawford, P. A. Altered systemic ketone body metabolism in advanced heart failure. *Tex Heart Inst J* **38**, 533-538
147. Rudolph, W., and Schinz, A. (1973) Studies on myocardial blood flow, oxygen consumption, and myocardial metabolism in patients with cardiomyopathy. *Recent advances in studies on cardiac structure and metabolism* **2**, 739-749
148. Longo, N., Fukao, T., Singh, R., Pasquali, M., Barrios, R. G., Kondo, N., and Gibson, K. M. (2004) Succinyl-CoA:3-ketoacid transferase (SCOT) deficiency in a new patient homozygous for an R217X mutation. *Journal of inherited metabolic disease* **27**, 691-692
149. Fukao, T., Sakurai, S., Rolland, M. O., Zobot, M. T., Schulze, A., Yamada, K., and Kondo, N. (2006) A 6-bp deletion at the splice donor site of the first intron resulted in aberrant splicing using a cryptic splice site within exon 1 in a patient with succinyl-CoA: 3-Ketoacid CoA transferase (SCOT) deficiency. *Mol Genet Metab* **89**, 280-282
150. Al-Zaid, N. S., Dashti, H. M., Mathew, T. C., and Juggi, J. S. (2007) Low carbohydrate ketogenic diet enhances cardiac tolerance to global ischaemia. *Acta Cardiol* **62**, 381-389
151. Wang, P., Tate, J. M., and Lloyd, S. G. (2008) Low carbohydrate diet decreases myocardial insulin signaling and increases susceptibility to myocardial ischemia. *Life Sci* **83**, 836-844

152. Krebs, P., Fan, W., Chen, Y. H., Tobita, K., Downes, M. R., Wood, M. R., Sun, L., Li, X., Xia, Y., Ding, N., Spaeth, J. M., Moresco, E. M., Boyer, T. G., Lo, C. W., Yen, J., Evans, R. M., and Beutler, B. (2011) Lethal mitochondrial cardiomyopathy in a hypomorphic Med30 mouse mutant is ameliorated by ketogenic diet. *Proc Natl Acad Sci U S A* **108**, 19678-19682
153. Zou, Z., Sasaguri, S., Rajesh, K. G., and Suzuki, R. (2002) dl-3-Hydroxybutyrate administration prevents myocardial damage after coronary occlusion in rat hearts. *Am J Physiol Heart Circ Physiol* **283**, H1968-1974
154. Snorek, M., Hodyc, D., Sedivy, V., Durisova, J., Skoumalova, A., Wilhelm, J., Neckar, J., Kolar, F., and Herget, J. (2012) Short-term fasting reduces the extent of myocardial infarction and incidence of reperfusion arrhythmias in rats. *Physiological research / Academia Scientiarum Bohemoslovaca*
155. Mayr, M., Yusuf, S., Weir, G., Chung, Y. L., Mayr, U., Yin, X., Ladroue, C., Madhu, B., Roberts, N., De Souza, A., Fredericks, S., Stubbs, M., Griffiths, J. R., Jahangiri, M., Xu, Q., and Camm, A. J. (2008) Combined metabolomic and proteomic analysis of human atrial fibrillation. *J Am Coll Cardiol* **51**, 585-594
156. Doepner, B., Thierfelder, S., Hirche, H., and Benndorf, K. (1997) 3-hydroxybutyrate blocks the transient K⁺ outward current in myocardial mouse cells in a stereoselective fashion. *J Physiol* **500 (Pt 1)**, 85-94
157. Ito, M., Fukui, T., Kamokari, M., Saito, T., and Tomita, K. (1984) Purification and characterization of acetoacetyl-CoA synthetase from rat liver. *Biochim Biophys Acta* **794**, 183-193
158. Lincoln, B. C., Des Rosiers, C., and Brunengraber, H. (1987) Metabolism of S-3-hydroxybutyrate in the perfused rat liver. *Arch Biochem Biophys* **259**, 149-156
159. Reed, W. D., and Ozand, P. T. (1980) Enzymes of L-(+)-3-hydroxybutyrate metabolism in the rat. *Arch Biochem Biophys* **205**, 94-103
160. Scofield, R. F., Brady, P. S., Schumann, W. C., Kumaran, K., Ohgaku, S., Margolis, J. M., and Landau, B. R. (1982) On the lack of formation of L-(+)-3-hydroxybutyrate by liver. *Arch Biochem Biophys* **214**, 268-272
161. Wang, X., Levi, A. J., and Halestrap, A. P. (1996) Substrate and inhibitor specificities of the monocarboxylate transporters of single rat heart cells. *Am J Physiol* **270**, H476-484
162. Fink, G., Desrochers, S., Des Rosiers, C., Garneau, M., David, F., Daloze, T., Landau, B. R., and Brunengraber, H. (1988) Pseudoketogenesis in the perfused rat heart. *J Biol Chem* **263**, 18036-18042
163. Des Rosiers, C., Montgomery, J. A., Garneau, M., David, F., Mamer, O. A., Daloze, P., Toffolo, G., Cobelli, C., Landau, B. R., and Brunengraber, H. (1990) Pseudoketogenesis in hepatectomized dogs. *Am J Physiol* **258**, E519-528
164. Orii, K. E., Fukao, T., Song, X. Q., Mitchell, G. A., and Kondo, N. (2008) Liver-specific silencing of the human gene encoding succinyl-CoA: 3-ketoacid CoA transferase. *Tohoku J Exp Med* **215**, 227-236
165. Avogaro, A., Doria, A., Gnudi, L., Carraro, A., Duner, E., Brocco, E., Tiengo, A., Crepaldi, G., Bier, D. M., and Nosadini, R. (1992) Forearm ketone body metabolism in normal and in insulin-dependent diabetic patients. *Am J Physiol* **263**, E261-267
166. Rosca, M. G., Lemieux, H., and Hoppel, C. L. (2009) Mitochondria in the elderly: Is acetylcarnitine a rejuvenator? *Adv Drug Deliv Rev* **61**, 1332-1342
167. Phillips, J. W., and Hird, F. J. (1977) Ketogenesis in vertebrate livers. *Comp Biochem Physiol B* **57**, 133-138
168. Zammit, V. A., Beis, A., and Newsholme, E. A. (1979) The role of 3-oxo acid-CoA transferase in the regulation of ketogenesis in the liver. *FEBS Lett* **103**, 212-215
169. MacDonald, M. J., Longacre, M. J., Stoker, S. W., Brown, L. J., Hasan, N. M., and Kendrick, M. A. (2008) Acetoacetate and beta-hydroxybutyrate in combination with other metabolites release

- insulin from INS-1 cells and provide clues about pathways in insulin secretion. *Am J Physiol Cell Physiol* **294**, C442-450
170. Hasan, N. M., Longacre, M. J., Seed-Ahmed, M., Kendrick, M. A., Gu, H., Ostenson, C. G., Fukao, T., and Macdonald, M. J. (2010) Lower succinyl-CoA:3-ketoacid-CoA transferase (SCOT) and ATP citrate lyase in pancreatic islets of a rat model of type 2 diabetes: Knockdown of SCOT inhibits insulin release in rat insulinoma cells. *Arch Biochem Biophys* **499**, 62-68
 171. MacDonald, M. J., Hasan, N., and Longacre, M. (2008) Studies with leucine, β -hydroxybutyrate and ATP citrate lyase-deficient beta cells support the acetoacetate pathway of insulin secretion. *Biochimica et Biophysica Acta*, 966–972
 172. MacDonald, M. J. (2007) Synergistic potent insulin release by combinations of weak secretagogues in pancreatic islets and INS-1 cells. *J Biol Chem*. **282** 6043-6052
 173. Newsholme, P., Gordon, S., and Newsholme, E. A. (1987) Rates of utilization and fates of glucose, glutamine, pyruvate, fatty acids and ketone bodies by mouse macrophages. *Biochem J*. **242**, 631-636.
 174. Newsholme, P., Curi, R., Gordon, S., and Newsholme, E. A. (1986) Metabolism of glucose, glutamine, long-chain fatty acids and ketone bodies by murine macrophages. *Biochem J*. **239**, 121-125.
 175. Odegaard, J. I., and Chawla, A. (2011) Alternative Macrophage Activation and Metabolism. *Annu. Rev. Pathol. Mech. Dis.*, 275–297
 176. Schneider, J. G., Yang, Z., Chakravarthy, M. V., Lodhi, I. J., Wei, X., Turk, J., and Semenkovich, C. F. (2011) Macrophage fatty-acid synthase deficiency decreases diet-induced atherosclerosis. *J Biol Chem* **285**, 23398-23409
 177. Yamasaki, M., Hasegawa, S., Suzuki, H., Hidai, K., Saitoh, Y., and Fukui, T. (2005) Acetoacetyl-CoA synthetase gene is abundant in rat adipose, and related with fatty acid synthesis in mature adipocytes. *Biochem Biophys Res Commun* **335**, 215-219
 178. Aguilo, F., Camarero, N., Relat, J., Marrero, P. F., and Haro, D. (2010) Transcriptional regulation of the human acetoacetyl-CoA synthetase gene by PPARgamma. *Biochem J* **427**, 255-264
 179. Lodhi, I. J., Yin, L., Jensen-Urstad, A. P., Funai, K., Coleman, T., Baird, J. H., El Ramahi, M. K., Razani, B., Song, H., Fu-Hsu, F., Turk, J., and Semenkovich, C. F. (2012) Inhibiting Adipose Tissue Lipogenesis Reprograms Thermogenesis and PPARgamma Activation to Decrease Diet-Induced Obesity. *Cell Metab*
 180. Yoo, H., Stephanopoulos, G., and Kelleher, J. K. (2004) Quantifying carbon sources for de novo lipogenesis in wild-type and IRS-1 knockout brown adipocytes. *J Lipid Res* **45**, 1324-1332
 181. Ahmed, K., Tunaru, S., and Offermanns, S. (2009) GPR109A, GPR109B and GPR81, a family of hydroxy-carboxylic acid receptors. *Trends Pharmacol Sci* **30**, 557-562
 182. Taggart, A. K., Kero, J., Gan, X., Cai, T. Q., Cheng, K., Ippolito, M., Ren, N., Kaplan, R., Wu, K., Wu, T. J., Jin, L., Liaw, C., Chen, R., Richman, J., Connolly, D., Offermanns, S., Wright, S. D., and Waters, M. G. (2005) (D)-beta-Hydroxybutyrate inhibits adipocyte lipolysis via the nicotinic acid receptor PUMA-G. *J Biol Chem* **280**, 26649-26652
 183. Tunaru, S., Kero, J., Schaub, A., Wufka, C., Blaukat, A., Pfeffer, K., and Offermanns, S. (2003) PUMA-G and HM74 are receptors for nicotinic acid and mediate its anti-lipolytic effect. *Nat Med* **9**, 352-355
 184. Lukasova, M., Malaval, C., Gille, A., Kero, J., and Offermanns, S. (2011) Nicotinic acid inhibits progression of atherosclerosis in mice through its receptor GPR109A expressed by immune cells. *J Clin Invest* **121**, 1163-1173
 185. Kimura, I., Inoue, D., Maeda, T., Hara, T., Ichimura, A., Miyauchi, S., Kobayashi, M., Hirasawa, A., and Tsujimoto, G. (2011) Short-chain fatty acids and ketones directly regulate sympathetic nervous system via G protein-coupled receptor 41 (GPR41). *Proc Natl Acad Sci U S A* **108**, 8030-8035
 186. Shimazu, T., Hirschey, M. D., Newman, J., He, W., Shirakawa, K., Le Moan, N., Grueter, C. A., Lim, H., Saunders, L. R., Stevens, R. D., Newgard, C. B., Farese, R. V., Jr., de Cabo, R., Ulrich,

- S., Akassoglou, K., and Verdin, E. (2012) Suppression of Oxidative Stress by beta-Hydroxybutyrate, an Endogenous Histone Deacetylase Inhibitor. *Science* **Epub ahead of print**. **PMID: 23223453**
187. Gordon, J. I. (2012) Honor thy gut symbionts redux. *Science* **336**, 1251-1253
188. Holmes, E., Kinross, J., Gibson, G. R., Burcelin, R., Jia, W., Pettersson, S., and Nicholson, J. K. (2012) Therapeutic modulation of microbiota-host metabolic interactions. *Sci Transl Med* **4**, 137rv136
189. Hooper, L. V., Littman, D. R., and Macpherson, A. J. (2012) Interactions between the microbiota and the immune system. *Science* **336**, 1268-1273
190. Nicholson, J. K., Holmes, E., Kinross, J., Burcelin, R., Gibson, G., Jia, W., and Pettersson, S. (2012) Host-gut microbiota metabolic interactions. *Science* **336**, 1262-1267
191. Blumberg, R., and Powrie, F. (2012) Microbiota, disease, and back to health: a metastable journey. *Sci Transl Med* **4**, 137rv137
192. Backhed, F., and Crawford, P. A. (2010) Coordinated regulation of the metabolome and lipidome at the host-microbial interface. *Biochim Biophys Acta* **1801**, 240-245
193. (2012) Structure, function and diversity of the healthy human microbiome: The Human Microbiome Project Consortium. *Nature* **486**, 207-214
194. (2012) A framework for human microbiome research: The Human Microbiome Project Consortium. *Nature* **486**, 215-221
195. Tremaroli, V., and Backhed, F. (2012) Functional interactions between the gut microbiota and host metabolism. *Nature* **489**, 242-249
196. Ley, R. E., Backhed, F., Turnbaugh, P., Lozupone, C. A., Knight, R. D., and Gordon, J. I. (2005) Obesity alters gut microbial ecology. *Proc Natl Acad Sci U S A* **102**, 11070-11075
197. Cani, P. D., Bibiloni, R., Knauf, C., Waget, A., Neyrinck, A. M., Delzenne, N. M., and Burcelin, R. (2008) Changes in gut microbiota control metabolic endotoxemia-induced inflammation in high-fat diet-induced obesity and diabetes in mice. *Diabetes* **57**, 1470-1481
198. Wu, X., Ma, C., Han, L., Nawaz, M., Gao, F., Zhang, X., Yu, P., Zhao, C., Li, L., Zhou, A., Wang, J., Moore, J. E., Millar, B. C., and Xu, J. (2010) Molecular characterisation of the faecal microbiota in patients with type II diabetes. *Curr Microbiol* **61**, 69-78
199. Cani, P. D., Amar, J., Iglesias, M. A., Poggi, M., Knauf, C., Bastelica, D., Neyrinck, A. M., Fava, F., Tuohy, K. M., Chabo, C., Waget, A., Delmee, E., Cousin, B., Sulpice, T., Chamontin, B., Ferrieres, J., Tanti, J. F., Gibson, G. R., Casteilla, L., Delzenne, N. M., Alessi, M. C., and Burcelin, R. (2007) Metabolic endotoxemia initiates obesity and insulin resistance. *Diabetes* **56**, 1761-1772
200. Membrez, M., Blancher, F., Jaquet, M., Bibiloni, R., Cani, P. D., Burcelin, R. G., Corthesy, I., Mace, K., and Chou, C. J. (2008) Gut microbiota modulation with norfloxacin and ampicillin enhances glucose tolerance in mice. *FASEB J* **22**, 2416-2426
201. Cani, P. D., Possemiers, S., Van de Wiele, T., Guiot, Y., Everard, A., Rottier, O., Geurts, L., Naslain, D., Neyrinck, A. M., Lambert, D. M., Muccioli, G. G., and Delzenne, N. M. (2009) Changes in gut microbiota control inflammation in obese mice through a mechanism involving GLP-2-driven improvement of gut permeability. *Gut*
202. Turnbaugh, P. J., Backhed, F., Fulton, L., and Gordon, J. I. (2008) Diet-induced obesity is linked to marked but reversible alterations in the mouse distal gut microbiome. *Cell Host Microbe* **3**, 213-223
203. Turnbaugh, P. J., Ley, R. E., Mahowald, M. A., Magrini, V., Mardis, E. R., and Gordon, J. I. (2006) An obesity-associated gut microbiome with increased capacity for energy harvest. *Nature* **444**, 1027-1031
204. Turnbaugh, P. J., Ridaura, V. K., Faith, J. J., Rey, F. E., Knight, R., and Gordon, J. I. (2009) The effect of diet on the human gut microbiome: a metagenomic analysis in humanized gnotobiotic mice. *Sci Transl Med* **1**, 6ra14

205. Backhed, F., Ding, H., Wang, T., Hooper, L. V., Koh, G. Y., Nagy, A., Semenkovich, C. F., and Gordon, J. I. (2004) The gut microbiota as an environmental factor that regulates fat storage. *Proc Natl Acad Sci U S A* **101**, 15718-15723
206. Backhed, F., Manchester, J. K., Semenkovich, C. F., and Gordon, J. I. (2007) Mechanisms underlying the resistance to diet-induced obesity in germ-free mice. *Proc Natl Acad Sci U S A* **104**, 979-984
207. Zhang, H., DiBaise, J. K., Zuccolo, A., Kudrna, D., Braidotti, M., Yu, Y., Parameswaran, P., Crowell, M. D., Wing, R., Rittmann, B. E., and Krajmalnik-Brown, R. (2009) Human gut microbiota in obesity and after gastric bypass. *Proc Natl Acad Sci U S A* **106**, 2365-2370
208. Li, J. V., Ashrafian, H., Bueter, M., Kinross, J., Sands, C., le Roux, C. W., Bloom, S. R., Darzi, A., Athanasiou, T., Marchesi, J. R., Nicholson, J. K., and Holmes, E. (2011) Metabolic surgery profoundly influences gut microbial-host metabolic cross-talk. *Gut* **60**, 1214-1223
209. Qin, J., Li, Y., Cai, Z., Li, S., Zhu, J., Zhang, F., Liang, S., Zhang, W., Guan, Y., Shen, D., Peng, Y., Zhang, D., Jie, Z., Wu, W., Qin, Y., Xue, W., Li, J., Han, L., Lu, D., Wu, P., Dai, Y., Sun, X., Li, Z., Tang, A., Zhong, S., Li, X., Chen, W., Xu, R., Wang, M., Feng, Q., Gong, M., Yu, J., Zhang, Y., Zhang, M., Hansen, T., Sanchez, G., Raes, J., Falony, G., Okuda, S., Almeida, M., LeChatelier, E., Renault, P., Pons, N., Batto, J. M., Zhang, Z., Chen, H., Yang, R., Zheng, W., Li, S., Yang, H., Wang, J., Ehrlich, S. D., Nielsen, R., Pedersen, O., Kristiansen, K., and Wang, J. (2012) A metagenome-wide association study of gut microbiota in type 2 diabetes. *Nature* **490**, 55-60
210. Dumas, M. E., Barton, R. H., Toye, A., Cloarec, O., Blancher, C., Rothwell, A., Fearnside, J., Tatoud, R., Blanc, V., Lindon, J. C., Mitchell, S. C., Holmes, E., McCarthy, M. I., Scott, J., Gauguier, D., and Nicholson, J. K. (2006) Metabolic profiling reveals a contribution of gut microbiota to fatty liver phenotype in insulin-resistant mice. *Proc Natl Acad Sci U S A* **103**, 12511-12516
211. Claus, S. P., Tsang, T. M., Wang, Y., Cloarec, O., Skordi, E., Martin, F. P., Rezzi, S., Ross, A., Kochhar, S., Holmes, E., and Nicholson, J. K. (2008) Systemic multicompartmental effects of the gut microbiome on mouse metabolic phenotypes. *Mol Syst Biol* **4**, 219
212. Holmes, E., Loo, R. L., Stampler, J., Bictash, M., Yap, I. K., Chan, Q., Ebbels, T., De Iorio, M., Brown, I. J., Veselkov, K. A., Davignus, M. L., Kesteloot, H., Ueshima, H., Zhao, L., Nicholson, J. K., and Elliott, P. (2008) Human metabolic phenotype diversity and its association with diet and blood pressure. *Nature* **453**, 396-400
213. Wang, Z., Klipfell, E., Bennett, B. J., Koeth, R., Levison, B. S., Dugar, B., Feldstein, A. E., Britt, E. B., Fu, X., Chung, Y. M., Wu, Y., Schauer, P., Smith, J. D., Allayee, H., Tang, W. H., DiDonato, J. A., Lusis, A. J., and Hazen, S. L. (2011) Gut flora metabolism of phosphatidylcholine promotes cardiovascular disease. *Nature* **472**, 57-63
214. Wen, L., Ley, R. E., Volchkov, P. Y., Stranges, P. B., Avanesyan, L., Stonebraker, A. C., Hu, C., Wong, F. S., Szot, G. L., Bluestone, J. A., Gordon, J. I., and Chervonsky, A. V. (2008) Innate immunity and intestinal microbiota in the development of Type 1 diabetes. *Nature* **455**, 1109-1113
215. Hoverstad, T., and Midtvedt, T. (1986) Short-chain fatty acids in germfree mice and rats. *J Nutr* **116**, 1772-1776
216. Pryce, J. W., Weber, M. A., Heales, S., Malone, M., and Sebire, N. J. (2011) Tandem mass spectrometry findings at autopsy for detection of metabolic disease in infant deaths: postmortem changes and confounding factors. *J Clin Pathol* **64**, 1005-1009
217. Seyfried, T. N., Kiebish, M. A., Marsh, J., Shelton, L. M., Huysentruyt, L. C., and Mukherjee, P. (2011) Metabolic management of brain cancer. *Biochim Biophys Acta* **1807**, 577-594.
218. Yang, X., and Cheng, B. (2010) Neuroprotective and anti-inflammatory activities of ketogenic diet on MPTP-induced neurotoxicity. *J Mol Neurosci* **42**, 145-153.
219. Kossoff, E. H., and Hartman, A. L. (2012) Ketogenic diets: new advances for metabolism based therapies. *Curr Opin Neurol* **25**, 173-178

220. Yao, J., Chen, S., Mao, Z., Cadenas, E., and Brinton, R. (2011) 2-Deoxy-D-glucose treatment induces ketogenesis, sustains mitochondrial function, and reduces pathology in female mouse model of Alzheimer's disease. *PLoS One* **6**, e21788.
221. McNally, M. A., and Hartman, A. L. (2012) Ketone Bodies in Epilepsy. *J Neurochem*
222. Browning, J. D., Baker, J. A., Rogers, T., Davis, J., Satapati, S., and Burgess, S. C. (2011) Short-term weight loss and hepatic triglyceride reduction: evidence of a metabolic advantage with dietary carbohydrate restriction. *Am J Clin Nutr* **93**, 1048-1052
223. Foster, G. D., Wyatt, H. R., Hill, J. O., Makris, A. P., Rosenbaum, D. L., Brill, C., Stein, R. I., Mohammed, B. S., Miller, B., Rader, D. J., Zemel, B., Wadden, T. A., Tenhave, T., Newcomb, C. W., and Klein, S. (2010) Weight and metabolic outcomes after 2 years on a low-carbohydrate versus low-fat diet: a randomized trial. *Ann Intern Med* **153**, 147-157
224. Kwiterovich, P. O., Jr., Vining, E. P., Pyzik, P., Skolasky, R., Jr., and Freeman, J. M. (2003) Effect of a high-fat ketogenic diet on plasma levels of lipids, lipoproteins, and apolipoproteins in children. *Jama* **290**, 912-920
225. Suzuki, J., Shen, W. J., Nelson, B. D., Selwood, S. P., Murphy, G. M., Jr., Kanehara, H., Takahashi, S., Oida, K., Miyamori, I., and Kraemer, F. B. (2002) Cardiac gene expression profile and lipid accumulation in response to starvation. *Am J Physiol Endocrinol Metab* **283**, E94-E102
226. Bisschop, P. H., de Metz, J., Ackermans, M. T., Endert, E., Pijl, H., Kuipers, F., Meijer, A. J., Sauerwein, H. P., and Romijn, J. A. (2001) Dietary fat content alters insulin-mediated glucose metabolism in healthy men. *The American journal of clinical nutrition* **73**, 554-559
227. Clarke, K., Tchabanenko, K., Pawlosky, R., Carter, E., Todd King, M., Musa-Veloso, K., Ho, M., Roberts, A., Robertson, J., Vanitallie, T. B., and Veech, R. L. (2012) Kinetics, safety and tolerability of (R)-3-hydroxybutyl (R)-3-hydroxybutyrate in healthy adult subjects. *Regul Toxicol Pharmacol* **63**, 401-408
228. Kashiwaya, Y., Pawlosky, R., Markis, W., King, M. T., Bergman, C., Srivastava, S., Murray, A., Clarke, K., and Veech, R. L. (2010) A ketone ester diet increases brain malonyl-CoA and Uncoupling proteins 4 and 5 while decreasing food intake in the normal Wistar Rat. *J Biol Chem* **285**, 25950-25956
229. Srivastava, S., Kashiwaya, Y., King, M. T., Baxa, U., Tam, J., Niu, G., Chen, X., Clarke, K., and Veech, R. L. (2012) Mitochondrial biogenesis and increased uncoupling protein 1 in brown adipose tissue of mice fed a ketone ester diet. *Faseb J* **26**, 2351-2362
230. Roe, C. R., Yang, B. Z., Brunengraber, H., Roe, D. S., Wallace, M., and Garritson, B. K. (2008) Carnitine palmitoyltransferase II deficiency: successful anaplerotic diet therapy. *Neurology* **71**, 260-264
231. Roe, C. R., Sweetman, L., Roe, D. S., David, F., and Brunengraber, H. (2002) Treatment of cardiomyopathy and rhabdomyolysis in long-chain fat oxidation disorders using an anaplerotic odd-chain triglyceride. *J Clin Invest* **110**, 259-269
232. Sweetman, L., Weyler, W., Nyhan, W. L., de Cespedes, C., Loria, A. R., and Estrada, Y. (1978) Abnormal metabolites of isoleucine in a patient with propionyl-CoA carboxylase deficiency. *Biomed Mass Spectrom* **5**, 198-207
233. Kuhara, T., Inoue, Y., Shinka, T., Matsumoto, I., and Matsuo, M. (1983) Identification of 3-hydroxy-3-ethylglutaric acid in urine of patients with propionic acidemia. *Biomed Mass Spectrom* **10**, 629-632
234. Kinman, R. P., Kasumov, T., Jobbins, K. A., Thomas, K. R., Adams, J. E., Brunengraber, L. N., Kutz, G., Brewer, W. U., Roe, C. R., and Brunengraber, H. (2006) Parenteral and enteral metabolism of anaplerotic triheptanoin in normal rats. *Am J Physiol Endocrinol Metab* **291**, E860-866
235. Stern, J. R., Coon, M. J., and Del Campillo A. (1956) Enzymes of fatty acid metabolism. III. Breakdown and synthesis of beta-keto fatty acids. *J Biol Chem* **221**, 1-14
236. Schuler, A. M., and Wood, P. A. (2002) Mouse models for disorders of mitochondrial fatty acid beta-oxidation. *Ilar J* **43**, 57-65

237. Labarthe, F., Gelinas, R., and Des Rosiers, C. (2008) Medium-chain fatty acids as metabolic therapy in cardiac disease. *Cardiovasc Drugs Ther* **22**, 97-106
238. Bergman, B. C., Cornier, M. A., Horton, T. J., and Bessesen, D. H. (2007) Effects of fasting on insulin action and glucose kinetics in lean and obese men and women. *Am J Physiol Endocrinol Metab* **293**, E1103-1111
239. Bickerton, A. S., Roberts, R., Fielding, B. A., Tornqvist, H., Blaak, E. E., Wagenmakers, A. J., Gilbert, M., Humphreys, S. M., Karpe, F., and Frayn, K. N. (2008) Adipose tissue fatty acid metabolism in insulin-resistant men. *Diabetologia* **51**, 1466-1474
240. Skrha, J., Kunesova, M., Hilgertova, J., Weiserova, H., Krizova, J., and Kotrlíkova, E. (2005) Short-term very low calorie diet reduces oxidative stress in obese type 2 diabetic patients. *Physiol Res* **54**, 33-39
241. Valera, A., Pelegrin, M., Asins, G., Fillat, C., Sabater, J., Pujol, A., Hegardt, F. G., and Bosch, F. (1994) Overexpression of mitochondrial 3-hydroxy-3-methylglutaryl-CoA synthase in transgenic mice causes hepatic hyperketogenesis. *J Biol Chem* **269**, 6267-6270
242. Blomqvist, G., Alvarsson, M., Grill, V., Von Heijne, G., Ingvar, M., Thorell, J. O., Stone-Elander, S., Widen, L., and Ekberg, K. (2002) Effect of acute hyperketonemia on the cerebral uptake of ketone bodies in nondiabetic subjects and IDDM patients. *Am J Physiol Endocrinol Metab* **283**, E20-28
243. Roy, M., Nugent, S., Tremblay-Mercier, J., Tremblay, S., Courchesne-Loyer, A., Beaudoin, J. F., Tremblay, L., Descoteaux, M., Lecomte, R., and Cunnane, S. C. (2012) The ketogenic diet increases brain glucose and ketone uptake in aged rats: A dual tracer PET and volumetric MRI study. *Brain research*
244. Hawdon, J. M., Ward Platt, M. P., and Aynsley-Green, A. (1992) Patterns of metabolic adaptation for preterm and term infants in the first neonatal week. *Arch Dis Child* **67**, 357-365
245. Alaynick, W. A., Kondo, R. P., Xie, W., He, W., Dufour, C. R., Downes, M., Jonker, J. W., Giles, W., Naviaux, R. K., Giguere, V., and Evans, R. M. (2007) ERRgamma directs and maintains the transition to oxidative metabolism in the postnatal heart. *Cell Metab* **6**, 13-24
246. Denne, S., and Kalhan, S. C. (1986) Glucose carbon recycling and oxidation in human newborns. *Am J Physiol* **251**, E71-77
247. Hertz, L., and Diemel, G. A. (2002) Energy metabolism in the brain. *Int Rev Neurobiol* **51**, 1-102
248. Bougneres, P. F., Lemmel, C., Ferre, P., and Bier, D. M. (1986) Ketone body transport in the human neonate and infant. *J Clin Invest* **77**, 42-48
249. Afifi, A. K., and Bergman, R. A. (2005) Functional Neuroanatomy: Text and Atlas. (Afifi, A. K., and Bergman, R. A. ed.), McGraw-Hill Company, New York. pp 326-336
250. Nehlig, A. (1999) Age-dependent pathways of brain energy metabolism: the suckling rat, a natural model of the ketogenic diet. *Epilepsy Research* **37** 211-221
251. Quant, P. A., Robin, D., Robin, P., Girard, J., and Brand, M. D. (1989) Control of acetoacetate production from exogenous palmitoyl-CoA in isolated rat liver mitochondria. *Biochem Soc Trans* **17**, 1089-1090
252. Quant, P. A., Robin, D., Robin, P., Ferre, P., Brand, M. D., and Girard, J. (1991) Control of hepatic mitochondrial 3-hydroxy-3-methylglutaryl-CoA synthase during the foetal/neonatal transition, suckling and weaning in the rat. *Eur J Biochem* **195**, 449-454
253. Kaye, M. A. (2006) Disorders of ketone production and utilization. *Mol Genet Metab* **87**, 281-283
254. Bateman, K. S., Brownie, E. R., Wolodko, W. T., and Fraser, M. E. (2002) Structure of the mammalian CoA transferase from pig heart. *Biochemistry* **41**, 14455-14462
255. Tammam, S. D., Rochet, J. C., and Fraser, M. E. (2007) Identification of the cysteine residue exposed by the conformational change in pig heart succinyl-CoA:3-ketoacid coenzyme A transferase on binding coenzyme A. *Biochemistry* **46**, 10852-10863
256. Ferre, P., Pegorier, J. P., Williamson, D. H., and Girard, J. R. (1978) The development of ketogenesis at birth in the rat. *Biochem J* **176**, 759-765

257. Girard, J. R., Cuendet, G. S., Marliiss, E. B., Kervran, A., Rieutort, M., and Assan, R. (1973) Fuels, Hormones, and Liver Metabolism at Term and during the Early Postnatal Period in the Rat. *J Clin Invest* **52**, 3190-3200
258. Cahill, G. F., Jr., Herrera, M. G., Morgan, A. P., Soeldner, J. S., Steinke, J., Levy, P. L., Reichard, G. A., Jr., and Kipnis, D. M. (1966) Hormone-fuel interrelationships during fasting. *J Clin Invest* **45**, 1751-1769
259. Matsui, Y., Takagi, H., Qu, X., Abdellatif, M., Sakoda, H., Asano, T., Levine, B., and Sadoshima, J. (2007) Distinct roles of autophagy in the heart during ischemia and reperfusion: roles of AMP-activated protein kinase and Beclin 1 in mediating autophagy. *Circ Res* **100**, 914-922
260. Glick, D., Barth, S., and Macleod, K. F. (2010) Autophagy: cellular and molecular mechanisms. *J Pathol* **221**, 3-12
261. Yu, L., McPhee, C. K., Zheng, L., Mardones, G. A., Rong, Y., Peng, J., Mi, N., Zhao, Y., Liu, Z., Wan, F., Hailey, D. W., Oorschot, V., Klumperman, J., Baehrecke, E. H., and Lenardo, M. J. (2010) Termination of autophagy and reformation of lysosomes regulated by mTOR. *Nature* **465**, 942-946
262. Kuma, A., Hatano, M., Matsui, M., Yamamoto, A., Nakaya, H., Yoshimori, T., Ohsumi, Y., Tokuhiya, T., and Mizushima, N. (2004) The role of autophagy during the early neonatal starvation period. *Nature* **432**, 1032-1036
263. Barth, S., Glick, D., and Macleod, K. F. (2010) Autophagy: assays and artifacts. *J Pathol* **221**, 117-124
264. Barnett, S. A., and Widdowson, E. M. (1971) Organ weights and body composition of parturient and lactating mice, and their young, at 21°C and -3°C. *J. Reprod. Fertil.* , 39-57
265. Krebs, H. A. (1967) Role of the redox state of nicotinamide adenine dinucleotides in the regulation of metabolic processes. *Natl Cancer Inst Monogr* **27**, 331-343
266. Takahashi, M., Ueda, K., Tabata, R., Iwata, S., Ozawa, K., Uno, S., and Kinoshita, M. (1997) Arterial ketone body ratio as a prognostic indicator in acute heart failure. *J Lab Clin Med* **129**, 72-80
267. Burgess, S. C., Leone, T. C., Wende, A. R., Croce, M. A., Chen, Z., Sherry, A. D., Malloy, C. R., and Finck, B. N. (2006) Diminished hepatic gluconeogenesis via defects in tricarboxylic acid cycle flux in peroxisome proliferator-activated receptor gamma coactivator-1alpha (PGC-1alpha)-deficient mice. *J Biol Chem* **281**, 19000-19008
268. Reichard, G. A., Jr., Haff, A. C., Skutches, C. L., Paul, P., Holroyde, C. P., and Owen, O. E. (1979) Plasma acetone metabolism in the fasting human. *J Clin Invest* **63**, 619-626
269. Hagberg, H., Peebles, D., and Mallard, C. (2002) Models of white matter injury: comparison of infectious, hypoxic-ischemic, and excitotoxic insults. *Ment Retard Dev Disabil Res Rev* **8**, 30-38
270. Hew, K. W., and Keller, K. A. (2003) Postnatal anatomical and functional development of the heart: a species comparison. *Birth Defects Res B Dev Reprod Toxicol* **68**, 309-320
271. Ibanez, L., Sebastiani, G., Lopez-Bermejo, A., Dı́az, M., Gomez-Roig, M. D., and Zegher, F. (2008) Gender Specificity of Body Adiposity and Circulating Adiponectin, Visfatin, Insulin, and Insulin Growth Factor-I at Term Birth: Relation to Prenatal Growth. *J Clin Endocrinol Metab.* **93**, 2774-2778
272. McGarry, J. D., and Foster, D. W. (1977) Hormonal control of ketogenesis. Biochemical considerations. *Arch Intern Med* **137**, 495-501
273. Hondares, E., Rosell, M., Gonzalez, F. J., Giralt, M., Iglesias, R., and Villarroya, F. (2010) Hepatic FGF21 Expression Is Induced at Birth via PPARalpha in Response to Milk Intake and Contributes to Thermogenic Activation of Neonatal Brown Fat. *Cell Metab* **11**, 206-212
274. Chaussain, J. L., Georges, P., Calzada, L., and Job, J. C. (1977) Glycemic response to 24-hour fast in normal children: III. Influence of age. *J Pediatr* **91**, 711-714
275. Jenness, R. (1979) The composition of human milk. *Semin Perinatol* **3**, 225-239

276. Allen, J. C., Keller, R. P., Archer, P., and Neville, M. C. (1991) Studies in human lactation: milk composition and daily secretion rates of macronutrients in the first year of lactation. *The American journal of clinical nutrition* **54**, 69-80
277. Best, T. H., Franz, D. N., Gilbert, D. L., Nelson, D. P., and Epstein, M. R. (2000) Cardiac complications in pediatric patients on the ketogenic diet. *Neurology* **54**, 2328-2330
278. Chen, T. Y., Smith, W., Rosenstock, J. L., and Lessnau, K. D. (2006) A life-threatening complication of Atkins diet. *Lancet* **367**, 958
279. Owen, D., Little, S., Leach, R., and Wyncoll, D. (2008) A patient with an unusual aetiology of a severe ketoacidosis. *Intensive Care Med* **34**, 971-972
280. White, H., and Jencks, W. P. (1976) Properties of succinyl-CoA:3-ketoacid coenzyme A transferase. *J Biol Chem* **251**, 1708-1711
281. Williamson, J. R., Browning, E.T., and Scholz, R. (1969) Interactions between fatty acid oxidation and the citric acid cycle in perfused rat liver. *J Biol Chem* **244**, 4617-4627
282. Palermo, J., Gulick, J., Colbert, M., Fewell, J., and Robbins, J. (1996) Transgenic remodeling of the contractile apparatus in the mammalian heart. *Circ Res* **78**, 504-509
283. Testa, G., Schaft, J., van der Hoeven, F., Glaser, S., Anastassiadis, K., Zhang, Y., Hermann, T., Stremmel, W., and Stewart, A. F. (2004) A reliable lacZ expression reporter cassette for multipurpose, knockout-first alleles. *Genesis* **38**, 151-158
284. Agah, R., Frenkel, P. A., French, B. A., Michael, L. H., Overbeek, P. A., and Schneider, M. D. (1997) Gene recombination in postmitotic cells. Targeted expression of Cre recombinase provokes cardiac-restricted, site-specific rearrangement in adult ventricular muscle in vivo. *J Clin Invest* **100**, 169-179
285. Miniou, P., Tiziano, D., Frugier, T., Roblot, N., Le Meur, M., and Melki, J. (1999) Gene targeting restricted to mouse striated muscle lineage. *Nucleic Acids Res* **27**, e27
286. Zhu, Y., Romero, M. I., Ghosh, P., Ye, Z., Charnay, P., Rushing, E. J., Marth, J. D., and Parada, L. F. (2001) Ablation of NF1 function in neurons induces abnormal development of cerebral cortex and reactive gliosis in the brain. *Genes Dev* **15**, 859-876
287. Gaussin, V., Van de Putte, T., Mishina, Y., Hanks, M. C., Zwijsen, A., Huylebroeck, D., Behringer, R. R., and Schneider, M. D. (2002) Endocardial cushion and myocardial defects after cardiac myocyte-specific conditional deletion of the bone morphogenetic protein receptor ALK3. *Proc Natl Acad Sci U S A* **99**, 2878-2883
288. Rempe, D., Vangeison, G., Hamilton, J., Li, Y., Jepson, M., and Federoff, H. J. (2006) Synapsin I Cre transgene expression in male mice produces germline recombination in progeny. *Genesis* **44**, 44-49
289. Escartin, C., Pierre, K., Colin, A., Brouillet, E., Delzescaux, T., Guillermier, M., Dhenain, M., Deglon, N., Hantraye, P., Pellerin, L., and Bonvento, G. (2007) Activation of astrocytes by CNTF induces metabolic plasticity and increases resistance to metabolic insults. *J Neurosci* **27**, 7094-7104
290. Sakazaki, H., Hirayama, K., Murakami, S., Yonezawa, S., Shintaku, H., Sawada, Y., Fukao, T., Watanabe, H., Orip, T., and Isshiki, G. (1995) A new Japanese case of succinyl-CoA:3-ketoacid CoA-transferase deficiency. *J. Inher. Metab. Dis.* **18** 323-325
291. Garbow, J. R., Doherty, J. M., Schugar, R. C., Travers, S., Weber, M. L., Wentz, A. E., Ezenwajiaku, N., Cotter, D. G., Brunt, E. M., and Crawford, P. A. (2011) Hepatic steatosis, inflammation, and ER stress in mice maintained long term on a very low-carbohydrate ketogenic diet. *Am J Physiol Gastrointest Liver Physiol* **300** 956-967
292. Kennedy, A. R., Pissios, P., Otu, H., Xue, B., Asakura, K., Furukawa, N., Marino, F. E., Liu, F., Kahn, B. B., Libermann, T. A., Maratos-Flier, E., and Roberson, R. (2007) A high-fat, ketogenic diet induces a unique metabolic state in mice. *Am J Physiol Endocrinol Metab* **292**, E1724-1739

293. Badman, M. K., Kennedy, A. R., Adams, A. C., Pissios, P., and Maratos-Flier, E. (2009) A Very Low Carbohydrate Ketogenic Diet Improves Glucose Tolerance in ob/ob Mice Independent of Weight Loss. *Am J Physiol Endocrinol Metab* **297**, E1197-E1204
294. Badman, M. K., Koester, A., Flier, J. S., Kharitonov, A., and Maratos-Flier, E. (2009) Fibroblast Growth Factor 21-Deficient Mice Demonstrate Impaired Adaptation to Ketosis. *Endocrinology*
295. Thio, L. L., Erbayat-Altay, E., Rensing, N., and Yamada, K. A. (2006) Leptin contributes to slower weight gain in juvenile rodents on a ketogenic diet. *Pediatr Res* **60**, 413-417
296. Ruderman, N. B., Ross, P. S., Berger, M., and Goodman, M. N. (1974) Regulation of glucose and ketone-body metabolism in brain of anaesthetized rats. *Biochem J* **138**, 1-10
297. Murphy, M. P. (2009) How mitochondria produce reactive oxygen species. *Biochem J* **417**, 1-13
298. Masuda, R., Monahan, J. W., and Kashiwaya, Y. (2005) D-beta-hydroxybutyrate is neuroprotective against hypoxia in serum-free hippocampal primary cultures. *J Neurosci Res* **80**, 501-509
299. Mori, H., Hanada, R., Hanada, T., Aki, D., Mashima, R., Nishinakamura, H., Torisu, T., Chien, K. R., Yasukawa, H., and Yoshimura, A. (2004) Socs3 deficiency in the brain elevates leptin sensitivity and confers resistance to diet-induced obesity. *Nat Med* **10**, 739-743
300. Gaveriaux-Ruff, C., and Kieffer, B. L. (2007) Conditional gene targeting in the mouse nervous system: Insights into brain function and diseases. *Pharmacol Ther* **113**, 619-634
301. Cotter, D. G., Schugar, R. C., and Crawford, P. A. (2013) Ketone body metabolism and cardiovascular disease. *Am J Physiol Heart Circ Physiol* **304**, H1060-1076
302. Sunny N. E., Satapati S., Fu X., He T. T., Mehdibeigi R., Spring-Robinson C., Duarte J., Potthoff M. J., Browning J. D., and Burgess S. C. (2010) Progressive adaptation of hepatic ketogenesis in mice fed a high-fat diet. *Am J Physiol Endocrinol Metab* **298**, 1226-1235
303. Dietzen, D. J., Weindel, A. L., Carayannopoulos, M. O., Landt, M., Normansell, E. T., Reimschisel, T. E., and Smith, C. H. (2008) Rapid comprehensive amino acid analysis by liquid chromatography/tandem mass spectrometry: comparison to cation exchange with post-column ninhydrin detection. *Rapid Commun Mass Spectrom* **22**, 3481-3488
304. Ziegler, A., Zaugg, C. E., Buser, P. T., Seelig, J., and Kunnecke, B. (2002) Non-invasive measurements of myocardial carbon metabolism using in vivo ¹³C NMR spectroscopy. *NMR Biomed* **15**, 222-234
305. Andrews, M. T., Russeth, K. P., Drewes, L. R., and Henry, P. G. (2009) Adaptive mechanisms regulate preferred utilization of ketones in the heart and brain of a hibernating mammal during arousal from torpor. *Am J Physiol Regul Integr Comp Physiol* **296**, R383-393
306. Holness, M. J., and Sugden, M. C. (2003) Regulation of pyruvate dehydrogenase complex activity by reversible phosphorylation. *Biochem Soc Trans* **31**, 1143-1151
307. Taylor, S. I., Mukherjee, C., and Jungas, R. L. (1975) Regulation of pyruvate dehydrogenase in isolated rat liver mitochondria. Effects of octanoate, oxidation-reduction state, and adenosine triphosphate to adenosine diphosphate ratio. *J Biol Chem* **250**, 2028-2035
308. Preuveneers, M. J., Peacock, D., Crook, E. M., Clark, J. B., and Brocklehurst, K. (1973) D-3-hydroxybutyrate dehydrogenase from *Rhodospseudomonas spheroides*. Kinetics of radioisotope redistribution at chemical equilibrium catalysed by the enzyme in solutions. *Biochem J* **133**, 159-164
309. Burgess, S. C., Hausler, N., Merritt, M., Jeffrey, F. M., Storey, C., Milde, A., Koshy, S., Lindner, J., Magnuson, M. A., Malloy, C. R., and Sherry, A. D. (2004) Impaired tricarboxylic acid cycle activity in mouse livers lacking cytosolic phosphoenolpyruvate carboxykinase. *J Biol Chem* **279**, 48941-48949
310. Batenburg, J. J., and Olson, M. S. (1976) Regulation of pyruvate dehydrogenase by fatty acid in isolated rat liver mitochondria. *J Biol Chem* **251**, 1364-1370
311. Harris, D. L., Weston, P. J., and Harding, J. E. (2012) Incidence of Neonatal Hypoglycemia in Babies Identified as at Risk. *The Journal of pediatrics* **161**, 787-789

312. Miniño, A. M., Xu, J., and Kochanek, K. D. (2010) Deaths: Preliminary Data for 2008. *National Vital Statistics Reports: Centers for Disease Control and Prevention* **59**, 1-52
313. Cotter, D. G., Ercal, B., d'Avignon, D. A., Dietzen, D. J., and Crawford, P. A. (2013) Impact of peripheral ketolytic deficiency on hepatic ketogenesis and gluconeogenesis during the transition to birth. *J Biol Chem* **288**, 19739-19749
314. Rakhshandehroo, M., Sanderson, L. M., Matilainen, M., Stienstra, R., Carlberg, C., de Groot, P. J., Muller, M., and Kersten, S. (2007) Comprehensive Analysis of PPARalpha-Dependent Regulation of Hepatic Lipid Metabolism by Expression Profiling. *PPAR Res* **2007**, 26839
315. Mandard, S., Muller, M., and Kersten, S. (2004) Peroxisome proliferator-activated receptor alpha target genes. *Cell Mol Life Sci* **61**, 393-416
316. Kersten, S., Seydoux, J., Peters, J. M., Gonzalez, F. J., Desvergne, B., and Wahli, W. (1999) Peroxisome proliferator-activated receptor {alpha} mediates the adaptive response to fasting. *J Clin Invest* **103**, 1489-1498
317. Leone, T. C., Weinheimer, C. J., and Kelly, D. P. (1999) A critical role for the peroxisome proliferator-activated receptor alpha (PPARalpha) in the cellular fasting response: The PPARalpha -null mouse as a model of fatty acid oxidation disorders. *Proc Natl Acad Sci U S A* **96**, 7473-7478
318. Chakravarthy, M. V., Lodhi, I. J., Yin, L., Malapaka, R. R., Xu, H. E., Turk, J., and Semenkovich, C. F. (2009) Identification of a physiologically relevant endogenous ligand for PPARalpha in liver. *Cell* **138**, 476-488
319. Chakravarthy, M. V., Pan, Z., Zhu, Y., Tordjman, K., Schneider, J. G., Coleman, T., Turk, J., and Semenkovich, C. F. (2005) "New" hepatic fat activates PPARalpha to maintain glucose, lipid, and cholesterol homeostasis. *Cell Metab* **1**, 309-322
320. Patsouris, D., Mandard, S., Voshol, P. J., Escher, P., Tan, N. S., Havekes, L. M., Koenig, W., Marz, W., Tafuri, S., Wahli, W., Muller, M., and Kersten, S. (2004) PPARalpha governs glycerol metabolism. *J Clin Invest* **114**, 94-103
321. Xu, J., Xiao, G., Trujillo, C., Chang, V., Blanco, L., Joseph, S. B., Bassilian, S., Saad, M. F., Tontonoz, P., Lee, W. N., and Kurland, I. J. (2002) Peroxisome proliferator-activated receptor alpha (PPARalpha) influences substrate utilization for hepatic glucose production. *J Biol Chem* **277**, 50237-50244
322. Burgess, S., He, T., Yan, Z., Lindner, J., Sherry, A., Malloy, C., Browning, J., and Magnuson, M. (2007) Cytosolic Phosphoenolpyruvate Carboxykinase Does Not Solely Control the Rate of Hepatic Gluconeogenesis in the Intact Mouse Liver. *Cell Metab* **5** 313-320
323. Dean, J. T., Tran, L., Beaven, S., Tontonoz, P., Reue, K., Dipple, K. M., and Liao, J. C. (2009) Resistance to diet-induced obesity in mice with synthetic glyoxylate shunt. *Cell Metab* **9**, 525-536
324. Rardin, M. J., He, W., Nishida, Y., Newman, J. C., Carrico, C., Danielson, S. R., Guo, A., Gut, P., Sahu, A. K., Li, B., Uppala, R., Fitch, M., Riiff, T., Zhu, L., Zhou, J., Mulhern, D., Stevens, R. D., Ilkayeva, O. R., Newgard, C. B., Jacobson, M. P., Hellerstein, M., Goetzman, E. S., Gibson, B. W., and Verdin, E. (2013) SIRT5 Regulates the Mitochondrial Lysine Succinylome and Metabolic Networks. *Cell Metab* **18**, 920-933
325. Loomba, R., and Sanyal, A. J. (2013) The global NAFLD epidemic. *Nat Rev Gastroenterol Hepatol* **10**, 686-690
326. Michelotti, G. A., Machado, M. V., and Diehl, A. M. (2013) NAFLD, NASH and liver cancer. *Nat Rev Gastroenterol Hepatol* **10**, 656-665
327. Anstee, Q. M., Targher, G., and Day, C. P. (2013) Progression of NAFLD to diabetes mellitus, cardiovascular disease or cirrhosis. *Nat Rev Gastroenterol Hepatol* **10**, 330-344
328. Ratzl, V. (2013) Pharmacological agents for NASH. *Nat Rev Gastroenterol Hepatol* **10**, 676-685
329. Abdelmegeed, M. A., Yoo, S. H., Henderson, L. E., Gonzalez, F. J., Woodcroft, K. J., and Song, B. J. (2011) PPARalpha expression protects male mice from high fat-induced nonalcoholic fatty liver. *J Nutr* **141**, 603-610

330. Ip, E., Farrell, G. C., Robertson, G., Hall, P., Kirsch, R., and Leclercq, I. (2003) Central role of PPARalpha-dependent hepatic lipid turnover in dietary steatohepatitis in mice. *Hepatology* **38**, 123-132
331. Shiri-Sverdlov, R., Wouters, K., van Gorp, P. J., Gijbels, M. J., Noel, B., Buffat, L., Staels, B., Maeda, N., van Bilsen, M., and Hofker, M. H. (2006) Early diet-induced non-alcoholic steatohepatitis in APOE2 knock-in mice and its prevention by fibrates. *J Hepatol* **44**, 732-741
332. Fabbrini, E., Mohammed, B. S., Korenblat, K. M., Magkos, F., McCrea, J., Patterson, B. W., and Klein, S. (2010) Effect of Fenofibrate and Niacin on Intrahepatic Triglyceride Content, Very Low-Density Lipoprotein Kinetics, and Insulin Action in Obese Subjects with Nonalcoholic Fatty Liver Disease. *J Clin Endocrinol Metab* **95**, 2727-2735
333. Fernandez-Miranda, C., Perez-Carreras, M., Colina, F., Lopez-Alonso, G., Vargas, C., and Solis-Herruzo, J. A. (2008) A pilot trial of fenofibrate for the treatment of non-alcoholic fatty liver disease. *Dig Liver Dis* **40**, 200-205
334. Mannaerts, G. P., Thomas, J., Debeer, L. J., McGarry, J. D., and Foster, D. W. (1978) Hepatic fatty acid oxidation and ketogenesis after clofibrate treatment. *Biochim Biophys Acta* **529**, 201-211
335. Fabbrini, E., Sullivan, S., and Klein, S. (2010) Obesity and nonalcoholic fatty liver disease: biochemical, metabolic, and clinical implications. *Hepatology* **51**, 679-689
336. Yamamoto, K., Fukuda, N., Zhang, L., and Sakai, T. (1996) Altered hepatic metabolism of fatty acids in rats fed a hypolipidaemic drug, fenofibrate. *Pharmacol Res* **33**, 337-342
337. Oosterveer, M. H., Grefhorst, A., van Dijk, T. H., Havinga, R., Staels, B., Kuipers, F., Groen, A. K., and Reijngoud, D. J. (2009) Fenofibrate simultaneously induces hepatic fatty acid oxidation, synthesis, and elongation in mice. *J Biol Chem* **284**, 34036-34044
338. Tremblay-Mercier, J., Tessier, D., Plourde, M., Fortier, M., Lorrain, D., and Cunnane, S. C. (2010) Bezafibrate mildly stimulates ketogenesis and fatty acid metabolism in hypertriglyceridemic subjects. *J Pharmacol Exp Ther* **334**, 341-346
339. Wree, A., Broderick, L., Canbay, A., Hoffman, H. M., and Feldstein, A. E. (2013) From NAFLD to NASH to cirrhosis-new insights into disease mechanisms. *Nat Rev Gastroenterol Hepatol* **10**, 627-636
340. Mehal, W. Z. (2013) The Gordian Knot of dysbiosis, obesity and NAFLD. *Nat Rev Gastroenterol Hepatol* **10**, 637-644
341. Fabbrini, E., Magkos, F., Mohammed, B. S., Pietka, T., Abumrad, N. A., Patterson, B. W., Okunade, A., and Klein, S. (2009) Intrahepatic fat, not visceral fat, is linked with metabolic complications of obesity. *Proc Natl Acad Sci U S A*
342. Targher, G., and Byrne, C. D. (2013) Clinical Review: Nonalcoholic fatty liver disease: a novel cardiometabolic risk factor for type 2 diabetes and its complications. *The Journal of clinical endocrinology and metabolism* **98**, 483-495
343. Targher, G., Day, C. P., and Bonora, E. (2010) Risk of cardiovascular disease in patients with nonalcoholic fatty liver disease. *N Engl J Med* **363**, 1341-1350
344. Yang, L., Li, P., Fu, S., Calay, E. S., and Hotamisligil, G. S. (2010) Defective hepatic autophagy in obesity promotes ER stress and causes insulin resistance. *Cell Metab* **11**, 467-478
345. Masuoka, H. C., and Chalasani, N. (2013) Nonalcoholic fatty liver disease: an emerging threat to obese and diabetic individuals. *Ann N Y Acad Sci* **1281**, 106-122
346. Lin, H. V., and Accili, D. (2011) Hormonal regulation of hepatic glucose production in health and disease. *Cell Metab* **14**, 9-19
347. Samuel, V. T., and Shulman, G. I. (2012) Mechanisms for insulin resistance: common threads and missing links. *Cell* **148**, 852-871
348. Newgard, C. B. (2012) Interplay between lipids and branched-chain amino acids in development of insulin resistance. *Cell Metab* **15**, 606-614

349. Farese, R. V., Jr., Zechner, R., Newgard, C. B., and Walther, T. C. (2012) The problem of establishing relationships between hepatic steatosis and hepatic insulin resistance. *Cell Metab* **15**, 570-573
350. Sun, Z., and Lazar, M. A. (2013) Dissociating fatty liver and diabetes. *Trends Endocrinol Metab* **24**, 4-12
351. Serviddio, G., Sastre, J., Bellanti, F., Vina, J., Vendemiale, G., and Altomare, E. (2008) Mitochondrial involvement in non-alcoholic steatohepatitis. *Mol Aspects Med* **29**, 22-35
352. Wei, Y., Rector, R. S., Thyfault, J. P., and Ibdah, J. A. (2008) Nonalcoholic fatty liver disease and mitochondrial dysfunction. *World J Gastroenterol* **14**, 193-199
353. Serviddio, G., Bellanti, F., Vendemiale, G., and Altomare, E. (2011) Mitochondrial dysfunction in nonalcoholic steatohepatitis. *Expert Rev Gastroenterol Hepatol* **5**, 233-244
354. Vice, E., Privette, J. D., Hickner, R. C., and Barakat, H. A. (2005) Ketone body metabolism in lean and obese women. *Metabolism* **54**, 1542-1545
355. Sunny, N. E., Parks, E. J., Browning, J. D., and Burgess, S. C. (2011) Excessive Hepatic Mitochondrial TCA Cycle and Gluconeogenesis in Humans with Nonalcoholic Fatty Liver Disease. *Cell Metab* **14**, 804-810
356. Thumelin, S., Kohl, C., Girard, J., and Pegorier, J. P. (1999) Atypical expression of mitochondrial 3-hydroxy-3-methylglutaryl-CoA synthase in subcutaneous adipose tissue of male rats. *J Lipid Res* **40**, 1071-1077
357. Williamson, J. R., Browning, E.T., and Scholz, R. (1969) Effects of oleate on gluconeogenesis in perfused rat liver. *J Biol Chem* **244**, 4607-4616
358. Williamson, J. R., Rostand, S.G., and Peterson, M.J. (1970) Control Factors Affecting Gluconeogenesis in Perfused Rat Liver. Effects of 4-Pentenoic Acid. *J Biol Chem* **245**, 3242-3251
359. Cohen, J. C., Horton, J. D., and Hobbs, H. H. (2011) Human fatty liver disease: old questions and new insights. *Science* **332**, 1519-1523
360. Ramos, M., Menao, S., Arnedo, M., Puisac, B., Gil-Rodriguez, M. C., Teresa-Rodrigo, M. E., Hernandez-Marcos, M., Pierre, G., Ramaswami, U., Baquero-Montoya, C., Bueno, G., Casale, C., Hegardt, F. G., Gomez-Puertas, P., and Pie, J. (2013) New case of mitochondrial HMG-CoA synthase deficiency. Functional analysis of eight mutations. *Eur J Med Genet* **56**, 411-415
361. Wolf, N. I., Rahman, S., Clayton, P. T., and Zschocke, J. (2003) Mitochondrial HMG-CoA synthase deficiency: identification of two further patients carrying two novel mutations. *Eur J Pediatr*. **162**, 279-280
362. Morris, A. A., Lascelles, C. V., Olpin, S. E., Lake, B. D., Leonard, J. V., and Quant, P. A. (1998) Hepatic mitochondrial 3-hydroxy-3-methylglutaryl-coenzyme a synthase deficiency. *Pediatr Res* **44**, 392-396
363. Leonardi, R., Zhang, Y. M., Rock, C. O., and Jackowski, S. (2005) Coenzyme A: back in action. *Prog Lipid Res* **44**, 125-153
364. Hunt, M. C., and Alexson, S. E. (2002) The role Acyl-CoA thioesterases play in mediating intracellular lipid metabolism. *Prog Lipid Res* **41**, 99-130
365. Rogers, L. K., Valentine, C. J., Szczpyka, M., and Smith, C. V. (2000) Effects of hepatotoxic doses of acetaminophen and furosemide on tissue concentrations of CoASH and CoASSG in vivo. *Chem Res Toxicol* **13**, 873-882
366. Andringa, K. K., Bajt, M. L., Jaeschke, H., and Bailey, S. M. (2008) Mitochondrial protein thiol modifications in acetaminophen hepatotoxicity: effect on HMG-CoA synthase. *Toxicol Lett* **177**, 188-197
367. Thurston, J. H., and Hauhart, R. E. (1992) Amelioration of adverse effects of valproic acid on ketogenesis and liver coenzyme A metabolism by cotreatment with pantothenate and carnitine in developing mice: possible clinical significance. *Pediatr Res* **31**, 419-423
368. Thurston, J. H., and Hauhart, R. E. (1993) Reversal of the adverse chronic effects of the unsaturated derivative of valproic acid--2-n-propyl-4-pentenoic acid--on ketogenesis and liver

- coenzyme A metabolism by a single injection of pantothenate, carnitine, and acetylcysteine in developing mice. *Pediatr Res* **33**, 72-76
369. Tokutake, Y., Iio, W., Onizawa, N., Ogata, Y., Kohari, D., Toyoda, A., and Chohnan, S. (2012) Effect of diet composition on coenzyme A and its thioester pools in various rat tissues. *Biochem Biophys Res Commun* **423**, 781-784
370. Li, L. O., Hu, Y. F., Wang, L., Mitchell, M., Berger, A., and Coleman, R. A. (2010) Early hepatic insulin resistance in mice: a metabolomics analysis. *Mol Endocrinol* **24**, 657-666
371. Garcia, M., Leonardi, R., Zhang, Y. M., Rehg, J. E., and Jackowski, S. (2012) Germline deletion of pantothenate kinases 1 and 2 reveals the key roles for CoA in postnatal metabolism. *PLoS One* **7**, e40871
372. Leonardi, R., Rehg, J. E., Rock, C. O., and Jackowski, S. (2010) Pantothenate kinase 1 is required to support the metabolic transition from the fed to the fasted state. *PLoS One* **5**, e11107
373. Mahendran, Y., Vangipurapu, J., Cederberg, H., Stancakova, A., Pihlajamaki, J., Soininen, P., Kangas, A. J., Paananen, J., Civelek, M., Saleem, N. K., Pajukanta, P., Lusic, A. J., Bonnycastle, L. L., Morken, M. A., Collins, F. S., Mohlke, K. L., Boehnke, M., Ala-Korpela, M., Kuusisto, J., and Laakso, M. (2013) Association of ketone body levels with hyperglycemia and type 2 diabetes in 9,398 finnish men. *Diabetes* **62**, 3618-3626
374. Garber, A. J., Menzel, P. H., Boden, G., and Owen, O. E. (1974) Hepatic ketogenesis and gluconeogenesis in humans. *J Clin Invest* **54**, 981-989
375. Krebs, H. A. (1961) The physiological role of the ketone bodies. *Biochem J* **80**, 225-233
376. Aledo, R., Mir, C., Dalton, R. N., Turner, C., Pie, J., Hegardt, F. G., Casals, N., and Champion, M. P. (2006) Refining the diagnosis of mitochondrial HMG-CoA synthase deficiency. *Journal of inherited metabolic disease* **29**, 207-211
377. Fukao, T., Shintaku, H., Kusubae, R., Zhang, G. X., Nakamura, K., Kondo, M., and Kondo, N. (2004) Patients homozygous for the T435N mutation of succinyl-CoA:3-ketoacid CoA Transferase (SCOT) do not show permanent ketosis. *Pediatr Res* **56**, 858-863
378. Fukao, T., Song, X. Q., Watanabe, H., Hirayama, K., Sakazaki, H., Shintaku, H., Imanaka, M., Orii, T., and Kondo, N. (1996) Prenatal diagnosis of succinyl-coenzyme A:3-ketoacid coenzyme A transferase deficiency. *Prenat Diagn* **16**, 471-474

David G. Cotter

9450 Minerva Avenue
St. Louis, MO 63114
Cell: 702-279-8471
Email: Cotterd@wusm.wustl.edu

EDUCATION

- Combined MD/PhD training. Washington University School of Medicine. May 2015.
- B.S., Biological Sciences. University of Nevada Las Vegas, School of Life Sciences, Honors College. 2008. **Summa Cum Laude** and **Department Honors Scholar**.

GRANTS and FELLOWSHIPS

- American Skin Association Medical Student Grant Targeting Melanoma and Skin Cancer Research, Jan 2015-Dec 2015.
- Developmental Cardiology and Pulmonary Training Grant, T32 HL007873, 2012-2014
- American Society for Microbiology Student Travel Grant 2008
- Summer research fellowship at Washington University School of Medicine, 2008
- Biomedical Research Apprenticeship Program (BiomedRAP) internship at Washington University School of Medicine, 2007
- NSF-EPSCoR undergraduate research grant to study SUMOylation during hibernation in the golden mantled ground squirrel *Spermophilus lateralis*, 2007
- NSF-EPSCoR undergraduate research grant to study Hsp70 expression in the rotifer *Brachionus plicatilis* in response to osmotic stress, 2006
- UNLV undergraduate research award to study Hsp70 expression in the rotifer *Brachionus plicatilis* in response to osmotic stress, 2006

HONORS and AWARDS

- Best Student Poster, Annual Cardiovascular Research Day, WUSM, 2013
- UNLV Outstanding Graduate, Fall Commencement 2008
- UNLV Provost's Scholar, 2005-2009
- Governor Guinn Millennium Scholarship 2005-2009
- Barnes and Noble Book Scholarship, Spring 2008
- Mitzi and Johnny Hughes UNLV Honors Program Scholarship, 2007-2008
- UNLV Science and Art Scholarship Fund, 2006-2007
- UNLV College of Sciences Award for Academic Excellence, 2005-06, 2006-07, 2007-08
- UNLV Stan Fulton's Honors Program Scholarship, 2005-2006

PUBLICATIONS

- **Cotter DG, Eash K, Gordon S, Schaffer A, Musiek A.** Angiosarcoma of the scalp arising within a cutaneous hemangioma. *Submitted*.
- **Cotter DG, Ercal B, Leid J, Graham M, d'Avignon DA, Dietzen DJ, Brunt E, and Crawford PA.** Ketogenesis prevents nonalcoholic fatty liver injury and hyperglycemia through coenzyme A recycling. *Journal of Clinical Investigation*. E-published 27 Oct 2014.
- **Cotter DG, Ercal B, d'Avignon DA, Dietzen DJ, and Crawford PA.** Impairments of hepatic gluconeogenesis and ketogenesis in PPAR α -deficient neonatal mice. *Am J Physiol Endocrinol Metab*. 2014. E-published 27 May 2014.
- **Cotter DG, Ercal B, d'Avignon DA, Dietzen DJ, and Crawford PA.** Impact of peripheral ketolytic deficiency on hepatic ketogenesis and gluconeogenesis during the transition to birth. *J Biol Chem*. 2013. 288 (27): 19739-19749.
- **Cotter DG, Schugar RC, and Crawford PA.** Ketone body metabolism and cardiovascular disease.

- Am J Physiol Heart Circ Physiol. 2013. 304 (8): H1060-76.
- **Cotter DG**, Schugar RC, Wentz AE, d'Avignon DA, and Crawford PA. Successful adaptation to ketosis by mice with tissue-specific deficiency of ketone body oxidation. Am J Physiol Endocrinol Metab. 2013. 304 (4): 363-74.
 - **Cotter DG**, d'Avignon, DA, Wentz AE, Weber ML, and Crawford PA. Obligate role for ketone body oxidation in neonatal metabolic homeostasis. J. Biol. Chem. 2011. 286: 6902-6910.
 - Lenz JD, Lawrenz MB, **Cotter DG**, Gonzalez RJ, Palacios MG, and Miller VL. Expression during host infection and localization of *Yersinia pestis* autotransporter proteins (Yaps). J. Bacteriol. 2011. 193 (21): 5936-5949
 - Garbow JR, Doherty JM, Schugar RC, Travers S, Weber ML, Wentz AE Ezenwajiaku N, **Cotter DG**, Brunt EM, and Crawford PA. Hepatic steatosis, inflammation, and ER stress in mice maintained long term on a very low-carbohydrate ketogenic diet. Am J Physiol Gastrointest Liver Physiol. 2011. 300: G956-G967.
 - Wentz AE, d'Avignon DA, Weber ML, **Cotter DG**, Doherty JM, Kerns R, Nagarajan R, Sambandam N, and Crawford PA. Adaptation of myocardial substrate metabolism to a ketogenic nutrient environment. J Biol Chem. 2010. 285: 24447-24456

PUBLISHED ABSTRACTS

- **Cotter DG**, and van Breukelen F. (2008). Dysregulation of SUMOylation during hibernation. FASEB J. 22 (5): 757.31.
- **Cotter DG**, Lawrenz MB, Lenz JD, Lathem W, Goldman WE, Miller VL. (2008). Identification and Characterization of Four Autotransporter Proteins in *Yersinia pestis*. 108th American Society of Microbiology, June 2008.

PRESENTATIONS

- The Yin and Yang of ketone body metabolism: new insights into a classic metabolic pathway.
 - **Oral**- UNLV School of Life Sciences Spring Seminar Series (Feb. 28, 2014).
- Ketogenesis protects from hyperglycemia and liver injury.
 - **Poster**- Annual Cardiovascular Research Day, WUSM. (Dec. 5, 2013).
 - **Poster**- Diabetes Day, WUSM. (Nov. 14, 2013).
 - **Oral**- Cardiovascular Trainee Seminar Series, WUSM. (Oct. 15, 2013).
- Ketogenesis is a central regulator of hepatic lipid and glucose metabolism.
 - **Poster**- WUSM MSTP Retreat. (April 20, 2013).
- Hepatic adaptations to impairments of ketone body metabolism.
 - **Poster**- 1ST Annual Cardiovascular Research Day, WUSM. (Dec. 7, 2012).
 - **Poster**- Diabetes Day Symposium, WUSM. (Nov. 15, 2012).
- Impact of ketone body oxidation defects on hepatic ketogenesis and gluconeogenesis.
 - **Oral**- Cardiovascular Trainee Seminar Series, WUSM. (Nov. 14, 2012).
- Preservation of redox balance and bionergetic homeostasis by ketone body metabolism.
 - **Oral**- Cardiovascular Trainee Seminar Series, WUSM. (April 18, 2012).
 - **Oral**- WUSM MSTP Retreat, Pere Marquette, IL. (April 9, 2012).
- Diverse roles for ketone body utilization in neonatal and adult metabolic homeostasis.
 - **Poster**- Diabetes Day Symposium, WUSM. (Nov. 17, 2011).
- Obligate role for ketone body oxidation in neonatal metabolic homeostasis.
 - **Oral**- WUSM MSTP Retreat, Potosi, MO. (April 9, 2011).
 - **Oral**- Cardiovascular Trainee Seminar Series, WUSM. (Oct 20, 2010).
- Adaptation of myocardial substrate metabolism to a ketogenic nutrient environment.
 - **Oral**- Cardiovascular Trainee Seminar Series, WUSM. (Feb 17, 2010).
- Dysregulation of SUMOylation during hibernation.
 - **Poster**- Experimental Biology, San Diego, CA. (2008).

- **Oral-** Nevada Undergraduate Research Symposium, Reno, NV. (2008).
- Identification and characterization of four autotransporter proteins in *Yersinia pestis*.
 - **Poster-** ASM 108th General Meeting, Boston, MA. (2008).
 - **Poster-** BioMedRAP Research Symposium, WUSM. (2008).
 - **Poster-** BioMedRAP Research Symposium, WUSM. (2007).
- Differential regulation of Hsp70 in the rotifer *Brachionus plicatilis* in response to thermal and osmotic stress.
 - **Oral-** Nevada Undergraduate Research Symposium, Las Vegas, NV. (2007).

CURRENT RESEARCH INTERESTS

- **Ketone Body Metabolism in Health and Disease (2009-present)**
 - **Mentor:** Dr. Peter Crawford, Department of Medicine, Genetics, and Developmental Biology, Washington University School of Medicine
 - **Project:** My work utilizes genetic mouse models, nutritional models, and nuclear magnetic resonance (NMR) spectroscopy to elucidate the metabolic changes that occur in disease states. Specifically, my studies have revealed novel roles for ketone body metabolism during the transition to extrauterine life and in obesity, and thus, have direct relevance to sudden infant death syndrome (SIDS), type 2 diabetes, and nonalcoholic fatty liver disease. I have demonstrated an essential role for hepatic ketogenesis in prevention of hyperglycemia and fatty liver disease, which is the most common cause of chronic liver disease in the world and affects 30% of adults in the United States. Furthermore, my studies in neonatal mice have demonstrated that defective disposal of and generation of ATP from ketone bodies phenocopies SIDS and causes hypoglycemia in a manner that can be predicted by alterations in other serum metabolites. These findings have been leveraged into a clinical study aimed to establish metabolite profiles that can risk stratify human neonates for development of hypoglycemia, a high morbidity condition.
 - **Future Interests:** I am highly motivated to apply my technical expertise in mouse genetics, NMR spectroscopy, isotopic labeling strategies, and cell biology to identify targetable molecular and metabolic adaptations employed by cutaneous neoplasms, including malignant melanoma and cutaneous T cell lymphoma, and to disorders characterized by abnormal dermal and/ or epidermal proliferation, including psoriasis, keloids, and scleroderma.

PAST RESEARCH EXPERIENCES

- **Dysregulation of SUMOylation during hibernation (2007-2009):**
 - **Mentor:** Dr. Frank van Breukelen, School of Life Sciences, UNLV
 - **Project:** Examination of the post-translational modification, SUMOylation, in the hibernating ground squirrel, *Spermophilus lateralis*, demonstrated an inability to regulate SUMOylation during hibernation. Funded by a competitive, statewide grant from the National Science Foundation-Experimental Program to Stimulate Competitive Research.
- **Identification and Characterization of Four Autotransporter Proteins in *Yersinia pestis* (2007-2008):**
 - **Mentor:** Dr. Virginia Miller, Department of Molecular Microbiology, Washington University School of Medicine
 - **Project:** Examination of the expression, localization, and function of four autotransporter proteins in *Yersinia pestis*, the causal agent of plague. Funded by a nationally competitive Biomedical Research Apprenticeship Program offered through the Division of Biology and Biomedical Sciences at Washington University School of Medicine.

- **Effects of temperature and salinity on motility and stress protein production in the rotifer *Brachionus plicatilis* (2006-2008):**
 - **Mentor:** Dr. Peter Starkweather and Dr. Frank van Breukelen, School of Life Sciences, UNLV
 - **Project:** Examination of cellular and behavioral responses to thermal and saline stress in the planktonic organism, *B. plicatilis* to determine if stress protein production supplants motility as a primary mechanism to overcome changes in ambient conditions. Funded by a competitive grant from the UNLV Office of Research, and by a statewide grant from the National Science Foundation-Experimental Program to Stimulate Competitive Research.

MENTORING EXPERIENCE

- Jamison Leid. Post-baccalaureate research assistant, WUSM. Summer 2013-present.
- Debra Whorms. Undergraduate research assistant, WUSM, summer 2012.
- Charles Shyng. PhD rotation student, WUSM, Summer-Fall 2011.
- Baris Ercal. MD/PhD rotation student, WUSM. Summer 2011.
- Charles Washington. Young Scientist Program Student, WUSM, summer 2007.

TEACHING EXPERIENCE

- Teaching Assistant for Histology, Washington University School of Medicine, 2011-12
- Lab Instructor for General Biology: Fundamentals of Life Science, UNLV, 2009
- Teaching Assistant for Cell Physiology, UNLV, 2008

COMMUNITY SERVICE

- Foster home for Serendipity German Shepherd Rescue, St. Louis, MO, 2011-present
- Washington University Medical Plunge, St. Louis, MO, 2009
 - Week long immersion into public health and community outreach
- Habitat for Humanity, Las Vegas, NV, 2006-2008
- Biology and chemistry tutor, UNLV, 2008
- Martial arts instructor for Boys and Girls Club of Las Vegas, NV, 2006-2007
- Instructor for Honors/ Women's Self Defense Class, UNLV, 2006-2007
- Green Up Las Vegas Wash, Las Vegas, NV, 2006 and 2008

CAMPUS INVOLVEMENT

- Capstone Committee, Washington University School of Medicine, 2014-2015.
- Martial Arts Club, Washington University School of Medicine, 2011-2012
 - Founding member and head instructor to 20+ members
- Your Film Society, Washington University School of Medicine, 2009-2010
 - Event Coordinator, 2009-2010
- Beta Beta Beta (biological honor society), UNLV, 2008-2009
 - Executive Vice President, 2008-2009
- Honors Student Council, UNLV, 2006-2008
 - Activities Director, 2006-2007
- Alpha Epsilon Delta (pre-health honor society), UNLV, 2006-2008
 - Chair of Fundraising, 2007-2008